RHEOLOGY AND STABILITY OF OIL-IN-WATER EMULSIONS STABILISED WITH AFRICAN CATFISH MUCILAGE

By

ADEBANJI OLASUPO OLUWOLE

Thesis submitted in fulfilment of the requirements for the degree

Doctor of Engineering; Chemical Engineering in the Faculty of Engineering and the Built Environment at the Cape Peninsula University of Technology

Supervisors: Prof Daniel Imwansi Ikhu-Omoregbe

Prof Victoria Adaora Jideani

Bellville

December 2020

Declaration

I, **Adebanji Olasupo Oluwole** declare that the contents of this thesis represent my own unaided work and that the thesis has not previously been submitted for academic examination towards any qualification. Furthermore, it represents my own opinions and not necessarily those of the Cape Peninsula University of Technology.

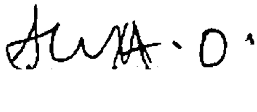

01/12/2020

Acknowledgements

I thank the Almighty God, the blessed and only potentate, for life, health, provision, and protection throughout the duration of this course. I could not have finished without the supernatural backing of God. I appreciate the people who yielded themselves as an instrument to be used by God for the success of this thesis.

I wish to express my gratitude

My supervisor Prof Daniel Imwansi Ikhu-Omoregbe I pray that God will reward your diligence, advice, and encouragements during the course of this research I am forever grateful because you believed in this research.

Prof Victoria Adaora Jideani my co-supervisor, for conveying to me the needed knowledge to complete my thesis and for your dedication to excellence.

Prof Tunde Ojumu for help and encouragements, I am forever grateful.

Prof Karabo Seteno Ntwampe for making resources available, facilitating, access to other institutions and encouragements.

Prof Percy Hlangothi for hosting my research at Nelson Mandela University.

Prof B. Y. Abubakar Executive Secretary Agricultural Research Council of Nigeria (ARCN) for providing institutional support and believing in me.

Late Dr A. Adekeye Deputy Director Fisheries ARCN for the push to aspire to be a researcher.

Prof O. Oni Ex-Director Research ARCN for his support.

The management and staff of Agricultural Research Council of Nigeria and te Federal Ministry of Agriculture and Rural Development, Nigeria.

Dr Abiola Ezekiel Taiwo for contributing to the writing of this theses, for your advice, encouragements, and prayers.

Rev. Amos and Pastor Esther Fenwa for help, encouragement and continuous prayers

Pastor and Pastor Mrs Moses Fenwa for their encouragement continuous prayers

Pastor and Pastor Mrs Ezekiel Fenwa for their continuous prayers.

Pastor and Pastor Mrs Taiwo Omojola for their encouragement continuous prayers

Rev. Robert and Dr. Titilayo Akande for help, encouragement and continuous prayers.

Pastor and Pastor Mrs Paulson Halliday for help, encouragement and continuous prayers.

Dr Stefan Abel and Ms Christa Van Schalwyke for providing alternatives.

Pastor and Pastor Mrs. Godwin Otobrise

Elder Peter Akata and family for prompt assistance

Ms Haneline Smal, Ms Ntobifuthi Bingo, and Mr Derick for help with laboratory supplies.

Ms Siyasanga Nqwazi, Ms Elizma Alberts and Ms Taylia Greene for administrative support.

My family, Holy Ghost Christian Center Worldwide for their support and prayers

Dedication

I dedicate this thesis to God Almighty for His loving kindness. I also dedicate it to my helpmeet, and succor, my beloved wife Mrs Oluwakemi Olufunmilayo Oluwole. You are a jewel of inestimable value. I appreciate God for your life daily.

Abstract

The mucilage secreted from African Catfish (*Clarias gariepinus)* when fish is stressed is a waste product that has lubricating properties and contains polysaccharides, proteins, and nucleic acid. African catfish mucilage (ACM) could be a potential emulsifier, however, information on its emulsification properties is scarce. Emulsions are thermodynamically unstable and could break down over time. Demand for sustainable natural emulsifiers has been documented in the literature and a number of them are used as food ingredients. Hence, my overall original contribution to knowledge is to characterise the physicochemical, stability, and rheological properties of ACM, a waste from African catfish to provide an effective suitable, eco-friendly alternative emulsifier that could stabilise food-grade, cosmetics, drug delivery, and personal care products.

The stability of freeze-dried ACM in MilliQ water was measured with a zetasizer and Turbiscan MA 2000. The functional groups in ACM were determined using Attenuated Total Reflection (ATR)-Fourier Transform Infrared (FTIR) spectroscopy while the flow and viscoelastic behavior of ACM was measured using a rheometer. ACM is a stable material with negatively charged (-38mV) loosely bound electrons having polar and non-polar portions. Turbiscan revealed that ACM in MilliQ water was stable after 180 minutes of storage. Wavelength peaks for ACM in the range of 400-4000 cm^{-1} showed that it contained amphiphilic protein as functional groups which is an essential characteristic for stability. ACM showed shear-thinning behavior when subjected to shear rates of 1, 10, and 100 s^{1}. ACM was found to be a pseudoplastic, non-Newtonian, and viscoelastic material with higher G' and lower G'' with increasing deformation at a fixed angular frequency of ω = 1 rad/s. The moduli in the linear viscosity range (LVR) was constant at low strains of up to 0.2 % and had cross-over points at about 10 %. Although ACM had a short LVR, rheological stability was conferred through the amphiphilic filamentous protein threads in ACM. Also, ACM could form strong interactive hydrogen and covalent bonds (emulsifying ability) with materials that have both polar and non-polar phases. The Casson model gave the best fit for African catfish mucilage.

A Zetasizer and Turbiscan were used to measure stability properties of ACM on soy milk, morphology was determined with Transmission electron microscopy (TEM), while functional groups in ACM and ACM-stabilised soya milk emulsions were determined using ATR-FTIR. The ATR-FTIR spectra of stabilised emulsion revealed synergies with soya milk droplets. Turbiscan revealed that ACM concentrations of 1, 3, and 5 % *w*/*w* stabilised soy milk emulsions within 180 min of storage. The particle size was determined with the zetasizer and stability was expressed as a function of Sauter mean diameter ($D_{(3,2)}$) calculated from the particle size. The higher the concentration of ACM, the more stable the emulsion i.e. the lower

the $D_{(3,2)}$ of stabilised emulsions. Also, the higher the ACM-emulsifier soy milk ratio (ESMR) the higher the stability i.e. the lower the $D_{(3,2)}$ of stabilised emulsions. The ESMR influenced the stability of ACM stabilised soy milk emulsions based on BS % flux and the $D_{(3,2)}$ values. The trend was that the higher ESMR the higher the BS % flux and the lower the $D_{(3,2)}$ values. The spectra of ACM stabilised soy milk emulsion revealed interactions between ACM and soya milk droplets. The results from TEM, ATR-FTIR, particle size, and BS % flux analysis showed that the mucins in ACM formed strong cohesive connections with stabilised soy milk emulsions and the ACM exhibited adhesive properties. Two-way analysis of variance (ANOVA) after Tukey's multiple comparisons (TMC) test established a significant difference ($\rho < 0.05$) on ACM stabilised soy milk emulsions with ESMRs of 5:10, 5:30, and % 5:50 %. ANOVA studies show that both BS % flux which closely fit the regression line by 99.94% and $D_{(3,2)}$ which had a 90% fit were good predictors of the stability of these emulsions.

Distinct physicochemical properties like functional groups, morphology, Sauter mean diameter ((D(3,2)), and backscattering (BS) % flux were measured to determine nanoemulsion stability using ultrasonication. The emulsifying ability of ACM on O/W-type nanoemulsions was investigated by D-optical mixture design methodology. The D-optical mixture design was used in preparing the ACM stabilised O/W-type nanoemulsion using ultrasonic cavitation. Turbiscan analysis confirmed the backscattering profile and Cryo-TEM studies confirmed the structural stability of the nanoemulsions. The ATR FTIR spectra revealed that the amphiphilic proteins in ACM formed interfaces with oil and water simultaneously to confer stability on ACM stabilised nanoemulsions which is consistent with micelle theory. The emulsifier-oil ratio (EOR) influenced the stability of O/W-type nanoemulsion based on BS % flux and the $D_{(3,2)}$. The trend was that the higher EOR the higher the stability i.e. the higher the BS % flux and the lower the $D_{(3,2)}$ of O/W-type nanoemulsion.

In this study, the D-Optimal mixture design was used in optimising O/W–type nanoemulsion formed by ultrasonication from sunflower oil, MilliQ water, and African catfish mucilage. Three mixture components constrained at lower and upper limits (ACM: 1 to 5 %, oil 3 to 10 %, and water: 85 to 96 %) were evaluated for their effects on responses of BS % flux and $\mathbf{D_{(3,2)}}$. A quadratic mixture model was the most appropriate for both BS % flux and $\mathbf{D_{(3,2)}}$. The quadratic mixture model for BS % flux was significant (F [557.86, 8.88] = 62.80; *p*-value < 0.0001). The model's lack of fit (F [19.98, *6.990E-003*] = *2858.24*; $p < 0.0001$) was also significant, however, the predicted R-squared value was 0.9123 and adequate precision was 20.186 indicating a model with adequate goodness-of-fit to the experimental data. Similarly, the quadratic mixture model for $\mathbf{D_{(3,2)}}$ was significant (F [235.71, 0.13] = 1805.99; *p*-value < 0.0001). The model lack of fit (F [0.17, 0.11] = 0.3104; $p = 1.49$) was not significant, and the predicted R-squared value was 0.9977 and adequate precision was 104.158 indicating a model with adequate goodness-

of-fit. Hence both BS % flux and the $D_{(3,2)}$ were good predictors of stability of O/W-type nanoemulsions. Desirability functions were chosen to either maximise BS % flux (γ_1) and minimise Sauter mean diameter (γ_2) or maximise BS % flux (γ_1) and maximise Sauter mean diameter (γ_2). Overall, positive physicochemical and functional properties were observed for ACM as it was established that it could stabilise O/W-type nanoemulsions, and it was shown that an optimal ACM stabilised O/W-type nanoemulsions could be produced.

The flow and viscoelastic properties were investigated to assess the stability and quality of ACMs' most stable emulsions and nanoemulsions based on rheological data. All the ACMs' most stable emulsions and nanoemulsions and control soya milk showed shear-thinning behavior as viscosity decreased as shear rate was increased from 0.01 to 1000 s^{-1}. The non-Newtonian flow of soy milk (control), ACM stabilised soya milk emulsion, ACM stabilised O/W-type nanoemulsion, and ACM stabilised O/W-type nanoemulsion enriched with soy milk fiber, was modeled with Power, Herschel-Buckley, Casson, and Bingham law equations, and the Casson model was observed to be the best fit. The moduli in the linear viscoelastic region (LVR) of ACM stabilised O/W-type nanoemulsions, and ACM stabilised O/W-type nanoemulsions enriched with soya milk fiber was constant at low strains of 0.4 and 0.6 % and cross-over points of about 30 and 50 % respectively at a fixed angular frequency of ω = 1 rad/s. The moduli in the LVR indicated improved stability for ACM stabilised O/W-type nanoemulsion enriched with soy milk fiber in comparison to that of ACM stabilised O/W-type nanoemulsion. This was due to the synergy between ACM and soy milk fiber which improved the moduli of ACM stabilised O/W-type nanoemulsion as the moduli did not match-up to the simple addition of each modulus. This synergistic effect enhanced the web-like stable matrix structure of the mixture as a phase change was not observed. All ACM stabilised O/W-type nanoemulsions formed a stable network structure as phase separation was not observed within the frequency range of 1.0 to 100 rad/s. At low frequencies, the elastic portion dominated the curves as the storage modulus was always higher than the loss modulus. Both ACM stabilised O/W-type nanoemulsion and ACM stabilised O/W-type nanoemulsion enriched with fiber behaved as weak gels. Refrigerating i.e. keeping at temperatures of 5°C sustained and improved the structural stability and viscoelastic rheological properties of the ACM, ACM stabilised O/W-type nanoemulsion and ACM stabilised O/W-type nanoemulsions enriched with soya milk fiber. An increase in time duration did not have significant negative effects on the structural stability and viscoelastic properties of the ACM, ACM stabilised O/W-type nanoemulsion and ACM stabilised O/W-type nanoemulsions enriched with soya milk fiber as ACM and all its most stable nanoemulsions remained stable with time. This was due to the filamentous proteins of ACM which was responsible for the cross-linkage stable structure network of ACM and ACMs' most stable nanoemulsions.

Consequently, the results from morphology, BS % flux, $\mathbf{D_{(3,2)}}$ (particle size), spectral functional groups and mucoadhesive property of ACM correlated with rheological properties as the stability and viscoelastic properties of ACM stabilised O/W-type nanoemulsions were ascribed to the amphiphilic filamentous protein threads present in the African catfish mucilage. These results show that African catfish mucilage is an effective suitable, an eco-friendly alternative emulsifier that could serve as feedstock in food-grade, cosmetics, drug delivery, and personal care industry.

Key Words: African catfish mucilage, African catfish mucilage stabilised soy milk emulsion, African catfish mucilage stabilised O/W-type nanoemulsion, amphiphilic proteins, D-Optimal mixture design, emulsifier-oil ratio, emulsifier soy milk ratio, homogenisation, micelle theory, mucoadhesive, O/W-type nanoemulsion, D-optical mixture design methodology, soymilk emulsion, ultrasonication.

List of Acronyms

Terms/ abbreviation	Definition/explanation
ACM	African catfish mucilage
FSM	Fish skin mucus
AMPs	Antimicrobial peptides
ANOVA	Analysis of variance
DOMD	D-Optical Mixture Design
DoE	Design of experiments
CMC	Critical micelle concentration
EA	Emulsifier activity
EOR	Emulsifier oil ratio
ESMR	Emulsifier soy milk ratio
IFT	Interfacial tension
HLB	Hydrophilic Lipophilic balance
PSR	Premixing, sonication, and rest ultrasonication method used to sonicate oil flocs.

Classification of terms

ACM	A waste product obtained from mucosal glands of the African catfish as a waste product when fish is stressed.
Amphiphilic emulsifier	An agent that contains hydrophobic and hydrophilic portions that binds to other molecules by lowering surface tension
Bioemulsifier	A surface acting agent of natural origin that stabilises an emulsion
Coalescence	Unprompted linking of small droplets of an emulsion to form larger droplets.
Creaming	Natural affinity of droplet of an emulsion to rise as a result of gravitational force.
Critical micelle concentration	Characteristic point at which amphiphilic emulsifier concentration forms micelles and all additional added surfactants go to micelles. At this point, the surface tension is comparatively stable irrespective of the emulsifier concentration.
Emulsion	Mixture of two immiscible liquids in the presence of an emulsifying agent
Emulsifier	Surface acting agent that stabilises an emulsion
Emulsifier oil ratio (EOR)	Ratio of emulsifier to oil
FSM	Mucus obtained from the skin of the fish that is not contaminated by droplets from reproductive tract
Flocculation	Phase at which the distance between the droplets of and emulsion diminishes due to the weakening of the net attractive force between them.
Hydrophilic Lipophilic (HLB) number	Number ranged from 0 to 20 which determine the nature of the emulsion.
Interfacial Tension (IFT)	Adhesive force between two phases (e.g. milk/oil and water) in emulsion.
Live African catfish	African catfish put under anaesthesia using 100 mg per liter methanesulfonate
Mucoadhesive property	An entrapment property that a material uses to adhere two phase together

Ultrasonication	Process of shearing the interface between oil and water to form stable droplets.

Table of contents

Contents

List of figures

List of tables

List of awards, publications, presentations, and training

Awards

Oluwole.A.O., Ikhu-Omoregbe, D.I. and Jideani, V.A., 2018. 'Soya milk gelation with African catfish mucus aliquots produces innovative integrated food emulsions'.

Quality, novelty and significance award for the oral presentation under the Young Researcher Forum category (page 70) at the third international Conference on Food Chemistry and Nutrition May, 16-18, 2018, Montreal, Canada

Oluwole.A.O., Ikhu-Omoregbe, D.I. and Jideani, V.A., 'Rheology and stability of oil in Water emulsions stabilised with African catfish mucus'.'

Novelty recognition by the Technology Transfer Office Cape Peninsula University of Technology, Bellville for the Deng Chemical Engineering study.

Publication

Oluwole, A.J.O., Ikhu-Omoregbe, D.I. and Jideani, V.A., 2020. Physicochemical Properties of African catfish mucilage and Its Effect on the Stability of Soya Milk Emulsions. Applied Sciences, 10(3), p.916.

Presentations

Oluwole.A.O., Ikhu-Omoregbe, D.I. and Jideani, V.A., 2018 'Soya milk gelation with African catfish mucilage aliquots produces innovative integrated food emulsions'. Oral presentation at the Food Chemistry and nutrition international conference May, 16-18, 2018, Montreal, Canada. Journal of Experimental Food Chemistry, 2018, Vol. 4, p, 70.

Oluwole.A.O. Ikhu-Omoregbe, D.I. and Jideani, V.A., 2018. Physicochemical and rheological properties of African catfish slime. Oral presentation at the U6 Postgraduate international conference, Bio-economy and biotech stream Research, Innovation and Technology for African Development, held at Cape Peninsula University of Technology September 4-6, 2018, Cape Town, South Africa.

Chapter 1

INTRODUCTION

1.1 Background of the Research Problem

The mucilage secreted from the fish skin when fish is stressed ends up as waste as fish farmers and researchers have been concerned about how to apply the benefits of this resource to ful potential (Conceição et al., 2016; Guardiola, Cuesta, & Esteban, 2016; Pérez-Sánchez et al., 2017; Fernández-Alacid et al., 2019). The disposal of this mucilage is currently raising economic and environmental concerns in the fish industry (Pérez-Sánchez et al., 2017; Bahadir & Tulun, 2019). According to 2011 figures, post-harvest waste during fish processing is estimated to be about 12 Mt annually, representing approximately 10% of global capture and cultured fish (Munesue, Masui, & Fushima, 2015). Food security has been viewed as vital for many years mainly because poverty still exists in some continents (Conceição et al., 2016). Statistics from the United Nations Development Program in 2012 indicated that malnourishment still exists in about 25% of individuals that live in Sub-Saharan Africa (Conceição et al., 2016). The 2030 program for sustainable development suggests that value be added to foods such as bread, fish, and meat by applying innovative technologies (Conceição et al., 2016; Wikström et al., 2019). Consequently, researchers have sought ways to add value to fish and fish products for sustainable fisheries development while trying to limit fish wastes (Béné et al., 2016; Stevens et al., 2018).

Emulsions are mixtures of two non-miscible liquids in which droplets in one the dispersed phase is immersed into the other one the continuous phase (McClements, 2015; Perazzo, Preziosi, & Guido, 2015). Emulsions could change phases thermodynamically and destabilise overtime via processes such as coalescence, creaming, flocculation, phase inversion, and Ostwald ripening (McClements, 2015; Liu et al., 2016; McClements, & Jafari, 2018). The thermodynamic phase changes in an emulsion and its break down over time is due to specific gravity differences in in the milk/oil globule and the aqueous phase (McClements, 2015; Tadros, 2015; Liu et al., 2016). Kinetic stability of emulsions can be achieved by using emulsifiers that allow the dispersed phase to be suspended in a continuous phase due to the intrinsic properties of the emulsifier (McClements, 2015; Li et al., 2018). Previously, synthetic biopolymers (κ-Carrageenan); synthetic surfactants (Spans and Tweens); animal-based (egg protein, gelatin whey protein) and other surfactants (poly-glycerol esters of fatty acids and sucrose fatty acid ester have been used as emulsifiers (Cheong et al., 2016; Li et al., 2018). However, due to preference displayed by consumers, researchers have been inspired to use natural bio-products as emulsifiers instead of synthetic biopolymers

and surfactants (McClements & Gumus, 2016). Food ingredients sourced from plants have been used as emulsifiers; reports on Bambara groundnut flour (Maphosa, Jideani, & Adeyi, 2017) soy lecithin and quillaja saponin (Chung et al., 2017), lutein (Weigel et al., 2018), and hydrolyzed rice glutelin and quillaja saponin (Xu, Sun, & McClements, 2019) has been documented in the literature. Emulsifiers sourced from plants although natural, are subject to sustainability challenges because they are also food ingredients. Fish skin mucus (FSM) has potentials as a natural emulsifier because it contains hydrocolloids that have adhesive properties (Shavandi et al., 2017; Petrou & Crouzier, 2018). African catfish mucilage (ACM) could serve as an alternative emulsifier compared with synthetic emulsifiers since it is sourced sustainably as waste during fish processing. Furthermore, ACM is not a food source combined with the fact that its application could lead to a eco-friendly habitats makes it a better sustainable source in comparison to synthetic emulsifier sources; however, researchers have not been interested in investigating the emulsifying ability of ACM despite the value it adds to fhe fishing industry.

Rheology has been identified as a science that deals with the study of deformation and flow of matter in emulsions on the application of stress (Guzmán et al., 2017; Zhu et al., 2019). A material such as an emulsion would undergo structural changes known as a strain when force is applied (Foudazi et al., 2015; Berton-Carabin et al., 2018; Kwok, Sun, & Ngai 2019; Tang, 2020). The stress of a material/emulsion is defined as the force per unit/drop area for materials/emulsions respectively (Rao, & Wong, 2018; Håkansson, 2019)). Authors have reported that for certain materials to undergo flow the stress needs to exceed a specific value known as the yield stress (Bonn et al., 2017; Malkin et al., 2017; Townsend et al., 2019). Hence, a materials' internal structure would respond to applied force based on its physical state and the response would show its rheological properties (Geremias-Andrade et al., 2016; Adeyi, Ikhu-Omoregbe, & Jideani et al., 2018; Khayat et al., 2019; Liu et al., 2019). Hence, a materials' internal structure would respond to applied force based on its physical state and the response would show its rheological properties (Geremias-Andrade et al., 2016; Adeyi et al., 2018; Khayat et al., 2019; Liu et al., 2019). Data obtained from rheological parameters can be fit into mathematical equations known as flow models which explain relationships between the deformation and the applied force (Dickinson, 2012; Rao, 2014; Hamza, 2016). Hence the degree of fit of the data on the flow models can be used to describe flow characteristics and predict the quality of the material. (Rao, 2014; Bhardwaj et al., 2019; Zhu et al., 2019). The rheological response of ideal materials to the applied force is governed by Hooke's law and Newton's law of elasticity which depends on a materials' flow characteristics (Fecarotti, Celauro, Pirrotta, 2012; Rao, & Wong, 2018).

Several authors have used sweep tests to investigate the responses of a specific value

for various rheological parameters over a specific strain/stress range. (Jamshidi et al., 2015; Alghooneh et al., 2017; Kolawole, Combrinck, & Boshoff, 2020). Rheological sweep tests are divided into oscillatory and rotational measurements and are executed using either small or large deformations (Läuger & Stettin, 2016; Barzic & Ioan, 2016). Rotational tests investigate a material's rheological behaviour at large deformation and correspond to brushing, pumping, and stirring operations (Vignali et al., 2019). Oscillatory tests at small deformations investigate a material's rheological behaviour and provide information on the structural state of a material at rest (Meerts et al., 2017). Small amplitude oscillatory tests correspond to long term elasticity and storage stability (Yuan et al., 2017). There are two types of rotational sweep tests controlled shear rate and controlled shear stress but the tests can be ramped or conducted in a stepwise manner (Tadros, 2011; Stettin, 2016; Whaley et al., 2019). Rotational and oscillatory measurements can be conducted via steady-state or non-steady state settings (Blau, 2015). Authors have conducted steady-state rheological measurements to characterize time-independent properties of materials (Morales-Contreras et al., 2018; Jiao, Shi, & Yuan, 2019). Shear stress and shear rate sweep tests under steady-state conditions is appropriate for very low to medium viscosity fluids while dynamic stress/strain sweep is appropriate for high viscosities (Tadros, 2011). Reliable data can be obtained from samples that are allowed to equilibrate, however, the physical instability of food systems to attain equilibrium is a challenge (Aditya, Espinosa, & Norton et al., 2017).

Fluid materials can be grouped rheologically according to their flow behaviour. Fluids are ideal if the relationship between shear rate and shear stress is linear and the proportionality constant is referred to as viscosity. Viscosity is the resistance the fluid shows under shear. When a material is deformed continuously under shear stress it displays flow behaviour (Yang & Pan, 2017; Qian & Kawashima, 2018; Jia et al 2019). A flow curve characterises the flow behaviour for a material and is expressed by the relationship between stress and strain (Ducloué et al., 2017; Zheng, 2019). Flow behaviour is categorised as either Newtonian or non-Newtonian (Sharma et al., 2016; Malkin & Isayev, 2017). Ideal fluids are referred to as Newtonian fluids because they obey Newton's law. Examples are air, milk, water, oil, clarified juices, and juice serum. Newtonian fluids show a linear proportionality between the stress and strain rate with a viscosity which remains constant (Mohammadi, Saffarian, & Mohammadi, 2015). Conversely, because the structural arrangement of almost all fluid foods changes when subject to applied forces they do not obey Newton's law they are referred to as non-Newtonian fluids (Figure 2.5). Non-Newtonian fluids show a non-linear proportionality between the stress and strain rate with varying viscosity. Non-Newtonian fluids show different flow behaviour and are categorised as time-independent, time-dependent, or viscoelastic (Kubo et al., 2019; Souza Mendes de & Thompson, 2019). Four divergent

behaviours occur in time-independent non-Newtonian fluids they are: Bingham, dilatant, Herschel–Bulkley, and pseudoplastic (Kubo et al., 2019; Ionescu et al., 2020).

Reports by researchers have shown that fish offers about 3 billion people with about 19% of animal protein globally (Béné et al., 2015; Chan et al., 2019). Also, authors have reported that the per person annual consumption of fish which contain long-chain key polyunsaturated fatty acids (PUFAs) in Africa, Asia, Europe, Latin America and the Caribbean, North America, Oceania and other parts of the world is about 10.8 kg, 21.4 kg, 21.9 kg, 9.9 kg, 21.6 kg, 26.9 kg, and 19.0 kg respectively (Agbekpornu et al., 2017; Lee & Nam, 2019; Chan et al., 2019; Obiero et al., 2019). Similarly, plant-based proteins such as soy milk that are fiber-rich has been used in bioproducts due to its low-cost, and its easy storage parameters (Cazón et al., 2017; Arif et al., 2018). Animal and plant-based adhesives such as milk proteins, mucilage, starch, and tree gums, are ecofriendly, adhere effectively with other materials, are safe and can be sustainably sourced (Ellis, Rowe, & Lotze, 2015; Guo & Wang, 2016). In the past, animal and plant sourced adhesives were steadily replaced by synthetic adhesives because they were more expensive but consumer preferences for natural products has led researchers to focus on the application of sustainably sourced bioadhesives as emulsifiers (Guo & Wang, 2016). Also, food scientists have suggested the use of fish slime as emulsifiers based on the fact that they are consumed for its animal protein, micronutrients, and long-chain key PUFAs; for instance, hagfish, which includes its mucilage, is part of the diet in Japan and Korea (Ellis et al., 2015; Böni, et al. 2016b; Böni et al. 2016b) . Consequently, authors have reported that hagfish mucilage have been applied as emulsifiers in food-grade emulsions (Böcker et al., 2016; Böni, et al. 2016a; Böni et al. 2016b; Kuster et al 2017).

Emulsions are basic constituents of many products in industries such as beverages, cosmetics, drug delivery, foods, nutraceuticals, and personal care products (Bai et al., 2017; McClements & Jafari, 2018; Mikulcová et al., 2017; Azmi et al., 2019). They can be classified as flavor emulsions which exist as colloids that are kinetically unstable and contain small oil globules dispersed within an aqueous phase (McClements, 2015; Bai et al., 2017; Maphosa et al., 2017). Kinetic instability of O/W emulsions can be ascribed to the presence of positive free energy made available when dispersions are formed that allows colloids to separate through creaming, coalescence, flocculation, Ostwald ripening, and sedimentation (Maphosa et al., 2017; McClements & Jafari, 2018; Bai et al., 2019). Emulsifiers are materials that kinetically stabilise emulsions by coating the oil globules and generate repulsive forces that hinder oil globules aggregation (Ozturk & McClements, 2016; McClements $ Jafari, 2018; Xu et al., 2019). The food industry has legally approved the use of several food-grade emulsifiers, however, costs, ease of use, and functionality make it difficult for food scientists to select the most proper emulsifier for an application (Bai et al., 2017; McClements & Jafari, 2018; Ferreira

and Nunes, 2019). Kinetic stability of O/W emulsion has been increased by adding emulsifiers, stabilisers, and biopolymers (Maphosa et al., 2017; McClements & Jafari, 2018; Drapala et al., 2018; Focsan et al., 2019). Literature supports the efficacy of emulsifiers such as biopolymers, hydrocolloids, and polysaccharides in stabilising O/W emulsions (Dickinson, 2017; Felix, Romero, & Guerrero, 2017; Maphosa et al., 2017; Maravić et al., 2019). Emulsifiers made from natural biopolymers are available, biocompatible, cost-effective, non-toxic, therapeutic, and can be sourced sustainably than synthetic ones (McClements & Gumus, 2016; Koller, 2018). Authors have reported that FSM protects the fish by incapacitating the binding of pathogens, and also acts as carriers of mucins and humoral immune factors (Peatman et al., 2015; Borges et al; 2018; Brinchmann et al., 2018). The humoral immune factors are antimicrobial peptides, cytokines, immune-globulins, and lectins while mucins are glycoproteins joined to considerable amounts of high molecular weight sugars that play a vital role in fish defense (Guardiola et al., 2017; Reverter et al., 2018). The use of fish skin mucus (FSM), as an efficient natural emulsifier, has been reported in the literature Böni et al. (2016a) and Böni et al. (2016b); African catfish mucilage (ACM) is a waste product formed when fish undergoes stress (Cabillon & Lazado, 2019). Authors have reported that the mucus from fish has antimicrobial and lubricating properties; and contains proteins, sugars, and nucleic acid (Böcker et al., 2016; Böni et al., 2016a; Reverter et al., 2018).

Literature supports the claim that the low free fatty acid content in sunflower oil makes it an oil of good quality and its low peroxide value makes its consumption reduce the risk of coronary and inflammatory health conditions (Ruiz Ruiz, Ortiz Vazquez, & Segura Campos, 2017; Bush et al., 2019; Konuskan et al., 2019; Salles et al., 2019). Food scientists have been faced with the challenge of formulating biologically nutritious semi-solid foods either as colloids, emulsions, gels, or simple solutions for different classes of individuals (Leong, Martin, & Ashokkumar, 2017a; Krasulya et al., 2016; Tiong et al., 2019). The challenges have been complicated because the biologically nutritious components tend to be immiscible with water (Krasulya et al., 2016; Leong et al., 2017a; Tiong et al., 2019). Researchers have therefore shifted focus to high-energy techniques of delivering (McClements & Jafari, 2018; Trujillo-Cayado et al., 2019). The high-energy techniques include systems that apply systems that require high-pressure, microfluidics, rotors, or ultrasonic equipment (Muschiolik & Dickinson, 2017; McClements & Jafari, 2018; Trujillo-Cayado et al., 2019). High-energy emulsification techniques use machine-driven devices that create strong disruptive forces that fragment the dispersed phase and result in small oil globules (McClements & Jafari, 2018; Patil & Gogate, 2018; Villalobos-Castillejos et al., 2018; Trujillo-Cayado et al., 2019) Authors have proposed ultra-sonication which involves shearing the interface between oil and water globules to form stable dispersions (Krasulya et al., 2016; Leong et al., 2017a; Tiong et al., 2019).

D-optical mixture design methodology (RSM) is a multivariate statistical method that has been commonly used to optimize food processing techniques (Yeom et al., 2015; Derrien et al., 2017; Yolmeh and Jafari, 2017). RSM is a regression-based analysis that fits mathematical models, such as linear, square or quadratic polynomial functions, and other models, to the experimental response observed in the experiment by applying multivariate statistical analysis methods (Myers et al., 2016; Yolmeh and Jafari, 2017; Selamat et al., 2018). The RSM strategy establishes relationships between input factors and responses with the aid of a mathematical model, deals with hindrances of optimizing with sole parameters, and provides an efficacious way to develop formulate emulsions (Montgomery, 2017; Trujillo-Cayado et al., 2019).

Various techniques have been used to investigate the physicochemical properties of O/W emulsions stabilised with bio-emulsifiers in other to explain how the bio-emulsifier influences the stability of the O/W emulsion (Maphosa et al., 2017; Shao et al., 2017; Gharibzahedi et al., 2019). Researchers have proposed other explanations that could better address O/W emulsion stability. For instance, it has been established that an emulsion could become kinetically unstable because its particle size increases with time (McClements & Gumus, 2016; Kale & Deore, 2017). However, an emulsifier reduces the repelling force between two liquids and diminishes the attractive forces between the molecules of the same liquid within an emulsion (McClements & Gumus, 2016; Kale & Deore, 2017). Hence an emulsifier lowers the interfacial tension between two immiscible liquids and stabilises an emulsion by the surface-tension theory (McClements & Gumus, 2016; Kale & Deore, 2017). Similarly, the interfacial-film theory states that the emulsifier forms a thin film on the oil globules by adsorbing onto the surface of the internal phase droplets and prevents contact or coalescence with the dispersed phase (Rajak et al., 2016; Kale & Deore, 2017; Zhang et al., 2018b; Saani et al., 2019). Increased concentration or larger molecular weight of the emulsifier results in a more stable emulsion because a more resilient film has been formed on the internal phase of the oil globules (Rajak et al., 2016; Kale & Deore, 2017; Saani et al., 2019). Similarly, authors have reported that the amphiphilic polymers in bio-emulsifiers influence stability of O/W emulsions by forming nanoemulsions through a thermodynamic process when the concentration of polymeric micelles (PMs) of the bio-emulsifiers is much lower than the concentration called critical micellar concentration (CMC) (Cagel et al., 2017; McClements, Bai, & Chung, 2017; Reneeta et al., 2018; McClements & Jafari, 2018; Liang et al., 2018; Bergenståhl & Spicer, 2019; Langevin, 2019). PMs are beneficial because their interior core contains a hydrophobic portion that can entrap materials that have a low affinity for water and an outer hydrophilic wall that encapsulates materials that have a high affinity for water (Cagel et al., 2017; Hussein & Youssry, 2018; Wang et al., 2019). In recent times, this benefit of PMs has been exploited in beverages, cosmetics, drug delivery, foods, nutraceuticals, and personal

care products because they provide improved solubility and stability for the incorporation of hydrophobic materials in O/W emulsions (Cagel et al., 2017; Hussein & Youssry, 2018; Wang et al., 2019). Furthermore, the literature supports the claim that the water solubility of an emulsifier is a rough estimate of hydrophilic-lipophilic balance (HLB) of an emulsifier and emulsifiers with HLB values between 8 and 15 are used to stabilise O/W emulsions (Burgos - Díaz et al., 2016; Nejadmansouri et al., 2016; Kale & Deore, 2017). The combination of data obtained from physicochemical properties such as particle size, backscattering flux %, and functional groups of bio-emulsifiers in conjunction with CMC and HLB correlations have been used by researchers to explain how bio-emulsifiers stabilise O/W emulsions (Burgos - Díaz et al., 2016; Nejadmansouri et al., 2016; Kale & Deore, 2017, Hussein & Youssry, 2018). Literature supports the micelle theory which proposes that bio-emulsifiers stabilised O/W emulsions is achieved through a hydrophobic portion that can entrap materials and simultaneously encapsulates materials that have a high affinity for water through its outer hydrophilic wall (Cagel et al., 2017; Hussein & Youssry, 2018; Laredj-Bourezg et al., 2017, López-Martínez & Rocha-Uribe, 2018; Wang et al., 2019).

Authors have reported research on the ability of hagfish mucus a waste product secreted from hagfish as an emulsifier (Böcker et al., 2016; Böni, et al. 2016a; Böni et al. 2016b; Bai et al., 2017; Böni et al., 2017; Böni et al., 2018: Chaudhary et al 2018: Kim, Beak, & Song, 2018; Jeewanthi & Paik, 2018). Although FSM a waste as both lubricating properties and antimicrobial properties research has focused on its antimicrobial properties (Elavarasi et al., 2013; Guardiola et al., 2017). Similarly, studies by Gobinath & Ravichandran, (2011) and Elavarasi et al, (2013) stated that the FSM of freshwater fishes such as estuarine catfish, African catfish, and tilapia have anti-microbial properties because it contains of anti-microbial peptides (Tyor & Kumari, 2016; Mahadevan et al., 2019). Hence, African catfish mucilage (ACM) could be a potential emulsifier, however, the literature on its physicochemical properties is scarce. Also, in spite of the lubricating and anti-microbial benefits of African catfish mucilage knowledge about the literature on its physicochemical properties and how it affects the stability and rheological properties of emulsions is limited.

Even though automated and rheological analyses were earlier used to characterise biopolymers, studies have revealed that the investigations on microstructure, stability and spectra, could be used to describe the physicochemical properties of biopolymers. Fourier Transform Infrared (FTIR) spectroscopy has been used in the analysis of biomaterials for more than half a century (Glassford, Byrne, & Kazarian, 2013; Sarroukh et al., 2013; Fernando et al., 2017). In the last decade FTIR in conjunction with attenuated total reflectance (ATR) spectroscopy, has been used to ascertain the structure of biopolymers (Staniszewska Malek, & Baranska. 2014; Moghaddam et al., 2017). FTIR-ATR is now commonly used to express

highly automated subcellular investigations, for examining spectra of bio-systems and chemical changes at a molecular level that can be used to predict detailed information on the structural and functional groups in a biopolymer (Angulo & do Amaral Sobral, 2016). Also, transmission electron microscopy (TEM) has been used to investigate the microstructure of bio-polymers because it produces highly magnified images (Fudge & Schorno, 2016; Drapala, Mulvihill, & O'mahony, 2018; Zielke, Stradner, & Nilsson, 2018). However, the literature on the allocation of functional groups, morphology, and stability has been scarce; also an in-depth study of the functional groups, morphology, rheological, and stability properties of African catfish mucilage limited in the literature.

The South African fishing industry is currently plagued with under-utilisation of wastes from fish that could add value to the industry. The research work focuses on the use of ACM as a sustainable natural emulsifier resource while ensuring that the ACM a waste product from African catfish is disposed of in an environmentally friendly way. Therefore, the objective of this work is to characterise the physicochemical properties of African catfish mucilage (ACM) with the focus to investigate the effectiveness of ACM as an emulsifier in stabilising dispersions and emulsions for food-grade, personal care, and drug delivery emulsion systems.

1.2 Rationale

The research is intended to be an innovation in the advancement of an emulsifier that could be used as feedstock in food-grade, personal care, and drug-release products. This was carried out by investigating the role of the emulsifier in stabilising soy milk emulsions and oil in water (O/W) emulsions. Economic advantages would be visible, through sales and exportation of the freeze-dried African catfish skin mucilage that could have possible applications as stabilisers in food-grade emulsions, creams in personal care products and drug carriers in the pharmaceutical industries. The product is in line with the national goal of achieving global competitiveness, optimizing the investment in science through improving social, economic and environmental benefits. A key goal of the South African National Research Priorities is economic growth and wealth creation which are based on innovation. This work seeks to fulfill this goal by attempting to create innovation in the area of advancing and producing ACM as a natural alternative emulsifier that could be used as a feedstock in food-grade, personal care, and pharmacological industries.

1.3 Problem Statement

The application of emulsion technology to foods, cosmetics, and medicine has received much attention lately as researchers are focusing on novel techniques to improve the stability and rheological properties of dispersions and emulsions. Previously, synthetic biopolymers such

acacia gum, polylactic acid, poly-lactic-co-glycolic acid which are polysaccharides have been used as emulsifiers (Li et al., 2018). However, due to consumer choices, researchers have been inspired to use natural bio-products as acacia gum, emulsifiers instead of synthetic biopolymers and surfactants (McClements & Gumus, 2016). Although a plant-based emulsifier is sourced, from nature its sustainability is in question as it is also a food source.

African catfish mucilage (ACM) obtained as a waste product from fish production could be a potential natural emulsifier and its usage could lead to eco-friendly environment. The polysaccharide composition of ACM shows that it has emulsification potential as feed-stocks in food, cosmetic and medical industry. This benefit coupled with consumer preference for natural products and the added advantage of its apploication could lead to greener environments However, not much is documented about its potential as an emulsifier. It is therefore of interest to investigate the potential of ACM in stabilising dispersions and emulsions.

1.4 Alignment to CPUT focus area

This research aligns with the focus area “Farmer to Pharma” value chain identified by the Department of Science and Technology’s Innovation in its Ten-Year Plan for South Africa to strengthen the bioeconomy. It also aligns with the National Development Plan: enabling milestones.

1.1.1 Economic growth and international competitiveness

African catfish mucilage (ACM) a waste product sustainably sourced from fish production has potential as a natural emulsifier as it stabilises dispersions and emulsions. Moreover, ACM has the benefit of customer preference, its application as an emulsifier could reduce its disposal challenges and result in greener environments. The use of the ACM a waste product as an emulsifier in feed-stocks for food, personal care, and pharmaceutical industries would lead to economic growth through creating employment opportunities and income generation. Also, the use of ACM as an emulsifier would lead to the development of a knowledge base that could enhance global competitiveness for South Africa.

1.5 Research aim

The study aims to investigate the performance of African catfish mucilage (ACM) as an emulsifier on the stability and rheological properties of dispersions and oil in water (O/W) emulsions with a view for its possible application as feedstock in food, personal care, and pharmaceutical industries.

1.5.1 Research objectives

The objectives of this study were to:

1. To collect and preserve African catfish mucilage from the African catfish.
2. To characterise African catfish mucilage by determining its physicochemical properties.
3. Investigate the effect of African catfish mucilage (ACM) on the stability of soya milk emulsions using Ultra-Turrax T-25 homogenizer.
4. Investigate the effect of ACM on the stability of oil in water-type nanoemulsions prepared by ultrasonication using D-optimal mixture design.
5. Investigate the flow and viscoelastic rheological behaviour of ACM, and ACMs' most stable emulsion and nanoemulsions.

1.5.2 Research questions

The research questions were:

1 How do the chemical and physical constituents of African catfish mucilage affect its use as an emulsifying agent in dispersions and O/W emulsions?

2 What optimum concentrations of African catfish mucilage are more suitable for stability of soya milk emulsions?

3 Would ultrasonication of oil and water using D-optimal mixture design methodology result in O/W-type nanoemulsions?

4 What optimum concentrations of African catfish mucilage are more suitable for stability of ultrasonified O/W-type nanoemulsions using d-optimal technique?

5 Does soy milk emulsion and O/W-type nanoemulsions stabilised with African catfish mucilage has shear-thinning and viscoelastic properties?

1.6 Delineation

Laboratory studies would be conducted to determine, assess and predict the influence of various factors on the parameters of soy milk and oil-in-water emulsions stabilised with African catfish mucilage (ACM). Sensory study was not conducted on the ACM, ACM stabilised soya milk emulsions and O/W-type nanoemulsions systems. The metabolic profile and microbial activity of ACM were not investigated in this study. This work focussed only on mucus of African catfish. Sunflower oil/soya milk served as the hydrophobic phase for this work. The properties investigated in this work iwere, emulsion stability and rheological properties of ACM and emulsions stabilised with African catfish mucus. This work did not focus on testing the

freeze-dried ACM or its emulsion systems for its pharmacological properties or benefits.

1.7 Research outcomes

Findings from the current study was presented in international/national conferences and one article has been published in peer-reviewed accredited academic journals. Other articles would subsequently follow. The outcome of the study would also increase the economic value of the African catfish mucilage.

1.8 Summary

This chapter provided a broad overview of the problem statement and research questions. The main aim and objectives of the study as well as the significance and contribution of the research were presented. The problem statement elucidated throughout literature is that the application of emulsion technology to foods, cosmetics, and medicine has resulted in the need for novel techniques to improve the stability and rheological properties of dispersions and emulsions. The problem statement has led to the formulation of fish research questions: (1) how do the chemical and physical constituents of African catfish mucilage affect its use as an emulsifying agent in dispersions and O/W emulsions? (2) What optimum concentrations of African catfish mucilage are more suitable for stability of soya milk emulsions? (3b) would ultrasonication of oil and water using D-optimal mixture design methodology result in O/W-type nanoemulsions? (d) What optimum concentrations of African catfish mucilage are more suitable for stability of ultrasonified O/W-type nanoemulsions using d-optimal technique? (e) soy milk emulsions and O/W-type nanoemulsions stabilised with African catfish mucilage has Shear-thinning and viscoelastic properties. Therefore, the study aimed to investigate the role of African catfish mucilage (ACM) as an emulsifier on the stability and rheological properties of dispersions and oil in water (O/W) emulsions with a view for its possible application as feedstock in food, personal care, and pharmaceutical industries.

The overarching significance of the study is to provide the food, cosmetics, drug delivery, and personal care industry with a low cost, eco-friendly alternative emulsifier. The African catfish mucilage (ACM) was collected and preserved from a fish farm after obtaining ethical clearance Faculty of Engineering. The mucus was collected based on South African Bureau of Standards approved procedures, the Guidelines for Ethical conduct in the care and use of nonhuman animals in research and Ethical considerations for field research on fishes (SABS, 2008; Dunbar et al., 2012; Bennett et al., 2016). Scientific tests were carried out on the ACM, ACM stabilised soy milk emulsions and ACM stabilised O/W-type nanoemulsions. A Zetasizer and Turbiscan were used to measure stability, morphology was determined with Transmission electron microscopy (TEM), while functional groups in ACM, ACM-stabilised soya milk

emulsions and ACM stabilised O/W-type nanoemulsions were determined using Attenuated Total Reflection Fourier Transform Infra-red spectroscopy. In addition rheological tests were carried out to determine the flow and viscoelastic properties of ACM, ACM-stabilised soya milk emulsions and ACM stabilised O/W-type nanoemulsions. A description on how the data were collected and analyzed is presented in the thesis. Findings from the research revealed how a low cost, eco-friendly alternative emulsifier such as African catfish mucilage (ACM) could be used in stabilising soy milk and O/W-type nanoemulsions.

1.9 Organisation of the thesis

This dissertation consists of seven chapters and it includes references and appendices. The chapters are organized to link the progression of the thesis from the title through to the

conclusion. The clarification of how each of the chapters are organised is elucidated in

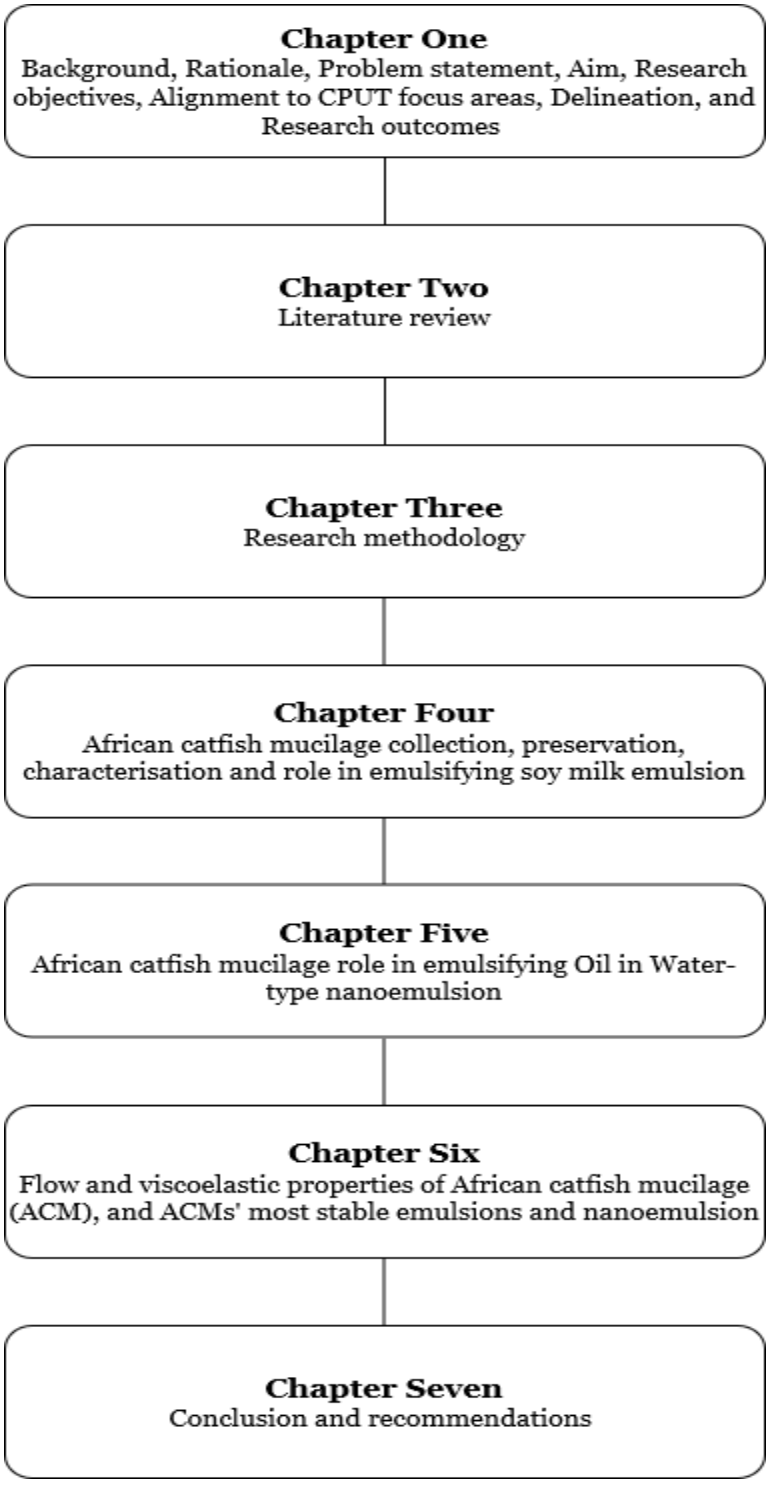

Figure 0.1.

Chapter One: The first chapter is as described under the summary section. The chapter concludes with the layout of the thesis.

Chapter Two: Provides an in-depth review of the literature on the issues of that currently affect application of emulsion technology to foods, cosmetics, and medicine. It highlights the novel techniques that researchers are focusing on to improve the stability and rheological properties of dispersions and emulsions. This chapter reviews the literature on emulsions, formulations of emulsions, the use of ultrasonication in formulating biologically nutritious semi-solid foods either as colloids, emulsions, gels or simple solutions, emulsion stability and mechanisms of emulsion breakdown during storage and techniques used to investigate emulsion stability. Furthermore, the chapter reviews the literature on rheology, flow and viscoelastic behaviour of emulsions. Also the chapter reviews literature on mixture design methodology and different designs that could be used to model the effect of independent variables on dependent variables in a mixture component. In addition the chapter reviews the literature on biology, characteristics, antimicrobial function and immunological components of fish skin mucus (FSM), its rheological characteristics and application of fish skin mucus as bioemulsifiers.

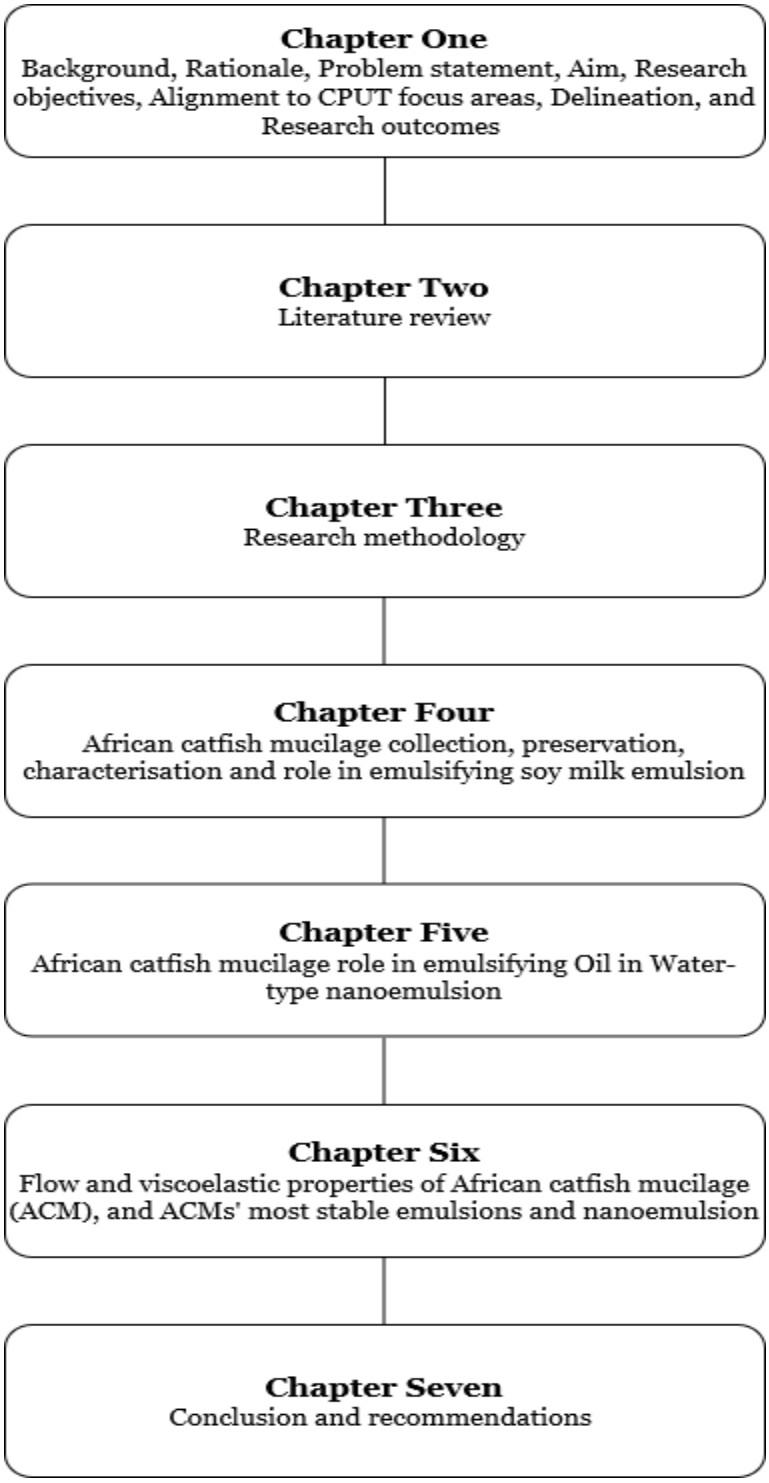

Figure 0.1: Clarification for the organisation of chapters

Chapter Three: Details the research materials and methods used in the investigations. In addition, it details the scientific tests conducted, the equipment used and how the data obtained were analyzed using statistical tools. It also presents the experimental design used and the data analytical methods. The ethical guidelines used are also indicated. The African catfish mucilage (ACM) was collected and preserved from a fish farm after obtaining ethical

clearance Faculty of Engineering. The ACM was collected based on South African Bureau of Standards approved procedures, the Guidelines for Ethical conduct in the care and use of nonhuman animals in research and Ethical considerations for field research on fishes (SABS, 2008, Dunbar et al., 2012; Bennett et al., 2016).

Chapter Four: Provides a description of the collection and preservation of the African catfish mucilage (ACM), the investigations conducted and the data collected, analysis, and findings for research objectives one, two and three. The chapter describes the findings on the extraction, and characterisation of African catfish mucilage and details role of ACM as a bioemulsifier that stabilises soy milks. It also details the result of the analysis of the data obtained on ACM stabilised soy milk emulsions using the GraphPad Prism version 5.00 for Windows, GraphPad Software, La Jolla, CA, USA.

Chapter Five: Provides a description of the investigations conducted and the data collected, analysis, and findings for research objectives two, three and four. The chapter describes the findings on the characterisation of African catfish mucilage and details role of ACM as a bioemulsifier that stabilises oil in water (O/W)-type nanoemulsions. It details the results of the D-optical mixture design used in preparing the ACM stabilised O/W-type nanoemulsion. It also details the result of the effect of the independent variables (ACM, oil and water) on the dependent variables Sauter mean diameter and backscattering % flux.

Chapter Six: Provides a description of the investigations conducted and the data collected, analysis, and findings for research objective five. The chapter describes the findings on the Investigate the flow and viscoelastic rheological behaviour of ACM, ACM stabilised soya milk emulsions and ACM stabilised O/W-type nanoemulsions. It details the results of the effect of African catfish mucilage on the viscosity of o/w type nanoemulsions, Shear-thinning behaviour of ACM and ACM stabilised emulsions, flow behaviour of o/w emulsions as described by different models. It also details the results obtained from the response of ACM, soya milk, ACM stabilised O/W-type nanoemulsion, ACM stabilised O/W-type nanoemulsion enriched with soya milk Fiber, and ACM stabilised soya milk emulsion at various strains, frequency, temperature and time.

Chapter Seven: Summarizes the discussion of findings and closing the thesis through presenting the recommendations and conclusion of the study.

The next chapter presents the literature review with a special focus on keywords featuring in the context of the background and problem statement.

Chapter 2

LITERATURE REVIEW

2.1 Overview of Emulsion

Emulsions are mixtures of two non-miscible liquids in which droplets in one the dispersed phase is immersed into the other one the continuous phase (McClements, 2015; Perazzo et al., 2015). An emulsion could also be defined as a dispersion made up of two non-miscible liquid phases homogenised with the aid of mechanical shear and emulsifiers (Kale & Deore, 2017). Amphiphilic surface acting agents of natural/synthetic origins have been used in stabilising emulsions because they reduce the interfacial tension between the two phases thereby contributing to the stability of dispersed droplets with electrostatic or steric effects (Kale & Deore, 2017; George, Shah, & Shrivastav, 2019). Emulsions could change phases thermodynamically and can destabilise overtime via processes such as coalescence, creaming, flocculation, phase inversion, and Ostwald ripening (McClements, 2015; Lu, Kelly, & Miao, 2016; McClements & Jafari, 2018). Emulsions are also grouped as bi-phasic systems of granular meta-stable dispersions that comprise of two liquids that are non-miscible, commonly oil/milk and water where one of the liquids forms small sphere-shaped droplets known as dispersions in the other which act as an aqueous dispersion vehicle; (McClements, 2015; McClements & Jafari, 2018). Commonly, emulsions are generated when oil/milk and water are homogenised; but, after homogenisation stops the emulsion starts to become unstable due to thermodynamic instability (McClements & Jafari, 2018). In categorising emulsions, the relationship between the spatial distribution of the oil/milk and aqueous phase has to be considered. If the emulsion particles are ordered as oil droplets distributed in an aqueous phase it is known as oil-in-water (O/W) emulsion, commonly used for lotions, hand cream, mayonnaise and beverages (McClements, 2015). However, if the water droplets of the emulsion are distributed in the oil phase is known as water-in-oil (W/O) emulsion, commonly used for topical ointments (Tadros, 2011). A key material needed to disperse two immiscible liquids is an emulsifier and emulsions are categorised based on the kind of the emulsifier or the system composition (Tadros, 2011; Foudazi et al., 2015).

Emulsion with various appropriate compositions has been patented for the delivery and protected encapsulation of many kinds of bioactive nutrients with major health benefits (Tadros, 2011; Lu et al., 2016). Industrially, emulsions have been used as essential encapsulation systems in the cosmetics, food, nutraceuticals, and pharmaceutical industries, therefore, current research has focused on its preparation, composition, function relationship and delivery characteristics (Tadros, 2015; Zhu et al., 2019; Choi & McClements, 2020). Emulsification, a method used industrially to formulate cosmetic, food and pharmaceutical

products involves dispersing two immiscible liquids, one a dispersed phase into another a continuous phase (Fasinu et al., 2015; Lu et al, 2016). This process results in a system in which the molecules of the two phases are indirectly interfacing with each other and have a great propensity for phase separation i.e. thermodynamic instability (Fasinu et al., 2015; McClements, 2015; Lu et al., 2016).

2.2 Emulsion formulation

In formulating emulsions, homogenisation which involves blending at elevated speeds is used, this process causes the dispersed phase to be suspended in the continuous phase (Fasinu et al., 2015). This process increases the system entropy but does not counteract the upsurge in enthalpy that arises when the hydrophilic and hydrophobic molecules of the system come in contact (Fasinu et al., 2015). Therefore; emulsions are unstable due to the presence of interfacial forces that cause repulsion between the hydrophilic and hydrophobic molecules of the system (Fasinu et al., 2015). The stages in emulsification include droplet deformation, droplet disruption and interface stabilization with the aid of an emulsifier (Dickinson, 2017; McClements & Jafari, 2018). The effectiveness of emulsifiers in producing small droplets during homogenisation is determined by its physicochemical features (McClements, 2015). These features are its adsorption kinetics, surface-activity, stabilization, surface coverage and its ability to reduce interfacial tension (McClements, 2015). Successful homogenisation involves the use of emulsifiers that speedily adsorb to droplet surfaces as this facilitates a reduction in interfacial tension and prevents droplet aggregation. The emulsion forming ability of natural emulsifiers depends on how they can lower interfacial tensions, inhibit aggregation droplet and adsorb to surfaces (McClements, 2015).

2.3 Emulsion ultra-sonication

Food scientists have been faced with the challenge of formulating biologically nutritious semi-solid foods either as colloids, emulsions, gels or simple solutions for different classes of individuals (Krasulya et al., 2016; Leong et al., 2017a; Leong et al., 2017b; Dickinson, 2018). This challenge have been complicated because the biologically nutritious components tend to be immiscible with water (Krasulya et al., 2016; Dickinson, 2018). Consequently, new methods of delivery as emulsions apart from homogenisation have been on-going. Authors have proposed ultra-sonication which involves shearing the interface between oil and water to form stable droplets (Krasulya et al., 2016; Leong et al., 2017a; Leong, et al., 2017b; Dickinson, 2018). Ultrasonication is the science and technology of using acoustic wave-fields with vibrations in the range 18 kHz to 1 GHz (Guimarães et al., 2019; Madhu et al., 2019). Ultrasonication has been grouped into sonochemistry with frequency ranging from 18–100

kHz and intensities higher than 1W/m^2, and diagnostic ultrasound with frequencies higher than 500 MHz (Guimarães et al., 2019; Madhu et al., 2019). Acoustic cavitation depends on dissolved gas content, fluid viscosity, temperature of the emulsion, acoustic and oscillatory pressure (Krasulya et al., 2016; Leong et al., 2017a; Leong et al., 2017b).

Acoustic cavitation involves two key stages the formation of unstable unrefined bubbles by breaking-up the droplets in dispersed phase into the continuous phase and an extreme cavitation of the bubbles that results in breaking-up and homogenising the oil and water phases to formulate droplet with micro or nano sizes (Patil & Gogate, 2018; Modarres-Gheisari et al., 2019). Authors have reported the application of ultrasound cavitation in sunflower oil in water emulsions, and milk and juice nutraceuticals (Krasulya et al., 2016; Leong et al, 2017b; Patil & Gogate, 2018). Authors have reported that droplet formation and size which determines emulsion stability is affected by pH, ionic strength, and emulsifier concentration (Ozturk & McClements, 2016; Maphosa et al., 2017; Schmidt, Schütz, & Schuchmann, 2017). Ultra-sonication has being used to internalise bio-nutrients through encapsulation as it stabilises internalised components from degradation and provides a mode of delivering bio-nutrients efficiently (Leong et al., 2017a; Leong et al., 2017b).

2.4 Emulsion stability

Emulsion stability is the capacity of an emulsion to sustain its physicochemical properties during long periods of storage (McClements, 2015). In characterising emulsions; emulsion stability, texture interfacial properties and interactions are vital. Also, emulsion stability has been described as the preservation of the composition accomplished after the homogenisation of the two (or more) phases. Emulsions are thermodynamically unstable and tend to breakdown over time (McClements, 2015; Dickinson, 2017; McClements & Jafari, 2018). Solutions to thermodynamic instability, are emulsifiers and stabilisers, which are substances that can adsorb at the interfacial areas of emulsions (McClements, 2015; McClements & Jafari, 2018).

During storage, emulsion breakdown can arise due to certain processes which are influenced by phase inversion, the distribution of the oil droplets and the difference in density between the droplets and the medium, and the solubility of the dispersed droplet (Komaiko,. & McClements, 2016; Kumar, & Mandal, 2018). This processes determines Ostwald ripening, the stability of the liquid film between the droplets, which determines coalescence and the magnitude of the attractive versus repulsive forces, and flocculation (Tadros, 2013; Tadros, 2015). Instability of emulsions commonly occurs based on more than one phenomenon and can run concurrently. Emulsions need to retain their stability throughout its shelf-life; however, they may become unstable through creaming, flocculation, and coalescence (Ozturk &

McClements, 2016).

2.5 Mechanisms of emulsion breakdown during storage

Emulsion droplets are interfaced mainly by three kinds of interaction energies namely: Electrostatic repulsion, the van der Waals attractions of which London dispersion interactions are the most important and steric repulsion. The van der Waals forces of attraction are commonly accountable for the breakdown of an emulsion during storage (McClements, 2015). Emulsions become unstable due to flocculation, creaming or sedimentation, coalescence, and phase inversion. Figure.0.1 outlines different emulsion destabilisation mechanisms.

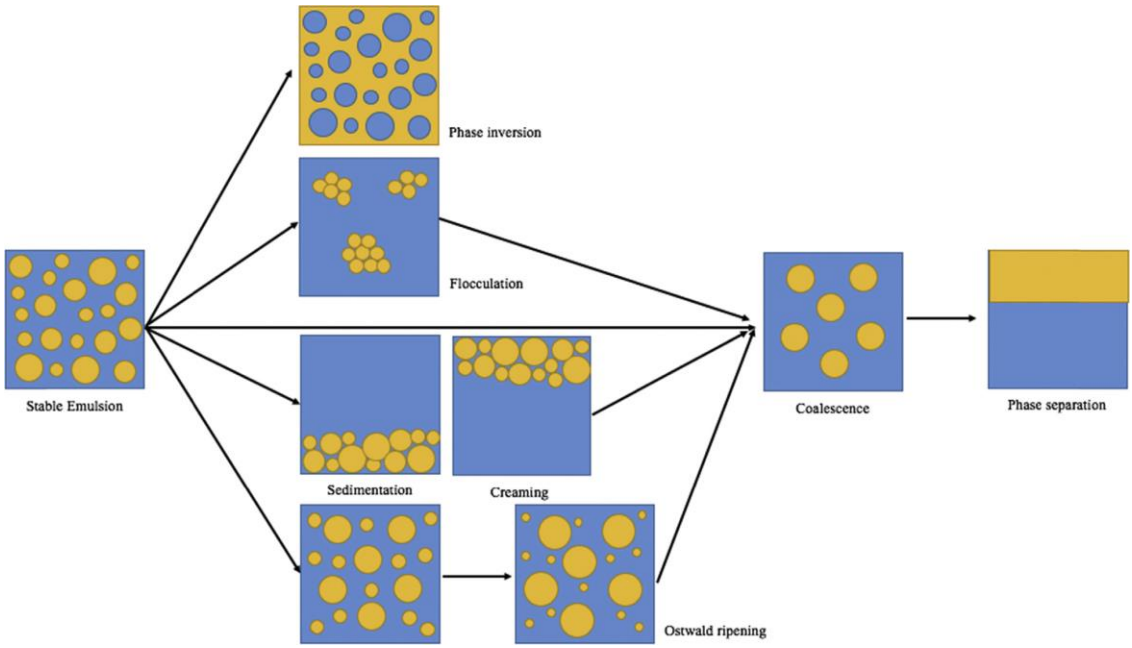

Figure.0.1: Pictorial image of emulsion breakdown mechanisms
Source: (Whitby & Wanless, 2016; Yamashita, Miyahara, & Sakamoto, 2017)

Flocculation occurs when two or more droplets in an emulsion aggregate without the interface stabilising layer rupturing (Whitby et al., 2016; Dickinson, 2017; McClements and Jafari, 2018). Flocculation depends on Brownian, centrifugal and gravitational forces which cause creaming or sedimentation (Karthik, Ezhilarasi, & Anandharamakrishnan, 2017; Gharehbeglou et al., 2019). An emulsion can undergo creaming or sedimentation due to the difference in density between the continuous or dispersed phases (Gupta et al., 2016). Sedimentation occurs when the droplet has a higher density than the fluid it is dispersed in while creaming arises when the density of the droplets is lower than that of the medium (Tadros, 2013; Stounbjerg et al., 2018). An emulsion can undergo coalescence when droplets irreversibly merge into each other to form a sole larger droplet (McClements, 2015; Jin et al., 2017). Due to the increase

in particle size the droplets of the emulsion rapidly cream or sediment and results in oiling off in beverages, a situation in which a layer of oil develops on top of the emulsion (Piorkowski & McClements, 2014, Karthik et al., 2017). This phenomenon called oiling off is observed as shiny layers of oil on top of unstable emulsions and the mechanism of coalescence involves; film drainage and film rupture (Piorkowski & McClements, 2014).

Ostwald ripening results from the solubility difference within small and large particles in an emulsion which allows large particles in an emulsion to grow larger at the expense of small particles (Gustafsson & Holmberg, 2017; Zhang & McClements, 2018). Ostwald ripening is common in oils which are highly water-soluble such as essential oils but less common in oils which are less water-soluble such as sunflower oils and fish oils (Karthik et al., 2017; Salvia-Trujillo et al., 2017) . Ostwald ripening has been controlled in emulsions by enhancing the Gibbs elasticity or by controlling interfacial tension (Powell, Damitz, & Chauhan, 2017; McClements & Jafari, 2018). Another mechanism of destabilisation is phase inversion which results from phase exchange whereby the continuous phase inverts into the diffused droplets while the disperse phase inverts into the droplets such as when a W/O emulsion reverts to an O/W emulsion or vice versa (Dickinson, 2017; Powell et al., 2017). Therefore, when inversion takes place in an emulsion, there is a reversal of the continuous and dispersed phases, this occurrence is exploited in nanoemulsions (McClements & Jafari, 2018). Phase inversion commonly occurs when the composition of an emulsion is changed and can be triggered by solvent types, amount and kind of emulsifying agent used, mechanical forces or the volume fraction of the disperse phase (McClements, 2015; McClements & Jafari, 2018). The goal of emulsification is to maintain the initial state attained after the homogenisation of two immiscible liquids (McClements, 2015; McClements & Jafari, 2018). In the food industry, emulsions that are kinetically stable for days, or weeks, months or even years require the incorporation of emulsifiers (McClements, 2015; Costa et al., 2017; McClements & Jafari, 2018).

As surface acting agents, emulsifiers must possess a good surface activity and the ability to form a condensed interfacial film (Dickinson, 2018). Various theories of emulsification have been proposed in order to explain the stabilising effects of emulsifiers. The surface tension theory explains emulsification as the lowering of the interfacial tension between the aqueous and the oily phase leading to a reduction in the repellant forces between the two liquids and a decrease in the attraction between the molecules of the same liquid (Kale & Deore, 2017). The oriented-wedge theory proposes the formation of a mono-molecular layer of the emulsifying agents which is curved around the droplets of the dispersed phase (Kale & Deore, 2017; Dickinson, 2018). The interfacial film theory explains emulsification as the prevention of contact and coalescence of dispersed phase due to the formation of a film of emulsifying agents which stabilise the emulsion (Kale & Deore, 2017). In addition to the ability to hold

together the dispersed phase in the continuous phase, an ideal emulsifier must be a stable material or compound, be non-toxic, must not inflict unacceptable color, taste or odor on the emulsion system, and must be compatible with other components of the preparation (McClements, 2015; McClements & Jafari, 2018).

2.6 Techniques used to investigate emulsion stability

In characterising emulsions the evaluation of emulsion particle size is vital as it affects emulsion qualities such as appearance, creaming velocity, flavor, texture, and rheology (Chung & McClements, 2014; Hu et al., 2017). The common techniques used to investigate emulsion stability are:

2.6.1 Emulsion particle size

One of the common ways of predicting the stability of an emulsion to gravitational separation is the use of mathematical model described by Stokes' Law (McClements, 2015). The Stokes' law relates emulsion stability to the particle size of bi-phasic systems of granular meta-stable dispersions that comprises of two non-miscible liquids with diverse densities (Miyagawa et al., 2015; Querol, Barreneche, & Cabeza, 2017). According to this law, the rate (v) at which an isolated rigid spherical droplet particles creams/sediments in an ideal liquid environment is directly proportional to the particle size (measured as particle radius r) and the density difference between the particle and the medium (ρ2 − ρ1); and inversely proportional to the viscosity (η_1) of the medium (McClements, 2015) as shown in Equation 2.1:

$$\boldsymbol{V = \frac{2gr^2(\rho_2 - \rho_2)}{9\eta_1}} \qquad \textbf{Equation 0.1}$$

Where g is the acceleration due to gravity.

Hence the rate at which discrete droplet particles cream/sediments (V) can be controlled as negative V is ascribed to sedimentation while positive V is ascribed to creaming. Therefore, for homogenous emulsions, emulsion stability can be attained when shear viscosity is increased; and density difference between the dispersed and continuous phases is small and the droplet size is decreased (McClements, 2015; Hu et al., 2017). However, the Stokes law is limited in non-homogenous dispersions as droplets are poly-diverse (Tadros, 2015). Other factors that influence non-homogenous dispersion include; droplet to droplet interface, interfacial thickness, droplet charge and concentration, and non-Newtonian fluid behaviour of the continuous face (Tadros, 2015). Several authors have investigated emulsion particle size and reported it as the volume mean diameter (Hu et al., 2015; Santos, Carignano, & Campanella, 2017), equivalent volume mean diameter (McClements, 2015; McClements &

Jafari, 2018), mean diameter number (Dapčević Hadnađev et al., 2013) and Sauter mean diameter (Dokić, Krstonošić, & Nikolić, 2012; Gordiychuk et al., 2016; Martinez et al., 2019). The particle or droplet size has a considerable influence on emulsion creaming stability (Maphosa et al., 2017; Nieto de Castro et al., 2017). An emulsion can attain stability when particle size is reduced, the density difference between the dispersed and continuous phases is low, or when the viscosity of the continuous phase is high. However, charges, droplet concentration, interfacial forces between the droplets, interfacial thickness, non-Newtonian fluid behaviour of the continuous phase and non-homogeneity of the droplets limit the Stokes law (Tadros., 2015).

2.6.2 Optical scrutiny

Various authors have identified optical scrutiny as a cheap, easy, simple and quick technique to investigate emulsion stability affects as it affects' the products' appearance, and it is directly observed by the naked human eye (McClements, 2015; Hu et al., 2017). Many researchers have visually observed emulsions and quantified emulsion stability using the creaming index method. For instance, Zhang et al. (2020) studied how oil phase volume fraction, pH and particle size affected the morphology, rheological, and stability of O/W emulsions stabilised with cellulose and soy protein stabilised by concentrated flaxseed protein stored for seven days in tightly sealed glass test tubes The total height of the emulsion (HE) and the height of the serum (HS) were measured and extent of creaming (CI) was determined using Equation 2.2 (Zhang et al., 2020).

$$\boldsymbol{CI = 100[HS/HE]} \qquad \textbf{Equation 0.2}$$

Optical scrutiny investigations are best performed through agitation tests using transparent tubes where the phase separation of the emulsion is assessed with the human eye (McClements, 2015; Hu et al., 2017). Phase separation of non-miscible emulsions can occur through creaming or sedimentation (Tadros., 2013; McClements, 2015; Hu et al., 2017). The extent of phase separation can be determined as the creaming index (CI) according to Equation 2.3. (Zhang et al., 2020).

$$\boldsymbol{CI = \frac{Hc}{He} \times 100} \qquad \textbf{Equation 0.3}$$

Where *Hc* is the height of the creamed layer and *He* the total height of the emulsion. The Creaming index has been recommended as a test of emulsion stability by many researchers as it is a good test of stress during long-term stability (McClements, 2015; McClements & Jafari, 2018). The creaming index is used to identify the extent of droplet aggregation in an emulsion as faster creaming of droplets results in larger particle size. (McClements, 2015;

McClements & Jafari, 2018). Data obtained from creaming tests can be used in assessing emulsion instability as information on the factors that affect the stability of the emulsion can be deciphered from creaming tests (McClements, 2015; Dickinson, 2018; McClements & Jafari, 2018).

Although the extent of phase separation by observation of thickness of creaming/sedimentation layers with naked eyes has been reported, optical scrutiny though convenient, is not appropriate in studying other mechanisms of emulsion breakdown during storage such as flocculation, coalescence, and Ostwald ripening (McClements, 2015; Hu et al., 2017). Researchers have noted that thickness in the creaming layer is only observed when the extent of phase separation is substantial. Therefore accurate investigations of emulsion stability have been performed by analyzing data from backscattering flux percentage, electron microscopy, and Zeta potential (McClements, 2015; Hu et al., 2017; McClements & Jafari, 2018).

2.6.3 Microscopic scrutiny

Microscopic scrutiny using devices such as atomic force, electron, optical, electron, and confocal fluorescent microscopy has been used in investigating mechanisms of emulsion breakdown for droplets that cannot be seen through optical scrutiny (Hu et al., 2017; Drapala et al., 2018*)*. Imaging studies have been used to investigate droplets distribution and sizes and also investigate factors that impact emulsion stability (Fudge & Schorno, 2016; Drapala et al., 2018). Emulsion stability has been described by observing droplet flocculation, coalescence or Ostwald ripening by using different modes of microscopy (Hu et al., 2017; Drapala et al., 2018*)*. Researchers have noted drawbacks such as tedious dilution and slide-spreading for microscopy samples; time-consuming preparations; subjective results which could be difficult to standardize; and the need to analyze a single sample slide from different angles to have reliable data (Hu et al., 2017, Drapala et al., 2018). Based on these drawbacks, authors combine data from other measurements such as backscattering flux, particle size and Zeta potential with the imaging studies to correctly analyze unstable emulsion mechanisms (Maphosa et al., 2017; Hu et al., 2017).

2.6.4 Zeta potential

The Zeta-potential is the potential difference between the neutral electrical area of the solution and the surface of the tightly bound layer of ions on the particle surface and it estimates the net charge on the particle (Bhattacharjee, 2016; Moussa et al., 2017). Zeta-potential is contingent upon the actual charge of the particle, nature, and composition of the medium surrounding the emulsion and the interfacial adsorbed layer (McClements, 2015;

Bhattacharjee, 2016; Moussa et al., 2017). It is influenced by pH, electrostatic attractive/repulsive forces and droplet charges of excited species in the dispersed phase (McClements, 2015; Hu et al., 2017; Moussa et al., 2017). Zeta-potential is influenced by droplet concentration, the electrical charge of the ions in the droplet and pH of the aqueous dispersions (Bhattacharjee, 2016; Hu et al., 2017). Hence the zeta potential of the particle strongly influences emulsion stability and analytical measurements have been carried out using electroacoustic or electrophoretic light scattering: techniques (McClements, 2015; Bhattacharjee, 2016; Hu et al., 2017).

2.6.5 Rapid stability

Several authors have reported that the Turbiscan Lab Expert (Formulation, France) can give accurate, rapid and reproducible measure of emulsion stability (Li et al., 2018; Xu et al., 2019). Hence this rapid technique has been used to predict long-term emulsion stability and investigate the destabilisation profiles of emulsions. This involves measurements made over relatively short times to extrapolate long-term effects. A number of authors have reported that analysis of Turbiscan results can characterise stability without emulsion dilution, provide data on particle migration, variations in particle size, optimising emulsion formulations, shelf life and quality control (Maphosa et al., 2017; Li et al., 2018; Xu et al., 2019). The Turbiscan MA 2000 operates on the principle of multiple light scattering Figure 2.2 and the Turbiscan MA 2000 is used in determining the instability mechanisms in an emulsion (Lu et al., 2016; Maphosa et al., 2017; Xu et al., 2019) The procedure involves using optical sensors to measure the changes in mean path length of photons in the dispersion as a function of backscattered and transmitted (T) light fluxes (Liu et al., 2014; Maphosa et al., 2017; Li et al., 2018; Xu et al., 2019). Figure 0.2 shows the Turbiscan MA 2000 measurement principle while Figure 0.3 shows the possible backscattering % profiles of an emulsion.

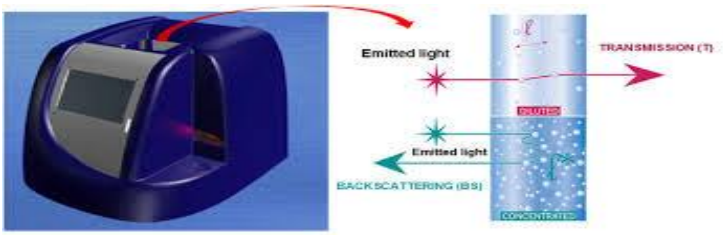

Figure 0.2: Turbiscan MA 2000 measurement principle
Source: (Liu et al., 2011; Liu et al., 2014)

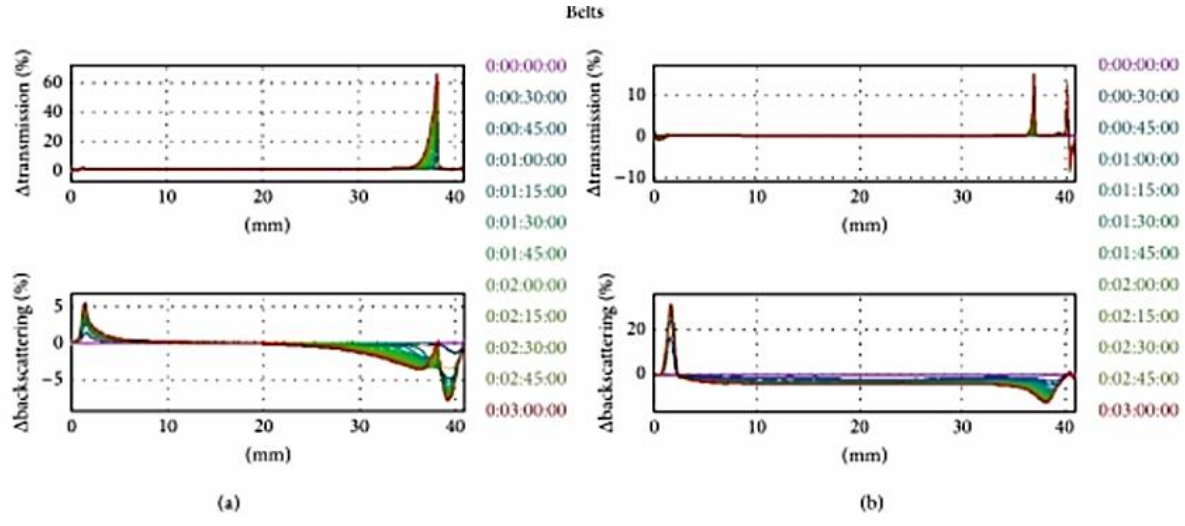

Figure 0.3: Backscattering profiles of Turbiscan.
Source: (Liu et al., 2011; Liu et al., 2014)

2.7 Rheology

Rheology has been identified as a science that deals with the study of deformation and flow flow of matter in emulsions on the application of stress (Guzmán et al., 2017; Zhu et al., 2019). A material such as an emulsion would undergo structural changes known as a strain when force is applied (Foudazi et al., 2015; Berton-Carabin et al., 2018; Kwok et al 2019; Tang ,2020). The stress of a material/emulsion is defined as the force per unit/drop area for materials/emulsions respectively (Rao, & Wong, 2018; Håkansson, 2019)). Authors have reported that for certain materials to undergo flow the stress needs to exceed a specific value known as the yield stress (Bonn et al., 2017; Malkin, Kulichikhin, & Ilyin, 2017; Townsend et al., 2019).

Hence, a materials' internal structure would respond to applied force based on its physical state and the response would show its rheological properties (Geremias-Andrade et al., 2016; Adeyi et al., 2018; Khayat et al., 2019; Liu et al., 2019). Data obtained from rheological parameters can be fit into mathematical equations known as flow models which explain relationships between the deformation and the applied force (Dickinson, 2012; Rao, 2014; Hamza, 2016). Hence the degree of fit of the data on the flow models can be used to describe flow characteristics and predict the quality of the material. (Rao, 2014; Bhardwaj et al., 2019; Zhu et al., 2019). The rheological response of ideal materials to the applied force is governed by Hooke's law and Newton's law of elasticity which depends on a materials' flow characteristics (Fecarotti et al., 2012; Rao, & Wong, 2018).

Authors have used sweep tests to investigate the responses of a specific value for various rheological parameters over a specific strain/stress range. (Jamshidi et al., 2015; Alghooneh

et al., 2017; Kolawole et al, 2020). Rheological sweep tests are divided into oscillatory and rotational measurements and are executed using either small or large deformations (Läuger & Stettin, 2016; Barzic & Ioan, 2016).

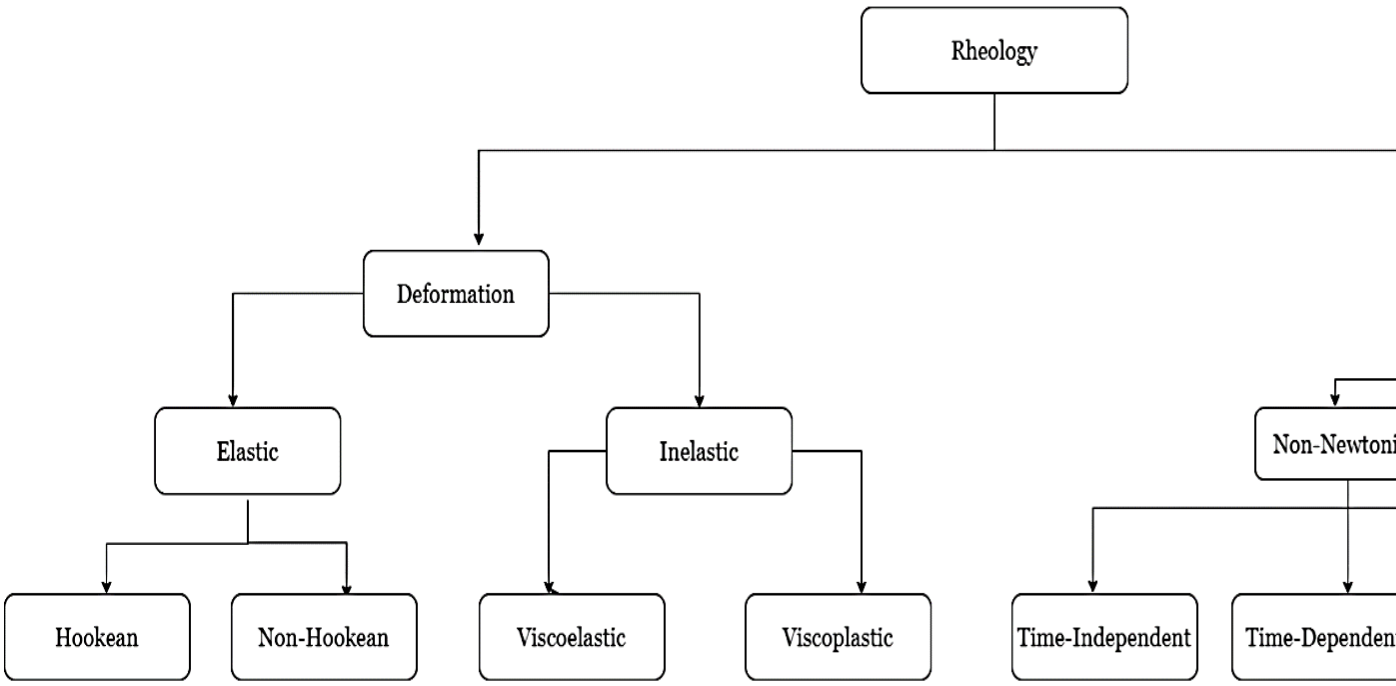

Figure 0.4: Schematic divisions of rheology

gives the schematic divisions of rheology.

Rotational tests investigate a material's rheological behaviour at large deformation and correspond to brushing, pumping, and stirring operations (Vignali et al., 2019). Oscillatory tests at small deformations investigate a material's rheological behaviour and provide information on the structural state of a material at rest (Meerts et al., 2017). Small amplitude oscillatory tests correspond to long term elasticity and storage stability (Yuan et al., 2017). There are two types of rotational sweep tests controlled shear rate and controlled shear stress but the tests can be ramped or conducted in a stepwise manner (Tadros, 2011; Stettin, 2016; Whaley et al., 2019). Rotational and oscillatory measurements can be conducted via steady-state or non-steady state settings (Blau, 2015). Authors have conducted steady-state rheological measurements to characterize time-independent properties of materials (Morales-Contreras et al., 2018; Jiao et al., 2019). Shear stress and shear rate sweep tests under steady-state conditions is appropriate for very low to medium viscosity fluids while dynamic stress/strain sweep is appropriate for high viscosities (Tadros, 2011). Reliable data can be obtained from samples that are allowed to equilibrate, however, the physical instability of food systems to attain equilibrium is a challenge (Aditya et al., 2017). This occurs because colloidal fluids and food materials are heterogeneous and structurally disordered therefore rheological investigations of this materials are complex (Fischer & Windhab, 2011; Rao, 2014). Also,

because of the structurally complex nature of these materials, their modelling has posed a challenge hence, rheological investigations of these complex material have been conducted under steady-state-conditions (Ivanova & Kotsilkova, 2018; Delgado et al., 2019).

.

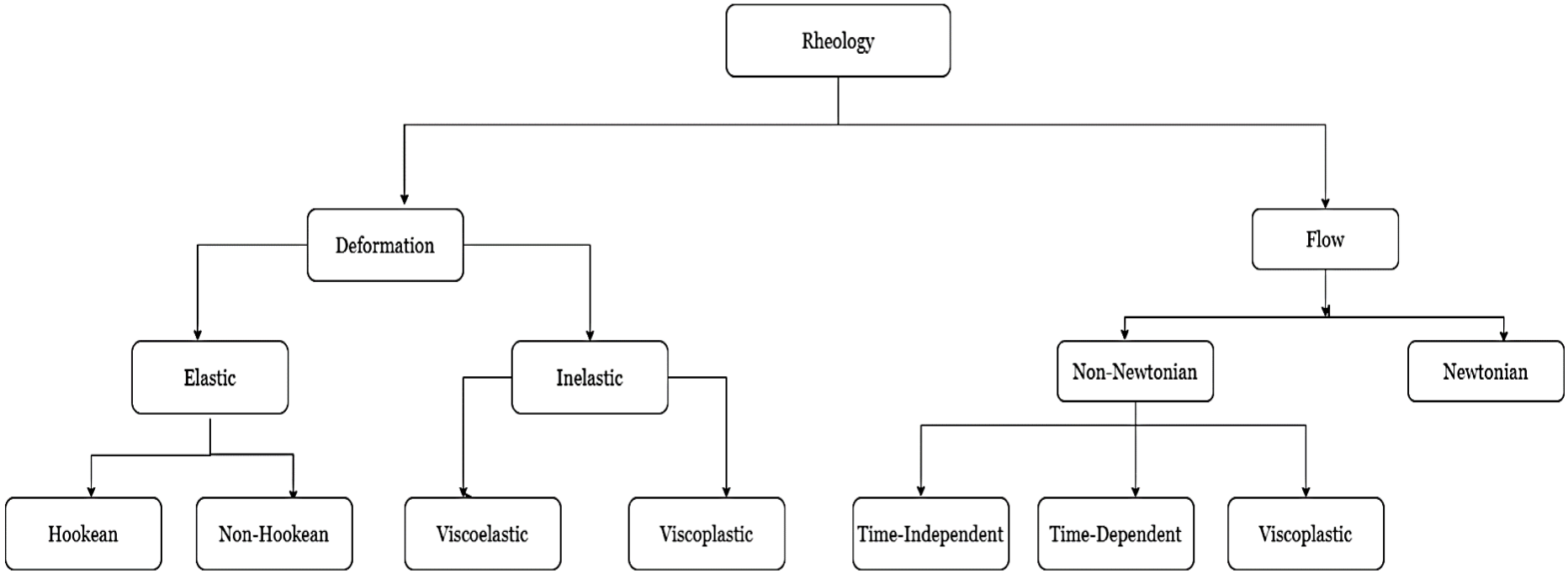

Figure 0.4: Schematic divisions of rheology

Source: (Malkin and Isayev, 2017; Kubo et al., 2019)

Error! Reference source not found. illustrates the rheological tests that are used to nvestigate the properties of materials. In food rheology, investigations are essential to design industrial machines, define the limits of packaging and storage plans, determine engineering factors, unit operations, quality control, and product development (Rao, 2014; Aguilera, 2018).In food emulsion systems, the measurement of viscosity which is the resistance of the material to deformation during flow or flow as a result of the applied stress on the food is vital (Zhu et al., 2019). Depending on flow properties a material can be classified as Newtonian or non-Newtonian. A Newtonian fluid is one with viscosity remains constant, no matter the amount of shear applied at at a constant temperature (Malkin & Isayev, 2017; Dickinson, 2018). Consequently, the relationship between the viscosity and shear stress of such fluids remains linearExamples of materials that exhibit Newtonian behaviour are air, water, chloroform, and glycerol. A non-Newtonian, material is one in which its viscosity depends on shear rate, hence a non-linear relationship exists between viscosity and shear stress (Malkin & Isayev, 2017; Dickinson, 2018). Examples include several hydrocolloids and polysaccharides which have been used as emulsifiers (McClements, 2015; Maphosa et al., 2017; McClements & Jafari, 2018).

The flow and viscoelastic characterisation of emulsions provide the necessary rheological information on both its viscous and elastic properties (Javidi et al., 2019). Several authors have related the long term physical stability with short term rheological measurements in the first few weeks of storage (Böni et al., 2016a; Böni et al., 2016b; Maphosa et al., 2017; Marín et al., 2018). For instance, Maphosa et al. (2017) investigated the stabilising effect of soluble fibers (SF) obtained from four varieties of Bambara groundnut (BGN) on orange oil emulsion. These authors' analysed results obtained from the chemical composition with the characteristics of the orange oil emulsions stabilised with SF BGN. They observed that BGN variants with higher arabinose, galactose, and xylose content were more stable than variants with lower arabinose, galactose, and xylose content as these sugars increased the viscosity of the SF BGN stabilised emulsions (Maphosa et al., 2017). The authors reported that SF BGN stabilised emulsions with variants that had higher viscosity had a higher consistency coefficient (Maphosa et al., 2017). Analysis of the hysteresis loop area of SF BGN stabilised emulsions stabilised with this high viscosity variant and a higher consistency coefficient recorded the lowest structural damage with respect to time and applied shear (Maphosa et al., 2017). Hence Maphosa et al. (2017) concluded that SD BGN fibers could improve the stability of orange oil emulsions. In the same vein, Böcker et al. (2016) investigated the effect of fibres on the cohesive property of hagfish stabilised emulsions. The authors investigated the flow behaviour of hagfish slime dissolved in Milli-Q water and solutions made with biopolymers to re-enforce the structural cohesive network of hagfish slime (Böcker et al., 2016). The

rheological tests involving amplitude sweep at an angular frequency of ω = 1 rad/s and specific strain amplitude of γ =1%, shear rates from 0.01 to 100 s^{-1} and back from 100 to 0.01 s^{-1} were

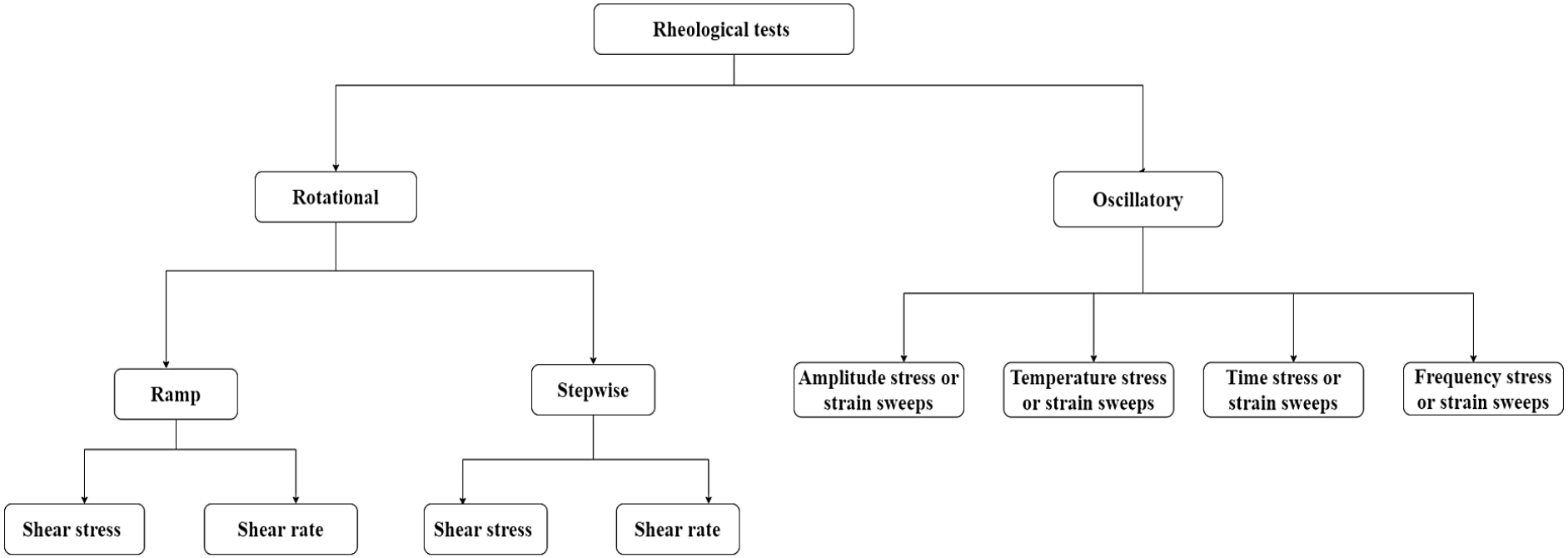

Figure 0.5: Rheological tests used to investigate the properties of materials

Source: (Stettin, 2016, Barzic & Ioan, 2016)

used to investigate the shear viscosity and obtain the flow parameter at 10 °C (Böcker et al., 2016; Böni et al., 2017; Böni et al., 2018). The authors observed that Hagfish slime had a viscoelastic network with G′ almost equal to G″, and an ordered linear viscoelastic behaviour at strains of about 100% even with slime concentrations of 0.01 w/w% in Milli-Q water (Böcker et al., 2016; Böni et al., 2017; Böni et al., 2018). Although the authors observed a hysteresis when hagfish slime concentrations were sheared the slime lost its viscosity and could not maintain its original interconnected network formation and reported that hagfish slime was not stable to shear (Böcker et al., 2016; Böni et al., 2017; Böni et al., 2018) The authors improved the mechanical stability of the slime with biopolymers such as chitosan ,starch and κ-carrageenan. Improvements with 1 w/w% aqueous chitosan solution led to aggregation, precipitation, and structural collapse of hagfish slime. Improvements with 1 w/w% of the starch solution formed an opaque and watery phase formed from hagfish slime and starch (Böcker et al., 2016; Böni et al., 2017; Böni et al., 2018). Elements of stabilised starch-hagfish slime complex did not show aggregation but were formed from low concentrations of hagfish slime and a watery phase (Böcker et al., 2016; Böni et al., 2017; Böni et al., 2018). The authors compared the amplitude sweeps of the stabilised starch-hagfish slime complex and native starch and observed a two-decade increase in G' and G" moduli (Böcker et al., 2016). Native starch was distinctly viscous while stabilised starch-hagfish slime complex had a clear G′ modulus even at strains within the range of 1-1000% (Böcker et al., 2016). Stabilised starch-hagfish slime complex was Shear-thinning, had a higher shear viscosity than the native starch solution, did not have a hysteresis loop compared with hagfish slime, and had an increased mechanically stabilised structure (Böcker et al., 2016). They reported that a homogeneous emulsion was formed when the κ-carrageenan solution was mixed with hagfish slime (Böcker et al., 2016). Although, the κ-carrageenan solution has a low viscosity and is entirely viscous the complex it forms with hagfish slime is viscoelastic and has a distinct G′ modulus. The addition of hagfish slime significantly increased both G' and G" moduli and led to a higher G' modulus and an ordered linear viscoelastic behaviour at strains of 100% (Böcker et al., 2016). Similarly, the authors reported that Shear-thinning characteristics were observed on κ-carrageenan biopolymer solution and hagfish slime−κ-carrageenan complex and higher shear viscosity as observed in stabilised starch-hagfish slime complex. The authors concluded that the complex formed with 1% (w/w) κ-carrageenan had improved mechanical stability and did not show network structural collapses like hagfish slime and Milli-Q mixtures. Authors have investigated the effect of fiber obtained from soy protein isolate and soy milk on hagfish slime (Böcker et al., 2016; Böni et al., 2016b). The rheological tests involving amplitude sweep at an angular frequency of ω

= 1 rad/s and specific strain amplitude of γ =1% were used to determine the Linear viscosity range. Viscosity was measured at shear rates ranging from 0.1 to 100 s^{-1} at a temperature of 20°C (Böni et al., 2016b). The authors reported that when subjected to frequency sweeps hagfish slime was an uncommonly mushy and delicate elastic substance, with a forcefully increasing G" at higher frequencies as a result of effects from inertia and a disappearing elastic modulus G' at ≥ frequencies of 3 rad/s (Böni et al., 2016b). Examples of materials that exhibit Newtonian behaviour are air, water, chloroform, and glycerol. A non-Newtonian, material is one in which its viscosity depends on shear rate, hence a non-linear relationship exists between viscosity and shear stress (Malkin & Isayev, 2017; Dickinson, 2018). Examples include several hydrocolloids and polysaccharides which have been used as emulsifiers (McClements, 2015; Maphosa et al., 2017; McClements & Jafari, 2018).The flow and viscoelastic characterisation of emulsions provide the necessary rheological information on both its viscous and elastic properties (Javidi et al.,2019). Several authors have related the long term physical stability with short term rheological measurements in the first few weeks of storage (Böni et al., 2016a, Böni et al., 2016b, Maphosa et al., 2017, Marín et al., 2018). For instance, Maphosa et al. (2017) investigated the stabilising effect of soluble fibers (SF) obtained from four varieties of Bambara groundnut (BGN) on orange oil emulsion. These authors' analysed results obtained from the chemical composition with the characteristics of the orange oil emulsions stabilised with SF BGN. They observed that BGN variants with higher arabinose, galactose, and xylose content were more stable than variants with lower arabinose, galactose, and xylose content as these sugars increased the viscosity of the SF BGN stabilised emulsions (Maphosa et al., 2017). The authors reported that SF BGN stabilised emulsions with variants that had higher viscosity had a higher consistency coefficient (Maphosa et al., 2017). Analysis of the hysteresis loop area of SF BGN stabilised emulsions stabilised with this high viscosity variant and a higher consistency coefficient recorded the lowest structural damage with respect to time and applied shear (Maphosa et al., 2017). Hence Maphosa et al. (2017) concluded that SD BGN fibers could improve the stability of orange oil emulsions. In the same vein, Böcker et al. (2016) investigated the effect of fibres on the cohesive property of hagfish stabilised emulsions. The authors investigated the flow behaviour of hagfish slime dissolved in Milli-Q water and solutions made with biopolymers to re-enforce the structural cohesive network of hagfish slime (Böcker et al., 2016). The rheological tests involving amplitude sweep at an angular frequency of ω = 1 rad/s and specific strain amplitude of γ =1%, shear rates from 0.01 to 100 s^{-1} and back from 100 to 0.01 s^{-1} were used to investigate the shear viscosity and obtain the flow parameter at 10 °C (Böcker et al., 2016; Böni et al., 2017; Böni et al., 2018). The authors observed that Hagfish slime had a viscoelastic network with G′ almost equal to G″, and an ordered

linear viscoelastic behaviour at strains of about 100% even with slime concentrations of 0.01 w/w% in Milli-Q water (Böcker et al., 2016; Böni et al., 2017; Böni et al., 2018). Although the authors observed a hysteresis when hagfish slime concentrations were sheared the slime lost its viscosity and could not maintain its original interconnected network formation and reported that hagfish slime was not stable to shear (Böcker et al., 2016; Böni et al., 2017; Böni et al., 2018). The authors improved the mechanical stability of the slime with biopolymers such as chitosan, starch, and κ-carrageenan. Improvements with 1 w/w% aqueous chitosan solution led to aggregation, precipitation, and structural collapse of hagfish slime. Improvements with 1 w/w% of the starch solution formed an opaque and watery phase formed from hagfish slime and starch (Böcker et al., 2016; Böni et al., 2017; Böni et al., 2018). Elements of stabilised starch-hagfish slime complex did not show aggregation but were formed from low concentrations of hagfish slime and a watery phase (Böcker et al., 2016; Böni et al., 2017; Böni et al., 2018). The authors compared the amplitude sweeps of the stabilised starch-hagfish slime complex and native starch and observed a two-decade increase in G' and G" moduli (Böcker et al., 2016). Native starch was distinctly viscous while stabilised starch-hagfish slime complex had a clear G′ modulus even at strains within the range of 1-1000% (Böcker et al., 2016). Stabilised starch-hagfish slime complex was Shear-thinning, had a higher shear viscosity than the native starch solution, did not have a hysteresis loop compared with hagfish slime, and had an increased mechanically stabilised structure (Böcker et al., 2016). They reported that a homogeneous emulsion was formed when the κ-carrageenan solution was mixed with hagfish slime (Böcker et al., 2016). Although, the κ-carrageenan solution has a low viscosity and is entirely viscous the complex it forms with hagfish slime is viscoelastic and has a distinct G′ modulus. The addition of hagfish slime significantly increased both G' and G" moduli and led to a higher G' modulus and an ordered linear viscoelastic behaviour at strains of 100% (Böcker et al., 2016). Similarly, the authors reported that Shear-thinning characteristics were observed on κ-carrageenan biopolymer solution and hagfish slime−κ-carrageenan complex and higher shear viscosity as observed in stabilised starch-hagfish slime complex. The authors concluded that the complex formed with 1% (w/w) κ-carrageenan had improved mechanical stability and did not show network structural collapses like hagfish slime and Milli-Q mixtures. Authors have investigated the effect of fiber obtained from soy protein isolate and soy milk on hagfish slime (Böcker et al., 2016; Böni et al., 2016b). The rheological tests involving amplitude sweep at an angular frequency of ω = 1 rad/s and specific strain amplitude of γ =1% were used to determine the Linear viscosity range. Viscosity was measured at shear rates ranging from 0.1 to 100 s^{-1} at a temperature of 20°C (Böni et al., 2016b). The authors reported that when subjected to frequency sweeps hagfish slime was an uncommonly mushy and delicate elastic substance,

with a forcefully increasing G" at higher frequencies as a result of effects from inertia and a disappearing elastic modulus G' at ≥ frequencies of 3 rad/s (Böni et al., 2016b).

However, the moduli of the complex formed from slime and soy protein isolate (SPI) were nearly independent of frequency sweep and about three dimensions higher than that of hagfish slime (Böni et al., 2017; Böni et al., 2018). The authors also reported lower strain values for amplitude tests for hagfish slime and the complex formed from slime and SPI (Böni et al., 2016b). The authors observed a low G' and high G" in hagfish slime but observed both low G' and G" in the complex formed from slime and SPI which is evident in soft glassy materials (Böni et al., 2016b). Hence the authors stated that the microstructure of the complex formed from slime and SPI was modified as a result of the gel-like nature of hagfish slime (Böni et al., 2016b). In the same vein, Felix et al. (2017) examined the viscoelasticity of emulsions derived from animal and vegetable oils emulsified with crayfish protein concentrate and xanthan gum stabilisers at pH range 3, 5 and, 8. The authors reported that fibers in Xanthan gum enhanced the viscoelasticity of the crayfish–XG stabilised emulsions key and resulted in the formation of a cohesive gel-like network (Felix et al., 2017).

2.8 Flow behaviour of fluids

Fluid materials can be grouped rheologically according to their flow behaviour. Fluids are ideal if the relationship between shear rate and shear stress is linear and the proportionality constant is referred to as viscosity. Viscosity is the resistance the fluid shows under shear. When a material is deformed continuously under shear stress it displays flow behaviour (Yang & Pan, 2017; Qian & Kawashima, 2018; Jia et al 2019). A flow curve characterises the flow behaviour for a material and is expressed by the relationship between stress and strain (Ducloué et al., 2017; Zheng, 2019). Flow behaviour is categorised as either Newtonian or non-Newtonian (Sharma et al., 2016; Malkin & Isayev, 2017). Ideal fluids are referred to as Newtonian fluids because they obey Newton's law. Examples are air, milk, water, oil, clarified juices, and juice serum. Newtonian fluids show a linear proportionality between the stress and strain rate with a viscosity which remains constant (Mohammadi et al., 2015). Conversely, because the structural arrangement of almost all fluid foods changes when subject to applied forces they do not obey Newton's law they are referred to as non-Newtonian fluids (Figure 2.5). Non-Newtonian fluids show a non-linear proportionality between the stress and strain rate with varying viscosity. Non-Newtonian fluids show different flow behaviour and are categorised as time-independent, time-dependent, or viscoelastic (Kubo et al., 2019; Souza Mendes de & Thompson 2019). Four divergent behaviours

occur in time-independent non-Newtonian fluids they are: Bingham, dilatant, Herschel–Bulkley, and pseudoplastic (Kubo et al., 2019; Ionescu et al., 2020).

Figure: 0.6 shows the schematic grouping of fluids based on their shear stress/shear rate relationship. The viscosity of non-Newtonian fluids is not a constant property in relation to the shear rate hence it is referred to as apparent viscosity. The apparent viscosity of a pseudoplastic fluid decreases as the shear rate is increased (Kubo et al., 2019; Ionescu et al., 2020). This occurs because the particles of the fluid align with the flow under shear examples are ketchup, mayonnaise, mustard, and fruit purees (Kubo et al., 2019; Ionescu et al., 2020). However, the apparent viscosity of dilatant fluids increases as the shear rate is increased. The apparent viscosity of a dilatant fluids increases because the suspended particles of the fluid collide under shear and increases its resistance to flow examples are crystallized honey, suspensions of sand in water and concentrated suspensions of starch in water (Kubo et al., 2019; Ionescu et al., 2020).

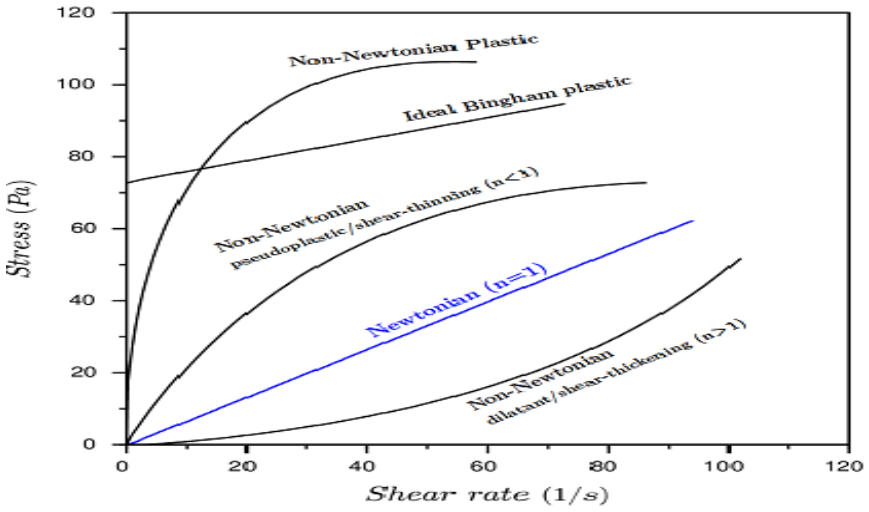

Figure: 0.6: Schematic grouping of fluids based on their shear stress/shear rate relationship. Source: (Whaley et al., 2019)

2.8.1 Steady flow characterisation of emulsions

Steady flow curves are used to show the rheological behaviour of fluids and this information is very useful in various industrial applications (Vadodaria et al., 2018; Kubo et al., 2019). It is used to describe product flow behaviour and is applied to machinery design and the design of unit operations such as heat transfer processes, mixing, and fluid moving (Kubo et al., 2019). The properties of fluids under steady-shear over wide ranges of shear rates have been described using several flow models. Flow models are mathematical equations that describe rheological data, for

instance, shear rate versus shear stress diagrams can be used as appropriate and succinct methods of depicting data obtained from rheological measurements (Rao, 2014). Fundamental flow models describe the simple flow behaviour of fluids. They are well suited to studying materials over a small shear range or where only a simple relationship is required.

In time-independent fluids the strain rate of the material at a specific point depends on the stress at the same point. When time-independent fluids are sheared they exhibit pseudoplastic or dilatant properties. Pseudoplastic fluids exhibit a shear-thinning flow behaviour i.e. an increase in shear rate results in decrease in viscosity (Anvari et al., 2016; Kelimu et al., 2017). Dilatant fluids exhibit a shear-thickening flow behaviour characterised by an increase in viscosity as the shear rate increases (Comtet et al., 2017; Gürgen, Kuşhan, & Li, 2017). Shear-thinning behaviour is common with ketchup, paints, slime, and syrups while shear-thickening flow behaviour is common with corn starch (Gürgen et al., 2017). The time-independent behaviour of food systems have been determined through rheological models such as Power Law, Hershel Bulkley, Casson, and Bingham plastic respectively.

The Power law model or Ostwald de waele is expressed by Equation 2.4 and the Herschel−Buckley model which is used when yield stress is taken into consideration can be expressed by Equation 2.5; (Vadodaria et al., 2018; Kubo et al., 2019; Hentati et al., 2020).

$$\boldsymbol{\tau} = \mathrm{K}\dot{\mathrm{Y}}^{\boldsymbol{\eta}} \qquad \textbf{Equation 0.4}$$

$$\boldsymbol{\tau} = \boldsymbol{\tau}_{\mathbf{0}} + \mathrm{K}\dot{\mathrm{Y}}^{\boldsymbol{\eta}} \qquad \textbf{Equation 0.5}$$

Where τ shear stress (Pa) is, τ_0 is yield stress (Pa), $\dot{\mathrm{Y}}$ is shear rate (s^{-1}), K is consistency coefficient (Pa s^{η}) and η is flow behaviour index (where η = 1 represents Newtonian behaviour, η > 1 (shear-thickening) dilatant and η < 1 (Shear-thinning) pseudoplastic (Wang et al., 2016; Vadodaria et al., 2018; Kubo et al., 2019; Hentati et al., 2020).

Also, other models like the Bingham and Casson, (Equations 2.6 and Equation 2.7), have used to characterise food-grade emulsions (Vadodaria et al., 2018; Kubo et al., 2019; Hentati et al., 2020).

$$\boldsymbol{\tau} = \boldsymbol{\tau}_0^B + \eta^B \dot{\mathrm{Y}} \qquad \textbf{Equation 0.6}$$

$$\boldsymbol{\tau}^{0.5} = \boldsymbol{\tau}(_0^C)^{0.5} + (\eta^C)^{0.5}\dot{Y}^{0.5} \qquad \textbf{Equation 0.7}$$

Where $\boldsymbol{\tau}$ is the shear stress, the $\boldsymbol{\tau}_0^B$ is the Bingham yield stress, the $\dot{\mathrm{Y}}$ is the shear rate (s^{-1}), η^B is the Bingham plastic viscosity (Pa.s), η^C is the Casson plastic viscosity (Pa.s),and $(\boldsymbol{\tau}_0^C)^{0.5}$ is

Casson yield and $\dot{Y}^{0.5}$ is the Casson shear rate (Vadodaria et al., 2018; Kubo et al., 2019; Hentati et al., 2020).

For time-dependent fluids, the time duration of shear and the applied shear amount are considered in expressing the relationship between apparent viscosity, and shear stress and the relationship is described by thixotropic and rheopectic behaviour (Kubo et al., 2019). When the effect of rheological parameters is examined with time duration of shear, relationships between structure and flow in food emulsions can be determined. Time-dependent rheological properties are related to changes in the internal structure and the equilibrium within the structure of a fluid as it is deformed when sheared and structure reorganization due to particle attractive forces. Thixotropic behaviour is observed when a fluids' viscosity decreases with the time duration of shear (Mortazavi-Manesh & Shaw, 2014; Souza Mendes de & Thompson, 2019). Thixotropy relates to breakdown of structure when the particles of the fluid interacts under shear. Thixotropic behaviour has been observed in colloids, gels and yogurt (Capitani et al., 2015; Hahn et al., 2015). Rheopectic behaviour is observed when a fluids' viscosity increases with the time duration of shear and this occurs when the internal structure reorganizes under shear stress (Souza Mendes de & Thompson, 2019; Tsugawa, et al.,, 2020). Rheopexy behaviour has been observed in non-food products such as cement pastes and paints (Souza Mendes de & Thompson, 2019; Tsugawa, et al., 2020).

In characterisng the time-dependent rheological behaviour of materials it is vital to note that the response could be reversible or irreversible (Mendes et al., 2015; Santos et al., 2016) The response is reversible if, the equilibrium viscosity of the time-dependent materials recovers after applied shear ceases and a relaxation time follows. It is however irreversible when the applied shear is above the yield stress and the material does not recover (Mendes et al., 2015; Santos et al., 2017). A reversible time-dependent response could be either thixotropic or anti-thixotropic. In thixotropic emulsions, the viscosity decreases as the applied stress increases with time and the structure recovers when the applied stress ceases e.g. colloids (Mendes et al.,2015; Santos et al., 2017). Hence the emulsion is said to display Shear-thinning behaviour. It is vital to note that some emulsions do not fully recover after the stress is applied e.g. yogurt. In anti-thixotropic emulsions, however, viscosity increases continuously as the stress is applied and displays a shear-thickening behaviour (Mendes et al.,2015; Santos et al., 2017). Figure: 0.77 shows the different responses a material could exhibit when subjected to applied stress and the time duration of the shear.

Time-dependent rheological characteristics of semi-solid food materials have been described by researchers to describe food thixotropic quality (Augusto et al., 2012; Mendes et al.,2015; Santos et al., 2017). The common time-dependent models are expressed by the Figoni and Shoemaker (Equation 2.8), Hahn (Equation 2.9), and Weltman (Equation 2.10) models respectively.

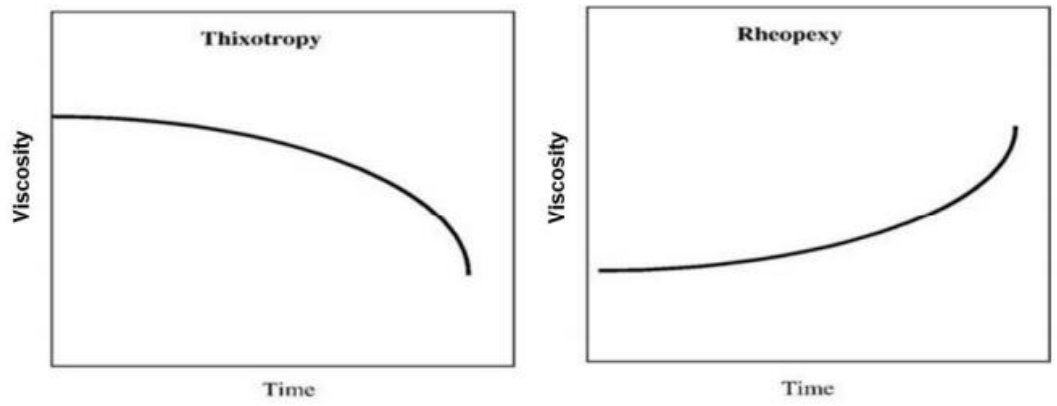

Figure: 0.7: Material responses to time-dependent applied stress.
Source: (Paraskevopoulou et al., 2017).

$$\boldsymbol{\tau = \tau_e + (\tau_{max} - \tau_e) exp(-kt)} \qquad \textbf{Equation 0.8}$$

Where τ_{max} represents the initial shear stress, τ_e the equilibrium shear stress, τ is the shear stress (Pa), t the time of shearing (s), and k the kinetic constant (Basu and Shivhare, 2013).

$$\boldsymbol{Log(\tau - \tau_e) = P - \alpha t} \qquad \textbf{Equation 0.9}$$

Where τe indicates the equilibrium shear stress, P the initial shear stress (Pa), t the time of shearing (s), and ∝ the sample's structural breakdown (s^{-1}) (Basu and Shivhare, 2013, Singla et al., 2013)

$$\boldsymbol{\tau = A - B\ int} \qquad \textbf{Equation 0.10}$$

Where τ is the shear stress (Pa), t the time of shearing (s), A the initial stress (Pa), and B the time coefficient (Basu and Shivhare, 2013).

The influence of temperature on the rheological behaviour of food emulsions is important as food emulsions are exposed to diverse temperatures in the course of processing, storage, and consumption. Several authors have investigated the influence of temperature on the parameters of rheological models in food emulsions using the Arrhenius model expressed as Equation 2.11 (Gonçalves et al., 2017; Junqueira et al., 2019; Kubo et al., 2019)

$$\eta = A_o \exp\left(\frac{Ea)}{RxT}\right) \qquad \textbf{Equation 0-11}$$

Where η is the is the viscosity (Pa s), A_0 is a constant, E_a is the activation energy (J mol^{-1}), R is the gas constant (J mol K^{-1}), and T is the temperature in K (Gonçalves et al., 2017; Junqueira et al., 2019; Kubo et al., 2019).

2.9 Viscoelastic Properties

Literature supports the claim that when fluids undergo applied stress they show both fluid-like (viscous) and solid-like (elastic) behaviour (Peters, Majumdar, & Jaeger, 2016; Majumdar et al., 2017). Hence, food emulsions exhibit *viscoelastic* properties and behave either as fluids or semi-solids (Patil & Gogate, 2018). Fluids that exhibit viscoelastic properties include lubricants, hagfish slime, tomato, and whipped cream (Junqueira et al., 2019; Kubo et al., 2019). Authors have investigated the stability of foods through viscoelastic properties and associated these rheological parameters with the structural changes that occur during processing. The fluid-like parameter is the loss modulus denoted by G'' while the solid-like parameter is the storage modulus denoted by G'. The storage modulus is the amount of the stored energy within the fluid while the loss modulus which is the energy within the fluid that is released in the form of when a stress is applied (Amirdivani & Baba, 2013). Another parameter the yield stress gives information about structure breakdown and is the least stress that would enable the fluid to start flowing (Augusto et al., 2012). The viscoelastic properties of food emulsions have been investigated using dynamic oscillatory tests or creep and recovery tests. (Rao, 2014; Kubo et al., 2019). The dynamic oscillatory tests involve applying sinusoidal shear stress with a determined amplitude within the linear behaviour and determining the resulting stress response over time (Kubo et al., 2019). The three rheological parameters involved in dynamic oscillatory tests are shear stress (σ), strain (γ), and oscillatory frequency (ω), and the test involves measuring one of the parameters by keeping one constant and varying the other (Kubo et al., 2019). Most tests involve, applying an oscillatory force to the fluid and measuring the strain as a response. Figure: 0. shows responses that could occur for purely viscous materials, viscoelastic, or purely viscous material dependent on the phase

difference. The deformation of purely elastic materials is in phase with the stress purely elastic, I.e. δ =0° and the deformation is directly proportional to the applied stress (Kubo et al., 2019). The stress response in viscoelastic materials has a phase angle δ <0° >90° while that of purely viscous material is 90° (Kubo et al., 2019). Oscillatory tests that can be used in assessing the viscoelasticity of a material are the amplitude, frequency, temperature, and time sweep tests.

Several authors have used creep-compliance tests to investigate the viscoelastic properties of food (Lorenzo et al., 2018; Kubo et al., 2019). The test involves the application of a rapid stress

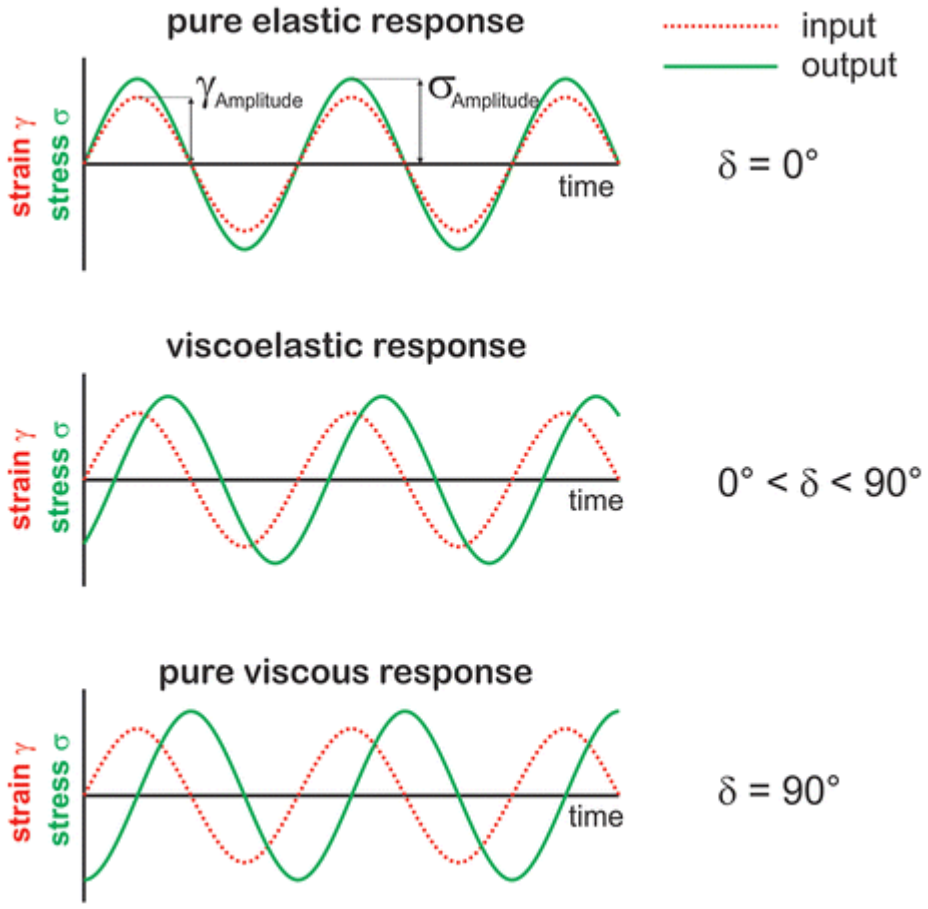

Figure: 0.8: Stress-strain response in a purely elastic, viscoelastic, or purely viscous material dependent on the phase difference

Source: (Kubo et al., 2019).

(σ) to a material, keeping the stress constant for a period of time, and measuring the changes in strain change (γ). The stress is then released, and the recovery behaviour is observed. Figure: 0. shows a pictorial outline of a creep and recovery process for a viscoelastic material. In creep and

recovery tests, a graph of compliance the inverse of the modulus of elasticity is plotted against time.to outline the viscoelastic properties.

2.9.1 Dynamic (oscillatory) characterisation of emulsions

Several authors have used oscillatory/ dynamic rheology to characterise the structure and texture of materials such as colloids, emulsions, gels or glass (Dickinson, 2012; Faber, Van Breemen, & Mckinley, 2017; Lorenzo et al., 2018). Oscillatory investigations involve subjecting the emulsion to oscillation stress-strain of varying frequency (Lorenzo et al., 2018; Zhu et al., 2019).

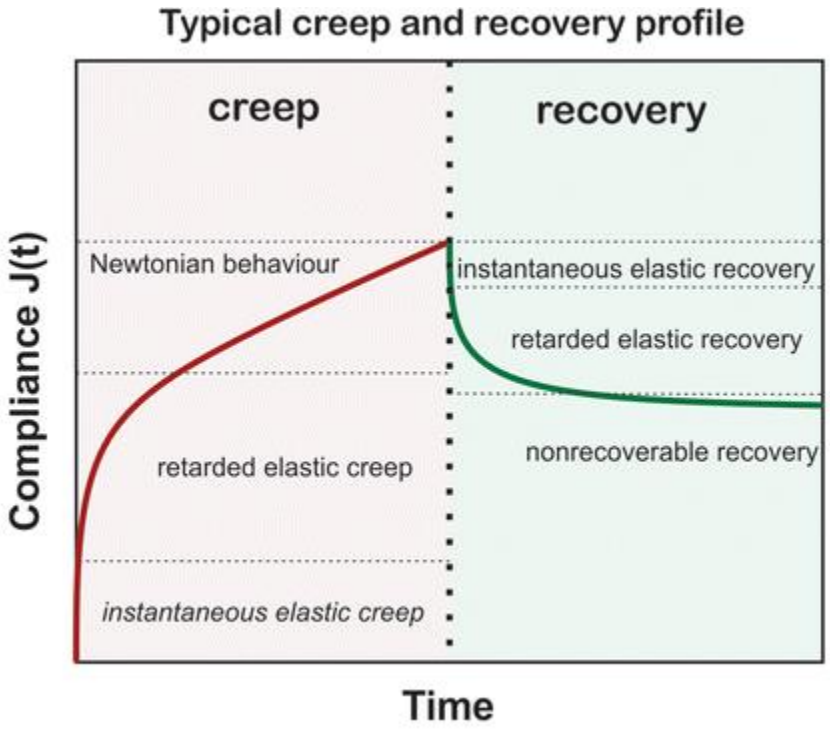

Figure: 0.9: Representation of a creep and recovery process for a viscoelastic material
Source: (Kubo et al., 2019)

Each investigation determines the amplitude and loss shift (δ) of the strain relative to the stress to evaluate shear modulus (G) that has both an elastic (G') and viscous (G') component. The ratio of the Storage modulus (G′) to the loss modulus G″ is evaluated as the loss angle (δ) which influences the structure and texture of emulsions (Zhu et al., 2019; Chen et al., 2020). Authors have established the importance of the linear viscoelastic region (LVR), which signifies strain domain in which emulsion basic structure is maintained when a stress is applied (Niu et al., 2016; Felix et al., 2017). Hence larger LVR implies that the emulsion is highly stable (Chen et al., 2019; Javidi et al., 2019). Javidi et al. (2019) indicated that the LVR is the phase at which the rate of

structural breakdown and reorganization are balanced. Several authors have established that the rheological parameters G′ and G″ influence emulsion stability. Niu et al. (2016) studied the viscoelastic behaviour of oil-in-water emulsions emulsified with gum Arabic (GA) and ovalbumin (OVA) at different proportions and pH range 3.8 - 7. These authors established that the emulsions investigated had a weak gel-like structural network with G′ > G″ at frequency range 0.01 to 10 Hz with a 0.5% strain in the LVR (Niu et al., 2016). The authors also noted that G' increased gradually as the dynamic frequency increased in the LVR which implied that interface that contributed to higher G' relaxed with time (Niu et al., 2016). Felix et al. (2017) examined the viscoelasticity of emulsions derived from animal and vegetable oils emulsified with crayfish protein concentrate and xanthan gum stabilisers at pH range 3, 5, and, 8. The authors established that the fabricated emulsions had strong gel-like properties with G′ > G″ at frequency range 0.01 to 20 Hz at a constant strain amplitude of 0.01 and 0.30% within the linear viscoelastic region at low pH of 3 (Felix et al., 2017);. However, an increase in pH led to progressive weak gel-like properties. The authors noted that the emulsion structural network was reinforced at low pH consequent upon electrostatic interactions between crayfish protein and oil in water emulsion interface (Felix et al., 2017).

The viscoelastic properties of materials have been done using oscillatory tests such as amplitude, frequency, temperature, and time sweep tests (Figure 2.4). The amplitude sweep is used in establishing the limit of the viscoelastic region (LVR) and is the point where the storage modulus starts becoming non-linear (Safaei & Castorena, 2017) The amplitude sweep test is also used to establish the flow point (Notani et al., 2019). Amplitude sweeps are performed at constant frequency but at various strains to establish the flow point and the LVR but low frequencies of about 1 HZ are usually used (Anvari & Joyner, 2017; Mendoza et al., 2018). Oscillatory shear tests have however been performed at large and small shear amplitudes (Melito, Daubert, & Foegeding, 2012). Small amplitude oscillatory shear tests that apply small strains/stress do not disrupt the materials' structure hence it is used designate the LVR (Lorenzo et al., 2018). However, large shear amplitude tests are used to establish elastic and viscous behaviour in complex fluids and also characterize the texture and sensory properties of food (Faber et al., 2017). Figure: 0.8 is a schematic representation of a sweep test with increasing strain at a fixed frequency. The strain point chosen in the linear region is normally used to conduct the frequency sweep (Lorenzo et al., 2018; Irani et al., 2019). Authors have used a frequency range of 0.01 to 100 rad/s to determine the viscoelastic properties of food emulsions (Silva et al., 2017; Chen et al., 2019). The structural network of dispersed and entangled polymers of hydrocolloids can be

shown through oscillatory viscoelastic frequency sweeps (Mahmood et al., 2017; Pérez-Orozco, Sánchez-Herrera, & Ortiz-Basurto, 2019; Velásquez-Cock et al., 2019). Therefore, a hydrocolloid can be classified based on its viscosity and elasticity data under frequency sweeps into:

1. Entangled networks which have solid-like structures at higher frequencies indicated by G' and G'' crossing at the middle of the frequency range (Wang et al., 2018).
2. Dilute polymer solutions where both G' and G'' are frequency-dependent with the G' smaller than the G'' over the entire frequency range (Mahmood et al., 2017).

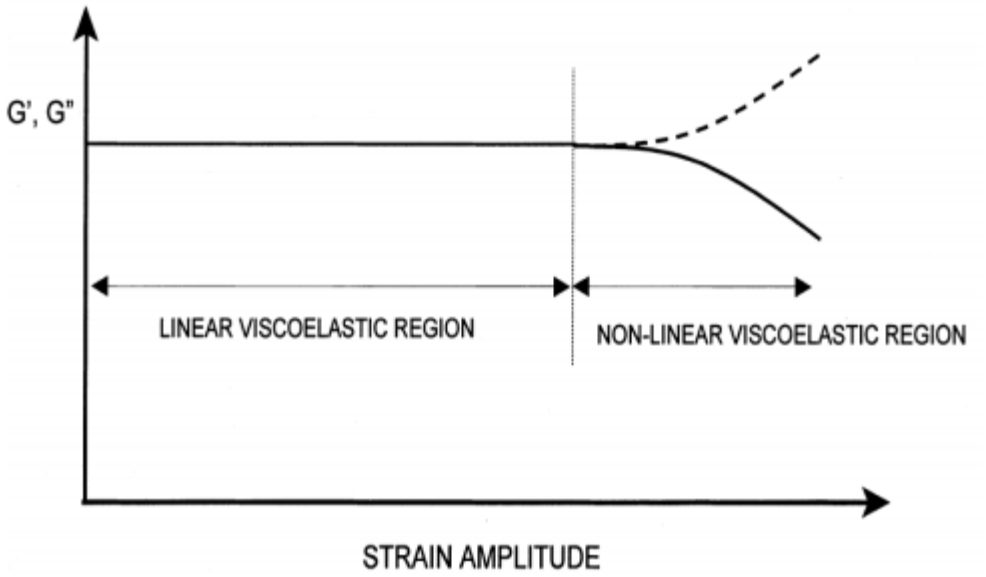

Figure: 0.80: Schematic representation of a sweep test with increasing strain at a fixed frequency. Source: (Safaei and Castorena, 2017).

3. Weak gels where both moduli moderately depends on frequency and G' is slightly greater than G'' (Mahmood et al., 2017; Hess et al., 2020). The tan δ of a weak gel is higher than the tan δ of a strong gel (Rafe and Razavi, 2017).
4. Strong gels where both moduli are independent of frequency and G' is far greater than G'' (Mahmood et al., 2017; Douglas, 2018). Strong gels are defined by $G''/G'(w) \leq 0.1$ (Patel et al., 2015).

High-frequency sweep tests mimic short-term storage stability while low-frequency sweep tests mimic long-term storage stability (Nasr & Pakshir, 2019). Authors have used time sweep tests to

determine G’ and G’’ as a function of time at a constant frequency and temperature (Torres, Chenlo, & Moreira, 2018). It has also being used to determine the gelling time of the material (Rafe & Razavi, 2013; Kazazi et al., 2017; Torres et al., 2018). Authors have also used a temperature sweep test to describe the effect that temperature on G’ and G’’ at a constant frequency (Hesarinejad et al., 2014; Sherahi et al., 2018). It has also being used to characterize gel formation in materials containing protein (Saini, Sharma, & Sharma, 2018). Literature supports the claim that food and hydrocolloids should be stored at different temperatures in order to maintain its quality and authors have proposed guidelines for food storage (Hygreeva & Pandey, 2016; Sohail et al., 2018; Tsang et al., 2018). In this work, temperature sweeps were performed to determine the effect of temperature (5 to 50°C) on the viscoelastic properties of African catfish mucilage (ACM), ACM stabilised O/W-type nanoemulsion ACM stabilised O/W-type nanoemulsion enriched with soya milk fiber The purpose of increasing the temperature up to 50°C was to determine the rheological characteristics of ACM and its stabilised O/W-type nanoemulsion at temperatures above room.

2.9.2 Constant stress (creep) characterisation of emulsions

When constant stress is applied to materials such as colloids, emulsions, gels or glass a slow deformation occurs which can be reversed if the stress does not get to the critical fracture point (Lidon, Villa, & Manneville, 2017; Malkin & Isayev, 2017; Bonn et al., 2017; Minami, Suzuki, & Urayama, 2019). Hence the material is referred to as plastic in nature. However, when constant stress is applied to materials such as metals, ceramics, or minerals they permanently deform even when the constant stress applied does not get to the fracture point (Lidon et al., 2017). This phenomenon which occurs because the material is deformed as a result of the application of constant stress is called creep (Lidon et al., 2017; Malkin & Isayev, 2017). Therefore depending on the morphology, these materials can exhibit slow deformation if the constant stress does not rise above the critical fracture point (Lidon et al., 2017; Malkin & Isayev, 2017). This ability allows colloids, emulsions, gels or glass to behave as both elastic and viscous materials simultaneously and is referred to as viscoelastic materials (Lidon et al., 2017; Minami et al., 2019).

Literature has shown that a creep test involves applying constant stress to materials and evaluating the strain with respect to time (Kim & Mason, 2017; Lidon et al., 2017; Lorenzo, Zaritzky, & Califano, 2018). Therefore, colloid, emulsions, and gels exhibit viscoelasticity and the strain behaviour for these materials are non-linear when constant stress applied (Joshi & Petekidis, 2018; Felix et al., 2019). Several authors have evaluated creep compliance as the ease

of deformity of material and it has been evaluated as the ratio of strain to stress with respect to time (Joshi & Petekidis, 2018; Lorenzo et al., 2018; Minami et al., 2019).

2.10 Mixture design methodology

Mixture design methodology is a regression-based analysis that fits mathematical models, such as linear, square or quadratic polynomial functions, to obtain experimental data observed in the experiment by applying multivariate statistical analysis methods (Myers et al., 2016; Yolmeh & Jafari, 2017; Selamat et al., 2018). The development of complicated formulations gernerally requires time and the use of enormous resources when it is approached traditionaly (Myers et al., 2016; Yolmeh & Jafari, 2017). Thus, applying designing and modeling experiments has been used to develop of complicated multi-variable formulations (Myers et al., 2016; Montgomeryi, 2017). Box-Behnken designs, central composite designs factorial designs, and D-optical mixture design are available and used by many scientists for multi-variable formulation. The components of the mixture (factors) affect other components of the mixture to produce an experimental response depending on the physicochemical property studies. Mixture designs are a type of statistical design that involve mixture components where, acceptable component values is constrained.

The mixture experimental design, all data analysis, desirability optimisation ability and all graphical plots was done using the Design-Expert statistical software. In Scheffe polynomial mixture models it is suggested that mixture design surfaces are used to interpret the effects of mixture constituents rather than being interpreted with quadratic coefficients which depends on the difference between the coefficients rather than their absolute magnitude (Baugreet et al., 2017; Konar et al., 2019). Two plots, the Trace (Piepel), and three dimensional surface plots were therefore used to interpret the effects of the mixture components on the measured responses. The trace plot was compared with the component effects on the design space, while the 3D plot desribes the mixture design surface.

2.11 Fish skin mucus

Wastes such as fish skin mucus (FSM) have generated much attention lately due to its function and immunological constituents and have been applied in medicine, cosmetics, and cell cultures (Elavarasi et al., 2013; Guardiola et al., 2017). Authors have reported that fishes exhibit a high diversity and represent about half of the vertebrates living today (Tyor, & Kumari, 2016). Global estimates in fisheries production were about 171 million tonnes in 2016 out of which about 20

million tonnes of fisheries by-products end up as wastes which humans discard (Tyor, & Kumari, 2016). However, authors have reported that discarded by-products from fish are vast stores of valuable in enzymes, flavors, long-chain key polyunsaturated fatty acids, micronutrients, minerals, pigments and proteins (Béné et al., 2016; Tyor, & Kumari, 2016; Chen et al., 2019).

The mucus obtained as a by-product of fish when it is stressed is a natural protective barrier for the skin against microbial attack and it also serves the dual purpose of immunization for the fish. (Tyor, & Kumari, 2016; Guardiola et al., 2017; Bansil & Turner, 2018). Several authors have reported that mucus on fish skin has lubricating properties as they act as a barrier between the inner and outer skin surfaces (Tyor, & Kumari, 2016; Guardiola et al., 2017; Bansil & Turner, 2018). Authors have noted that fish epithelial surfaces are enveloped by an intricate adhesive discharge known as mucus which is a colloidal adhesive gel that adherently covers the fishes' entire body (Tyor, & Kumari, 2016; Guardiola et al., 2017; Bansil & Turner, 2018). Thus mucus which occurs in the alimentary tract, gills, and the epithelium is secreted from the mucosa-associated lymphoid tissue of fish (Salinas, 2015; Guardiola et al., 2017; Jiang et al., 2018; Wang et al., 2019). Mucus from teleost fish is predominantly made up of water and mucins and is much like mucus from mammals (Guardiola et al., 2017; Salinas & Magadán, 2017; Reverter et al., 2018). Mucus protects the fish by incapacitating the binding of pathogens, and also acts as carriers of mucins and humoral immune factors. The humoral immune factors are antimicrobial peptides, cytokines, immune-globulins, and lectins while mucins are glycoproteins joined to considerable amounts of high molecular weight sugars that play a vital role in fish defense (Guardiola et al., 2017; Salinas & Magadán, 2017; Reverter et al., 2018). Mucus has been defined as an adhesive gel that contains antibacterial enzymes, proteins, and water that serves as a vital role in natural defense (Dash et al., 2018). Mucosal composition, consistency, and how often the mucus is secreted depend on the fish species and stress conditions in the environment, microbes present, and pH of the medium. (Tyor, & Kumari, 2016; Guardiola et al., 2017; Bansil & Turner, 2018). Authors have reported that mucus obtained from fish shields it from neural pain, heals wounds, has bactericidal, anti-inflammation, and anti-fungal properties and also helps to aggregate platelets (Tyor, & Kumari, 2016; Guardiola et al., 2017; Rahman et al., 2018). Furthermore, the secreted mucus plays the role of lubricant that has mechanical protective properties by serving as a barrier between the interior and exterior environment of the fish (Gobinath & Ravichandran 2011; Böni et al., 2016a; Böni et al., 2016b). Hence authors have investigated the bacteriocidal affinity, biochemical, biological, defensive and ecological characteristics of the mucus of fish and its metabolites (Tyor, & Kumari, 2016; Guardiola et al., 2017; Reverter et al., 2018). Literature has shown that the external epithelium of fish namely the alimentary tract, gills, and the skin secretes

mucus which is the first line of defense against microbial attack (Reverter et al., 2018). Furthermore, Gobinath & Ravichandran (2011), Elavarasi, et al. (2013), and Shabir et al. (2018) reported that the fish skin mucus (FSM) of freshwater fishes such as African and South Australian catfish, and tilapia have bactericidal properties due to the presence of anti-microbial peptides (AMP) which impart them with immunological properties. The authors further stated that the fish skin mucus (FSM) of African and South Australian catfish are bio-active, therapeutic, exhibits a broad spectrum activity on pathogens and are prospective sources of designing novel drugs against bacterial ailments. The literature has shown that the FSM acts as an exchange portal for the fish and its habitat, where it functions by chemically conveying messages for defense for the fish and protection from other species in its habitat (Reverter et al., 2018; Legrand et al., 2020). Several authors studied the FSM of marine and freshwater fishes and observed that FSM stimulated immune activity and could be used to boost human immunity (Su, 2011; Tsutsui et al., 2011; Tyor & Kumari, 2016). Su (2011) observed that the isolated AMP, pelteobagrin was an intrinsic part of the defensive mechanism of yellow catfish. Similarly, Tsutsui et al. (2011) identified lectins in the mucus of catfish which serve as an immunity booster by binding to saccharides on the surface of pathogenic microbes.

The elements of the FSM include; carbohydrates, enzymes, lipids, metabolites, proteins, and water (Dash et al., 2018; Reverter et al., 2018). Several authors have established that vital enzymes and proteins have been identified in FSM which is responsible for its natural defense (Guardiola et al., 2017; Dash et al., 2018; Reverter et al., 2018). These include antimicrobial peptides (AMP), glycoproteins, immunoglobulin, lectins, lysozyme, mucins, complement proteins, proteases, transferrins, and various other antibacterial proteins and peptides. (Guardiola et al., 2017; Dash et al., 2018; Reverter et al., 2018). Glycoproteins that exist in FSM exist either as carboxylated monosaccharides or sulfated monosaccharides (Dash et al., 2018; Reverter et al., 2018). The carbohydrate portion of FSM is involved in protective roles but occurs in the form of glycoconjugates and is different from other types of mucus by its ability to bind with lectins (Guardiola et al., 2017; Dash et al., 2018). Mucus from finfish and mammals mainly contains mucins (Guardiola et al., 2017; Salinas & Magadán, 2017; Reverter et al., 2018). Carbohydrate sequences called mucins which exist as thread-like objects with high molecular mass form the bulk of the FSM and is about 50% of FSM dry matter; (Guardiola et al., 2017; Dash et al., 2018). Mucins adhere forcefully to any material, play a key function in the defense mechanism of the FSM, and are the structural backbone of bacteriocidal molecules (Guardiola et al., 2017; Dash et al., 2018; Reverter et al., 2018). Mucins described as vastly glycosylated glycoproteins with a high molecular weight that confer rheological and viscoelastic properties on the mucus. (Bansil &

Turner, 2018; Dash et al., 2018). Mucins commonly contain side by side recurrent units abundant in proline serine and threonine amino acids which are protein functional sites that form hydrogen bonds with polar substrates (Guardiola et al., 2017; Dash et al., 2018; Svensson et al., 2018). The fatty acids in FSM are a vital part of the defensive action of mucus on pathogenic attacks while the metabolites in FSM such as azelaic acid, N-acetylneuraminic acid, and N-acetylglucosamine, have been reported to hinder bacteria (Ekman et al., 2015; Guardiola et al., 2017; Dash et al., 2018). The other constituents of mucus include anti-microbial peptides (AMPs), immunoglobulins, lectins, lysozymes., toxins, mycosporine-like amino acid, and unidentified semiochemicals (Salinas, 2015; Guardiola et al., 2017; Salinas & Magadán, 2017; Reverter et al., 2018). Consequently, FSM protection to the fish in its aquatic habitat, lubrication, and a first-line of defense harmful microbes via AMPs, lectins, lysozyme, complement proteins, and proteases.

2.12 Antimicrobial peptides

Antibacterial polypeptides (AMPs) are a class of short polypeptides that have amphipathic-helical configurations and occur naturally (Dash et al., 2018; Ongey et al., 2018; Chrom et al., 2019). They are found in animals and plants where they fulfill the purpose of defense and are essential parts of immune systems (Shabir et al., 2018; Chrom et al., 2019). AMPs are categorised by, its biological functions and sources, bio-genesis mechanism, covalent boding type, type of surface targeted, structure peptides, and secondary structure (Gonzalez Moreno, Lombardi, & Di Luca, 2017; Ongey et al., 2018; Shabir et al., 2018). The secondary structures exist as alpha-helical, beta-sheet, alpha-beta and non-alpha-beta peptide conformations (Gonzalez Moreno et al., 2017; Ongey et al., 2018; The alpha-helical (cecropins, dermaseptin) and beta-sheet (defensins, protegrin) peptide secondary structures are both common in nature (Gonzalez Moreno et al., 2017; Ongey et al., 2018; Shabir et al., 2018).

Researchers have reported that AMPs have broad-spectrum bactericidal activity, function as immunity agents and signaling molecules hence many studies have been carried out on its biology and structure to ascertain why it resists disease (Bansil & Turner, 2018; Dash et al., 2018; Jiang et al., 2018; Shabir et al., 2018). Although AMPs are found in other organisms such as animals, microbes, and plant it plays a more vital role in fish as the fish depends on AMPs as a form of defense in its aquatic habitat. An abundance of AMPs occurs in fish and major categories of peptides which include cathelicidins, defensins, hepcidins, histone-derived peptides, and piscidins specifically occur in fish species (Valero et al., 2013; Dash et al., 2018). Fish AMPs perform more vital roles than AMPs of other organisms because they can act in diverse ways depending on the stress condition. Table 0.1 shows the bioactivity and homology of some vital antimicrobial peptides

present in fish skin mucmucilage as adapted from Dash et al. (2018). Apart from the benefits of broad-spectrum activity of AMPs on microbes researchers have focused on detecting and extracting AMPs because they have been used in treating tumors and wounds and are produced with minimal energy (Su, 2011; Elavarasi et al., 2013; Zhu et al., 2015; Dash et al., 2018; Reverter et al., 2018; Shabir et al., 2018).

2.12.1 Lectins

Lectins belong to a class of glycoproteins that act against infections by initiating an immunity barrier while eliminating pathogens (Dash et al., 2018).These innate glycoproteins possess several domains that agglutinate cells or precipitate glycoconjugates (Dash et al., 2018; Reverter et al., 2018). Lectins are also glycoproteins that contain sites that accept electrons and binds to carbohydrates that are not catalytic in targeted microbes' or viruses and this is used to destroy matching and phagocytic cells. Lectins have also been shown to identify links associated with glycosides, sugar, and polysaccharides associated with bacteria. Authors have reported the bacteriocidal action of lectins that bind with fructose, galactose, and mannose in catfish, and Atlantic salmon (Tsutsui, et al., 2011; Valdenegro-Vega et al., 2014; Stowell, Ju, Cummings, 2015; Cordero et al., 2016; Dash et al., 2018). Authors have suggested that lectins are abundant in the FSM of many fish species because hemagglutination a major characteristic of lectins occurs in many species (Dash et al., 2018). Several authors have researched on fish mucus to report on the bioactivity of anti-body lectins of fisheries resources and have categorised lectins into four major categories (Ogawa et al., 2011; Coelho et al., 2017; Dash et al., 2018; Palanisamy et al., 2018). Lectins are categorised on the basis of; basic framework, the cation required and fold formations (Anju et al., 2013). They include C-type lectins which bind with lactose; galectins which bind with galactose; the fucolectins (F-type lectins) which bind with fucose and rhamnose binding lectin (RBL). C-type lectins attach to sugars when calcium ions are present to adhere, transport materials into a cell, and neutralize pathogens (Ogawa et al., 2011; Allam & Espinosa, 2015)). Authors have reportedly identified C-type lectins in freshwater eels (Tsutsui et al., 2015), Japanese yellowtail, (Nakamoto et al., 2017); and pearl spot (Rubeena et al., 2019). Table 0.2 shows some lectins in FSM based on lectin type and sugar bioactivity as adapted from Ogawa et al. (2011).

Table 0.1: Bioactivity and homology of some vital antimicrobial peptides in fish mucilage

Peptide	Species	Homology	Bioactivity	References
Cathelicidins	Atlantic salmon (*Salmo salar*)	Cationic, amphipathic, α-helix	Bacteria	Scocchi et al. (2016) Dash et al. (2018)
Epinecidins	Orange-spotted grouper (*Epinephelus coioides*)	Cationic, amphipathic, α-helix	Bacteria, virus	Dash et al. (2018) Sathyamoorthi et al. (2019)
Gaduscidins	Atlantic cod (*Gadus morhua*)	Cationic, amphipathic, á-helix	Bacteria, virus	Browne et al. (2011); Valero et al, (2013); Dash et al.,(2018)
Grammistins	Goldenstriped soapfish (*Grammistes sexllineatus*)	Cationic, amphipathic, á-helix	Bacteria	Valero et al. (2013); Dash et al. (2018); Cipolari et al. (2020)
Hipposin	Atlantic halibut (*Hippoglossus hippoglossus*)	Histone H2A N-terminal fragment	Gram-positive and Gram-negative bacteria	Bustillo et al. (2014); Dash et al. (2018)
Moronecidins	Hybrid striped bass (*Morone saxatilis*)	Cationic, amphipathic, á-helix	Gram-positive and Gram-negative bacteria, fungi, yeast	Shin et al. (2017); Dash et al. (2018) Mohammadi et al. 2018)
Oncorhyncin III R	Rainbow trout (*Oncorhynchus mykiss*)	A cleavage product of the non-histone chromosomal protein H6	Gram-positive and Gram-negative bacteria	Rajanbabu & Chen (2011); Dash et al. (2018)

Adapted from Dash et al.,(2018).

Peptide	Species	Homology	Bioactivity	References
Pardaxin	Moses sole (*Pardachirus marmoratus*)	Cationic, amphipathic, á-helix	Gram-positive and Gram-negative bacteria	Scocchi et al. (2016); Dash et al. (2018)
Parasin I	Amur catfish (*Parasilurus asotus*)	Histone H2A N-terminal fragment	Gram-positive and Gram-negative bacteria, fungi	Falanga et al. (2016); Dash et al. (2018)
Pelteobagrin	Yellow catfish (*Pelteobagrus fulvidraco*)	Unclear homology with any known bioactive peptides.	Gram-positive and Gram-negative bacteria, fungi,	Su (2011); Dash et al. (2018) Reverter et al. (2018)
Pluerocidin	Winter flounder (*Pseudopleuronectes americanus*)	Cationic, amphipathic, á-helix	Gram-positive and Gram-negative bacteria	Falanga et al. (2016); Dash et al. (2018)
Piscidins	Atlantic cod (*Gadus morhua)*	Cationic, amphipathic, á-helix	Bacteria	Ruangsri et al. (2012); Dash et al. (2018)
Salmon antimicrobial peptide (SAMP 1)	Atlantic salmon (Salmo salar)	Proline-rich histone H1 Nterminal peptide fragment	Gram-positive and Gram-negative bacteria	Rajanbabu & Chen (2011); Dash et al.,(2018); Wu et al. (2019)

Adapted from Dash et al. (2018).

Table 0.2: Type and sugar bioactivity of some lectins isolated from fish skin mucus

Species	Lectins	Sugar bioactivity	Lectin type	References
Catfish (*Silurus asotus*)	saIntL	d-Mannose	intelectin	Tsutsui et al. (2011); Watanabe et al. (2013) Ogawa et al. (2014);
1. Catfish (*Arius thalassinus*)	1. OLL	1. l-Rhamnose	1. RBL	1. Ogawa et al. (2014)
2. Catfish (*Silurus asotus*)	2. SAL	2. l-Rhamnose	2. RBL	2. Hosono et al. (2013)
3. Carp (*Cyprinus carpio*)	3. CarpFEL	3. GlcNAc	3. 6x β-propeller /Tectonin	3. Watanabe et al. (2013); Capaldi et al. (2015)
Chum salmon (*Oncorhynchus keta*)	CSL-1–3	l-Rhamnose	RBL	Watanabe et al. (2013); Ogawa et al. (2014)
Conger eel (*Conger myriaster*)	1. Congerin I	1. Lactose	1. Galectin	1. Ogawa et al. (2014); Tsutsui et al. (2019).
	2. Congerin II	2. Lactose	2. Galectin	2. Ogawa et al. (2014); Tsutsui et al. (2019).
	3. Congerin P	3. Lactose /mannose	3. Galectin	3. Ogawa et al. (2014); Tsutsui et al. (2016); Brinchmann et al. (2018); Tsutsui et al. (2019).
	4. conCL-s	4. Mannose	4. C-type	4. Ogawa et al. (2014); Tsutsui et al. (2015).
Electric eel (*Electrophorus electricus*)	Electrolectin	Lactose	Galectin	Ballarin et al. (2013); Zhou et al. (2016).
European eel (*Anguilla anguill*a)	AAA	Fucose	F-type	Brinchmann et al. (2018)

Species	Lectins	Sugar bioactivity	Lectin type	References
Far-East dace (*Tribolodon brandti*)	TBL-1–3	l-Rhamnose	TBL	Ogawa et al. (2011); Watanabe et al. (2013)
Japanese eel (*Anguilla japonica*)	AJL-1; AJL-2; eCL-1/eCL-2	β-Galactoside, Lactose	Galectin C-type (,3)	Ogawa et al. (2011); Tsutsui et al. (2016); Brinchmann et al. (2018).
Japanese sea perch (*Lateolabrax japonicus*)	JspFL	Fucose	F-type	Ogawa et al. (2011); Watanabe et al. (2013); Vasta et al., (2017)
Ponyfish (*Leiognathus nuchalis*)	PFL-1,2	l-Rhamnose	RBL	Ogawa et al. (2011);Watanabe et al. (2013)
Pufferfish (*Fugu rubripes*)	Pufflectin	d-Mannose	Lily-type	Tasumi et al. (2016).
Scorpionfish (*Scorpaena plumieri)*	plumieribetin	d-Mannose	Lily-type	Ogawa et al. (2011); Costa et al.,(2014)
Sea bass (*Dicentrarchus labrax*)	DlFBL	Fucose	F-type	Ogawa et al. (2011); Parisi et al. (2015).
Shishamo smelt (*Osmerus lanceolatus*)	OLABL	d-Galactose	C-type	Ogawa et al. (2011); Zhang et al. (2011
Steelhead trout (*Oncorhynchus mykiss*)	STL-1–3	l-Rhamnose	RBL	Ogawa et al. (2011); Watanabe et al. (2013); Motohashi et al. 2017)
Spanish mackerel (*Scomberomorus niphonius*)	SML	l-Rhamnose	RBL	Ogawa et al. (2011); Hosono et al. (2013); Watanabe et al. (2013)
Japanese sea perch Striped bass (*Morone saxatilis*)	DlFBL	Fucose	F-type	Ogawa et al. (2011); Vasta et al. (2017).; Mahajan et al. (2017)

Species	Lectins	Sugar bioactivity	Lectin type	References
White-spotted charr (*Salvelinus leucomaenis*)	WCL-1, 3	l-Rhamnose	RBL	Ogawa et al. (2011); Watanabe et al. (2013)
Windowpane flounder (*Lophopsetta maculate*)	AJL-1	d-Galactose	Galectin	Ogawa et al. (2011); Dash et al.,(2018).
Zebrafish (*Danio rerio*)	Drgal1-L1–L3	LacNAc	Galectin	Ogawa et al. (2011); Brinchmann et al. (2018).

Adapted from Ogawa et al. (2011)

Galectins are lectins that attach to carbohydrates such as β-galactosides even when calcium ions are absent to aid in cell death and malignant cell inactivity, differentiation, growth, morphogenesis, and infection resistance of the fish. Galectins reported in the literature are Japanese eel (Tsutsui et al., 2016), electric eel ((Zhou et al., 2016), channel catfish (Brinchmann et al., 2018), windowpane flounder (Dash et al., 2018), zebrafish (Brinchmann et al., 2018), and conger eel (Tsutsui et al., 2019). F-type lectins (FTLs) are glycoproteins that serve as receptors based on patterns that they recognise (Anju et al., 2013; Dash et al., 2018). FTLs identify and attach to carbohydrate elements such as fucose which occur on surfaces of likely fish pathogens via carbohydrate recognition spheres (Anju et al., 2013; Bishnoi et al., 2015; Dash et al., 2018). Authors have categorised FTLs as immunity recognition units in fishes such as gilthead bream (Cammarata et al., 2012), and Japanese eel (Vasta et al., 2017).

2.12.2 Proteases

Several authors have reported that fish skin is vital because the exudate from the skin the fish skin mucus (FSM) lubricates, protects and is the first line of defense from pathogenic attack (Elavarasi et al., 2013; Zhu et al., 2015; Dash et al., 2018; Reverter et al., 2018; Shabir et al., 2018; Tsutsui et al., 2019). Another natural immunity component of the FSM is the protease an enzyme that efficiently degrades attacking pathogens by hydrolyzing peptide bonds in the proteins infectious microorganisms (Nigam et al., 2012; Esteban & Cerezuela, 2015; Dash et al., 2018). Fish proteases trigger and boost the generation of constituents such as antimicrobial peptides and immunoglobulin that supplement fish natural immunity (Nigam et al., 2012; Esteban & Cerezuela, 2015; Dash et al., 2018). Proteases are categorised into; aspartic, cysteine, serine, and metalloprotease on the basis of radicals that stimulate the natural immunity mechanism (Nigam et al., 2012; Dash et al., 2018). Authors have reported serine protease in over 25% of fishes they include; bagrid catfish (Nigam et al., 2012), Indian major carp (Srivastava et al., 2018), Rohu carp (Balasubramanian et al., 2012), South Asian carp (Dash et al., 2018) and spotted snakehead (Balasubramanian et al., 2012). Aspartic protease (cathepsin D), cysteine protease (cathepsin B and L), serine protease (trypsin) and metalloproteases have been characterized in fish mucus of Atlantic salmon, coho, Japanese eel, Indian major carp, and Rainbow trout (Nigam et al., 2012; Dash et al., 2018; Srivastava et al., 2018). Proteases characterized in the mucus of diverse fish have been classified based on function in Table 2. 3.

Table 2. 3: Classification of proteases characterised in fish skin mucus based on function

Proteases	Species	Function	Reference
Amino proteases	Epidermal cell layer of Japanese eel/dorsal surface of European eel	Bacteriolytic activity against the fish pathogen	Dash et al. (2018)
Amino-peptidase	Epidermal cell layer of Japanese eel/dorsal surface of European eel	Bacteriolytic activity against the fish pathogen	Dash et al. (2018)
Cathepsin B	Epidermal cell layer of Japanese eel/dorsal surface of European eel	Bacteriolytic activity against the fish pathogen	Dash et al. (2018)
Cathepsin D	Mucous surface of catfish	Regulate production of parasin I	Ren et al., (2015): Dash et al. (2018)
L-like proteases	Epidermal cell layer of Japanese eel/dorsal surface of European eel	Bacteriolytic activity against the fish pathogen	Dash et al. (2018)
Metalloproteases	Epidermal cell layer of Japanese eel/dorsal surface of European eel	Bacteriolytic activity against the fish pathogen	Dash et al. (2018)
Trypsin like proteases	Rainbow trout/Atlantic salmon	Bacteriolytic activity against the Gram-negative fish pathogen/act against salmon louse	Dash et al. (2018)

Adapted from Dash et al.,(2018).

2.12.3 Lysozyme

Lysozyme is one of the class of non-specific antibody defense mechanisms in bony fishes which also function in roles in sustaining homeostasis (Firdaus-Nawi & Zamri-Saad, 2016; Kordon, Karsi, & Pinchuk, 2018). The non-specificity of lysozyme allows it to be multi-functional as it also mediates defense against pathogenic attack (Dash et al., 2018; Kordon, Karsi, & Pinchuk, 2018).

Lysozymes originate from the leucocyte and is a mucopeptide that has adhesive properties. They hydrolyze β-(1,4)-glycosidic bonds that alternate between N-acetylmuramic acid (NAM) and N-acetyl glucosamine (Monaghan et al., 2018), residues of peptidoglycan of the bacterial cell wall and result in swift cell destruction in highly osmotic habitats. The non-specificity of lysozyme allows it to be multi-functional as it mediates defense against pathogenic attack and also hinders fungi, parasites, and viruses that do not have peptidoglycan units (Dash et al., 2018; Kordon et al., 2018). Lysozyme also directly activates polymorph nuclear leukocytes and macrophages or indirectly marks an antigen for immune responses to stimulate phagocytosis (Dash et al., 2018; Kordon et al., 2018), There are five broad categories of lysozymes namely bacterial lysozyme, chicken-type lysozyme (c-type), goose-type lysozyme (g-type), plant-type lysozyme, and T4 phage lysozyme known as the phage-type (Dash et al., 2018). Only the chicken-type and the goose-type lysozyme has been identified in FSM (Seppola et al., 2016; Dash et al. 2018; Zhang et al., 2018a). Authors have reported that the response of lysozymes depends on the fish species and the location of the tissue to support the theory that lysozymes are non-specific antibody defense (Falfushynska et al., 2015; Dash et al., 2018). For instance, Dash et al. (2018) investigated the skin structure and non-specific antibody defense properties in Atlantic and coho salmon, and rainbow trout FSM and plasma. The authors reported a rise in lysozyme activity of FSM in Atlantic salmon and Rainbow trout at the onset of sea lice and reduced lysozyme activity as infestation progressed (Dash et al., 2018). In contrast, lysozyme activity of FSM was reduced at the onset of sea lice infestation in coho salmon but rose considerably as infestation progressed (Dash et al., 2018). Other authors have suggested lysozyme activity in fish is prompted very rapidly and is associated with the presence of bacteria and stress conditions that alarms the fish (Dash et al., 2018). Consequently, Dash et al. (2018) concluded that fish lysozymes acted as an acute-phase protein that was part of alarm responses in fishes.

2.13 Rheological characteristics of fish skin mucus

Authors have reported characteristics of fish skin mucus (FSM) that enables it to have lubricating properties (Böni et al., 2016a; Bansil & Turner, 2018). The FSM is a complex viscoelastic sticky exudate produced and secreted in the epithelia by unique goblet and mucous cells (Bansil & Turner, 2018; Rahman et al., 2018). Böcker et al. (2016), Böni et al. (2016a), and Böni et al. (2016b) described the FSM of hagfish as a soft gel with a complex moist network of elongated proteins strands and glycol-proteins of about 15 cm. However, in contrast to other hydrogels, the mucus of hagfish is highly diluted as it contains 99.996% water temporarily kept within the protein fibers (Böni et al., 2016a; Böni et al., 2016b; Bansil & Turner, 2018). The protein like fibers of

hagfish FSM consists of intermediate filaments (IFs) that have the same phylogeny as type II keratins (Böni et al., 2016a; Böni et al., 2016b). They occur as coiled protein coils and when exposed to deformation they experience α to β sheet transitions that significantly improves their mechanical characteristics (Böcker et al., 2016). Furthermore, the transition of hagfish FSM and deformations also imparts FSM of hagfish with better bio-physical features and handling potentials than spider silk (Böcker et al., 2016). Studies by Böcker et al. (2016) on hagfish FSM stated that when combined with biopolymers such as starch and κ-Carrageenan the resultant emulsion had higher cohesiveness, stability, interaction, water retention, and visco-elasticity. These researchers concluded that hagfish FSM and biopolymers could be applied in food, cosmetics, and medicinal industries as novel fiber enforced gels (Böcker et al., 2016).

The roles that mucus plays depends on the nature of FSM, its deformation, and flow characteristics (Guardiola et al., 2017; Bansil & Turner, 2018; Reverter et al., 2018). Authors have established that mucus structure and exudate amount increases under pathogenic attack and this enables defensive action by the fish (Guardiola et al., 2017; Bansil & Turner, 2018; Reverter et al., 2018). Authors have defined mucus as a viscoelastic adhesive exudate made by special goblet and mucous cell in the epithelium that covers glands and organs which are vulnerable to external habitats (Corfield, 2018; Bansil & Turner, 2018).

2.14 Application of fish skin mucus in emulsions

Formally, researchers had focused on describing the biology and anti-microbial properties of fish skin mucus (FSM) generated from marine and freshwater fishes and stated that it could be used to boost human immunity (Su, 2011; Tsutsui et al., 2011; Tyor & Kumari, 2016; Guardiola et al., 2017). However, research into ways of adding value to natural foods has targeted fish and fishery products for food security globally. Consequently, efforts in preventing wastage have led to studies on the rheology of FSM due to its antimicrobial and lubricating properties (Elavarasi et al., 2013; Conceição et al., 2016). Studies by Böni et al. (2016a) showed that the FSM obtained from hagfish are used as food in Japan and Korea as it compares very well to cooked “tofu”. The authors further stated that FSM generated from hagfish could be exploited in food-grade applications (Böni et al., 2016a). Several authors also established that the FSM of fish is used to defend them from predators and boost immunity (Su, 2011; Tsutsui et al., 2011; Böni et al., 2016a; Tyor & Kumari, 2016; Reverter et al., 2018). Consequently, the suggestion by some authors that FSM of estuarine and African catfish could be used as potential sources of effective replacements for antibiotics could pave the way for novel natural antibiotics (Su, 2011; Tsutsui et al., 2011; Tyor & Kumari, 2016). Hence, a knowledge of the rheological behaviour of emulsions stabilised with FSM could

innovate the use of catfish skin mucus as natural emulsion stabilisers in cosmetics and pharmaceutical industries (Gobinath & Ravichandran 2011; Elavarasi et al., 2013; Su, 2011; Tyor & Kumari, 2016).

2.15 Role of emulsifiers in Oil in water emulsions

Oil-in-water (O/W) emulsions are basic constituents of many products in industries such as beverages, cosmetics, drug delivery, foods, nutraceuticals, and personal care products (Bai et al., 2017; McClements & Jafari, 2018; Mikulcová et al., 2017; Azmi et al., 2019). They can be classified as flavor emulsions which exist as colloids that are kinetically unstable and contain small oil globules dispersed within an aqueous phase (McClements, 2015; Bai et al., 2017; Maphosa et al., 2017). Kinetic instability of O/W emulsions can be ascribed to the presence of positive free energy made available when dispersions are formed that allows colloids to separate through creaming, coalescence, flocculation, and sedimentation (Maphosa et al., 2017; McClements & Jafari, 2018; Bai et al., 2019). Emulsifiers are materials that kinetically stabilise emulsions by coating the oil globules and generate repulsive forces that hinder oil globules aggregation (Ozturk & McClements, 2016; McClements $ Jafari, 2018; Xu et al., 2019). The food industry has legally approved the use of several food-grade emulsifiers, however, costs, ease of use, and functionality make it difficult for food scientists to select the most proper emulsifier for an application (Bai et al., 2017; McClements & Jafari, 2018; Ferreira and Nunes, 2019). Kinetic stability of O/W emulsion has been increased by adding emulsifiers, stabilisers, and biopolymers (Maphosa et al., 2017; McClements & Jafari, 2018; Drapala et al., 2018; Focsan, Polyakov, & Kispert, 2019). Literature supports the efficacy of emulsifiers such as biopolymers, hydrocolloids, and polysaccharides in stabilising O/W emulsions (Dickinson, 2017; Felix et al., 2017; Maphosa et al., 2017; Maravić et al., 2019). Emulsifiers made from natural biopolymers are available, biocompatible, cost-effective, non-toxic, therapeutic, and can be sourced sustainably than synthetic ones (McClements & Gumus, 2016; Koller, 2018). Authors have reported that FSM protects the fish by incapacitating the binding of pathogens, and also acts as carriers of mucins and humoral immune factors (Peatman et al., 2015; Borges et al., 2018; Brinchmann et al., 2018). The humoral immune factors are antimicrobial peptides, cytokines, immune-globulins, and lectins while mucins are glycoproteins joined to considerable amounts of high molecular weight sugars that play a vital role in fish defense (Guardiola et al., 2017; Reverter et al., 2018). The use of fish skin mucus (FSM), as an efficient natural emulsifier, has been reported in the literature Böni et al. (2016a) and Böni et al. (2016b); African catfish mucilage (ACM) is a waste product formed when fish undergoes stress (Cabillon & Lazado, 2019). Authors have reported that the mucus from fish

has antimicrobial and lubricating properties; and contains proteins, sugars, and nucleic acid (Böcker et al., 2016; Böni et al., 2016a; Reverter et al., 2018).

Mixture design methodology is a multivariate statistical method that has been commonly used to optimize food processing techniques (Yeom et al., 2015; Derrien et al., 2017; Yolmeh and Jafari, 2017). RSM is a regression-based analysis that fits mathematical models, such as linear, square or quadratic polynomial functions, and other models, to the experimental response observed in the experiment by applying multivariate statistical analysis methods (Myers et al., 2016; Yolmeh and Jafari, 2017; Selamat et al., 2018). The RSM strategy establishes relationships between input factors and responses with the aid of a mathematical model, deals with hindrances of optimizing with sole parameters, and provides an efficacious way to develop formulate emulsions (Montgomery, 2017; Trujillo-Cayado et al., 2019).

Various techniques have been used to investigate the physicochemical properties of O/W emulsions stabilised with bio-emulsifiers in other to explain how the bio-emulsifier influences the stability of the O/W emulsion (Maphosa et al., 2017; Shao et al., 2017; Gharibzahedi et al., 2019). Researchers have proposed other explanations that could better address O/W emulsion stability. For instance, it has been established that an emulsion could become kinetically unstable because its particle size increases with time (McClements & Gumus, 2016; Kale & Deore, 2017). However, an emulsifier reduces the repelling force between two liquids and diminishes the attractive forces between the molecules of the same liquid within an emulsion (McClements & Gumus, 2016; Kale & Deore, 2017). Hence an emulsifier lowers the interfacial tension between two immiscible liquids and stabilises an emulsion by the surface-tension theory (McClements & Gumus, 2016; Kale & Deore, 2017). Similarly, the interfacial-film theory states that the emulsifier forms a thin film on the oil globules by adsorbing onto the surface of the internal phase droplets and prevents contact or coalescence with the dispersed phase (Rajak et al., 2016; Kale & Deore, 2017; Zhang et al., 2018b; Saani, Abdolalizadeh, & Heris, 2019). Increased concentration or larger molecular weight of the emulsifier results in a more stable emulsion because a more resilient film has been formed on the internal phase of the oil globules (Rajak et al., 2016; Kale & Deore, 2017; Saani et al., 2019). Similarly, authors have reported that the amphiphilic polymers in bio-emulsifiers influence stability of O/W emulsions by forming nanoemulsions through a thermodynamic process when the concentration of polymeric micelles (PMs) of the bio-emulsifiers is much lower than the concentration called critical micellar concentration (Cagel et al., 2017; McClements et al., 2017; Reneeta et al., 2018; McClements & Jafari, 2018; Liang et al., 2018; Bergenståhl & Spicer, 2019; Langevin, 2019). PMs are beneficial because their interior core contains a hydrophobic portion

that can entrap materials that have a low affinity for water and an outer hydrophilic wall that encapsulates materials that have a high affinity for water (Cagel et al., 2017; Hussein & Youssry, 2018; Wang et al., 2019). In recent times, this benefit of PMs has been exploited in beverages, cosmetics, drug delivery, foods, nutraceuticals, and personal care products because they provide improved solubility and stability for the incorporation of hydrophobic materials in O/W emulsions (Cagel et al., 2017; Hussein & Youssry, 2018; Wang et al., 2019). Furthermore, the literature supports the claim that the water solubility of an emulsifier is a rough estimate of hydrophilic-lipophilic balance (HLB) of an emulsifier and emulsifiers with HLB values between 8 and 15 are used to stabilise O/W emulsions (Burgos - Díaz et al., 2016; Nejadmansouri et al., 2016; Kale & Deore, 2017). The combination of data obtained from physicochemical properties such as particle size, backscattering flux %, and functional groups of bio-emulsifiers in conjunction with CMC and HLB correlations have been used by researchers to explain how bio-emulsifiers stabilise O/W emulsions (Burgos - Díaz et al., 2016; Nejadmansouri et al., 2016; Kale & Deore, 2017, Hussein & Youssry, 2018). Literature supports the micelle theory which proposes that bio-emulsifiers stabilised O/W emulsions is achieved through a hydrophobic portion that can entrap materials and simultaneously encapsulates materials that have a high affinity for water through its outer hydrophilic wall (Cagel et al., 2017; Hussein & Youssry, 2018; Laredj-Bourezg et al., 2017, López-Martínez & Rocha-Uribe, 2018; Wang et al., 2019).

2.16 Recent applications of Affrican catfish mucus

The skin of fish contains goblet and peneth cells which play a focal role in defending the fish by producing humoral immune factors and mucins (Guardiola et al., 2017; Salinas & Magadán, 2017; Reverter et al., 2018). The humoral immune factors include antimicrobial peptides, cytokines, immune-globulins, and lectins (Guardiola et al., 2017; Reverter et al., 2018).. Mucins on the other hand are glycoproteins joined to considerable amounts of high molecular weight sugars that play a vital role in fish defense (Guardiola et al., 2017; Salinas & Magadán, 2017; Reverter et al., 2018). Glucoproteins are structurally intricate chemical compounds that comprise of proteins and carbohydrates (Bansil & Turner, 2018; Tang et al., 2019). Aurthors have reported that oligosaccharide chains of glycoproteins are covalently attached to the polypeptide side-chains and proteins secretd from fish are glycosylated (Bieczynski et al., 2017; Bansil & Turner, 2018; Tang et al., 2019).

Studies on plant mucilage abound in literature, for instance the physicochemical properties of thale cress, cochineal cactus and coastal mallow has been documented in literature (McGee et

al., 2019; Zhou et al., 2018). Mucillage is secreted from various parts of the plant such as the leafy parts, seeds, stem and root wnd this mucilage have adhesive, defensive, nutritive, protective purposes (Galloway et al., 2020). The constituents in mucilage plant cell walls are normally include cellulose, hemicellulose,proteins, and pectin (Galloway et al., 2020). Authors have reported that stabilized oil in water emuslsions have been formulated with amphiphilic emulsifiers such as hagfish or saliva mucins which have the potentials to form crosslinked stable structures (Edwards et al., 2020). These emulsions were also shown to adhere to pig mucus in the buccal cavity, which confirms that amphiphilic emulsifiers can be used to formulate mucoadhesive oil-in-water (O/W) emulsions (Edwards et al., 2020). In the past, hagfish mucilage have been used as emulsifiers because of its mucoadhesive properties the authors concluded that hagfish mucilage could emulsify soy milk emulsions (Böni et al., 2016b). The literature claims that the catfish mucilage contains about 2.3 % ash, 1 0 % fat 2 0 % fibre, 7.4 % protein, 10.9 % moisture 76.3% carbohydrates (Akune et al., 2016) .The mucin extract from fish has been reported to have exceptional antimicrobial, lubricating and wound healing properties (Akune et al 2016; Böni et al., 2016b). Hence authors have proposed that it can be used to formulate nutritious neutraceutical, ccosmetic and drug-delivery systems.for animals and humans (Kouhi, Prabhakaran, & Ramakrishna, 2020).

2.17 Summary

African catfish mucilage (ACM) a waste product sustainably sourced from fish production has potential as a natural emulsifier that could be applied as feedstock in food emulsion formulations, in the cosmetic, and pharmaceutical industries. This chapter introduced the thesis and reviewed the literature on fish skin mucus, emulsions, ultrasonication, mixture design methodology, rheology of emulsions, characteristics of mucus and application of fish skin mucus in emulsions. The objective of the review was to discuss how emulsions can become kinetically unstable, the role of emulsifiers in emulsion formation, techniques used to investigate emulsion stability, emulsion rheology, and flow and viscoelastic properties of emulsions, The chapter provides an in-depth review of the literature on the issues that currently affect application of emulsion technology to foods, cosmetics, and medicine. It highlights the novel techniques that researchers are focusing on to improve the stability and rheological properties of dispersions and emulsions. This chapter reviews the literature on emulsions, formulations of emulsions, the use of ultrasonication in formulating biologically nutritious semi-solid foods either as colloids, emulsions, gels or simple solutions, emulsion stability and mechanisms of emulsion breakdown during storage and techniques used to investigate emulsion stability. Furthermore, the chapter reviews the literature

on rheology, flow, and viscoelastic behaviour of emulsions. Also the chapter reviews the literature on biology, characteristics, antimicrobial function and immunological components of fish skin mucus (FSM), its rheological characteristics, and application of fish skin mucus as bioemulsifiers.

Chapter 3

METHODOLOGY

3.1 Source of materials, equipment and chemicals

Cold pressed sunflower oil was purchased from Puris Natural Aroma Chemicals, South Africa. Clover brands of soy milk was procured from a Pick 'n' Pay hypermarket in Cape Town, Western Cape, South Africa.The equipment used were a fish stimulation gadget (HPG1, Velleman Instruments, (18 V, 80 Hz), Perkin Elmer universal total reflectance-Fourier Transform Infra-Red spectrum II spectrometer (UATR-FTIR, Llantrisant, Wales, UK), shear rheometer (Physica MCR502), Anton Paar, Austria), FEI/Tecnai T20 transmission electron microscope (TEM) and FEI/Tecnai F20 Cryo-TEM with a high-resolution camera and electron energy loss spectroscopy system, a Turbiscan Lab Expert (MA 2000), and a particle electrophoresis Nano series ZS instrument (Zetasizer Nano-ZS, Malvern Instruments, Worcestershire, UK). The chemicals used in this work were laboratory grade ammonium chloride, MCT oil (medium chain triglycerides), methanesulfonate, PIPES buffer [piperazine-N,N′-bis(ethanesulfonic acid)], protease inhibitor cocktail (broad range of amino acids such as alanine, aspartic, cysteine & serine etc). Sodium bicarbonate, and sodium citrate purchased at Sigma Aldrich.

3.2 Methods

The methods used in this work have been sectioned based on the research objectives. Section 3.3 details methods used in determining research objectives 1, 2, and 3, section 3.4 details with the methods used to determine research objective 4 while, section 3.5 details with the methods used in determining research objective 5.

3.3 African catfish mucilage extraction, characterisation, and role in stabilising soy milk emulsions.

This section deals with the methods used in achieving the collection and preservation of African catfish mucilage (ACM) and its characterisation. It also details the methods used to investigate the role of ACM in stabilising soy milk emulsions. The African catfish mucilage (ACM) was collected and preserved from a fish farm after obtaining ethical clearance Faculty of Engineering. The ACM was collected based on South African Bureau of Standards approved procedures, the Guidelines for Ethical conduct in the care and use of nonhuman animals in research and Ethical considerations for field research on fishes (SABS, 2008; Dunbar et al., 2012; Bennett et al., 2016).

3.3.1 Collection and preservation of African catfish mucilage

The African catfish mucilage (ACM) was collected based on South African Bureau of Standards approved procedures, the Guidelines for Ethical conduct in the care and use of nonhuman animals in research and Ethical considerations for field research on fishes (SABS, 2008; Dunbar et al., 2012; Bennett et al., 2016). Before acquiring ACM, the African catfish was put under anesthesia using 100 mg per liter methanesulfonate (Guardiola et al., 2017). Figure: 0.1 shows the fish stimulation gadget being used in collecting ACM. The anesthesised African catfish were blotted dry on a dissection tray, then placed in a bowl and a fish stimulation gadget (HPG1, Velleman Instruments, 18 V, 80 Hz) was used to enhance mucus discharge aseptically from mucus glands by placing the gadget on the ventral lateral section of the catfish (Gobinath & Ravichandran, 2011; Böni et al., 2016a). ACM secreted was collected from anaesthetised African catfish as described by Herr et al. (2010). The secreted ACM collected was stabilised in MCT oil or in a high osmolarity citrate/PIPES bufer (0.9M sodium citrate and 0.1M PIPES at pH 6.7, 0.02% sodium azide and protease inhibitor, using the method modified by Böni et al. (2018) and instantly stored at 4 °C for measurements that involved ACM mucins (Herr et al., 2014; Böni et al., 2018). Proteolysis was avoided by adding 1 mL of protease inhibitor cocktail to every 100 mL of citrate/PIPES buffer using the method modified by Böni, et al. (2018). The ACM stabilised in MCT could be used throughout the day that it was collected, while ACM stabilised in high osmolarity citrate/PIPES bufer (HOC/PIPES) could only be used for measurements immediately, as skeins stopped untangling when exposed to (HOC/PIPES) for too long (Bernards et al., 2014). Part of the retained ACM was frozen in liquid nitrogen and freeze-dried for storage at −80°C. The anesthesised African catfish were conveyed to a recuperation bath after the ACM was collected.

A portion of the freeze-dried ACM was dissolved in Milli Q Water and used for zeta potential, morphology, and stability tests while the freeze-dried ACM was used to acquire wavelength peaks.

3.3.2 African catfish mucus stabilised soy milk emulsion formulation

The hydrophobic dispersed state used was Clove brands of soy milk. ACM stabilised soy milk emulsion was formulated from a dispersed state comprised of soya milk and a continuous state comprising of freeze-dried ACM dispersion. Precise quantities of freeze-dried ACM [1, 3 and 5 % (w/w)] was dissolved in Milli-Q water. Measured quantities of soya milk [10, 30, 50 and 75 % (w/w)] were added into the ACM dispersions to attain different soya milk emulsion concentrations. The precise quantities of freeze-dried ACM in Milli-Q water and measured quantities of soya milk were homogenized with the aid of an Ultra Turrax T-25 homogenizer

(IKA, Germany) at 11000 rpm for 10 min (Adeyi, khu-Omoregbe, & Jideani et al., 2014). The temperature was controlled using a thermal ice jacket at 20 ± 1ºC.

Figure: 0.1: Use of the fish stimulation gadget in the collection of ACM

3.3.3 Transmission Electron Microscopy and particle size analysis

Transmission electron microscopy (TEM) was used to investigate the microstructure of African catfish mucus (ACM) and soya milk emulsions stabilised by ACM using modifications of a method described by Kasiri & Fathi (2018**).**and soya milk emulsions stabilised by ACM using modifications of a method described by Kasiri & Fathi (2018**).** Figure: 0.2 shows the picture of the FEI/Tecnai T20 Transmission electron microscope. The microstructure of ACM and soya milk emulsions stabilised by ACM was investigated using aFEI/Tecnai T20 Transmission electron microscope (TEM) with a high-resolution camera and electron energy loss spectroscopy (EELS) system using modifications of methods described by Park et al. (2015) and Kasiri & Fathi (2018). An accelerating voltage of 200 kV was used in investigating the ACM dispersion and each emulsion sample. One droplet of ACM in MilliQ water was transferred over the surface of the carbon-coated copper grid, negatively spotted with a 2% (w/w) solution of uranyl acetate and then dried at room temperature as described by Park et al. (2015) and Kasiri & Fathi (2018). Digital image analysis was used to determine the particle size. The TEM images were acquired using the FEI/Tecnai T20 TEM and a charge-coupled device (CCD) camera size of 2048 × 2048; [Gatan, USA] as described by Park et al. (2015) and Kasiri & Fathi (2018). The images at 50 and 100 nm were taken to quantify the particle size of each soya milk globule and its distribution in each emulsion sample using the method adapted by Dokić, et al. (2012).

Figure: 0.2: FEI/Tecnai T20 Transmission electron microscope

The particle size distribution of ACM stabilised emulsions was elucidated by calculating Sauter mean diameter ($D_{(3,2)}$) using Equation 3.1 while the standard deviation i.e. value of the width of the milk goblets distribution in the ACM stabilised emulsion was calculated using . The average droplet size is given by Equation 3.3 where n_i is the number of goblets in each size class, d_i is the particle diameter, ∑ni is the total number of droplets, and d_n is average droplet size (Dokić et al., 2012).

$$D_{(3,2)} = \frac{\sum n_i d_i^3}{\sum n_i d_i^2} \qquad \textbf{Equation 0.1}$$

$$\sigma = \frac{\sum n_i (d_i - d_n)^2}{\sum n_i} \qquad \textbf{Equation 0.2}$$

$$d_n = \frac{\sum n_i d_i}{\sum n_i} \qquad \textbf{Equation 0.3}$$

Source: (Dokić et al., 2012)**.**

3.3.4 Absorption bands analysis

Infrared spectra of ACM were gathered with a Perkin Elmer universal total reflectance Fourier Transform Infra-Red spectrum II spectrometer (UATR-FTIR, Llantrisant UK), run with

spectrum software as described by Zide et al. (2018). Figure: 0.3 shows the Perkin Elmer universal total reflectance Fourier Transform Infra-Red spectrum II spectrometer equipment. Wavelength bands were collected in the region of 4000 cm^{-1}-400 c m^{-1} to categorize the functional groups in the ACM and ACM stabilised soy milk emulsion (Zide et al., 2018).

Figure: 0.3: Perkin Elmer universal total reflectance Fourier Transform Infra-Red spectrum II spectrometer

3.3.5 Zeta potential and particle size measurements

The electrical charge was investigated with the aid of a particle electrophoresis Nano series ZS instrument (Zetasizer Nano-ZS, Malvern Instruments, Worcestershire, UK) by determining the electrophoretic mobility of the droplets using a capillary electrophoresis cell. The particle size was measured using the principle of direct light scattering with the aid of a particle electrophoresis Nano series (Zetasizer Nano-ZS, Malvern Instruments, Worcestershire, UK). The ACM dispersion electrical charge and ACM stabilised soy milk emulsion was analyzed in three replicates.

3.3.6 Stability studies

The Turbiscan MA 2000 (Formulaction, Toulouse, France) was used to evaluate the stability of the ACM stabilised soy milk emulsion as described by Adeyi et al. (2014). Figure: 0.4 shows the schematic representation of transmission and backscattering. African catfish mucilage stabilised soy milk emulsion of about 7 mL was measured into a Turbiscan tube (65 mm length) and measurements were taken. The measurement involved scanning each dispersion and emulsion along with its height for 3 h at 30 min intervals (Maphosa et al., 2017). The backscattering (BS) and transmission curve acquired provided the BS and transmission flux

percentage in relation to the instrument's internal standard as a function of the height of the sample. To study the effect of ACM on the stability of ACM stabilised soy milk emulsion multiple scans was analyzed using the principle of Multiple Light Scattering in both Transmission (T) and Backscattering (BS) % flux mode.

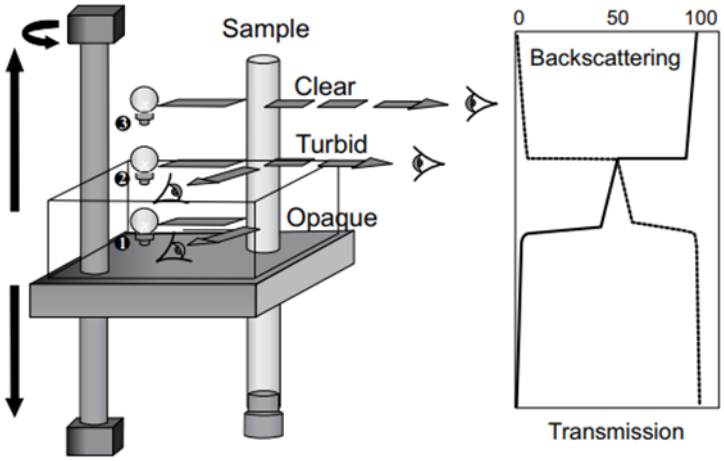

Figure: 0.4: Schematic representation of transmission and backscattering
Source: (Qi et al 2017)

3.3.7 Data and statistical analysis

Data were expressed as mean, ± standard deviation, and as mean ± standard error for the backscattering flux percentage and particle size as a function of stability. GraphPad Prism version 5.00 for Windows, GraphPad Software, La Jolla, CA, USA, was used for data analysis of ACM stabilised soy milk emulsion. The results were subject to a two-way analysis of variance test.

3.4 Investigation of the effect of African catfish mucilage on the stability of oil in water-type (O/W-type) nanoemulsions prepared by ultrasonication using D-Optimal mixture technique.

This section details the methods used in investigating the effect of African catfish mucilage (ACM) on the stability of oil in water-type (O/W-type) nanoemulsions that were prepared by ultrasonication. D-optical mixture design methodology was used to study the influence of three-component mixture on the stability s a function of back scattering percentage flux and particle size.

3.4.1 Experimental Design

The D-optical mixture design methodology was used to study the influence of the ACM, sunflower oil and MilliQ water concentrations on the stability. A D-optimal experimental mixture design design was used with the constraints African catfish mucus (A or ACM) + sunflower oil (B or Oil) + MilliQ water (C) = 100 %. The lower and high limits for ACM, oil and water were (1-to 5 %), (3-t0 10 %), and (85- to 96 %). The stability responses analysed using D-optical mixture design surface interface were backscattering flux percentage (BS % flux) and Sauter mean diameter ($D_{(3,2)}$) as a function of particle size (nm). Design Expert (version 10.0: Stat Ease, Inc. Minneapolis MN U.S.A) was used to generate the D-optimal mixture design experimental plan. The mixture studied was a three-component system: a mixture of ACM emulsifier (*A*), sunflower oil (*B*), and MilliQ water (*C*). The total sum of the mixture was 100 % (100 mL), The optimal combinations of ingredients proportions and levels of components for active oil water-type (O/W-type) nanoemulsions stabilised with free-dried ACM were determined by D-optimal mixture design using Design-Expert software (version 10, Stat-Ease, Inc.). The coded low and high for L_Pseudo Coding for ACM was (+0 ↔ 1 and +0.363636 ↔ 5), that of oil was (+0 ↔ 3 and +0.636364) ↔ 10 while that of water was (+0 ↔ 85 and +1 ↔ 96).

The trace plot and the 3D plot were used to compare the component effects on the design space L-pseudo phase diagrams were constructed to predict and establish the regions where stable o/w-type nanoemulsions were formulated. D-optimal mixture design was set up to enable definition of quadratic model to quantify the effect of concentration of ACM emulsifier on emulsion stability properties (BS % flux and $D_{(3,2)}$). Model equations were calculated after converting the actual values of emulsifier concentration into l-pseudo levels.

3.4.2 African catfish mucilage stabilised O/W-type nanoemulsion formulation

The ACM stabilised O/W-type nanoemulsions were formulated using a modification of the premixing, sonication, and rest method developed by Lourdes de Pérez-González et al. (2020). Figure: 0.5 shows the ultrasonic processor used in the formation of nanoemulsions. It involved cavitating the oil flocs in the MilliQ water aqueous medium with the aid of an ultrasonic processor (Sonics & Materials, Inc. Newtown, CT, USA). Sunflower oil and MilliQ water were premixed for 5 min at a temperature set to 10 ± 2 °C. Then ACM was added to the sunflower and MilliQ water and the mixture was stirred with an acoustic amplitude (ζ) of 40 % for 2 min in periods of 0.5 min of stirring and 0.5 min of rest using a 20-kHz Vibracel processor, 750 W Sonics, a tip diameter of 13 mm, and a temperature set to 10 ± 2 °C (Lourdes de Pérez-González et al., 2020). Oil-water mixtures containing 85-96 mL MilliQ water, and 3-10mL

sunflower oil were homogenized without ACM with the aid of an ultrasonic processor as control (Sonics & Materials, Inc. Newtown, CT, USA).

Figure: 0.5: Ultrasonic processor used in the formulation of O/W-type nanoemulsions

3.4.3 Cryo-Transmission Electron Microscopy and Particle Size Analysis

Figure: 0.6 shows the picture of the FEI/Tecnai F20 Cryo-Transmission electron microscope. The structure of ACM stabilised sunflower O/W-type nanoemulsion was analyzed with the aid of an FEI/Tecnai F20 Cryo-TEM and a charged coupled device camera size 4096 X 4096 Gatan UK Milton Park Innovation Centre Abingdon OX14 4RY United Kingdom Gatan, the USA (Tran et al., 2016, Acevedo-Estupiñan et al., 2019). The Sauter mean diameter ($D_{(3,2)}$) was calculated from the particle size distribution using equations 1, 2, and 3 (captured in section 3.3.3 page 65) using methods developed by Dokić et al. (2012).

Figure: 0.6: FEI/Tecnai F20 Cryo-TEM microscope

3.4.4 Stability studies

The Turbiscan MA 2000 (Formulaction, Toulouse, France) was used to evaluate the stability of the ACM stabilised O/W-type nanoemulsion, as described by Adeyi et al. (2014). Figure 3.4 shows the schematic representation of transmission and backscattering. African catfish mucus (ACM) dispersion of freeze-dried ACM in MiiliQ water, ACM stabilised O/W-type nanoemulsions, and ACM stabilised soy milk emulsion of about 7 mL separately, were measured into a Turbiscan tube (65 mm length) and measurements were taken. The measurement involved scanning each dispersion and emulsion along with its height for 3 h at 30 min intervals (Maphosa et al., 2017). The backscattering (BS) and transmission curve acquired provided the BS and transmission flux percentage in relation to the instrument's internal standard as a function of the height of the sample. To study the effect of ACM on the stability of both ACM stabilised emulsions multiple scans were analyzed using the principle of Multiple Light Scattering in both Transmission (T) and Backscattering (BS) mode.

3.4.5 Optimisation and statistical analyses

In determining the optimum ACM stabilised O/W-type nanoemulsion formulation, a D-optimal mixture design was chosen as the desirable design type based on the number and constraints of the selected mixture components. The 3 mixture constituents were: (A) ACM, (B) oil, and (C) water. Each constituent was constrained with lower and upper limits; the 3 components in real scale amounted to 100% (1 % to 5 % for ACM, 3 % to 10 % for oil, and 85 % to 96 % for

water) respectively. The design consisted of 16 formulations (Table 0.1) with which comprised 11 different runs, and 5 runs had two replicates. The optimised formulation was used to determine experimental results of stability as a function of Backscattering (BS) flux % and Sauter mean diameter ($D_{(3,2)}$). The research objective was to evaluate how the physicochemical properties of ACM affect its role as an emulsifier in sunflower O/W-type nanoemulsion using ultrasonication with a view to optimise the emulsion formation to provide the food, cosmetics, drug delivery, and personal care industry with a low cost, eco-friendly alternative emulsifier

The optimisation was set to explain results on (a) maximising ACM concentration and minimising oil concentration and (b) maximising ACM concentration and maximising oil concentration. By applying the optimisation methods desired amounts of each variable for the final O/W-type nanoemulsions were obtained and choices could be made depending on purposes for either food, cosmetics, drug delivery, or personal care. A quadratic model was chosen for responses Y (BS flux % and $D_{(3,2)}$) for the interpretation of results. The quadratic equation generated using statistical analysis of software, established the relationship between

Table 0.1: Formulation sets as determined by the three-component D-optimal mixture design[a, b]

	Independent variable		
Formulation	**A: ACM (%)**	**B: Oil (%)**	**C: Water (%)**
1	1	9.6	89.4
2	1	9.6	89.4
3	1	3	96
4	5	7.3	87.7
5	1	5.7	93.3
6	5	3	92
7	5	3	92
8	5	10	85
9	2.3	10	87.7
10	1	3	96
11	2.9	3.1	93.9
12	3.3	6.2	90.5
13	5	10	85
14	1	8.00	91.0
15	5	4.6	90.4
16	3.3	6.2	91.0

[a]Correspondent values indicated in actual scale.

[b]African catfish mucilage.

the formulation variables and responses. Each of the measured responses (dependent variables) was fitted to a quadratic model (Equation 3.4).

$$Y = \beta_1 x_1 + \beta_2 x_2 + \beta_3 x_3 + \beta_4 x_i x_2 + \beta_5 x_1 x_3 + \beta_6 x_2 x_3. \qquad \textit{Equation 3.4}$$

where β_1–β_6 represent the regression coefficients. The values of these coefficients were calculated based on the synergy between the response and formulation variables. The terms x_1, x_2, and x_3 represent the coded formulation variables, Y represents the measured response Analysis of variance (ANOVA) was used to assess both models' level of significance. P-value and Lack-of-fit of the selected models should be either significant ($P < 0.05$) or not significant ($P > 0.05$) respectively (Patel et al., 2015; Yeom et al., 2015). The model is adequate if it has a positive predicted R squared value and lack of fit value P - value of > 0.1 (Yeom et al., 2015). The trace and contour plot were used to examine the role of mixture parameters ACM, oil and water on the studied stability properties (BS % flux and $D_{(3,2)}$). The Piepel trace plot was used to assess the effect of changing each variable of the mixture on the studied responses, along an imaginary line from a reference blend to the vertex, while the proportion between the other components was kept constant (Yadav et al., 2017; Radfar et al., 2020). Trace plots ascertains the Independent variable that influence and have a dominant effect on the studied responses (Djuris et al., 2014; Radfar et al., 2020). The selected Independent variables from trace plots were used to construct the contour plots. The contour plot method provides a meaningful way to visualize the changes of a response that has various levels of constituents (Radfar et al., 2020). The D-optical mixture design surface in a contour plot connects all points that have the same responses within a two-dimensional plane (Nassar,Thom, & Parry, 2016; Radfar et al., 2020).

3.4.6 Absorption bands analysis

Infrared spectra of ACM stabilised O/W-type nanoemulsion was gathered with a Perkin Elmer universal total reflectance Fourier Transform Infra-Red spectrum II spectrometer (UATR-FTIR, Llantrisant UK), run with spectrum software as described by Zide et al. (2018). Figure: 0.3 shows the Perkin Elmer universal total reflectance Fourier Transform Infra-Red spectrum II spectrometer equipment. Wavelength bands were collected in the region of 4000 cm^{-1}-400 cm^{-1} to categorize the functional groups in the ACM stabilised O/W-type nanoemulsion (Zide et al., 2018).

3.4.7 Zeta potential and particle size measurements

The electrical charge was investigated with the aid of a particle electrophoresis Nano series ZS instrument (Zetasizer Nano-ZS, Malvern Instruments, Worcestershire, UK) by determining the electrophoretic mobility of the droplets using a capillary electrophoresis cell. The particle

size was measured using the principle of direct light scattering with the aid of a particle electrophoresis Nano series (Zetasizer Nano-ZS, Malvern Instruments, Worcestershire, UK). The particle size of ACM stabilised O/W-type nanoemulsion was analyzed in three replicates.

3.5 Flow and viscoelastic rheological behavior of African catfish mucilage (ACM) and ACM''most stable emulsions

This section details the methods used in investigating the flow and viscoelastic rheological **behavior** of African catfish mucilage (ACM), ACM stabilised soy milk emulsion, ACM stabilised O/W-type nanoemulsion and ACM stabilised O/W-type nanoemulsions enriched with soy milk fibre. The ACM stabilised O/W-type nanoemulsions enriched with soy milk fibre was formulated by using a modification of the premixing, sonication, and rest method developed by Lourdes de Pérez-González et al. (2020). It involved cavitating the oil flocs in the MilliQ water aqueous medium with the aid of an ultrasonic processor (Sonics & Materials, Inc. Newtown, CT, USA). Sunflower oil and MilliQ water were premixed for 5 min at a temperature set to 10 ± 2 °C. Then soymilk and ACM was added to the sunflower and MilliQ water and the mixture was stirred with an acoustic amplitude (ζ) of 40 % for 2 min in periods of 0.5 min of stirring and 0.5 min of rest using a 20-kHz Vibracel processor, 750 W Sonics, a tip diameter of 13 mm, and a temperature set to 10 ± 2 °C (Lourdes de Pérez-González et al., 2020). Oil-water mixtures containing 85-96 mL MilliQ water, and 3-10mL sunflower oil were homogenized without ACM with the aid of an ultrasonic processor as control (Sonics & Materials, Inc. Newtown, CT, USA).

3.5.1 Formation of mucilage

The ACM stabilised in MCT and instantly stored at 4 °C was used to carry out rheological measurements that involved charcterising ACM In preparing ACMs most stable emulsions, MilliQ water was added to specific grams of freeze-dried ACM was placed in a glass flask with a plastic spatula based on the concentrations of each emulsion and nanoemulsion. The mixture was mixed by a gentle sloshing of heads for about eight times (Ewoldt, Winegard, & Fudge, 2011; Böni et al., 2016a; Böni et al., 2018). The resulting exudate concentration of the measurements was determined according to the assumption of Ewoldt et al, (2011) that the density of the exudate is close to 1 g/ml, as about 66% of the exudate mass is water.

3.5.2 Flow and viscoelastic rheological tests

The rheological tests were carried out using a controlled stress/strain rheometer (Physica MCR 502 rheometer, Anton Paar Com with sandblasted parrale plates geometry (and a gap size of 0.5 mm using a method developed by Böni et al. (2016a) with slight modifications (Figure: 0.7 and Figure: 0.8). Oscillatory and rotational tests were performed using the DIN EN

ISO 6721-10 and DIN 53019 standard to determine the flow and viscoelastic properties of ACM dispersion, soya milk, ACM stabilised O/W-type nanoemulsions, ACM stabilised soy milk emulsion, and African catfish mucus stabilised O/W-type nanoemulsion enriched with soya milk fiber respectively. ACM and its most stable emulsions were equilibrated for 10 minutes before conducting oscillatory tests as described by Adeyi et al. (2014).

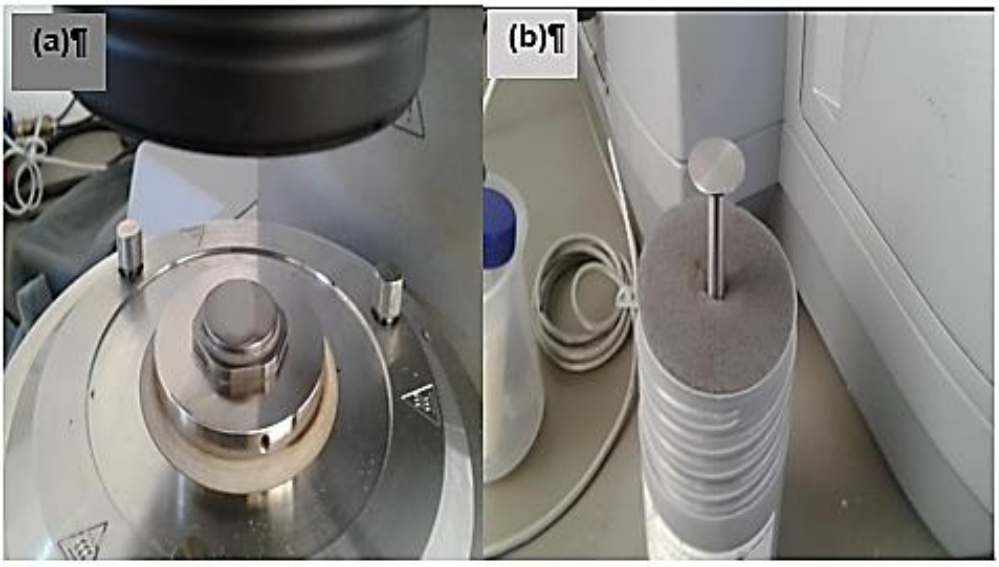

Figure: 0.7: Anton Paar Stress/strain controlled rheometer Physica MCR 502 rheometer, with (a) 25 mm diameter stainless steel plates (b) geometry

Figure: 0.8: Anton Paar Stress/strain controlled Physica assembled MCR 502 rheometer equipment

3.5.3 Flow and viscoelastic rheological test

All samples were subjected to a constant shear rate of 100 s^{-1} for 10 minutes after which the shear rate was varied from 100 to 1000 s^{-1} at 25°C. The relationship between the shear stress versus shear rate was used to obtain the apparent viscosity. The data obtained from the rotational steady-state test was fitted to conventional time-independent models such as Power law, Bingham, Herschel-Bulkley and Casson using the Microsoft Excel solver function. The generalized reduced gradient (GRG2) nonlinear optimization code was used in optimizing the rheological flow data using a method described by Adeyi et al. (2014). The Analysis ToolPak regression tool under the Solver function in Microsoft Excel was used to calculate the R-squared, adjusted R-squared, sum of square error (SSE) and root mean square error (RMSE).

3.5.3.1 Oscillatory Amplitude Strain test

The amplitude strain tests was performed within the strain range of 0.1 to 100% under a fixed frequency of 1 Hz. The plot obtained was used to determine the linear viscoelastic region (LVR) and the crossover point. Amplitude tests were limited to ACM dispersion, ACM stabilised O/W-type nanoemulsions, and ACM stabilised O/W-type nanoemulsion enriched with soya milk.

3.5.3.2 Oscillatory frequency sweep test

The frequency test was performed within the frequency range of 0.01 to 100 Rad/s at a fixed temperature 25°C and a constant strain of 0.1% obtained from the amplitude strain test. The G’ and G’’ were obtained at the various frequencies to show the effect of frequency on the rheological properties of ACM dispersion, soya milk, ACM stabilised O/W-type nanoemulsions, and ACM stabilised soy milk emulsion. Frequency sweep tests were limited to ACM dispersion, ACM stabilised O/W-type nanoemulsions, and ACM stabilised O/W-type nanoemulsion enriched with soya milk.

3.5.3.3 Oscilatory temperature strain test

The effect of storage temperature on the rheological properties of ACM dispersion, ACM stabilised O/W-type nanoemulsion, and ACM stabilised soy milk emulsion were investigated at a temperature of 0 to 50°C, at a constant strain of 0.1% and a constant frequency of 1 Hz. Temperature sweep tests were limited to ACM dispersion, ACM stabilised O/W-type nanoemulsions, and ACM stabilised O/W-type nanoemulsion enriched with soya

3.5.3.4 Oscillatory time strain test

The effect of time on the rheological properties of ACM dispersion, ACM stabilised O/W-type nanoemulsion, and ACM stabilised soy milk emulsion were investigated by subjecting these samples to a constant strain of 0.1% for 1 hour, at a frequency of 1 Hz and temperature of

25°C. Time sweep tests were limited to ACM dispersion, ACM stabilised O/W-type nanoemulsions, and African catfish mucus stabilised O/W-type nanoemulsion enriched with soya milk.

3.5.3.5 Data and statistical analysis

The rheological tests were conducted in three replicates and mean and standard deviation of the data were calculated with IBM SPSS version 21 software. Flow curve fitting was conducted using the Microsoft Excel solver function. The rheological parameters were determined by adopting the generalized reduced gradient (GRG2) nonlinear optimization code. The rheological parameters fitted for Power and Herschel-Buckley law were τ the shear stress, (Pa), τ_0 the yield stress, (Pa), K the consistency coefficient (Pa s^n}, and η the flow behavior index (where η = 1 represents Newtonian behavior, η > 1 (shear-thickening) dilatant and η < 1 (Shear-thinning) pseudoplastic Wang et al., 2016; Vadodaria et al., 2018; Kubo et al., 2019; Hentati et al., 2020). The rheological parameters fitted for Bingham and Casson laws were $\boldsymbol{\tau}$ the shear stress (Pa), $\boldsymbol{\tau}_0^B$ the Bingham yield stress (Pa), $\dot{\gamma}$ the shear rate (s^{-1}), η^B the Bingham plastic viscosity (Pa.s), η^C the Casson plastic viscosity (Pa.s),and $(\boldsymbol{\tau}_0^C)^{0.5}$ Casson yield, and $\dot{Y}^{0.5}$ the Casson shear rate (Vadodaria et al., 2018; Kubo et al., 2019) The best fit line was defined by the minimum sum of square errors (SSE) and this was the only criterion used during curve fitting. The goodness of fit, R^2 was calculated as $R^2 = 1 - (SSE/SST)$, where SST is the total corrected sum of squares (Adeyi et al., 2014; Myers et al., 2016; Okuro et al., 2019). The best fit model was selected on the basis of coefficient of determination R^2 and the root mean square error (RMSE) which was calculated using Equation 3.5 (Adeyi et al.., 2014; Dertli et al., 2016).

$$\mathbf{RMSE} = \left[\frac{\sum \mathbf{Y_m - Y_p}}{\mathbf{n}}\right)^{\frac{1}{2}} \qquad \textit{Equation 0.5}$$

Where $\boldsymbol{Y_m}$ is the measured shear stress data value (Pa), Y_p is the predicted shear stress data value (Pa) for each data point and $\boldsymbol{n}$ is the number of observations made.

The flow data for ACM, soy milk, ACM stabilised soya milk emulsion, ACM stabilised O/W-type nanoemulsion, and ACM stabilised O/W-type nanoemulsion enriched with soy milk fiber were evaluated and fitted according to the rheological models of Power, Herschel-Buckley, Bingham and, Casson models (Equations 3.6, Equation 3.7, Equation 3.8, and Equation 3.9).

$$\boldsymbol{\tau} = \mathrm{K}\dot{\mathrm{Y}}^{\boldsymbol{\eta}} \qquad \textit{Equation 0.6}$$

$$\boldsymbol{\tau} = \boldsymbol{\tau}_{\mathbf{0}} + \mathrm{K}\dot{\mathrm{Y}}^{\boldsymbol{\eta}} \qquad \textit{Equation 0.7}$$

Where τ shear stress (Pa) is, τ_0 is yield stress (Pa), $\dot{Y}$ is shear rate (s^{-1}), K is consistency coefficient (Pa s^n) and η is flow behaviour index (where η = 1 represents Newtonian behaviour, η > 1 (shear-thickening) (shear-thickening) dilatant and η < 1 (Shear-thinning) pseudoplastic (Wang et al., 2016; Vadodaria et al., 2018; Kubo et al., 2019; Hentati et al., 2020).

$$\boldsymbol{\tau = \tau_0^B + \eta^B \dot{Y}} \qquad \textit{Equation 0.8}$$

$$\boldsymbol{\tau^{0.5} = \tau(_0^C)^{0.5} + \left(\eta^C\right)^{0.5} \dot{Y}^{0.5}} \qquad \textit{Equation 0.9}$$

Where $\boldsymbol{\tau}$ is the shear stress, the $\boldsymbol{\tau_0^B}$ is the Bingham yield stress, the $\dot{Y}$ is the shear rate (s^{-1}), η^B is the Bingham plastic viscosity (Pa.s), η^C is the Casson plastic viscosity (Pa.s),and $(\boldsymbol{\tau_0^C})^{0.5}$ is Casson yield and $\dot{Y}^{0.5}$ is the Casson shear rate (Vadodaria et al., 2018; Kubo et al., 2019).

The adequacy of the rheological models were checked based on the R^2 and adjusted-R^2. The quality of fit was evaluated by regression coefficient of determination along with an analysis of residuals (Ortiz-Viedma et al., 2018). The fitting ability of the tested rheological models was also appraised by calculating the root mean squared error (RMSE) according to the literature (Rasouli-Pirouzian et al., 2017).

Chapter 4

AFRICAN CATFISH MUCILAGE EXTRACTION, CHARACTERISATION, AND ROLE IN STABILISING SOY MILK EMULSIONS

4.1 Extraction, characterisation, and role of ACM in stabilising soy milk emulsions

This chapter details results and discussion on the results of the research objectives which involved: collecting and preserving African catfish mucilage (ACM) from the African catfish, characterising ACM by determining its physicochemical properties and investigating the effect of African catfish mucilage (ACM) on the stability of soya milk emulsions. My original contribution to knowledge from my research is that the results generated from the extraction of ACM could give the guidelines to enable the fish industry to collect and preserve ACM that could be used as an emulsifier in food-grade emulsions, cosmetic, and drug release products. Also, the results generated on the resuscitation and full recuperation of live fish could give the guidelines for the re-use of live African catfish for collection of ACM. Another original contribution to knowledge from my research is that the knowledge-base collected could result in the guidelines for the application of ACM in food-grade emulsions.

The methodology for this research objective is described in Section 3.3 chapter three. The African catfish mucilage (ACM) was collected and preserved from a fish farm after obtaining ethical clearance Faculty of Engineering. The ACM was collected based on South African Bureau of Standards approved procedures, the Guidelines for Ethical conduct in the care and use of nonhuman animals in research and Ethical considerations for field research on fishes (SABS, 2008; Dunbar et al., 2012; Bennett et al., 2016).

4.2 Results and discussion

4.2.1 African catfish recuperation

After the collection of ACM, the live African catfish were resuscitated and none of the live fish died. All the African catfish sampled fully recovered within three hours. The live fish were observed for five days and it was noted that the methanesulfonate used as anesthesia was excreted from the skin and the gills of the fish into the water. The water in the recuperation bath was changed every day and by day 4 there were no traces of the methanesulfonate in the water. It was vital to observe the fish sampled to ensure that the methanesulfonate was not present on the catfish skin or tissues as the catfish could be harvested and sold for consumption. The catfish sampled were not harvested until two weeks after methanesulfonate was excreted out

of the catfish system. In addition, the same fish samples could be used to further collect fresh ACM samples.

4.3 Structural characteristics of African catfish mucilage

Unmagnified freeze-dried African catfish mucilage (ACM) was found to be greyish-brown with a powdery appearance as shown in **Error! Reference source not found.**1 Freeze-dried frican catfish mucilage in MilliQ

Figure 0.1: Structural characteristics of unmagnified ACM

water formed a gel aggregate of fibrous material. Figure 4.1 shows the photographic image of the dispersion of freeze-dried ACM, and TEM images of ACM at 0.2 micrometre. Structure studies with the transmission electron microscope revealed that the ACM dispersion is spherical and forms aggregate networking into gel fibers (Figure 4.2). It was also observed that the ACM contained filamentous thread-like fibers. The particle size of ACM measured under TEM analysis and Zetasizer was 73-80 nm. The freeze-dried African catfish mucilage (Figure 0.2), was found to entrap the MilliQ water and formed a dilute hydrogel that was adhesive (Böni et al., 2016a; Böni et al., 2016b). The TEM image of African catfish mucilage in MilliQ water (Figure 0.2), show intermediate filaments which entrap MilliQ water. The formation of intermediate filaments and elastic gel-like stable structure (Figure 4.2), agrees with results obtained in TEM investigations of Atlantic and Pacific hagfish mucus as reported by other authors (Fudge & Schorno, 2016; Böni et al., 2017).

4.3.1 Structural characteristics of ACM stabilised soy-milk emulsion

Transmission electron microscopy (TEM) imaging of soy milk emulsion stabilised with ACM

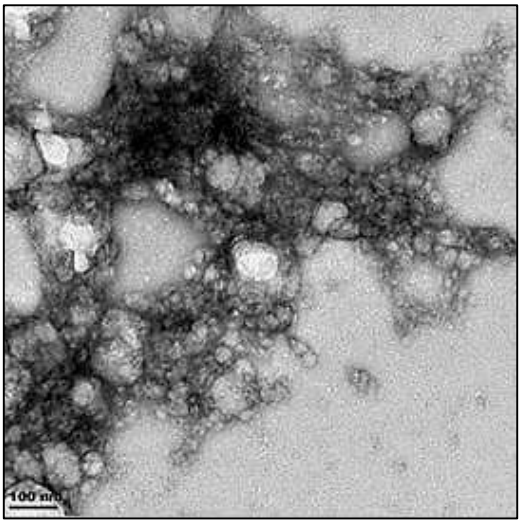

Figure 0.2: Structural characteristics of ACM at 0.2 micrometer

was investigated with concentrations of 30% and 50% (w/v) soy-milk to 3% and 5% concentrations of ACM (Figure 0.3). Figure 0.3a and Figure 0.3b depict the TEM Images of ACM stabilised soy-milk emulsion with ACM-emulsifier soy milk ratio (ESMR) of 3:30, and 5:30 % at 50 nm. The images show the encapsulation of the soy-milk emulsion by the ACM to form a cohesive aggregate structure. Encapsulation was achieved when the emulsions were formulated through high shear homogenization. Furthermore, the images show that aggregates of thread-like filamentous fibers of ACM encapsulate the soy milk emulsion leading to the bridging and flocculation of the soy milk emulsion. Figure 0.3c and Figure 0.3d show the TEM Images of ACM stabilised soy-milk emulsion with ACM-emulsifier soy milk ratio (ESMR) of 5:30, and 5:50% at 50 nm respectively. In the same way, the images show the encapsulation of the soy-milk emulsion by the ACM to form a cohesive aggregate structure. The particle size measured for ACM stabilised soy-milk emulsion with ESMR 3:30 % (w.v) was 118-120 nm while that for 5:30 % (w/v) was between 113-115 nm. The particle size measured for ACM stabilised soy-milk emulsion with ESMR 5:30 % (w.v) was 176-178 nm while that for 5:50 % (w/v) was between 172-174 nm. The trend followed was the higher the concentration of ACM the lower the particle size of ACM stabilised soy-milk emulsion. Hence, the ESMR influences the particle size of the emulsions and the trend is the higher the ESMR the lower the particle size. Also, the TEM images obtained for both emulsions showed that the soy-milk emulsion was encapsulated by the ACM to form a cohesive aggregate raw structure. Thus, encapsulation of the soya-milk stabilised emulsion could be a result of the ACM potential to adhere to the soy milk emulsions' droplets which induces a kind of cohesive interaction and confers stability as suggested by (Böni et al., 2016b). Encapsulation was achieved by high shear hmogenisation of soymilk globules which resulted in low particle size. ACM adsorbs at the soymilk/water interface resulted in ACM stabilized soymilk emulsions.

Even though automated and rheological analysis have been used to depict that biopolymers could be mucoadhesive, studies have revealed that the analysis of spectrum and image analysis could be used to establish the bio-adhesive properties of mucus based

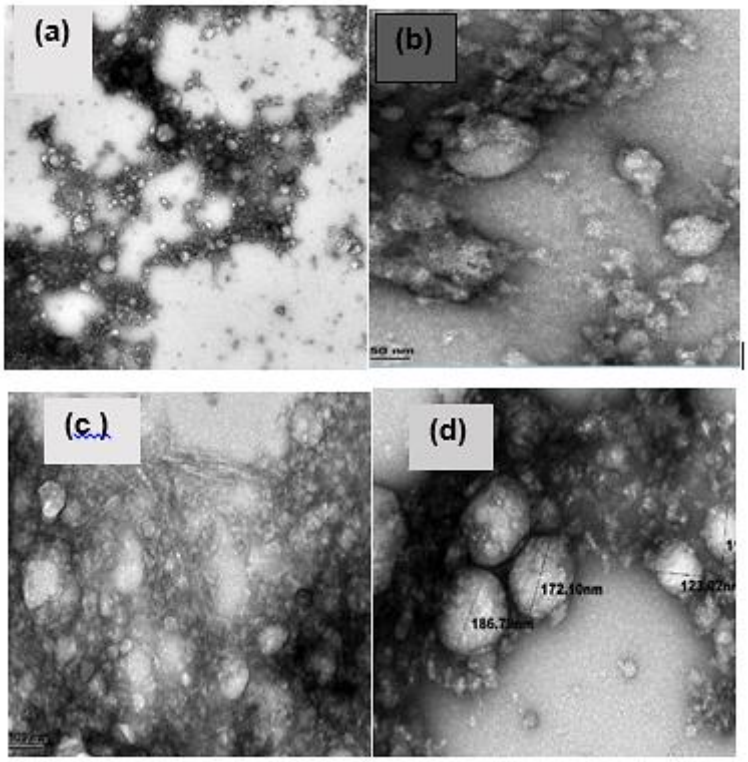

Figure 0.3: Structural characteristics at 50 nm magnification for ACM-emulsifier soy-milk ratio (a) 3:30 % with thread like-fibers (b) 5:30 % (c) 3:50 % (d) 5:50 %.

bio-polymers (Albaldawi, 2015; Mahdizadeh Barzoki et al., 2016). 'The ACM contains amphiphilic filamentous threads that stabilises the network structure of stabilised emulsions. However, this stabilisation does not occur in every part of the matrix hence the stability is preferential as seen in Figure 4.3. It is more pronounced with stabilised emulsions having EOR of 5:30 and 5:50 % as they are more stable than emulsions containing 3 % ACM concentration. TEM imaging results of ACM stabilised soy milk emulsions revealed a form of entrapment by which the mucins in the African catfish entrapped and adhered to the droplets of the soy milk emulsion to confer stability.

4.3.2 Functional group characteristics of freeze-dried ACM

Several authors have reported that Attenuated Total Reflectance-Fourier transform infrared (ATR-FTIR) spectroscopy is a good tool to determine the functional groups of biopolymers (Staniszewska et al., 2014; Moghaddam et al., 2017). Attenuated Total Reflectance-Fourier transform infrared spectroscopy was employed in analyzing the functional groups of

unprocessed ACM (Table 0.1 and Figure 0.). The ATR-FTIR spectra of freeze-dried African catfish mucilage showing the wavelength peaks in the range 4000-400 cm^{-1} with the focal functional group are presented in Figure 0.. Table 0.1 also shows the focal functional groups in freeze-dried African catfish mucilage. Twelve vital absorption peaks were observed from the spectrum of ACM (Table 0.1). The peaks at 3301 and 3080 cm^{-1} were designated to stretching vibrations of hydroxyl groups of hydrophilic amino and defined aromatic overtone that may be due to aromatic amino acids(Choo et al., 2016; Trapella et al., 2018). The peak at 2958 cm^{-1} could be attributed to CH_2, [1] could be attributed to the C—H symmetric and

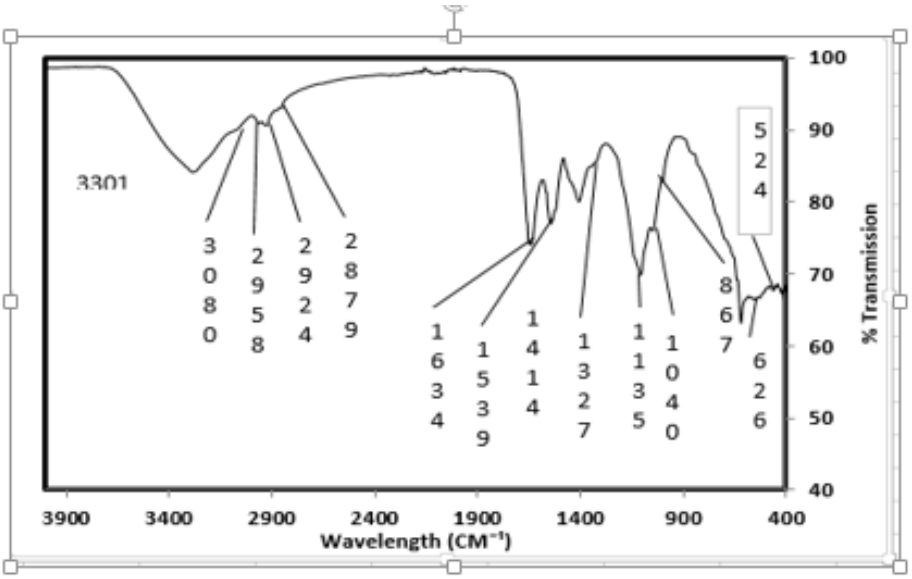

Figure 0.4: ATR-FTIR spectra of raw freeze-dried ACM

antisymmetric stretching vibrations in CH_2 ascribed to pyranose rings which point to aliphatic (—CH) chains in the mucilage (Angulo & do Amaral Sobral, 2016). The peaks at 1634 and 1539 cm^{-1} could be as a result of amide stretch, from ß-sheets absorption bands (Amide I bands) and aromatic C=C bending or C=C stretch in the ring (Amide II) (Pellegrini, et al., 2016; Trapella et al., 2018). The peak at 1414 cm^{-1} represents a C—O of carboxyl COO group accepting zero or one H-bond or O—H (alcohols) bend while the peak at 1136cm^{-1} could represent anti-symmetric C—O—C glycoside bond, C—O strong bond stretch (Tabrizi et al., 2016; Fernando et al., 2017). The peak at 1040 cm^{-1} is ascribed to a primary amine stretching, secondary R-carbon of amino acids for glycoprotein or mucus while the peak at 867 cm^{-1} represents C—H out of plane bending (Lewis et al., 2013; Balasubramanian et al., 2016)Also, the peaks at 626 cm^{-1} are attributed to CH vibrating bends in RC=CH sites while peaks at 524 cm^{-1} are linked to S—S disulfide stretch in biopolymers with proteins and collagen (Balasubramanian et al., 2016; Monaghan et al., 2018). The presence of amide A (N—H) stretching vibration found at around 3301 cm^{-1}, amide I at 1634 cm^{-1}, and amide II near 1539

cm^{-1} in ACM suggests the presence of α helix with ß-turns (Glassford et al., 2013). Authors have. reported that although, amide I, II, and III bands could be used to affirm protein secondary structure, FTIR investigations of amide I give better results as it is most responsive to changes in conformation and establish the presence of peptide bonds. (Glassford et al., 2013). The peak of amide I occurs as a result of stretching vibration of C—O bonds and N–H bending while C—H stretching vibration is responsible for the amide II band (Glassford et al., 2013; Lewis et al., 2013). In the same way, studies by other authors revealed that amide I bands were found in the range 1600-1700 cm^{-1} with bands that show C—O stretching vibrations of protein-peptide bonds which is consistent with the results obtained in the ACM (Sarroukh et al., 2013). The distinctive absorption bands of 3301 cm^{-1}, 1634 $cm^{-1}$and 1539 cm^{-1}in the ACM designates the presence of peptide bonds (Lewis et al., 2013; Sarroukh et al., 2013, Trapella et al., 2018).

African catfish mucilage also showed wavelength peaks of 1136 cm^{-1}, which suggested the possibility of anti-symmetric glycoside bond, C—O strong bond stretch. Several authors investigated the physicochemical characteristics of glycoprotein present in green algae and suggested that asymmetric stretch of bonds with intense bands around 1130 cm^{-1} could be used to identify glycosidic linkages (Lewis et al., 2013; Chylińska, Szymańska-Chargot, & Zdunek, 2016; Fernando et al., 2017; Tabrizi et al., 2016). Furthermore, FTIR analysis of brown algae polysaccharides indicated peaks around 1,135 cm^{-1} which are characteristics of vibrational stretches of the glycosidic C—O group of biopolymers. The authors stated further that broad peaks in the range 1,120-1,270 cm^{-1} pointed to S═O stretch for molecular branches of alginic acid or fucoidan (Lewis et al., 2013; Fernando et al., 2017). Hence, the wavelength peak of 1136 cm^{-1} recorded in the spectra of raw FTIR spectra of ACM could be attributed to the anti-symmetric glycoside bond. Several authors have established that the presence of the glycosidic bond in glycoproteins is the reason why a glycan can covalently attach to polypeptide side-chains and form stable structures that are suitable for biological processes (Lamriben et al., 2016; Varki et al., 2017; Xie et al., 2017). It can be inferred that the raw FTIR spectrum of African catfish mucilage probably has glycosidic linkages similar to other glycoproteins. Hence the presence of glycosidic linkages in ACM is similar to that found in other glycoproteins that have the potential of stabilising emulsions by covalently bonding with polypeptide side chains to form stable structures in emulsions in agreement with the authors (Lamriben et al., 2016; Varki et al., 2017; Xie et al., 2017).

Table 0.1: Functional groups of freeze-dried African catfish mucilage

Wave number (cm^{-1})	Band assignment	References
3301	Broad peak stretching vibrations of hydroxyl groups of hydrophilic amino acids	(Choo et al., 2016)
3080	Defined aromatic overtone, due to aromatic amino acids	(Trapella et al., 2018)
2958	Mucus/glycoprotein CH_2 out of plane vibration	(Reneeta et al., 2018)
2924	CH_2 symmetric and out of plane vibration	(Angulo and do Amaral Sobral, 2016)
1634	Amide stretch, β-sheets absorption bands; Amide I	(Pellegrini, et al., 2016)
1539	Aromatic C=C bending or C=C stretch in a ring ; Amide II	(Trapella et al., 2018)
1414	C-O of carbonyl COO group accepting zero or one H-bond	(Fernando et al., 2017)
1136	Anti-symmetric C-O-C glycoside bond; C-O strong bond stretch;	(Tabrizi et al., 2016)
1040	Mucus/glycoprotein primary amine stretch or secondary R-carbon of amino acids	(Lewis et al., 2013)
867	C-H out of plane bending	Balasubramanian et al., 2016)
626	C-H bending vibration of RC=CH	(Balasubramanian et al., 2016, Monaghan et al., 2018)
524	S-S disulfide stretch in collagens and proteins	(Monaghan et al., 2018)

4.3.3 Functional group characteristics of ACM stabilised soy-milk emulsion

The ATR-FTIR spectra of Soya-milk emulsion stabilised with freeze-dried African catfish mucilage showing the wavelength peaks in the range 4000-400 cm^{-1} with the focal functional groups are shown in Figure 0.5. Also, Table 0.2 compares the wavelength peak changes noted in ACM with the ACM stabilised soya-milk emulsions The shift in the amide I at 3336 cm^{-1} is similar to the stretching vibrations of hydroxyl groups of hydrophilic amino in the spectra of raw ACM however; the peak is much wider and profound (Table 0.2). This might have occurred as a result of interactions between the hydroxyl groups of hydrophilic amino groups in ACM that interact with soy milk.

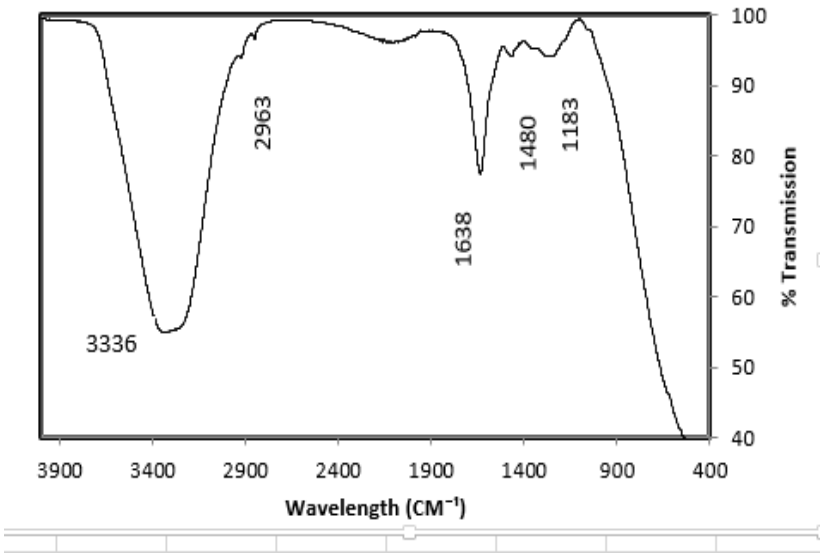

Figure 0.5: ATR-FTIR spectra of ACM stabilised soy milk emulsion

Similarly, the peak at 2924 cm^{-1} in ACM which was ascribed to CH_2 symmetric and antisymmetric stretching vibrations shifted to a peak 2963 cm^{-1} in the ATR-FTIR spectra of Soya-milk emulsion stabilised with freeze-dried ACM (Table 0.2).

Table 0.2 shows that the shifts for ACM stabilised soy milk emulsions were observed for amide I at 1638 cm^{-1}, C—O of carboxyl COO group accepting zero or one H-bond at 1480 cm^{-1} and anti-symmetric C—O—C glycoside bond, C—O strong bond stretch at 1183 cm^{-1}. This phenomenon was described by (Angulo & do Amaral Sobral, 2016) in the study of changes in the chemical composition of aloe vera and snail mucus composite scaffold using ATR-FTIR spectroscopy The higher wavelength bands for functional groups of amide A, amide I, C—O of carboxyl, COO group accepting zero or one H-bond, CH_2 symmetric and antisymmetric stretching vibrations and anti-symmetric C—O—C glycoside bond observed in the spectra of ACM stabilised soy milk emulsions in (Figure 0.5 and Table 0.2) might suggest a type of bonding that leads to a stable structure. This is consistent with results observed in TEM images of ACM stabilised soya-milk emulsion (Figure 0.3).

4.3.4 Stability of freeze-dried African catfish mucilage in MilliQ water using Zeta potential

Zeta potential is a vital tool that could be used to evaluate if an emulsifier can stabilise dispersions or emulsions. It depicts the potential charge in the boundary double layer at the droplet boundary of the continuous and dispersed phases (Cheong et al., 2016; Zhai et al., 2018). The absolute zeta potential of freeze-dried African catfish mucilage in MilliQ water was -36.2

Table 0.2: Comparison of the wavelength peak changes noted in ACM with the ACM stabilised soya-milk emulsions

Wave number ACM (CM^{-1})	**Wave number soy milk stabilised emulsion (CM^{-1})**	**Band assignments**	**References**
3301	3336	Possible broad peak stretching vibrations of hydroxyl groups of hydrophilic amino acids	(Angulo & do Amaral Sobral, 2016; Choo et al., 2016)
2958	2963	Possible mucus/glycoprotein CH_2 out of plane vibration	(Angulo & do Amaral Sobral, 2016, Reneeta et al., 2018)
2924	2963	Possible CH_2 symmetric and out of plane vibration	(Angulo and do Amaral Sobral, 2016)
1634	1638	Possible Amide stretch, β-sheets absorption bands; Amide I	(Angulo & do Amaral Sobral, 2016; Pellegrini, et al., 2016)
1414	1480	Possible C-O of carbonyl COO group accepting zero or one H-bond	(Angulo and do Amaral Sobral, 2016, Fernando et al., 2017)
1136	1183	Anti-symmetric C-O-C glycoside bond; C-O strong bond stretch;	(Angulo and do Amaral Sobral, 2016, Tabrizi et al., 2016)

mV at a pH of 7.83. Hence, sufficient repulsion exists between the droplets of the African Catfish mucins and MilliQ water to keep particles away from each other. Published works propose that a dispersion becomes stable if its zeta potential is more than ± 30 mV (Konkena & Vasudevan, 2012; Sankhla et al., 2016; Zhai et al., 2018). Stability is a result of static electrical repulsive forces between the particles hence the dispersion does not form aggregates because the absolute zeta potential is more than ± 30 mV (Nieto de Castro et al., 2017; Zhai et al., 2018). Hence African Catfish mucilage has the potential to stabilise emulsions.

4.3.5 Stability of ACM stabilised soy milk emulsions

Figures 4.6, 4.7, 4.8, and 4.9 show the changes in the stability of twelve ACM stabilised soy milk emulsions for 10, 30, 50, and 75 % soy milk with ACM concentrations of 1, 3, and 5 % respectively. Only the backscattering (BS) % flux for the ACM stabilised soy milk emulsions with ACM-emulsifier soy milk ratios (ESMR) of 1:50, 3:50 and 5:50 % was significant *p*-value < 0.05. The BS % flux for ACM stabilised soy milk emulsions with ESMR of 1:10, 3:10, 510, 1:30,3:30, 5:30 1:75, 3:75 and 5:75 % were not significant. The BS % flux as a function of stability was higher with 75 % soy milk than 50, 30, and 10 % respectively. For instance, the effect of 5 % concentration of ACM on 10, 30, 50, and 75 % soy milk was 35.7 ± 0.2, 46.4 ± 0.2, 55.4 ± 0.2, and 78.5 ± 0.2 %, respectively (Figure 0., Figure 0., and Figure 0.). In the same vein, ACM concentrations of 1 and 3 % had the same effect on 10, 30, 50, and 75, % soy milk Figure 0.6, Figure 0., Figure 0., and Figure 0.). For instance, the effect of 3 % ACM on 10, 30, 50 and 75 % soy milk was 31.8 ± 0.1, 36.3 ± 0.1, 43.8 ± 0.2, and 73.9 ± 0.2 % respectively (Figure 0.6, Figure 0., Figure 0., and Figure 0.). Also, the effect of 1 % ACM on 10, 30, 50, and 75 % soy milk was 20.4 ± 0.2, 28.4 ± 0.1, 41.4 ± 0.1, and 65.3 ± 0.2 %, respectively (Figures 4.6, 4.7, 4.8, and 4.9).

Although the stability of soy milk emulsions with 75 % was higher than that of 10, 30 and 50 % respectively further analysis on 75 % soy milk emulsions was discontinued to showcase the effect of ACM when the concentration of water was at least 45 % (Figure 0.6, Figure 0., Figure 0., and Figure 0.). Table 0.3 shows the effect of ACM on the stability of soy milk emulsions. Hence the higher the concentration of ACM the higher the stability (backscattering flux percentage) of the emulsions no matter the concentration of soy milk (Table 0.3 and Figure 0.6, Figure 0., Figure 0., and Figure 0.). Also, the ESMR influenced the stability of the emulsions, and the higher the ESMR the higher the stability of the emulsions as evidenced by BS flux %. To confirm if the stability (BS % flux) of the emulsions could be attributed to the ACM, the effect of homogenized mixtures of soy milk and MilliQ water emulsions were investigated with the Turbiscan to serve as a control Figure 0. shows that all emulsions

containing only homogenized soy milk 10, 30, 50, and 75 mL (w/v) and MilliQ water were unstable without the addition of ACM. This confirmed the role of ACM as an emulsifier. Based on stability tests for soy milk emulsions it is evident that the stability as a function BS % flux profile could only be attributed to the effect of African catfish mucilage which served as an emulsifier in the emulsion.

Error! Reference source not found. compares the particle sizes of 50 % soy milk emulsions tabilised with 1, 3, and 5 % ACM in terms of the Sauter mean diameter ($D_{(3,2)}$) and its standard deviation. Authors have

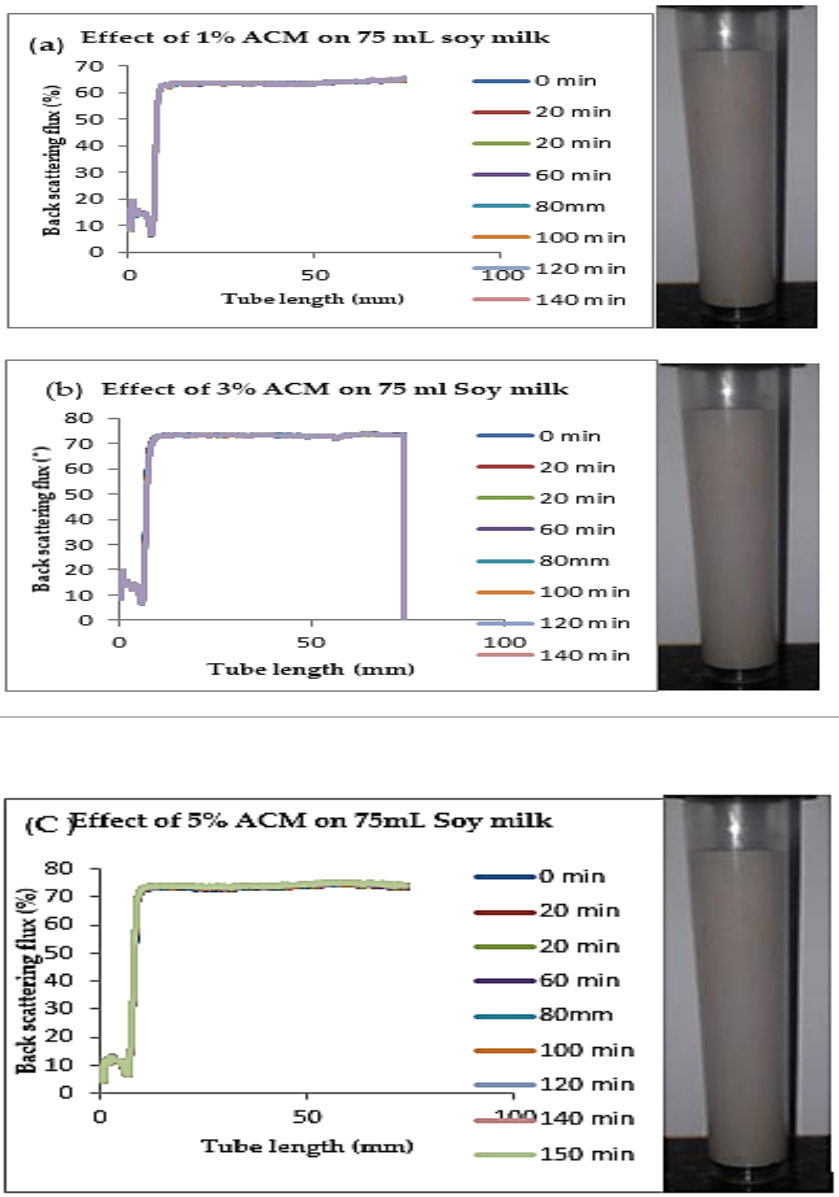

Figure 0.6: Changes in stability of ACM stabilised soy milk emulsions with emulsifier Soy milk ratios of (a) 1:75 % w/w (B) 3:75 % w/w (C) 5:75 % w/w.

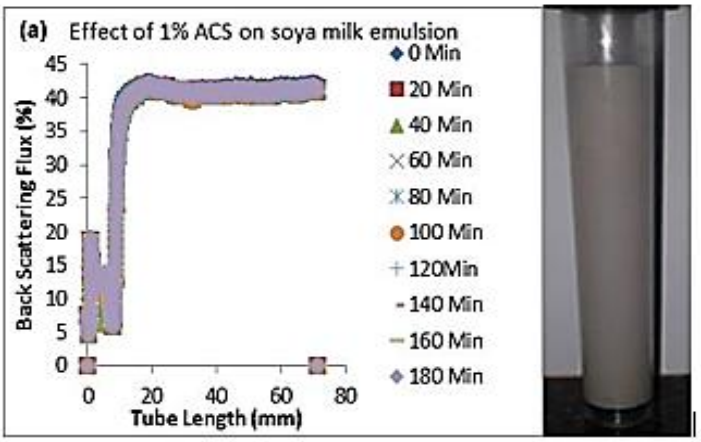

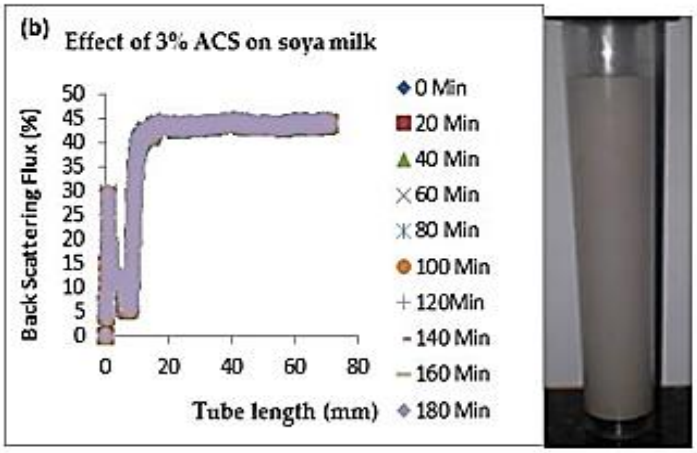

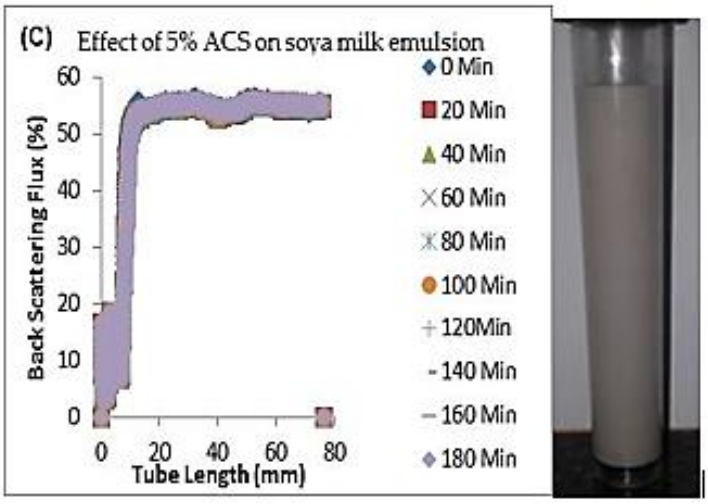

Figure 0.7: Changes in stability of ACM stabilised soy milk emulsions with emulsifier Soy milk ratio (a) 1:50 % w/w (B) 3:50 % w/w (C) 5:50 % w/w.

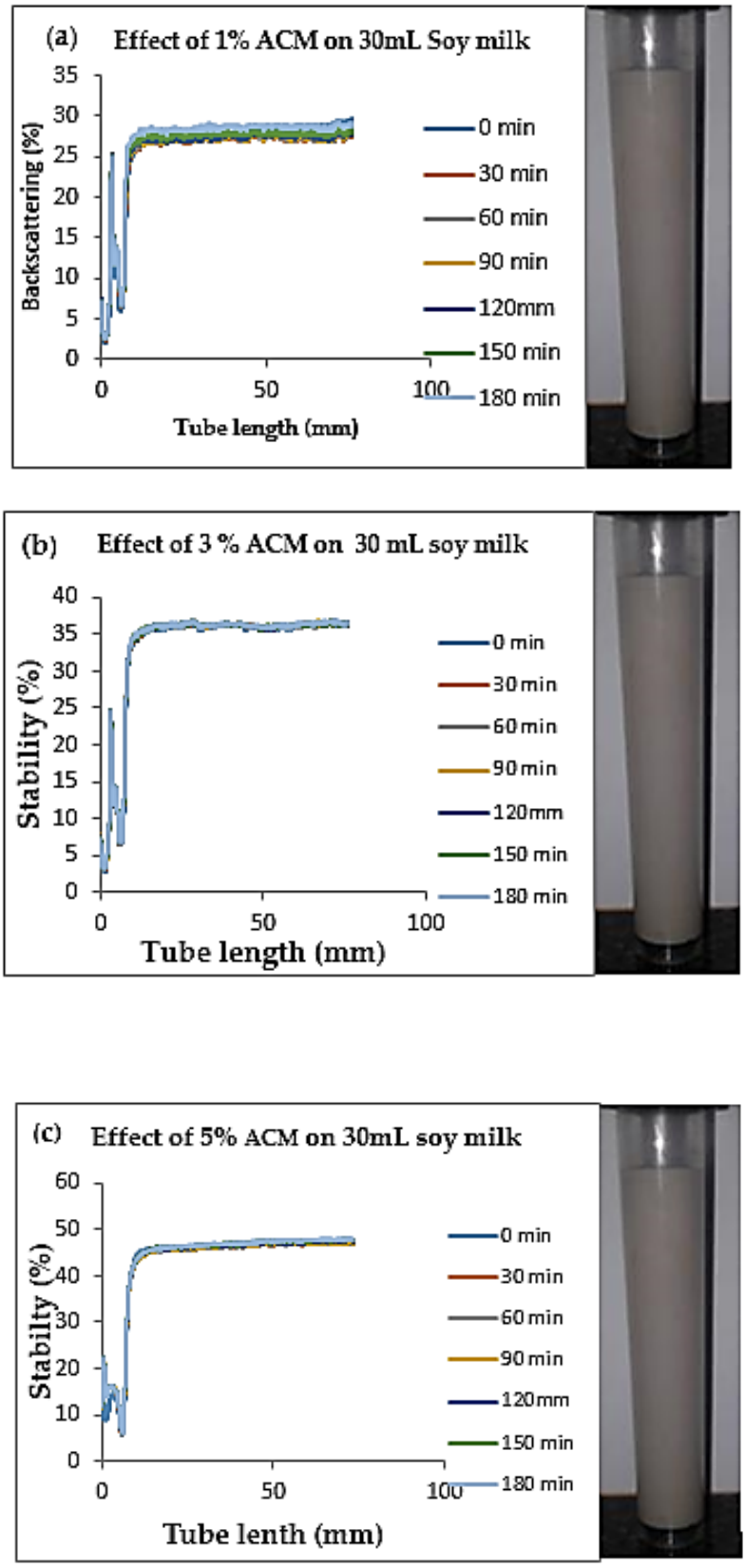

Figure 0.8: Changes in stability of ACM stabilised soy milk emulsions with emulsifier Soy milk ratio (a) 1:30 % w/w (B) 3:30 % w/w (C) 5:30 % w/w.

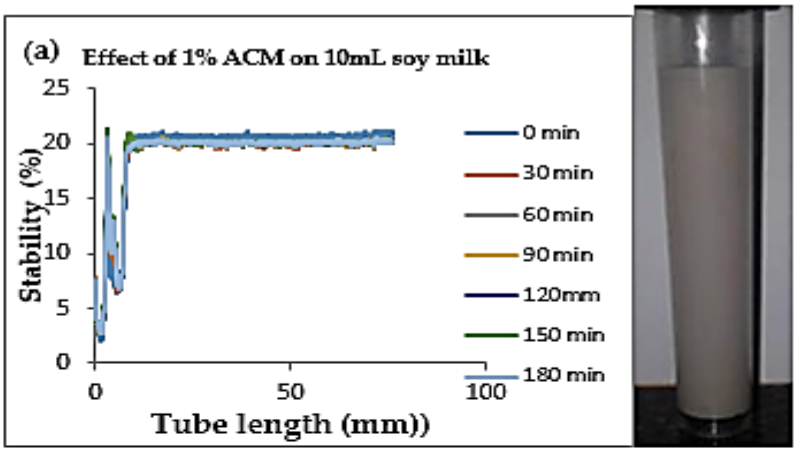

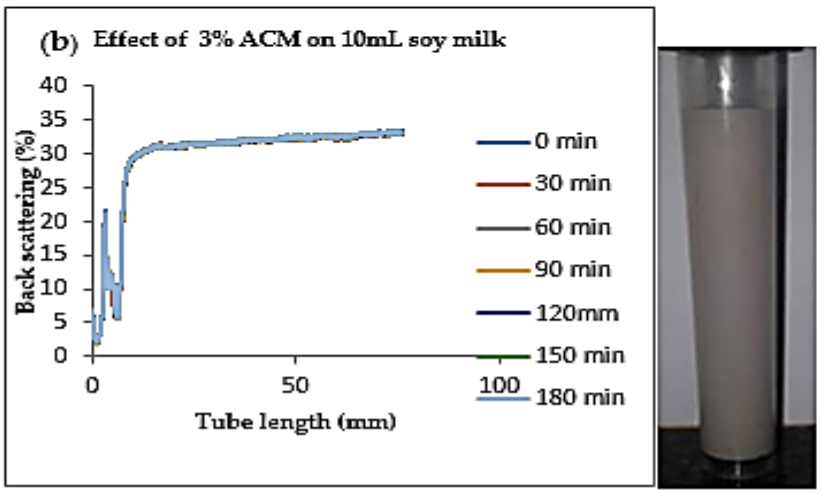

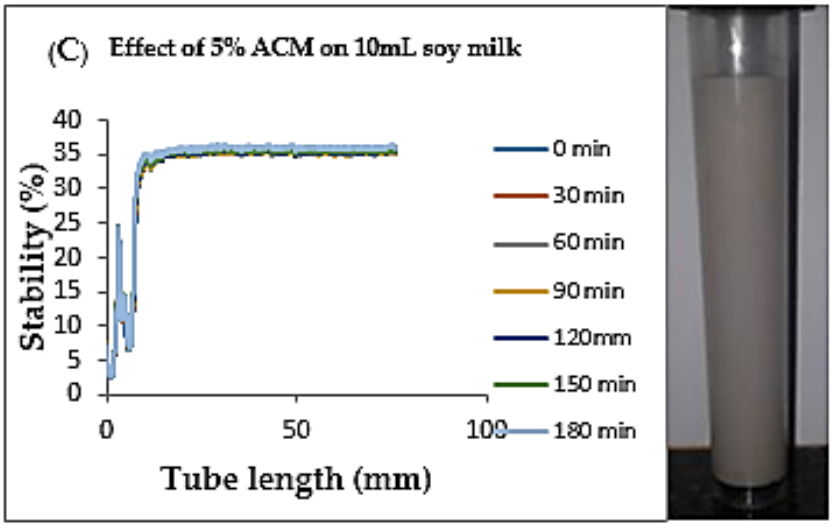

Figure 0.9: Changes in stability of ACM stabilised soy milk emulsions with emulsifier Soy milk ratio (a) 1:10 % w/w (B) 3:10 % w/w (C) 5:10 % w/w

.

Table 0.3: Effect of ACM on the stability of soy milk emulsions [a. b]

ACM (%)	Soy milk (%)	Water (%)	pH	$D_{(3,2)}$ (nm)	Stability (%)
1	50	49	7.85	179.2 ± 1.0[a]	41.4 ± 0.1[a]
3	50	47	7.92	176.1 ± 0.9[b]	43.8 ± 0.2[b]
5	50	45	7.95	172. 9 ± 0.6[c]	55.4 ± 0.2[c]
1	30	69	7.72	123.3 ± 0.7	28.4 ± 0.1
3	30	67	7.84	118.1 ± 0.5	36.3 ± 0.1
5	30	65	7.86	113.6 ± 0.3	46.4 ± 0.2
1	10	89	7.65	106.2 ± 1.0	20.4 ± 0.2
3	10	87	7.71	103.1 ± 0.8	31.8 ± 0.1
5	10	85	7.79	100.3 ± 0.6	35.7 ± 0.2

[a]Values are means ± standard deviations from 5 replicates.

[b]Indicated values within a column are significantly different (*p*-value < 0.05]

[c]$D_{(3,2)}$ is Sauter mean diameter**.**

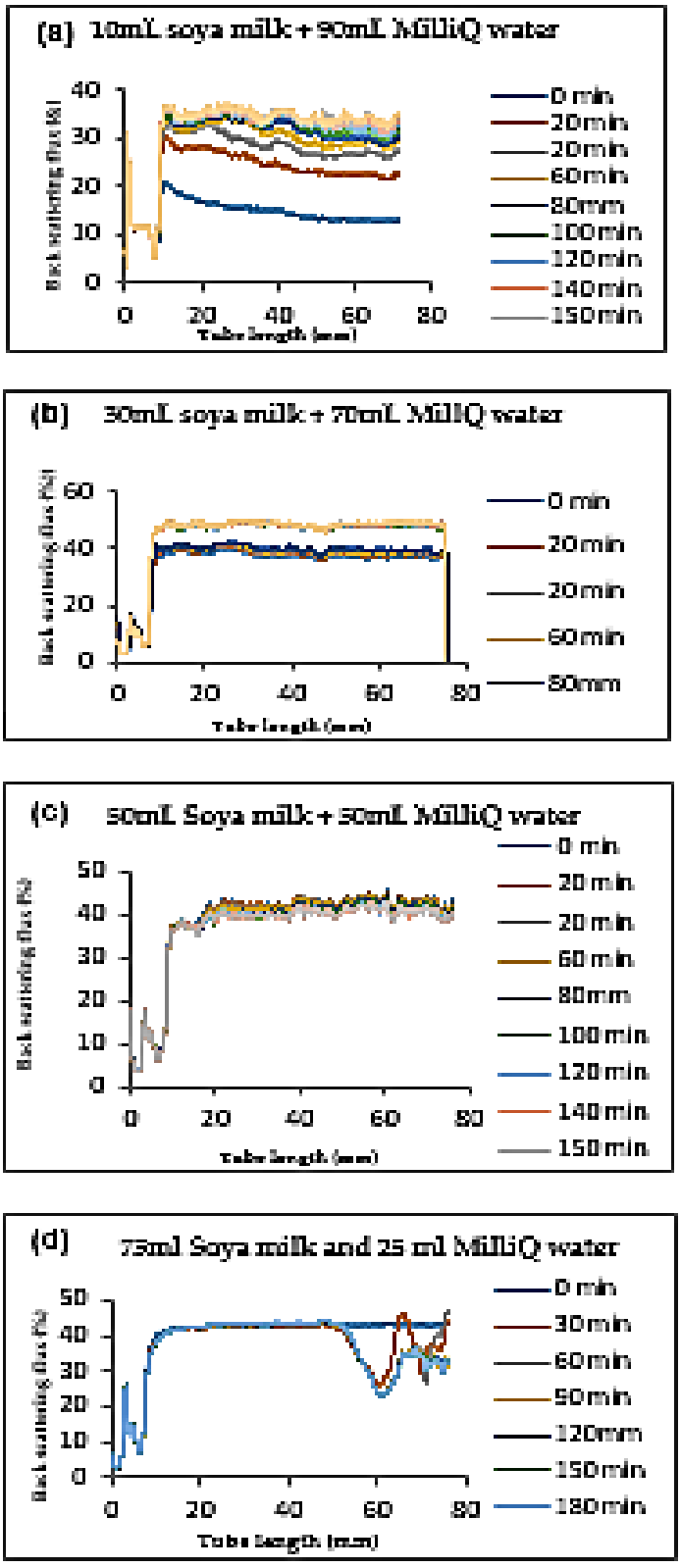

Figure 0.10: Instability in homogenized soy milk and MilliQ water for (a) 10. (b) 30 (c) 50, and (d) 75 % (w/v) soy milk emulsions

established that the lower the particle size the more stable an emulsion becomes (Adeyi et al., 2014; Maphosa et al., 2017). An increase in ACM concentration led to a decrease in $D_{(3,2)}$ of soy milk oil droplets for emulsions containing 50 % soy milk. The $D_{(3,2)}$ of the three emulsions formulated from 50 % soy milk and stabilised with ACM concentrations of 1. 3 and 5 % were 179.2 ± 1.0, 176.1 ± 0.9, and 172. 9 ± 0.6 nm respectively (Table 0.3 and Table 0.4). Hence the higher the concentration of ACM the more stable the emulsion (low $D_{(3,2)}$ of soy milk droplets).

Similarly, the $D_{(3,2)}$ of the three emulsions formulated from 30 % soya milk and stabilised with ACM concentrations of 1. 3 and 5% were 123.3 ± 0.7, 118.1 ± 0.5, and 113.6 ± 0.3 nm respectively (Table 0.3). In the same vein, the $D_{(3,2)}$ of the three emulsions formulated from 10 % soya milk and stabilised with ACM concentrations of 1. 3 and 5% were 106.2 ± 1.0, 103.1 ± 0.8, and 100.3 ± 0.6 nm respectively (Table 0.3). The smallest $D_{(3,2)}$ was found in emulsions stabilised with ESMR of 5:10 % (100.3 ± 0.6 nm), 5:30 % (113.6 ± 0.3 nm) and 5:50 % (172. 9 ± 0.6 nm) (Table 0.3 and Table 0.4). Literature supports the claim that the most physically stable emulsion has the lowest $D_{(3,2)}$ (Maphosa et al., 2017). Hence the trend followed was the higher the concentration of ACM, the more stable the emulsion i.e. the lower the $D_{(3,2)}$ of stabilised emulsions (Table 0.3 and Table 0.4). Also, the higher the ESMR the higher the stability i.e. the lower the $D_{(3,2)}$ of stabilised emulsions (Table 0.3 and Table 0.4). These observed results are in agreement with stability results as a function of backscattering % flux in Figure 0.6, Figure 0., Figure 0., and Figure 0.. The results also showed that the mean $D_{(3,2)}$ and stability (BS flux % and $D_{(3,2)}$) of ACM stabilised emulsions with ESMR of 1:50, 3:50, and 5:50 % was significantly different *p*-value < 0.05 (Table 0.3 and Table 0.4). Hence, the soy milk emulsions containing 50 % and stabilised with 5 % ACM (ACM-ESMR 5:50) were selected to showcase the rheological properties of the emulsion.

Table 0.4: Effect of ACM on the stability of soy milk ***emulsions*** [a, b, c, and d]

Concentration of ACM (%)	**Concentration of soy milk (%)**	**Concentration of water (%)**	**$D_{(3,2)}$ (nm)**	**BS % flux**
1	50	49	179.2 ± 1.0[a]	41.4 ± 0.1[a]
3	50	47	176.1 ± 0.9[b]	43.8 ± 0.2[b]
5	50	45	172. 9 ± 0.6[c]	55.4 ± 0.2[c]

[a]Indicated values are reported as means ± standard deviation (n = 5). Si
[b]Indicated values within a column are significantly different (*p*-value < 0.05]
[c]D(3,2) is the Sauter mean diameter; [d]BS % flux-Backscattering percentage flux.

The impact of ACM concentration on the particle size of an emulsion can also be revealed by changes in the particle size distribution of the emulsion as a function of the width of the

distribution. Several authors have computed the width of distribution i.e. standard deviation as a variance of the mean diameter of droplets in the diffuse state (Dokić et al., 2012; McClements, 2015). Table 0.3 and Table 0.4 presents the changes in the standard deviation of values of the particle size, dependent upon the ACM amount used to stabilise the emulsions.

Changes in backscattering flux percentage (BS % flux) as a function of tube length of emulsion containing 50 % (w/w) soy milk stabilised with (a) 1 % w/w (B) 3 % w/w (C) 5 % w/w African catfish mucilage after 180 mins were investigated as depicted in Figure 0.. Emulsion stability alludes to an emulsions' capacity to withstand changes in its physicochemical characteristics through time (Nieto de Castro et al., 2017). Due to the turbid appearance of all ACM stabilised emulsions after rapid stability tests, the analysis of the distinct backscattering characteristics of ACM stabilised soy milk emulsions as a function of tube magnitude were carried out to ascertain the stability of the system at room temperature (20 °C). The BS % flux for each concentration are presented in Figure 0.. The initial average BS % flux for ACM stabilised emulsions with ESMR of 1:50, 3:50, and 5:50 % were 41.4 ± 0.1 %, 43.8 ± 0.2 %, and 55.4 ± 0.2 % respectively. It was observed that the BS % flux of all emulsions investigated depended greatly on the concentration of ACM in agreement with reports by (Maphosa et al., 2017; Nieto de Castro et al., 2017). Literature studies have established relationships between the BS % flux and particle size for Bambara groundnut flour stabilised emulsions (Adeyi et al., 2014). Studies have shown that the BS % flux depicts the arrangement of molecules before it becomes unstable hence a high percentage in BS % flux infers a more stable structure (Maphosa et al., 2017).

In Figure 0., Figure 0., and Figure 0. the tube length is plotted on the x-axis while the BS % flux is plotted on the y-axis. It shows that all nine emulsions conformed to similar disintegration modes but, scans did not ideally align as slightly lower percentages in BS % flux were noted along the tube (Figure 0., Figure 0., and Figure 0.). The observed slightly lower percentages in BS flux % as emulsions disintegrate when particles aggregate could be as a result of kinetic instability. In all the three ACM stabilised soy milk emulsions, a peak was observed within the 0-20 mm range, followed by a stable phase within the 20-40 mm range, then a slight lowering within the 40-60 mm range and a final stage of rest within the 60-80mm range. All the ACM stabilised soy milk emulsions formed a cohesive network which suggests that the ACM stabilises emulsions through a different entrapment interaction as described for hagfish mucus stabilised soy milk emulsions by Böni et al. (2016b). The results also suggest that the ACM has the potential to emulsify emulsions even with low concentrations and form a cohesive interactive network as described by Böni et al. (2016b). The authors stated that a 1% concentration of hagfish mucus was able to stabilise soy milk emulsions as a result of a

different entrapment interaction called mucoadhesion (Böni et al., 2016b). The average initial BS flux % of 55.4 ± 0.2 % exhibited by the ACM stabilised soy milk emulsions with ESMR of 5:50 in comparison with other concentrations with ESMR of 1:50 (41.4 ± 0.1 %) and 3:50 (43.8 ± 0.2 %) showed that higher concentrations of ACM could lead to better stability. To better understand the stability kinetics of ACM stabilised soy milk emulsions, an evaluation of differences in BS flux % within the 20– 40 mm range over time was conducted using a Two-way analysis of variance. The effect of ACM on the stability of soy milk emulsions using two-way ANOVA on initial BS flux (%) and $D_{(3,2)}$ (nm) is presented in Tables 4.5 and 4.6 respectively. The selected data points on BS flux % within the 20– 40 mm range overtime was compared with particle size to decipher the best-fit predictor of stability in ACM stabilized soy milk emulsions. The goodness-of-fit was assessed using the coefficient of determination (R^2) to establish which effect was more significant in the response to stability between particle size and initial BS flux %. Two-way Analysis of variance (ANOVA) subsequent to Tukey's multiple comparisons (TMC) test was performed using GraphPad Prism version 5.00 for Windows to evaluate whether the stability as a function of initial BS flux or the $D_{(3,2)}$ as a function of particle size (nm) better explained the stability characteristics of the ACM soy milk stabilized emulsions. A significant difference ($p < 0.05$) was established on all three ACM soy milk stabilized emulsions with respect to BS flux % and particle size at pH range 7.85-7.95. The F statistic of BS flux % was 5078 while the F statistic of particle size was 27 (Table 4.7). This result implies that the means in both responses i.e. BS Flux % and particle size significantly responded to concentrations of ACM. This establishes that we can reject the null hypothesis that ACM concentrations would not affect or enhance the stability of ACM soy milk emulsions. Furthermore, the adjusted P-value was calculated for both responses to establish the most significant response. The Adjusted P-value obtained for BS flux % using the TMC test was <0.0001 for all African catfish mucus concentrations (1, 3, and 5% w/w). However, the adjusted P-value obtained for particle size using the TMC test for ACM concentration 1 and 3 % (w/w) was 0.024 at both concentrations while that of ACM concentration 5 % was <0.001 respectively (Figure 4.6) This result showed that the initial BS Flux % was a better response factor in comparison to particle size. A similar trend was followed with the R^2 statistic with the values. The data analysed for BS % flux were the selected data points within the 20– 40 mm range as it gave a stable phase profile over-time in comparison with the 0-20, 40-60, and 60-90 nm ranges (Figure 0.). The goodness-of-fit was assessed using the coefficient of determination (R^2) to establish the most dominant effect on stability between. Two-way Analysis of variance (ANOVA) with Tukey's multiple comparisons (TMC) test was performed using GraphPad Prism version 5.00 for Windows to evaluate whether the stability as a function of initial BS flux or the $D_{(3,2)}$ as a function of particle size (nm) better explained the stability characteristics of the ACM soy milk stabilised emulsions..

Table 0.5: Effect of ACM on the on average initial backscattering % flux of soy milk emulsions using Two-way ANOVA [a, b.]

Concentration of ACM (%)	Concentration of soya milk (%)	Average initial BS % flux	pH	Mean difference	SE of difference	Level of Significance	Adjusted P Value
1	50	41.39±0.13	7.85	-2.355	0.1488	Yes	<0.0001
3	50	43.75±0.17	7.92	-14	0.1488	Yes	<0.0001
5	50	55.39±0.23	7.95	-11.64	0.1488	Yes	<0.0001

aSE of difference –Standard error of difference between two means bBS % flux-Backscattering percentage flux

Table 0.6: Effect of ACM on the Sauter mean diameter of soy milk emulsions using Two-way ANOVA [a, b]

Concentration of ACM (%)	Concentration of soya milk (%)	$D_{(3,2)}$ (nm)	pH	Mean difference.	SE of difference	Level of Significance	Adjusted P Value
1	50	179±1	7.85	3	0.8165	Yes	0.024
3	50	176±1	7.92	6	0.8165	Yes	0.024
5	50	173±1	7.95	3	0.8165	Yes	<0.001

[a] SE of difference –Standard error of difference between two means

[b] **D(3,2)** -Sauter mean diameter

Table 0.7: Two-way ANOVA statistics for stability behaviour

Stability property	Degrees of freedom	P-value	F value	R squared
Average initial BS % flux	2	<0.0001	5078	0.9994
D(3,2) (nm)	2	<0.001	27	0.90

[a]BS % flux-Backscattering percentage flux, [b] $\mathbf{D_{(3,2)}}$ -Sauter mean diameter

A significant difference (*p*-value < 0.05) was established on all three ACM soy milk stabilised emulsions for BS % flux and $D_{(3,2)}$ at pH range 7.85-7.95. The F statistic of BS % flux was 5078 while the F statistic of particle size was 27 (Table 0.7). This result implies that the means in both responses i.e. BS % flux and $D_{(3,2)}$ significantly responded to changes in concentrations of ACM. This confirms earlier results obtained that the stability of ACM stabilised soy milk emulsions depends on the concentration of the ACM. It is also consistent with the inference that ACM-emulsifier soy milk ratio (ESMR) influences the stability of the emulsions. Furthermore, the adjusted *p*-value was calculated for both responses to establish the most significant response. The Adjusted *p*-value obtained for BS % flux using the TMC test was < 0.0001 for all African catfish mucilage concentrations (1, 3, and 5% w/w). However, the adjusted P-value obtained for particle size using the TMC test for ACM concentration 1 and 3 % (w/w) was 0.024 at both concentrations while that of ACM concentration 5 % was p < 0.001 respectively (Figure 0.6 and Figure 0.). This result showed that the initial BS % flux was a dominant response factor in comparison to particle size. A similar trend was followed with the R^2 statistic with the values 0.9994 and 0.9000 for BS % flux and and $D_{(3,2)}$ particle size respectively. The results show that data obtained from BS % flux closely fit the regression line by about 99.94% while the data for $D_{(3,2)}$ was 90% fit. Hence, both responses are good predictors of the stability of an emulsion.

.

Chapter 5

MODELING OF THE PERFORMANCE OF AFRICAN CATFISH MUCILAGE IN THE STABILITY OF OIL IN WATER-TYPE NANOEMULSIONS

5.1 Modeling fhe performance of ACM stabilised O/W-type nanoemulsions

This chapter details results and discussion on the results of the research objectives which involved: investigating the effect of African catfish mucilage (ACM) on the stability of oil in water-type nanoemulsions prepared by ultrasonication using D-optimal mixture design methodology. My original contribution to knowledge is that application of the results could streamline the conditions needed to determine the effect of process variables (ACM, oil and water) in the stability of O/W–type nanoemulsions in food-grade emulsions, personal care, and drug delivery emulsion systems. Also these guidelines would streamline the optimisation and validation of the stability of O/W–type nanoemulsions in food-grade emulsions, personal care, and drug delivery emulsion systems. The process variables (ACM, oil and water) were used to investigate the stability of O/W–type nanoemulsions based on backscattering % and Sauter mean diameter. The methodology for achieving this research objective is described in section 3.4, chapter three. Authors have reported the multi-faceted applications of O/W-type nanoemulsion in beverages, cosmetics, drug delivery, foods, nutraceuticals, and personal, and personal care products (Bai et al., 2017; Mikulcová et al., 2017; Azmi et al., 2019). Based on the multi-faceted applications of O/W-type nanoemulsions, the data on the effect of the independent variables (ACM, oil and MilliQ water) on the dependent variables Sauter mean diameter [$\mathbf{D_{(3,2)}}$] and backscattering (BS) % flux was modelled using D-optical mixture design surface methodology.

5.2 Results and discussion

5.2.1 Stability of ACM stabilised O/W-type nanoemulsion

The particle size data from TEM imaging studies were identical to the measurements of particle size made on the Zetasizer The literature established that the lower the particle size the more stable an emulsion becomes (Adeyi et al., 2014; Maphosa et al., 2017). The Sauter mean diameter ($D_{(3,2)}$) was calculated from the particle size distribution using equations 1, 2, and 3 as described in the methodology section 3.3.3 using methods developed by (Dokić et al., 2012; Nieto de Castro et al., 2017). Table 0.1 compares the $D_{(3,2)}$ of the sixteen different combinations in the randomized runs in the d-optimal mixture design of ACM stabilised O/W-

type nanoemulsion with the stability as a function of initial % backscattering. Higher concentrations of ACM led to a decreas in $D_{(3,2)}$ of oil globules for all investigated ACM stabilised O/W-type nanoemulsion. When ACM concentration was highest regardless of oil concentration the $D_{(3,2)}$ of emulsions was low. For instance, the average $D_{(3,2)}$ of stabilised O/W nanoemulsions containing an ACM-emulsifier oil ratio (EOR) of 5:3, 5:4.6. 5:7.3 and 5:10 were 6.6 ± 0.1, 6.7 ± 0.2, 6.9 ± 0.2, and 7.5 ± 0.2 nm respectively (Table 5.1). Similarly, the average $D_{(3,2)}$ of stabilised O/W nanoemulsions with EOR of 1:3, 1:5.7, 1:7.3, and 1:10 % was 10.0 ± 0.3, 23.2 ± 0.6, 29.1 ± 0.5, and 32.4 ± 0.6 nm respectively (Table 5.1). The $D_{(3,2)}$ of emulsions with EOR 2.3:10, 2.9:3.1, and 3.3:6.2% was higher than that of emulsions stabilised with 5 % ACM but lower than that of emulsions stabilised with 1 % ACM they were 15.4 ± 0.4, 15.9 ± 0.5, and 13.6 ± 0.4 nm (Table 5.1). It was also observed that particle size ($D_{(3,2)}$) of emulsions decreased as the ACM-oil ratio increased (Table5.1). The trend shows that the higher the EOR the lower the $D_{(3,2)}$ (particle size) as seen in Table 5.1. Consequently, the ACM-emulsifier oil ratio (EOR) directly influence the $D_{(3,2)}$ of ACM stabilised O/W-type nanoemulsions. The trend was the higher EOR the lower the $D_{(3,2)}$. Literature supports this claim as revealed by a study conducted by Nejadmansouri et al. (2016),) which investigated the key elements that influenced the formulation of non-ionic surfactants-stabilised fish oil nanoemulsions using high-intensity ultrasound. The study focused specifically on the influence of hydrophilic-lipophilic balance (HLB), emulsifier-oil ratio (EOR), and effect of temperature on storage, as well as the physicochemical attributes and oxidative stability of the of nanoemulsion (Nejadmansouri et al., 2016). The authors observed that when the EOR and HLB were high the particle size was low and concluded that EOR and HLB influenced particle size (Nejadmansouri et al., 2016). Hence the results obtained on the $D_{(3,2)}$ of ACM stabilised nanoemulsions that the higher the EOR the lower the $D_{(3,2)}$ of ACM stabilised nanoemulsions is consistent with results reported by Nejadmansouri et al. (2016) that the higher the EOR the lower the particle size of non-ionic surfactants-stabilised fish oil nanoemulsions.

The width of the distribution can also be used to access the influence of ACM concentration on the particle size distribution of an emulsion. The changes in the particle size distribution of ACM stabilised nanoemulsions are shown in Table 0.1. The particle size distribution of emulsions stabilised with 5 % ACM was between 0.1 and 0.2 nm while that of emulsions stabilised with 1 % was between 0.5 and 0.6 nm (Table 0.1). The middle-value ranges of ACM concentration were between 0.4 and 0.5 nm (Table 0.1). The results show that the particle size distribution decreased as the ACM concentration increased from 1-5 % of ACM. This signifies that as the ACM-emulsifier oil ratio (EOR) increased the particle size distribution of ACM stabilised nanoemulsions (ASE) decreased (Table 0.1). Hence the higher the ACM-EOR

Table 0.1: Composition and observed responses from randomized runs for D-optimal mixture design [a, b, and c.]

	Independent variable			Dependent variable	
Run	**A: ACM (%)**	**B: Oil (%)**	**C: Water (%)**	**Backscattering (%) flux**	**$D_{(3,2)}$ (nm)**
1	1.0	9.6	89.4	36.0 ± 0.9	31.9 ± 0.6
2	1.0	9.6	89.4	36.0 ± 0.9	32.4 ± 0.6
3	1.0	3.0	96.0	63.4 ± 0.2	10.0 ± 0.3
4	5.0	7.3	87.7	73.0 ± 0.5	6.9 ± 0.2
5	1.0	5.7	93.3	56.7 ± 0.2	23.2 ± 0.6
6	5.0	3.0	92.0	77.9 ± 0.1	6.7 ± 0.1
7	5.0	3.0	92.0	77.7 ± 0.1	6.6 ± 0.1
8	5.0	10	85.0	73.6 ± 0.1	7.4 ± 0.2
9	2.3	10	87.7	64.4 ± 0.1	15.4 ± 0.4
10	1.0	3.0	96.0	63.4 ± 0.2	10.4 ± 0.4
11	2.9	3.1	93.9	46.8 ± 0.1	15.9 ± 0.5
12	3.3	6.2	90.5	73.2 ± 0.1	13.8 ± 0.4
13	5.0	10.0	85.0	73.7 ± 0.1	7.5 ± 0.2
14	1.0	8.0	91.0	46.9 ± 0.2	29.1 ± 0.5
15	5.0	4.6	90.4	75.7 ± 0.3	6.7 ± 0.2
16	3.3	6.2	91.0	73.2 ± 0.1	13.6 ± 0.4

[a]Indicated values are reported as means ± standard deviation (n = 3).

[b]ACM-African catfish mucilage, oil-sunflower oil, and water-MilliQ water

[c]**$D_{(3,2)}$**- Sauter mean diameter.

the lower the $D_{(3,2)}$ (PS) and PSD and the higher the stability of the ASE. For instance (Sharif et al., 2017), studied the influence of EOR on the particle size (PS) and particle size distribution (PSD) of flaxseed O/W-type nanoemulsions stabilised with two different chemically modified starch (CMS) as emulsifiers (Sharif et al., 2017). The authors concluded that the $D_{(3,2)}$ (PS) and PSD of the flaxseed O/W-type nanoemulsions decreased as the concentration of the CMS-emulsifier increased and concluded that the higher EOR the lower the $D_{(3,2)}$ (PS) and PSD of the flaxseed O/W-type nanoemulsions (Sharif et al., 2017). Similarly, Dokić et al. (2012) investigated the $D_{(3,2)}$ (PS) and PSD of O/W emulsion containing 5-60 % of sunflower oil and 8- 16 % octenyl succinic anhydride-emulsifier. The authors reported that $D_{(3,2)}$ (PS) and PSD decreased as the emulsifier concentration octenyl succinic anhydride (OSA)concentration increased and concluded that the higher EOR the lower the $D_{(3,2)}$ (PS) and PSD i.e the higher the stability of the sunflower O/W-type emulsions (Dokić et al., 2012) . The results obtained on the $D_{(3,2)}$ (PS) and PSD of ACM stabilised nanoemulsions that the higher the EOR the lower the $D_{(3,2)}$ and PSD and the higher the stability are in agreement with results reported by the authors by Dokić et al. (2012), Nejadmansouri et al. (2016), Nieto de Castro et al. (2017)), and Sharif et al. (2017).

Emulsion stability investigates the capacity of an emulsion to resist physicochemical changes in its structure during storage (Nieto de Castro et al., 2017). The average initial back scattering (BS) % flux and Sauter mean diameter ($D_{(3,2)}$) for each run are shown in Table 0.1. When ACM concentration was highest regardless of oil concentration the initial average BS % flux of emulsions was high. For instance, the initial mean BS % flux for ACM stabilised O/W-type nanoemulsions stabilised with 5 % ACM was 77.7 ± 0.1 % (3 % oil), 75.7 ± 0.3 % (4.6 % oil), 73.0 ± 0.5 % (7.29 % oil), and 73.6 ± 0.1% (10 % oil), while that of emulsions stabilised with 1 % ACM was 63.4 ± 0.2 % (3 % oil), 56.7 ± 0.2 % (5.7 % oil), 46.9 ± 0.2 (8 0 oil), and 36.0 ± 0.9 % (9.6 % oil), respectively (Table 5.1). Similarly, the emulsions stabilised with EORs 2.3:10 2.9:3.1, and 3.3:6.2 as BS % flux was 64.4 ± 0.1, 46.8 ± 0.1 and 73.2 ± 0.1 % respectively (Table 0.1). Hence, the higher the concentration of ACM the higher the stability and BS % flux of ACM stabilised O/W-type nanoemulsions (Table 5.1). Also, the concentration of ACM-emulsifier oil ratio (EOR) influenced BS % flux of ACM stabilised O/W-type nanoemulsion because as the concentration of ACM increased from 1 to 5 % the BS % flux increased (Table 0.1). The results obtained that the higher the EOR the higher the stability and the higher the BS flux percentage of ACM stabilised O/W-type nanoemulsion is consistent with the results obtained by Nieto de Castro et al. (2017).. Consequently, high BS % flux means that the nanoemulsions structure is more stable as the BS % flux reflects the arrangement of molecules before it becomes unstable (Maphosa et al., 2017). The backscattering (BS) % flux profile of ACM stabilised O/W-type nanoemulsion within180 mins were investigated as depicted in Figure 0.1, Figure 0.2 and Figure 0.3. The tube length is

plotted on the x-axis while the BS % flux is plotted on the y-axis. The cohesion observed in the structural matrix network of all the ACM stabilised O/W-type nanoemulsions implies that the emulsion stability of ACM is achieved by encapsulation mechanism called mucoadhesion as defined for hagfish mucus stabilised soya milk emulsions Böni et al. (2016b). Encapsulaton

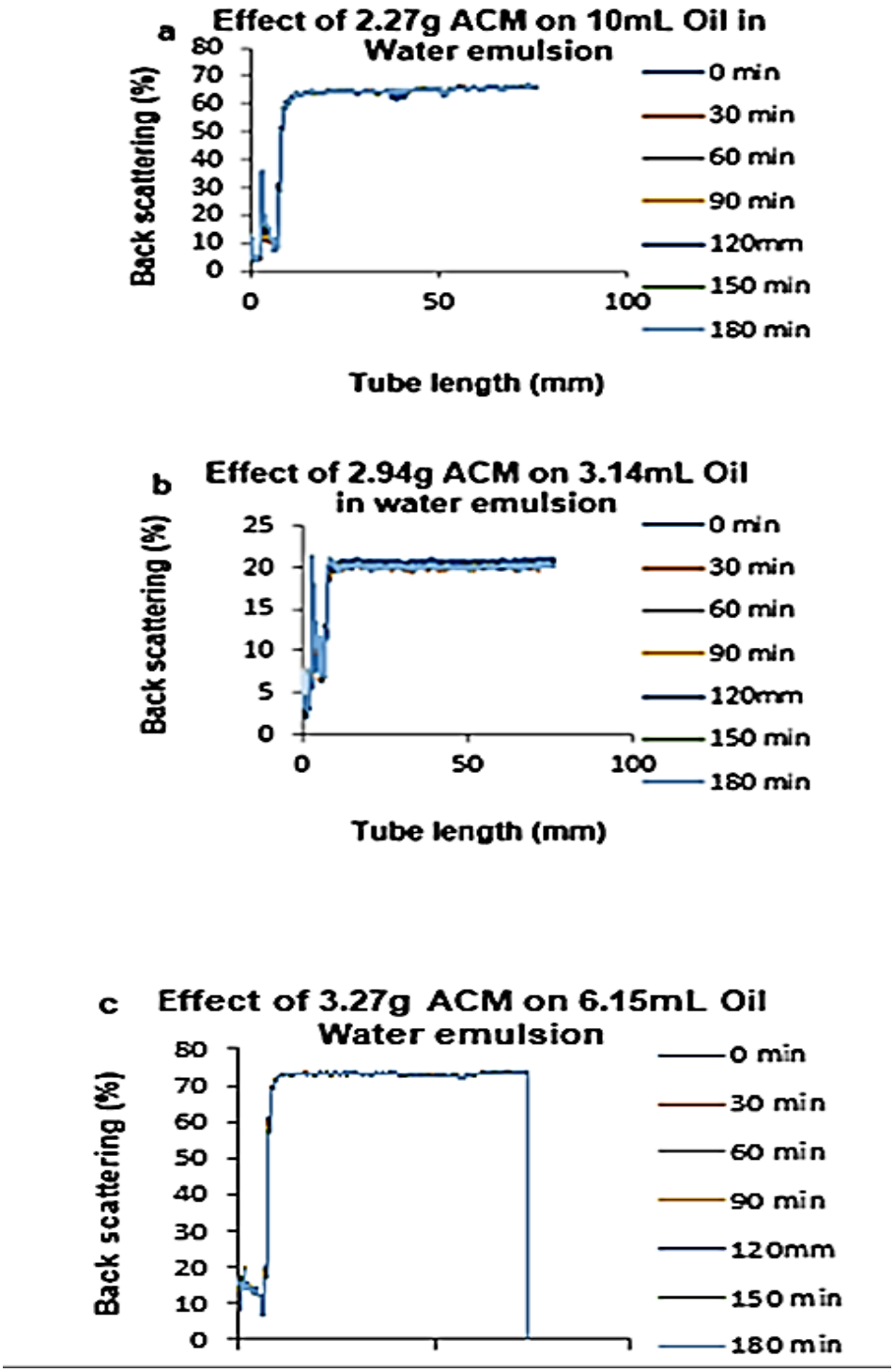

Figure 0.1: Changes in stability of ACM stabilised O/W-type nanoemulsions with emulsifier oil ratio (a) 2.27:10 % (b) 2.94:3.14 % (c) 3.27:6.15 %.

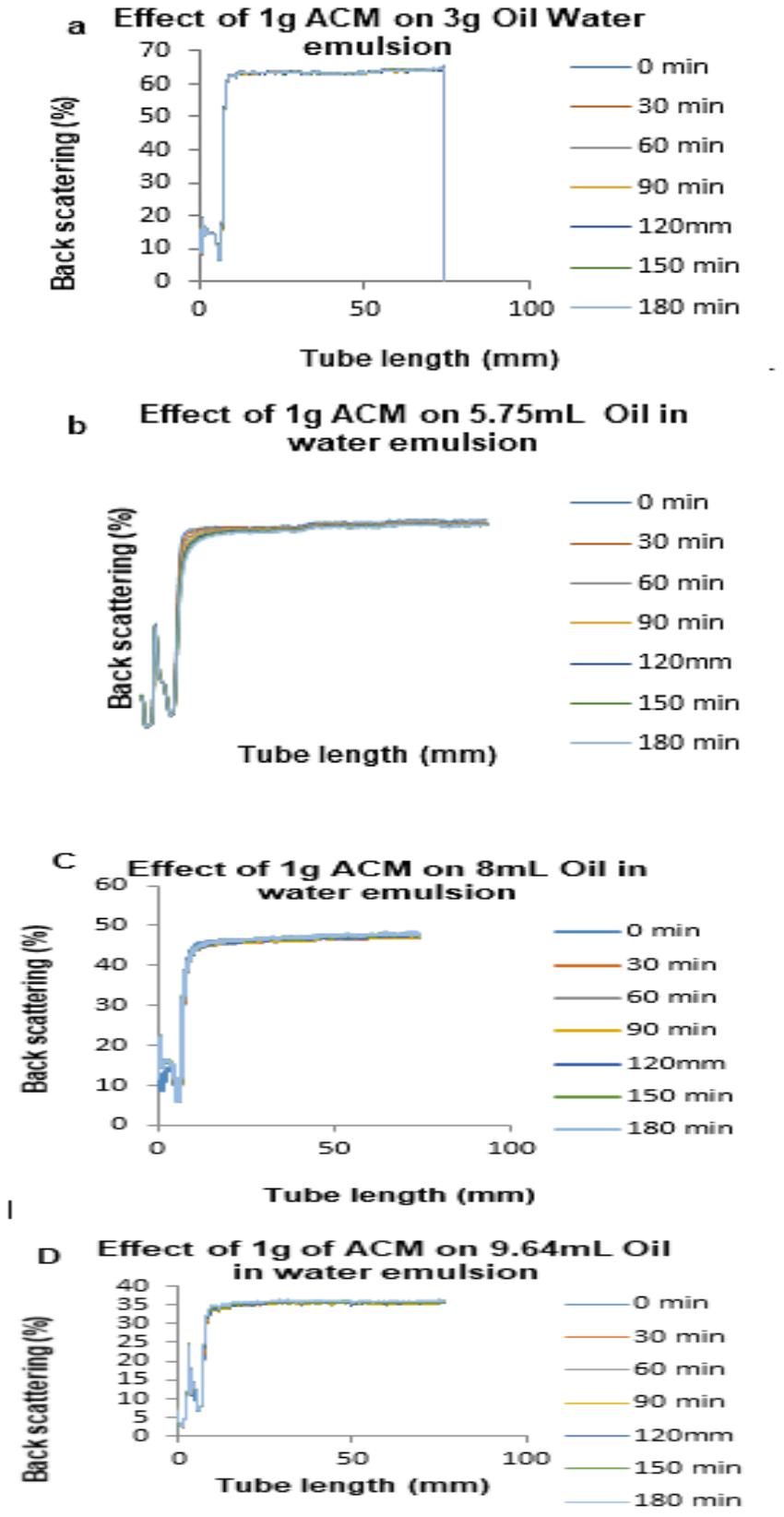

Figure 0.2: Changes in stability of ACM stabilised O/W-type nanoemulsions with ACM-emulsifier oil ratio (a) 1:3 % (b) 1:5.75 % (c) 1:8 % (d) 1:9.64 %

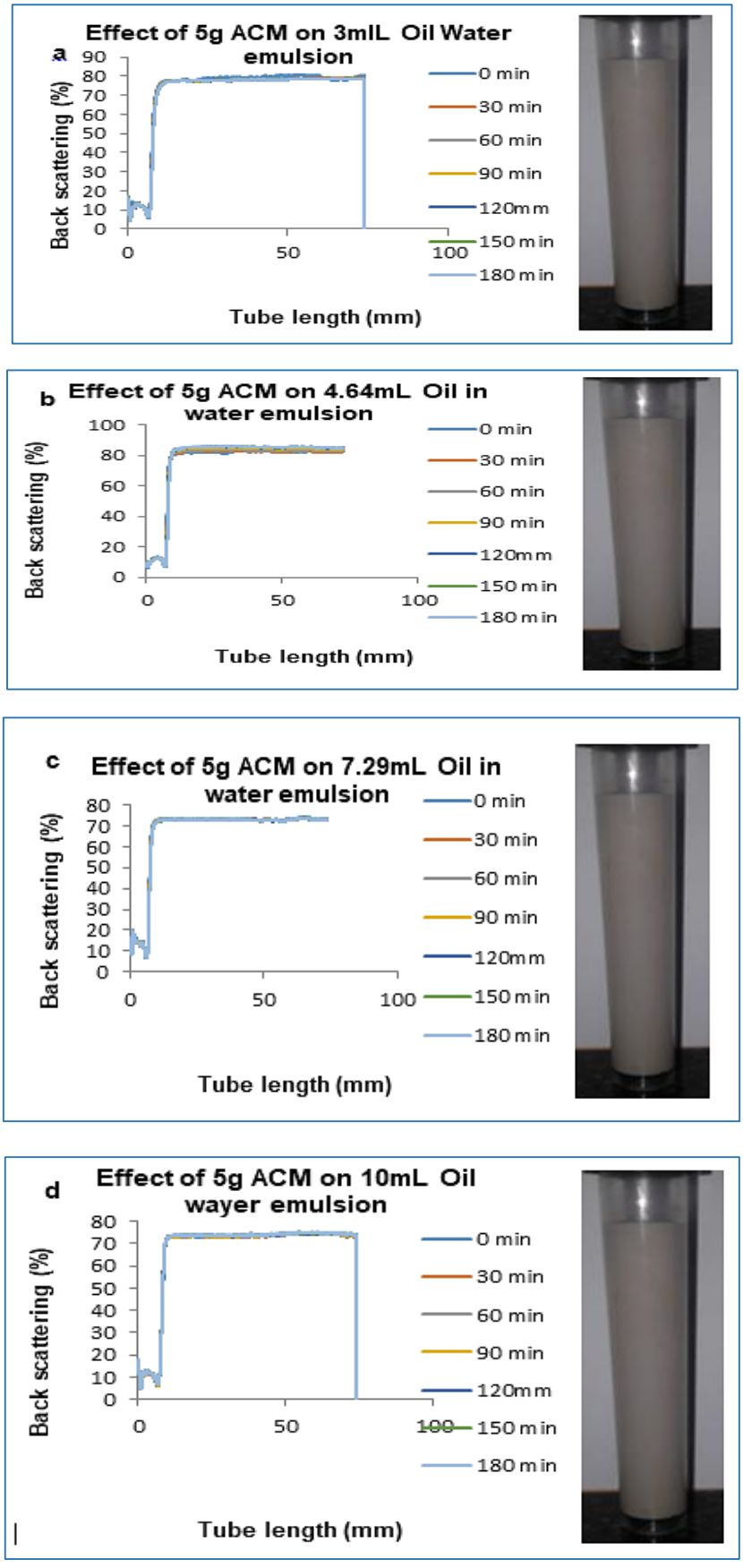

Figure 0.3: Changes in stability of ACM stabilised O/W-type nanoemulsions with emulsifier oil ratio (a) 5:3 % (b) 5:4.64 %l (c) 5:7.29 % (d) 5:10 %.

was achieved through ultrasonication a novel emulsification method which resulted in stable nanoemulsions (lower particle size and high BS% flux) as opposed to conventional homogenisation methods. The results are consistent with reports that ACM stabilises emulsions even with low concentrations and forms a cohesive interactive network as described by Böni et al. (2016b). The authors stated that 1 % concentration of hagfish mucus could stabilise soya milk emulsions as a result of a different entrapment interaction called mucoadhesion Böni et al. (2016b). The authors concluded that higher percentage concentrations of hagfish mucus led to higher stability. This phenomenon was also established in the previous chapter on the role of ACM as an emulsifier on soy milk emulsions. Hence ACM is an excellent natural emulsifier with mucoadhesive properties as it encapsulates soya milk to enhance stability.

5.2.2 Model fit and adequacy for the stability of ACM stabilised O/W-type nanoemulsion

The Design-Expert (Stat-Ease Inc., Minneapolis, Minnesota, U.S.A., version 10.0.7) statistical software was used to analyse the experimental data obtained for stability as a function of BS % flux. The precise stability parameters for BS % flux obtained from the mixture design for determining the ACM stabilised O/W-type nanoemulsion formulation is presented in Table 0.2. The summary of the model statistics and regression coefficients is shown in

Table 0.3. The quadratic mixture model for BS % flux obtained by analysng the experimental data was significant (F [557.86, 8.88] = 62.80; *p*-value < 0.0001) in describing the component effects (ACM, oil, and water) on BS % flux stability parameter (

Table 0.3). There was only a 0.01% chance that a model F-value this large could occur due to noise. The model's lack of fit (F [19.98, *6.990E-003*] = *2858.24*; $p < 0.0001$) was also significant, however, the predicted R-squared value was 0.9123 indicating a model with adequate goodness-of-fit (Table 5.3). This was also confirmed by the adequate precision (20.186) a value > 4 indicates adequate precision and a model, which can be used to navigate the design space. The precise stability parameters ($D_{(3,2)}$) obtained from the mixture design for determining the ACM stabilised O/W-type nanoemulsion formulation is presented in

Table 0.3. The summary of the model statistics and regression coefficients is shown in Table 0.4. The quadratic mixture model for $D_{(3,2)}$ was significant (F [235.71, 0.13] = 1805.99; *p*-value < 0.0001) in describing the component effects (ACM, oil, and water) on BS flux % stability parameter (Table 0.4.). There was only a 0.01% chance that a model F-value this large could occur due to noise. The model lack of fit (F [0.17, 0.11] = 0.3104; *p* = 1.49) was not significant, and the predicted R-squared value was 0.9977 and adequate precision was 104.158 indicating a model with adequate goodness-of-fit (Table 0.4.). This was also confirmed by the adequate precision (104.158) a value > 4 indicates adequate precision and a model, which can be used to navigate the design space. All variables were fitted to a quadratic model, and the residual errors calculated to determine the goodness of model fit. Based on these values, the quadratic mixture model was found to be suited to determine the effects of the three ingredients (ACM, oil, and water) on the precise stability parameters for BS % flux and $D_{(3,2)}$.

The experimental data obtained was used to obtain the best fitting mathematical model which was a polynomial quadratic equation. The model was significant and valid for the stability (BS % flux) of the ACM stabilised O/W emulsions. The resultant quadratic polynomial model adequately represented the experimental responses with the coefficients of multiple determinations R^2 of 0.9567 and adjusted R^2 of 0.9721, respectively (

Table 0.3), which indicates a good fit between the experimental values and the regression model.

Table 0.2: Formulation sets as determined by 3-component D-optimal mixture design[a, b]

	Independent variable		
Formulation	**A: ACM (%)**	**B: Oil (%)**	**C: Water (%)**
1	1.0	9.6	89.4
2	1.0	9.6	89.4
3	1.0	3.0	96.0
4	5.0	7.3	87.7
5	1.0	5.7	93.3
6	5.0	3.0	92.0
7	5.0	3.0	92.0
8	5.0	10.0	85.0
9	2.3	10.0	87.7
10	1.0	3.0	96.0
11	2.9	3.1	93.9
12	3.3	6.2	90.5
13	5.0	10.0	85.0
14	1.0	8.0	91.0
15	5.0	4.6	90.4
16	3.3	6.2	91.0

[a]Correspondent values indicated in actual scale

[b]African catfish mucilage

Table 0.3: Analysis of variance (ANOVA) for the effect of the three variables on backscattering % flux

Source	Sum of Squares	df	Mean Square	F Value	p-value Prob > F	Significance level
Model	2789.30	5	557.86	62.80	< 0.0001	significant
[1]Linear Mixture	*2288.36*	*2*	*1144.18*	*128.80*	*< 0.0001*	
AB	*381.64*	*1*	*381.64*	*42.96*	*0.0001*	
AC	*241.87*	*1*	*241.87*	*27.23*	*0.0006*	
BC	*5.18*	*1*	*5.18*	*0.58*	*0.4648*	
Residual	79.95	9	8.88			
Lack of Fit	*79.92*	*4*	*19.98*	*2858.24*	*< 0.0001*	*significant*
Pure Error	*0.035*	*5*	*6.990E-003*			
Cor Total	2869.25	14				
R-Squared	0.9721					
Adjusted R-Squared	0.9567					
Predicted R-Squared	0.9123					
Adequate Precision	20.186					

Table 0.4: Analysis of variance (ANOVA) for the effect of the three variables of Sauter mean diameter (D(3,2)

Source	Sum of Squares	df	Mean Square	F Value	p-value Prob > F	Significance level
Model	1178.55	5	235.71	1805.99	< 0.0001	significant
[1]*Linear Mixture*	909.19	2	454.60	3483.07	< 0.0001	
AB	32.44	1	32.44	248.53	< 0.0001	
AC	11.06	1	11.06	84.76	< 0.0001	
BC	26.97	1	26.97	206.65	< 0.0001	
Residual	0.91	7	0.13			
Lack of Fit	0.34	2	0.17	1.49	0.3104	not significant
Pure Error	0.57	5	0.11			
Cor Total	1179.46	12				
R-Squared	0.9992					
Adjusted R-Squared	0.9987					
Predicted R-Squared	0.9977					
Adequate Precision	104.158					

The final equation in terms of actual components is given by Equation 5.1.

γ_1 (BS flux %) = -267.43*(ACM) + 6.48*(Oil) + 0.64*(Water) + 3.55*(ACM * Oil) + 2.86*(ACM * Water) - 0.12 *(Oil * Water) **Equation 5.1**

The R^2 value for the BS % flux model is 0.9567 and the closeness of this value to 1 makes it represent a good fit. The adequate signal to noise ratio for BS % flux response was given as 20.186 (Table 5.3). Authors have reported that the adequate prediction compares the range of the predicted values at the design points to the average prediction error and a ratio greater than 4 is desirable (Gupta et al., 2016; Anupam et al., 2018). It can be observed that the signal to noise ratio for BS % flux is much higher than 4 as it is 20.186. Hence, it can be inferred that the stability design space as a function of BS % flux for ACM stabilised O/W-type nanoemulsion contains minor noise/errors i.e. the experimental data set transmits more useful information/signal about the developed stability model for BS % flux.

The experimental data obtained for Sauter mean diameter was used to obtain the best fitting mathematical model which was a polynomial quadratic equation. The model was significant and valid for the stability ($\mathbf{D_{(3,2)}}$) of the ACM stabilised O/W emulsions. The resultant quadratic polynomial model adequately represented the experimental responses with the coefficients of multiple determinations R^2 of 0.9992 and adjusted R^2 of 0.9987, respectively (Table 0.4), which indicates a good fit between the experimental values and the regression model. The final equation in terms of actual components is given by Equation 5.2

$\gamma_2 = (\mathbf{D_{(3,2)}})$ = 7906.40*(ACM) - 2601.19*(Oil) - 6.91*(Water) -12501.27*(ACM * Oil) + 8268.83*(ACM * Water) - +3436.43*(Oil * Water) **Equation 5.2**

The R^2 value for the $\mathbf{D_{(3,2)}}$ model is 0.9992 and the closeness of this value to 1 makes it represent a good fit. The adequate signal to noise ratio for $\mathbf{D_{(3,2)}}$ response was given as 104.158 (Table 0.34). Authors have reported that the adequate prediction compares the range of the predicted values at the design points to the average prediction error and a ratio greater than 4 is desirable (Gupta et al., 2016; Anupam et al., 2018). It can be observed that the signal to noise ratio for $\mathbf{D_{(3,2)}}$ is much higher than 4 as it is 104.158. Hence, it can be inferred that the stability design space as a function of $\mathbf{D_{(3,2)}}$ for ACM stabilised O/W-type nanoemulsion contains minor noise/errors i.e. the experimental data set transmits more useful information/signal about the developed stability model for $\mathbf{D_{(3,2)}}$..

All variables were fitted to a polynomial quadratic model, and the residual errors calculated to determine the goodness of model fit. Based on these values, the polynomial quadratic mixture model was found to be suited to determine the effects of the three

ingredients (ACM, oil, and water) on the back scattering (BS) % flux and Sauter mean diameter ($D_{(3,2)}$). Normality of data was confirmed with 2 model adequacy tools—Normality Plot of Residuals and the Box-Cox Plot (not shown). The straight line obtained from the plots, indicated a normal distribution of residuals (Jeirani et al., 2012; Diedericks & Jideani, 2015), and showed that a changes in transformation would not lead to any improvement of the analysed data. Authors have reported that the Box-Cox plot, defined as "the natural log of the sum of the squares of the residuals against lambda," indicates whether lambda should be transformed (Jeirani et al., 2012; Diedericks & Jideani, 2015; Habib, Sayed, & Elsayed, 2018). In this case the statistical tool did not recommend any transformation for the response variables of BS % flux and $D_{(3,2)}$) for the ACM stabilsed O/W-type nanoemulsions; Hence the model was found adequate to determine the effects of the three ingredients (ACM, oil, and water) on the precise stability parameters for BS % flux and $D_{(3,2)}$.

5.2.3 Effects of mixture components on stability (backscattering % flux).

The stability as a function of backscattering (BS) % flux obtained from the mixture design for ACM stabilised O/W-type nanoemulsion formulation is presented in Table 5.5. The formulations with the highest BS % flux had an ACM concentration of 5 % in Table 5.5. For instance, the average initial BS flux % of the formulation with the emulsifier oil ratio (EOR) of 5:3 (77.8 ± 0.1 %), 5:4.6 (75.8 ± 0.3 %), 5:7.3 (75.8 ± 0.3 %), and 5:10 (73.6 ± 0.1 %) as shown in Table 5.5. Similarly, the average initial BS flux % of the formulation with the EOR of 1:3 (63.4 ± 0.2 %), 1:5.7 (56.7 ± 0.2 %) 1: 8.0 (46.9 ± 0.2 %), and 1:9.6 (36.0 ± 0.9 %) as shown in Table 0.45. It was evident that the EOR directly influences the BS % flux and the higher the ACM concentration the higher the stability (BS % flux). This observation was confirmed in the dominance displayed by ACM in the quadratic synergies as the concentration of ACM directly influenced stability as evidenced by highest factor coefficients for BS % flux L_Pseudo and actual Components (Table 0.6). It was observed that the L_Pseudo and actual Components factor coefficient for ACM was higher than that of oil and water. The trend was ACM> water> oil. The factor coefficients for stability (BS % flux) L_Pseudo and actual Components in ACM was (-120.53 and -26742. 66), that of oil was (+28.51 and +647.56) while that of water was (+64.29 and +.64.04). Similarly, the synergy factors for ACM were higher than those of oil and water. The synergy factor coefficients for BS % flux L_Pseudo and actual Components of ACM* Oil was (+ 430.12 and +35546.82), for ACM * Water it was (+346.06 and +28600.28) while that of Oil * Water was (-14.46 and --1195.15). The factor component values of the L_Pseudo and actual Components predict that the relative impact of ACM was higher than that of oil and water therefore the concentration of ACM/EOR is vital in ensuring that the O/W nanoemulsion has stability as it leads to higher BS % flux.

Table 0.5: Experimental responses from randomized runs for D-optimal mixture design [a, b, and c]

Run	Dependent Variable	
	BS % flux	**$D_{(3,2)}$ (nm)**
1	36.0 ± 0.9	31.9 ± 0.6
2	36.0 ± 0.9	32.4 ± 0.6
3	63.4 ± 0.2	10.0 ± 0.3
4	72.99 ± 0.5	7.0 ± 0.2
5	56.7 ± 0.2	23.2 ± 0.6
6	77.9 ± 0.1	6.7 ± 0.1
7	77.7 ± 0.1	6.6 ± 0.1
8	73.6 ± 0.1	7.4 ± 0.2
9	64.4 ± 0.1	15.4 ± 0.4
10	63.4 ± 0.2	10.4 ± 0.4
11	46.8 ± 0.1	16.0 ± 0.5
12 (	73.2 ± 0.1	13.8 ± 0.4
13	73.7 ± 0.1	7.5 ± 0.2
14	46.9 ± 0.2	29.1 ± 0.5
15	75.8 ± 0.3	6.7 ± 0.2
16	73.2 ± 0.1	13.6 ± 0.4

[a]Indicated values are reported as means ± standard deviation (n = 5).
[b]ACM-African catfish mucilage, oil-sunflower oil, and water-MilliQ water
[c]**$D_{(3,2)}$**- Sauter mean diameter.

Table 0.6: Regression coefficient values for the quadratic model of L_Pseudo Components for BS % flux [a,] and [b]**.**

Source	**BS % flux**
ACM (*A*)	-267.42655
Oil (*B*)	+6.47560
Water (*C*)	+0.64043
ACM * Oil (*A***B*)l	+3.55468
ACM * Water (*A***C*)	+2.86003
Oil * Water (*B***C*)l	-0.11952

[a]BS .% flux-Backscattering % flux, [b]ACM - Afirican catfish mucilage; Oil - Sunflower oil; and [c]Water - MiliQ water

Figure 0.4 shows the Piepel trace and mixture design surface plot for the effect of 3 components (A: ACM, B: oil and C: water) on BS % flux. The observation of dominance of ACM concentration in the stability (BS % flux) as evidenced by higher RC values in the synergiess of oil and water with ACM was confirmed in the Piepel trace plots as the stability (BS % flux) was greatly influenced by ACM (Figure 0.4a). A curvature was observed in the Piepel trace plots for all independent variable ACM, oil, and water (Figure 0.4a). The relationship observed was that the stability (high BS % flux) increased as the concentration of ACM increased up a point when it decreased slightly with a marked curvature decline (Figure 0.4a). The curvature in ACM was sharp while that of oil and water was not sharp. This means that at a certain point depending on the concentration of the ACM-emulsifier to the concentration of the oil i.e. EOR the stability of the O/W nanoemulsion would be impacted negatively as the stability would not be affected by higher concentrations of the ACM.

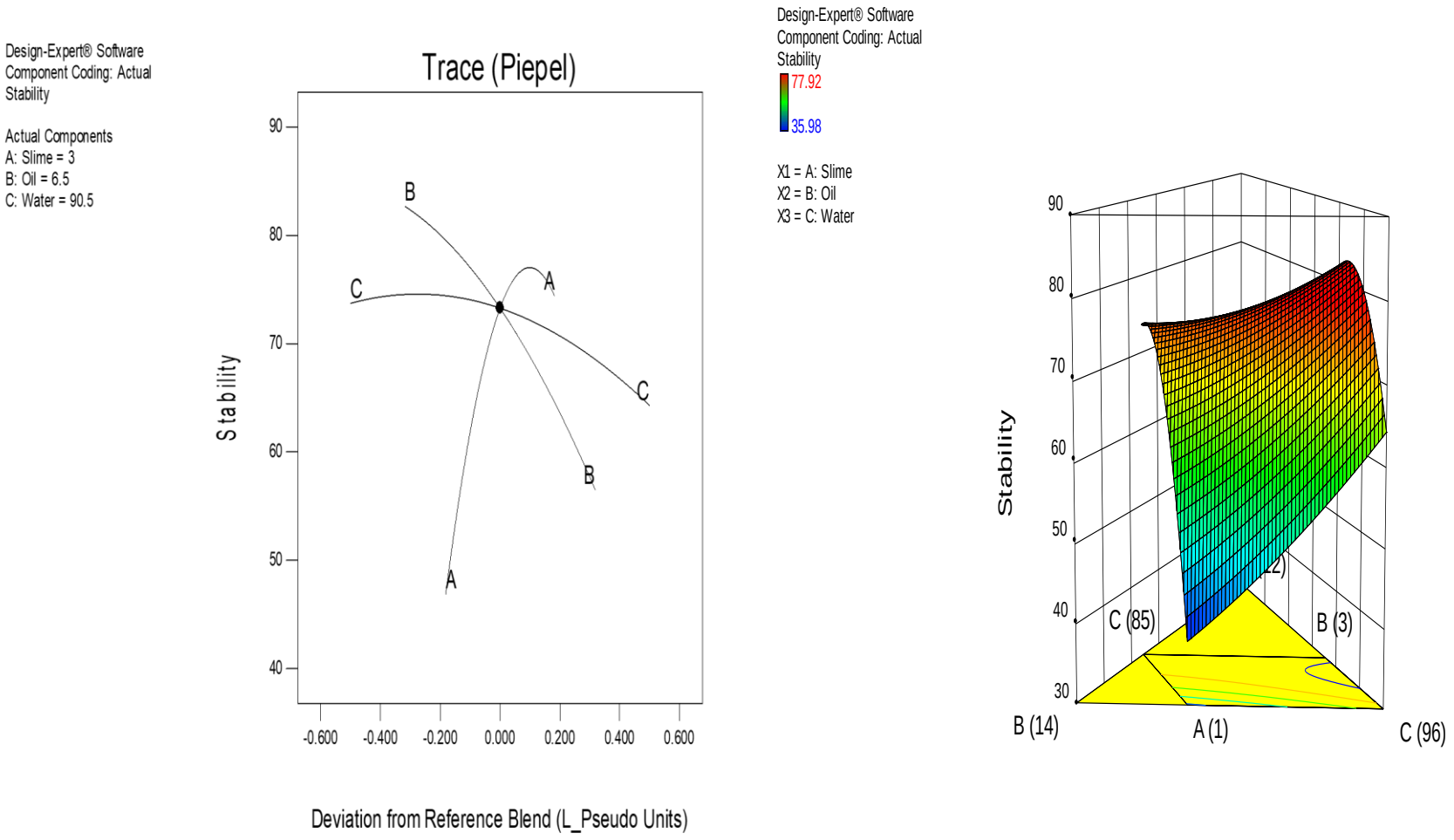

Figure 0.4: (a) Trace (Piepel) plot and (b) mixture design surface plot for the effect of 3 components (A: ACM, B: oil and C: water) on Backscattering % flux.

Authors have reported that when sharp curvature occurs on Piepel's trace plots, it shows that the specific constituent produces an extremely sensitive response in comparison to other constituents in the mixture (Diedericks & Jideani, 2015; Habib & AbouGhaly, 2016). Based on the literature, an extremely sensitive response by ACM shown by sharp curvature effect on stability as a function of BS % flux is the most dominant effect among the three mixture constituents. In the case of oil and water, the influence was not dominant as the stability (BS % flux) decreased as the concentration oil and water increased hence a pronounced curvature was experienced instead of a sharp curvature. Thus it could be deduced that if the concentration of ACM increases to a certain level where the curvature is observed, the stability-BS % flux of O/W-type nanoemulsions would be impacted negatively. This means that stability could reduce because the BS % flux reduces as a result of excess ACM that would not be dissolved in the system. The significance of this is that water-insoluble excess ACM concentrations could trigger instability i.e. lower BS % flux in an O/W-type nanoemulsion. The observation of dominance of ACM concentration in the stability (BS % flux) as evidenced by higher RC values in the isynergies of oil and water with ACM was confirmed in the mixture design surface plots as the stability (BS % flux) which was greatly influenced by ACM (Figure 5.4b). The actual stability value obtained on the mixture design surface plots (Figure 0.4b) was 77.9 % which compares favorably with the value obtained as the average initial BS % flux (77.9 ± 0.1 %) In BS % flux stability studies (Figure 0.3a). The mixture design surface plots (Figure 5.4b) also showed that as the concentration of ACM increased, the stability (BS % flux) increased up a point when it decreased slightly with a marked curvature decline as evidenced in the quadrilateral shape of the mixture design surface pots. Similar results were obtained for oil and water as stability (BS % flux) decreased with increasing concentrations of oil and water (Figure 0.4b). The effects of the three independent variables on stability (BS % flux) as shown in the Piepel trace plot (Figure 0.4a) agrees with the results obtained from the D-optical mixture design surface (Figure 0.4b), where high stability (high BS % flux) is as a result of the concentration of ACM which influenced the emulsifier-ACM oil ratio (EOR). The result that ACM by showing a sharp curvature effect on the effect of three mixture components on stability as a function of backscattering flux agrees with results reported by Diedericks & Jideani (2015) and Habib & AbouGhaly (2016).

5.2.4 Effects of mixture components on stability as a function of Sauter mean diameter of ACM stabilised O/W-type nanoemulsion.

The stability as a function of $D_{(3,2)}$ obtained from the mixture design for ACM stabilised O/W-type nanoemulsion formulation is presented in Table 0.5. The formulations with the highest $D_{(3,2)}$ had an ACM concentration of 5 %. For instance, the average of $D_{(3,2)}$ of the formulation

with the emulsifier oil ratio (EOR) of 5:3 (6.6 ± 0.1 nm), 5:4.6 (6.7 ± 0.2 nm), 5:7.3 (6.9 ± 0.2 nm), and 5:10 (7.5 ± 0.2 nm) as seen in Table 5.5 Similarly, the average $D_{(3,2)}$ of the formulation with the EOR of 1:3.0 (10.0 ± 0.3 nm), 1:5.7 (23.2 ± 0.6 nm) 1: 8.0 (29.1 ± 0.5 nm), and 1:9.6 (32.4 ± 0.6 nm) as seen in Table 0.5. It was evident that the EOR directly influences the $D_{(3,2)}$ and the higher the ACM concentration the higher the stability (low $D_{(3,2)}$). This observation was confirmed in the dominance displayed by ACM in the quadratic synergies as the concentration of ACM directly influenced stability as evidenced by highest factor coefficients for $D_{(3,2)}$ L_Pseudo and actual Components (0.7). The factor coefficients for stability [$D_{(3,2)}$] L_Pseudo and actual Components in ACM was (+64.06 and +7906.40), that of oil was (+30.17 and -2601.19) while that of water was (+10.23 and -6.91). Similarly, the synergy factors for ACM were higher than those of oil and water. The synergy factor coefficients for BS flux % L_Pseudo and actual Components of ACM* Oil was (-151.27 and -12501.27), for ACM * Water it was (-100.05 and -8268.83) while that of Oil * Water was (+41.58 and +3436.44). The factor component values of the L_Pseudo and actual Components predict that the relative impact of ACM was higher than that of oil and water therefore the concentration of ACM/EOR is vital in ensuring that the O/W nanoemulsion has higher stability as it leads to lower $D_{(3,2).}$

Figure 0.5 shows the Piepel trace and mixture design surface plot for the effect of 3 components (A: ACM, B: oil and C: water) on $D_{(3,2).}$ The observation of dominance of ACM concentration in the stability ($D_{(3,2)}$) as evidenced by higher RC values in the synergies of oil and water with ACM was confirmed in the Piepel trace plots as the stability (low $D_{(3,2)}$) was greatly influenced by ACM (Figure 0.5a). A curvature was observed in the Piepel trace plots for all independent variable ACM, oil, and water (Figure 0.5a). It was observed that as the concentration of ACM increased, the stability increased as $D_{(3,2)}$ values became lower also, a sharp curvature was observed as the concentration of ACM increased. This means that stability low $D_{(3,2)}$ can be achieved at a certain concentration of mixture constituents and subsequent increases in the concentration of ACM would continually lower $D_{(3,2)}$ and increase stability as shown in Figure 0.5a. For the influence of water, the curvature was more pronounced forming a parabola shape curvature. This means that higher concentrations concentration of water did not negatively impact the stability because the $D_{(3,2)}$ was low. This occurrence was confirmed with the high RC isynergy value of ACM and water and is in line with the theory that water-solubility enhances HLB values and ensures the stability of O/W-type nanoemulsions. The curvature for oil was slight hence as the concentration of oil increased, the stability decreased as evidenced by high $D_{(3,2)}$ values. In the same vein, the mixture design surface plot (Figure 0.5b).

Table 0.7: Regression coefficient values for the final reduced model of L_Pseudo Components for Sauter mean diameter [a, b c., and d]

Source	$D_{(3,2)}$ (nm)
ACM (*A*)	+7906.40251
Oil (*B*)	-2601.19300
Water (*C*)	-6.90902
ACM * Oil (*A***B*)l	-12501.27336
ACM * Water (*A***C*)	-8268.83095
Oil * Water (*B***C*)l	+3436.43482

aACM - Afirican catfish mucilage, bOil - Sunflower oil, cWater - MiliQ water, d$D_{(3,2)}$ - Sauter mean diameter

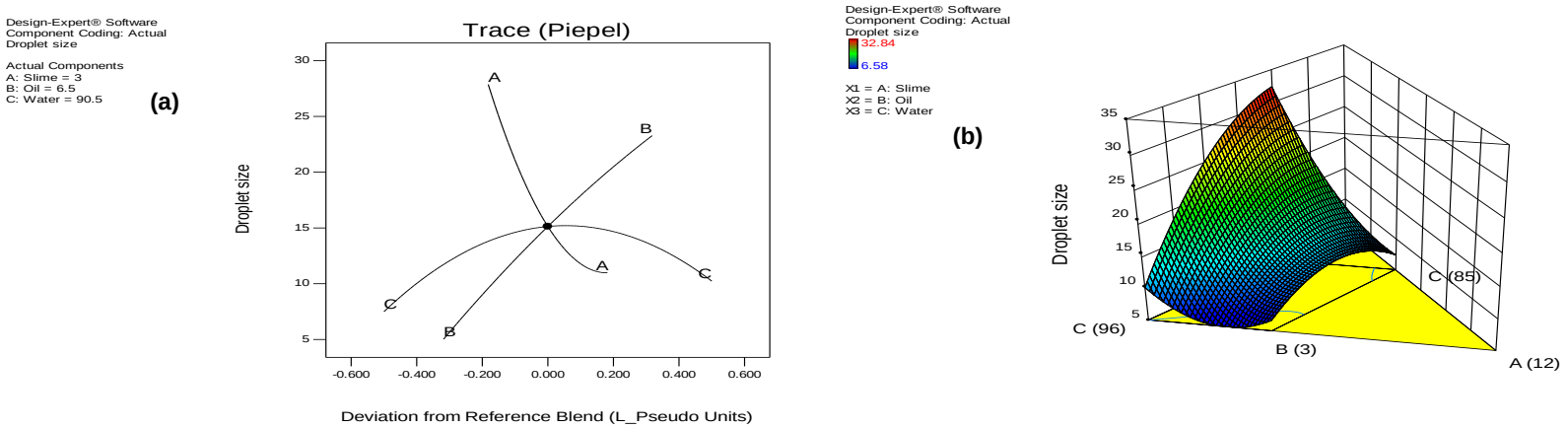

Figure 0.5: (a) Trace (Piepel) plot and (b) mixture design surface plot for the effect of 3 components (A: ACM, B: oil and C: water) on Sauter mean diameter

Based on the literature, an extremely sensitive response by ACM shown by sharp curvature effect on stability as a function of $D_{(3,2)}$ is the most dominant effect among the three mixture constituents. The observation of dominance of ACM concentration in the stability ($D_{(3,2)}$) as evidenced by higher RC values in the syergies between oil and water with ACM was confirmed in the mixture design surface plots as the stability (BS flux %) was greatly influenced by ACM (Figure 5.5b). The actual stability-$D_{(3,2)}$ value obtained on the mixture design surface plots (Figure 5.5b) was 6.6 nm which compares favorably with the value obtained as the average $D_{(3,2)}$ (6.7 ± 0.1 nm). The significance of a low $D_{(3,2)}$ is that the particles of the ACM stabilised O/W-type nanoemulsions are more tightly packed which makes it less susceptible to kinetic instability mechanisms. Hence with the low $D_{(3,2)}$ the nanoemulsion take a longer time to coalesce hence they remain stable. Although the $D_{(3,2)}$ is low, as a result of the adhesion of ACM at the oil and water interface, the creaming of the emulsion is avoided hence the nanoemulsion maintains stability. Literature supports the claim that emulsifiers reduce interfacial tension and reduce coalescence in oil droplets (McClements, 2015; Jin et al., 2017). The mixture design surface plots (Figure 0.5b) also showed that as the concentration of ACM increased, the stability increased as $D_{(3,2)}$ values became lower. Similar results were obtained for oil as stability ($D_{(3,2)}$) decreased with increasing concentrations of oil (Figure 0.5b). In the case of water, the stability increased with increasing concentrations of water as $D_{(3,2)}$ values became lower. This means that the water-solubility of ACM was needed to ensure stability (low $D_{(3,2)}$ values). The effects of the three independent variables on stability ($D_{(3,2)}$) as shown in the Piepel trace plot (Figure 0.5a) agrees with the results obtained from the mixture design surface (Figure 0.5b), where the stability (low $D_{(3,2)}$ values) is as a result of the concentration of ACM which influenced the emulsifier-ACM oil ratio (EOR). The result that ACM by showing a sharp curvature effect on the effect of three mixture components on stability as a function of $D_{(3,2)}$ values agrees with results reported by Diedericks & Jideani (2015) and Habib & AbouGhaly (2016).

5.2.5 Process optimisation for stability (backscattering % flux) of ACM stabilised O/W-type nanoemulsion

The stability as a function of backscattering (BS) % flux of the ACM stabilised O/W-type nanoemulsion obtained from all the observed responses from randomised runs in the D-optimal mixture design runs designed using the Design-Expert (10) software (StatEase, Inc., Minneapolis, USA) are given in the experimental responses from randomised runs in the D-optimal mixture design (Table 0.5). The experimental responses (Table 0.5) were used to calculate the coefficients of the polynomial equation, subject to the degree of fit, predictive power, and robustness of the model, and the derived equation was then used to predict the

predicted values of BS % flux of the nanoemulsions. The predicted values fitted well with the experimental responses obtained from the RSM design as seen in Figure 0.46. The parity plot of the predicted value versus the experimental values for BS % flux of ACM stabilised O/W-type nanoemulsion gave a good indication of a good agreement between predicted and experimental responses as a straight line was observed through the origin (Figure 0.46).

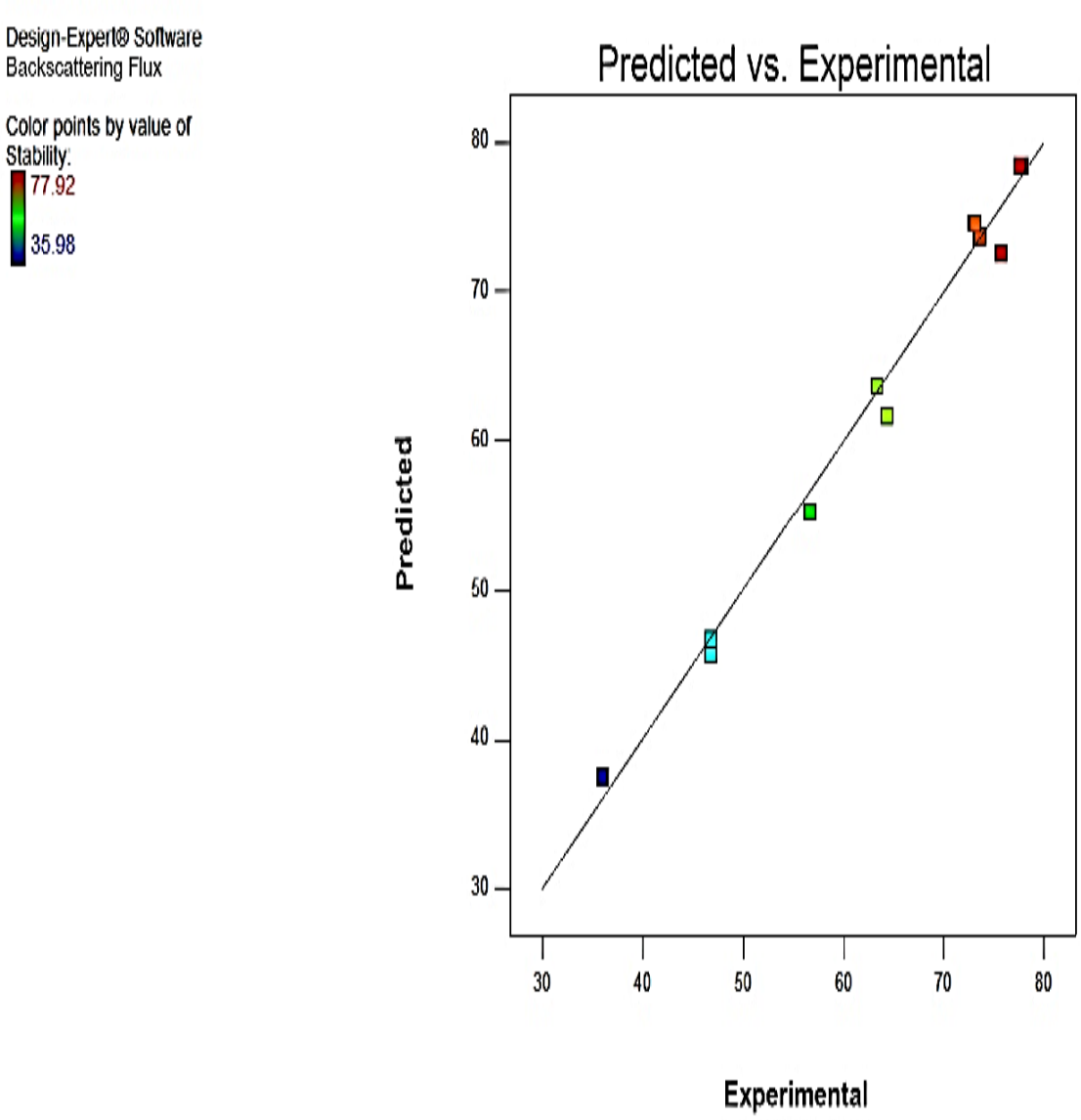

Figure 0.6: Parity plot of predicted and experimental values of backscattering flux % of ACM O/W-type stabilised nanoemulsion

The regression coefficients (RCs) obtained are shown in Table 0.67. Based on the regression coefficient values the greatest effect on the response BS flux % was caused by the

Table 0.8: Experimental responses from randomized runs for D-optimal mixture design[a, b, and c.]

Run	Dependent Variable	
	BS flux (%)	$D_{(3,2)}$ (nm)
1	36.0 ± 0.9	31.9 ± 0.6
2	36.0 ± 0.9	32.4 ± 0.6
3	63.4 ± 0.2	10.0 ± 0.3
4	72.99 ± 0.5	7.0 ± 0.2
5	56.7 ± 0.2	23.2 ± 0.6
6	77.9 ± 0.1	6.7 ± 0.1
7	77.7 ± 0.1	6.6 ± 0.1
8	73.6 ± 0.1	7.4 ± 0.2
9	64.4 ± 0.1	15.4 ± 0.4
10	63.4 ± 0.2	10.4 ± 0.4
11	46.8 ± 0.1	16.0 ± 0.5
12 (	73.2 ± 0.1	13.8 ± 0.4
13	73.7 ± 0.1	7.5 ± 0.2
14	46.9 ± 0.2	29.1 ± 0.5
15	75.8 ± 0.3	6.7 ± 0.2
16	73.2 ± 0.1	13.6 ± 0.4

[a]Indicated values are reported as means ± standard deviation (n = 5).
[b]ACM-African catfish mucilage, oil-sunflower oil, and water-MilliQ water
[c]**$D_{(3,2)}$**- Sauter mean diameter.

concentration of ACM as seen in Table 5.7. This could be due to the effect of the concentration of the bioemulsifier ACM on the stability as a function of BS % flux. It was established that ACM contains amide I functional/amino groups that bond with O/W nanoemulsions by adsorbing at the O/W interface resulting in stabilised nanoemulsions. Literature supports the claim that catfish mucus contains amphiphilic proteins which have been known to adsorb on nanoemulsion type interfaces (Hung et al., 2013; Shahkaramipour et al., 2017; Maravić et al., 2019). Hence, the amphiphilic proteins in ACM could assist with stabilising the O/W emulsions by influencing BS % flux. As seen from the results, the concentration of ACM had the greatest effect on the dependent variable BS % flux response (Table 0.67) and this result is consistent with the results that the concentration of ACM assists with stabilising the O/W emulsions by influencing BS % flux (Table 0.5).

Authors have established that a *p*-value lower than 0.05 is significant (Samson et al., 2016; Gharehbeglou et al., 2019). The *p*-value of the ANOVA results for the effect of the three independent variables on BS % flux response was significant < 0.0001 (Table 0.63). The R^2

value for the BS % flux model is 0.9567 and the closeness of this value to 1 makes it represent a good fit. The adequate signal to noise ratio for BS % flux response was given as 20.186 (

Table 0.3). Authors have reported that the adequate prediction compares the range of the predicted values at the design points to the average prediction error and a ratio greater than 4 is desirable (Gupta et al., 2016; Anupam et al., 2018). It can be observed that the signal to noise ratio for BS % flux is much higher than 4 as it is 20.186 (

Table 0.3). Hence, it can be inferred that the stability design space as a function of BS flux % for ACM stabilised O/W-type nanoemulsion contains minor noise/errors i.e. the experimental data set transmits more useful information/signal about the developed stability model for BS % flux.

The analysis of the BS % flux responses in the data sets gave a final reduced model with a significant *p*-value ($p < 0.0001$) as shown in Table 0.6. The regression coefficients (RCs) obtained are shown in Table 0.6. Authors have reported that negative RC values show antagonistic effect while positive RC values show a synergistic effect of the independent variables on the dependent variable/desired response (Alkhatib, Grunzke, & Chabot, 2016; Anupam et al., 2018). From the regression coefficient (RC) values for the final reduced model of L_Pseudo components for BS % flux, the highest RCs was found on the concentration of *ACM* (-26742. 66) this implied that the effect of concentration of ACM dominated the effects of the concentration oil +647.56) and water (+.64.04) respectively (Table 0.6). To further understand the effect of RC on the effect of BS % flux the main synergies on the quadratic relationship of parameters *A*, *B,* and *C* were analysed because they were significant. Authors have indicated that synergy effects on mixture design surface better interpret the effects of mixture constituents rather than linear coefficients which depend on the difference between the coefficients rather than their absolute magnitude (Baugreet et al., 2017; Konar et al., 2019). A close inspection of the synergy relationship between the parameters (Table 0.6) showed that *AB* and *AC* had high positive values, +35546.82 and +28600.28 respectively. This implied that the concentration of ACM was still the dominant factor in the sybergy relationship. Also, a positive value for synergies *AB* and *AC* shows that synergy was needed for stability (high BS % flux) to be achieved in ACM stabilised O/W-type nanoemulsions as ACM adheres to the oil and water interfaces of the O/W-type nanoemulsion to affect stability.

The significance of the synergy *AB* is that the ACM hydrophobic portion adsorbed at the oil interface of the O/W-type nanoemulsion thereby causing an adhesion at the ACM and oil interface to ensure stability. The reason for this occurrence could be that the hydrophobic tail parts of ACM could generate micelles in water that allowed the clustering of the ACM and oil together in other to form non-covalent bonds. Also, the significance of the synergy *AC* is that the ACM hydrophilic head adsorbed at the water interface O/W-type nanoemulsion thereby causing an adhesion at the ACM and water interface to ensure stability (Table 0.6). The reason for this occurrence could be that the hydrophilic head parts of ACM could generate micelles in water that allowed the

clustering of the ACM and water together in other to form hydrogen bonds. Also. It can be suggested that because of this solubility, ACM could adhere to the O/W interface and the high positive RC values could be the reason why both synergies were vital in ensuring high BS % flux values and ensure the stability of ACM stabilised O/W-type nanoemulsions. The significance of the simultaneous adhesion of the ACM to the oil and water interface is that kinetic instability is avoided. For instance coalescence which involves thinning and disruption of O/W-type nanoemulsion droplets to form larger ones is avoided as a result of stability with ACM. Also the presence of ACM also delays creaming or phase separation as the ACM covers and adheres to the oil-water interfaces of the O/W–type nanoemulsions which are stable because of the low $D_{(3,2)}$. The water-solubility of ACM could also have played a part as water solubility is essential for hydrophilic-lipophilic balance (HLB). This phenomenon could occur because ultrasonication of oil flocs could allow the ACM-emulsifier to cover oil and water particle interfaces which results in an interfacial layer that prevents phase separation and enhances stability evident in the high BS % flux values. The covering of the oil and water interfaces in the O/W-type nanoemulsion is due to adhesion and it was earlier established that ACM has mucoadhesive properties. Hence, the water solubility of ACM and its ability to stabilise O/W-type nanoemulsion could be as a result of its high HLB value. Literature supports the claim that emulsifiers that are water-soluble and stabilise O/W nanoemulsions have high HLB values (Burgos - Díaz et al., 2016; Nejadmansouri et al., 2016,; Kale & Deore, 2017). For instance, Nejadmansouri et al. (2016) conducted studies on the stability of fish oil nanoemulsions as a function HLB, emulsifier to oil ratio (EOR), and storage temperature. The authors reported that high HLB (9-15) was related to the solubility of different concentrations of the non-ionic surfactants that emulsified and enhanced the stability of the fish oil nanoemulsions (Nejadmansouri et al., 2016). The authors concluded that an emulsifier that could stabilise nanoemulsions should have high HLB values (Nejadmansouri et al., 2016). The high HLB value of the emulsifier would lead to the formation of interfacial layers that prevents phase separation and allows the emulsifier to cover oil and water interfaces (Burgos - Díaz et al., 2016, Nejadmansouri et al., 2016; Kale & Deore, 2017). Hence in agreement with other authors, the water-solubility of ACM and its ability to stabilise O/W-type nanoemulsion could establish its high HLB value and explain its stability as a function of high BS % flux. Also, the dominance of ACM in the quadratic synergy *AB* and *AC* shows that synergy was needed for stability (high BS % flux) to be achieved in ACM stabilised O/W-type nanoemulsions as reported by other authors. Therefore, the stability ACM stabilised O/W-type nanoemulsions (BS % flux) could be as a result of the simultaneous adhesion of hydrophobic tails of ACM to the oil interface, and the hydrophilic head of ACM and water interface to form stable bonds because it was within the critical micelle

concentration. Stability could be due to the presence of ACM amphiphilic proteins which contain both hydrophobic tails and the hydrophilic heads. The low negative RC value for *BC* (--1195.15) could be because oil and water do not mix normally hence an antagonistic effect was observed from the RC synergy of *BC* (Table 0.6*)*. However, mixing could occur when a high-energy technique such as ultrasonication is used to homogenize the oil and water to formulate stable nanoemulsions in the presence of ACM.

Literature supports the claim that an emulsifier can stabilise O/W emulsions if its HLB value is greater than 10 (Burgos - Díaz et al., 2016; Nejadmansouri et al., 2016; Kale & Deore, 2017). Hence, it can be deduced that the HLB value of ACM is aabove 10 as it stabilises O/W-type nanoemulsions. Hence stability is confirmed, from the combination of BS % flux response, significance *p*-value ($p< 0.0001$) of the effect of the three independent variables*,* the dominating RC values of the final reduced model for BS % flux in *AB, and AC* and the effect of ACM-emulsifier oil ratio (EOR) on O/W-type nanoemulsions. and literature evidence on HLB it can be deduced that stability of ACM stabilised O/W emulsions as a function of BS % flux could be explained by micelle theory.

5.2.6 Process optimisation for stability Sauter mean diameter of ACM stabilised O/W-type nanoemulsion.

The stability as a function of $D_{(3,2)}$ of the ACM stabilised O/W-type nanoemulsion obtained from all the observed responses from randomised runs in the D-optimal mixture design runs designed using the Design-Expert statistical software are given in experimental responses from randomized runs in the D-optimal mixture design (Table 0.5). The experimental responses (Table 0.5) were used to calculate the coefficients of the polynomial equation, subject to the degree of fit, predictive power, and robustness of the model, and the derived equation was then used to predict the optimised values of $D_{(3,2)}$ of the nanoemulsions. The predicted values fitted well with the experimental responses obtained from the RSM design as seen in Figure 0.57. The parity plot of the predicted value versus the actual values for $D_{(3,2)}$ of ACM stabilised O/W-type nanoemulsion gave a good indication of a good agreement between predicted and experimental responses (Figure 0.57).

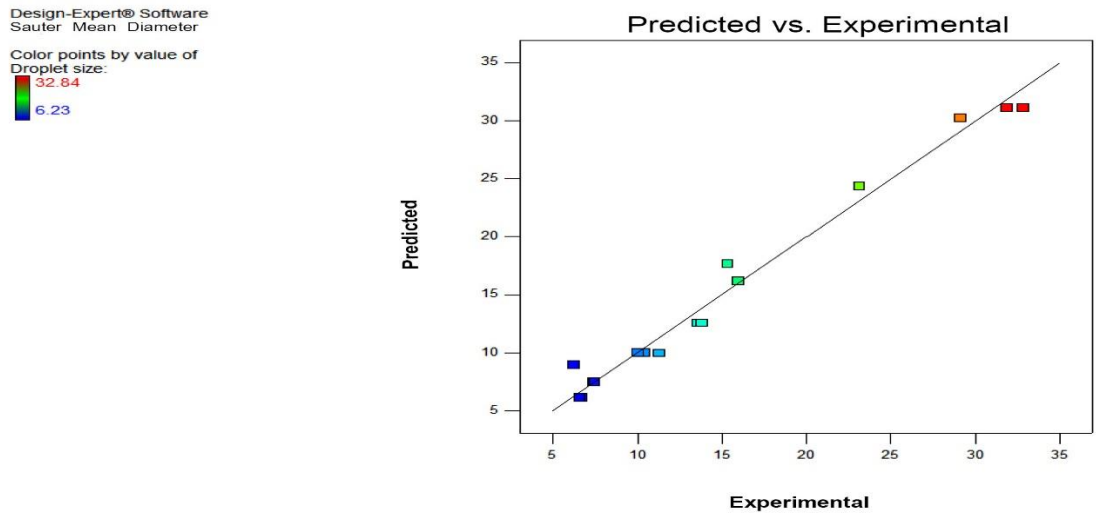

Figure 0.7: Parity plot of predicted and experimental values of Sauter mean diameter of ACM O/W-type stabilised nanoemulsion

To obtain the best fit model the experimental responses were statistically analysed using Analysis of variance (ANOVA) of the three independent variables. The regression coefficients (RCs) obtained are shown in 0.79. Based on the regression coefficient values the greatest effect on the response $\mathbf{D_{(3,2)}}$ was caused by the concentration ACM as seen in 0.79. This could be due to the effect of the concentration of the bioemulsifier ACM on the stability as a function of $\mathbf{D_{(3,2)}}$. It was earlier established that ACM contains amide I functional/amino groups that bond with O/W nanoemulsions by adsorbing at the O/W interface resulting in stabilised nanoemulsions. Also, amino groups are known to be building blocks of proteins. Literature supports the claim that catfish mucus contains amphiphilic proteins which have been known to adsorb on nanoemulsion type interfaces (Hung et al., 2013; Shahkaramipour et al., 2017; Maravić et al., 2019). It was also established that amphiphilic proteins in ACM assist with stabilising the O/W emulsions by influencing $\mathbf{D_{(3,2)}}$. As seen from the results, the concentration of ACM had the greatest effect on the dependent variable $\mathbf{D_{(3,2)}}$ response (Table 5.7) and this result is consistent with the results that the concentration of ACM assists with stabilising the O/W emulsions by influencing $\mathbf{D_{(3,2)}}$ (Table 0.5). Authors have established that a *p*-value lower than 0.05 is significant

Table 0.9: Regression coefficient values for the final reduced model of L_Pseudo Components for Sauter mean diameter[a, b c]**.**

Source	**$D_{(3,2)}$ (%)**
ACM (*A*)	+7906.40251
Oil (*B*)	-2601.19300

Water (*C*)	-6.90902
ACM * Oil (*A***B*)l	-12501.27336
ACM * Water (*A***C*)	-8268.83095
Oil * Water (*B***C*)l	+3436.43482

[a]ACM - Afirican catfish mucilage, [b]Oil - Sunflower oil, [c]Water - MiliQ water

(Samson et al., 2016; Gharehbeglou et al., 2019). The *p*-value of the ANOVA results for the effect of the three independent variables on $\mathbf{D_{(3,2)}}$ response was < 0.0001 which is lower than 0.05 and is significant (Table 0.4). The R^2 value for the $\mathbf{D_{(3,2)}}$ model is 0.9992 and the closeness of this value to 1 makes it represent a good fit. The adequate signal to noise ratio for $\mathbf{D_{(3,2)}}$ response was given as 104.158 (Table 0.4). Authors have reported that the adequate prediction compares the range of the predicted values at the design points to the average prediction error and a ratio greater than 4 is desirable (Gupta et al., 2016; Anupam et al., 2018). It can be observed that the signal to noise ratio for $\mathbf{D_{(3,2)}}$ is much higher than 4 as it is 104.158. Hence, it can be inferred that the stability design space as a function of $\mathbf{D_{(3,2)}}$ for ACM stabilised O/W-type nanoemulsion contains minor noise/errors i.e. the experimental data set transmits more useful information/signal about the developed stability model for $\mathbf{D_{(3,2)}}$.

The analysis of the $\mathbf{D_{(3,2)}}$ responses in the data sets gave a final reduced model with a significant *p*-value (*p*< 0.0001) as seen in 0.79. The regression coefficients (RCs) obtained are shown in 0.79. Authors have reported that negative RC values show antagonistic effect while positive RC values show a synergistic effect of the independent variables on the dependent variable/desired response (Alkhatib et al., 2016; Anupam et al., 2018). From the r*egression* coefficient (RC) values for the final reduced model of L_Pseudo components for $\mathbf{D_{(3,2)}}$, the highest RCs was found on the concentration of *ACM (*+7906.40) this implied that the effect of concentration of ACM dominated the effects of the concentration oil (-2601.19) and water (-6.91) respectively (0.79). To further understand the effect of RC on the effect of $\mathbf{D_{(3,2)}}$ the main synergy and quadratic relationship of parameters *A*, *B,* and *C* were analysed because they were significant. Authors have indicated that synergy effects on mixture design surface better interpret the effects of mixture constituents rather than linear coefficients which depend on the difference between the coefficients rather than their absolute magnitude (Baugreet et al., 2017; Konar et al., 2019). A close inspection of the synergy relationship between the parameters (0.79) showed that *AB* and *AC* had high negative values (-12501.27 and -8268.83) respectively. This implied that the concentration of ACM was still the dominant factor in the synergy relationship. A negative value for synergy in *AB* and *AC* shows that an antagonistic effect was needed for stability (low $\mathbf{D_{(3,2)}}$) to be achieved in ACM

stabilised O/W-type nanoemulsions as ACM adheres to the oil and water interfaces of the O/W-type nanoemulsion to affect stability. The significance of the synergy in *AB* is that the ACM hydrophobic portion adsorbed at the oil interface of the O/W-type nanoemulsion due to the low $\mathbf{D_{(3,2)}}$ thereby causing an adhesion at the ACM and oil interface to ensure stability. The reason for this occurrence could be that the hydrophobic tail parts of ACM could generate micelles in water that allowed the clustering of the ACM and oil together in other to form non-covalent bonds. Also, the significance of the synergy in *AC* is that the ACM hydrophilic head adsorbed at the water interface O/W-type nanoemulsion thereby causing an adhesion at the ACM and water interface to ensure stability. The reason for this occurrence could be that the hydrophilic head parts of ACM could generate micelles in water that allowed the clustering of the ACM and water together in other to form hydrogen bonds. Also. It can be suggested that because of this solubility, ACM could adhere to the O/W interface and the higher RC values could be the reason why both synergies were vital in ensuring high BS % flux values and ensure the stability of ACM stabilised O/W-type nanoemulsions. The low positive RC value of +3436.43 for *BC* could be because oil and water do not mix normally hence an antagonistic effect was observed from the RC synergy of *BC*. However, mixing could occur when a high-energy technique such as ultrasonication is used to homogenize the oil and water when the oil flocs were broken to assist in formulating stable nanoemulsions in the presence of ACM. Hence the result that the dominant effect on the ANOVA results for the effect of the quadratic synergys ACM*oil (*AB*) on the dependent variable $\mathbf{D_{(3,2)}}$ response (0.79) was due to the concentration of emulsifier- ACM which was antagonistic is consistent with the results that the emulsifier-ACM oil ratio (EOR) influences the $\mathbf{D_{(3,2)}}$ and ACM assists with stabilising the O/W-type nanoemulsions by influencing $\mathbf{D_{(3,2)}}$.

5.2.7 Optimisation of response

The final polynomial equations (Equations 5.1 and Equation 5.2) and the constituent were constrained with lower and upper limits. The 3 components in real scale amounted to 100% (1 % to 5 % for ACM, 3 % to 10 % for oil, and 85 % to 96 % for water) respectively listed in The numerical optimisation of an O/W-type nanoemulsion formulation was carried out according to the desirability function using the Design-Expert (Stat-Ease Inc., Minneapolis, Minnesota, U.S.A., version 10.0.7) statistical software. The research objective was to evaluate how the physicochemical properties of ACM affect its efficacy as an emulsifier in sunflower O/W-type nanoemulsion using ultrasonication to optimise the emulsion formation to provide the food-grade, cosmetics, drug delivery, and personal care industry with a low cost, eco-friendly alternative emulsifier. Desirability functions were chosen to either maximise BS % flux (γ_1) and minimise

Sauter mean diameter (γ_2) or maximise BS % flux (γ_1) and maximise Sauter mean diameter (γ_2). This desirability function was set to answer sub research objective questions on whether maximising BS % flux (γ_1) and minimising Sauter mean diameter (γ_2) or maximising BS % flux (γ_1) and maximising Sauter mean diameter (γ_2) would affect the desirability options. The sub research objective questions were also set to enable choices to be made for suitable mixture constituents' composition to fulfill emulsifier roles in the food, cosmetics, drug delivery, and personal care industry. Diverse nanoemulsion solutions representing different combinations of mixture constituents and independent variable levels were found by using the Design-Expert statistical software. These solutions were dependent on the degree to which the dependent variables BS flux (γ_1) and Sauter mean diameter (γ_2) were minimised and maximizsed. The overall desirability of the chosen formulation for option A (EOR 4.2:3) which involved maximising BS %flux (γ_1) and minimising Sauter mean diameter (γ_2) was 100%, which means that this formulation substantially satisfied the targeted constraints. Similarly, the overall desirability of the chosen formulation for option B (EOR 5:10) which involved maximising BS flux (γ_1) and maximising Sauter mean diameter (γ_2) was 95%, which means that this formulation substantially satisfied the targeted constraints. A study by Dokić et al. (2012) on the effect on oil concentration on the stability of octenyl succinic anhydride (OSA starch) stabilised sunflower O/W emulsions as a function of creaming rand apparent viscosity. The authors' investigated the effect of using 5-60% oil concentration in an emulsion and reported that emulsions containing 60% of dispersed sunflower oil with 8-16% concentrations of OSA starch were stable for 15 days of storage and creaming did not occur (Dokić et al., 2012). The authors observed that at the OSA starch concentration above 10% there was a drastic reduction in the creaming index values and stated that it was due to network structure formation through inter-molecular bonding of OSA starch molecules (Dokić et al., 2012). Hence, the structure formed increased the viscosity of the continuous phase, slowed down oil droplet movement, and reduced the rate of creaming, which means that increase in OSA starch concentration led to an increase in the physical stability of the investigated emulsions (Dokić et al., 2012). The authors concluded that an increase in the concentration of oil in emulsions stabilised by OSA starch caused a significant delay of creaming (Dokić et al., 2012). Furthermore, the authors also reported that as oil concentration increased from 5-60 % the apparent viscosity of the stabilised emulsions increased (Dokić et al., 2012).. Similarly, Xi et al (2019), investigated the effect of oil concentration (10-50 %) on the rheological, structural, and microstructural properties of ethanol- induced whey protein stabilised soy-bean oil emulsions: The authors observed that stabilised emulsions with higher oil concentration exhibited a higher degree of shear-thinning as the apparent shear viscosity decreased with increasing shear

rate. The authors concluded that the shear thinning displayed was consistent with the rheological properties of colloidal dispersions containing aggregated particles (Xi et al., 2019). Based on the literature (Dokić et al., 2012; Xi et al., 2019), the combination of independent variable constituents in option B (5 % ACM: 10 % oil: 85 % water) was selected for rheology tests because authors have reported that stabilised emulsions with higher oil concentration exhibited a higher degree of shear-thinning, viscosity, and viscoelastic rheological properties. The predicted stability value for BS % flux was 73.7 % while the $D_{(3,2)}$ value was 7.5 nm and the desirability was 95 %.

5.2.8 Validation of selected optimised formulation

The selected optimised formulation contains 5 % ACM: 10 % oil: 85 % water. The optimum formulations were selected to validate the chosen experimental domain and polynomial quadratic equations. Laboratory experiments were conducted in three replicates to determine the BS % flux and $D_{(3,2)}$ of the optimised formulation which contained 5 % ACM: 10 % oil: 85 % water. The predicted stability as a function of BS % flux and $\mathbf{D_{(3,2)}}$ was compared with the experimental stability values of the selected optimised formulation. The mean experimental values of BS % flux and $D_{(3,2)}$ were 73.6 ± 0.1 % and 7.5 ± 0.2 nm. The experimental stability of both BS % flux and $\mathbf{D_{(3,2)}}$ confirms the suitability of the model for food-grade, cosmetic, personal care, and drug delivery products.

5.2.8 Structural characteristics of O/W-type nanoemulsion formulation

Structural characterisation ACM stabilised O/W-type nanoemulsion formulation for the 16 randomised runs designed by Design-Expert software was conducted using Cryo-Transmission electron microscopy (TEM) imaging. The 16 random runs comprised of 11 different runs, with 5 runs that had two replicates.

Figure 0.8, Figure 0.9 and Figure 0.10 shows the TEM Images of O/W-type nanoemulsion stabilised with 1, 3, and 5 % concentration of ACM and oil concentrations in the range of 3.14-9.164 %.

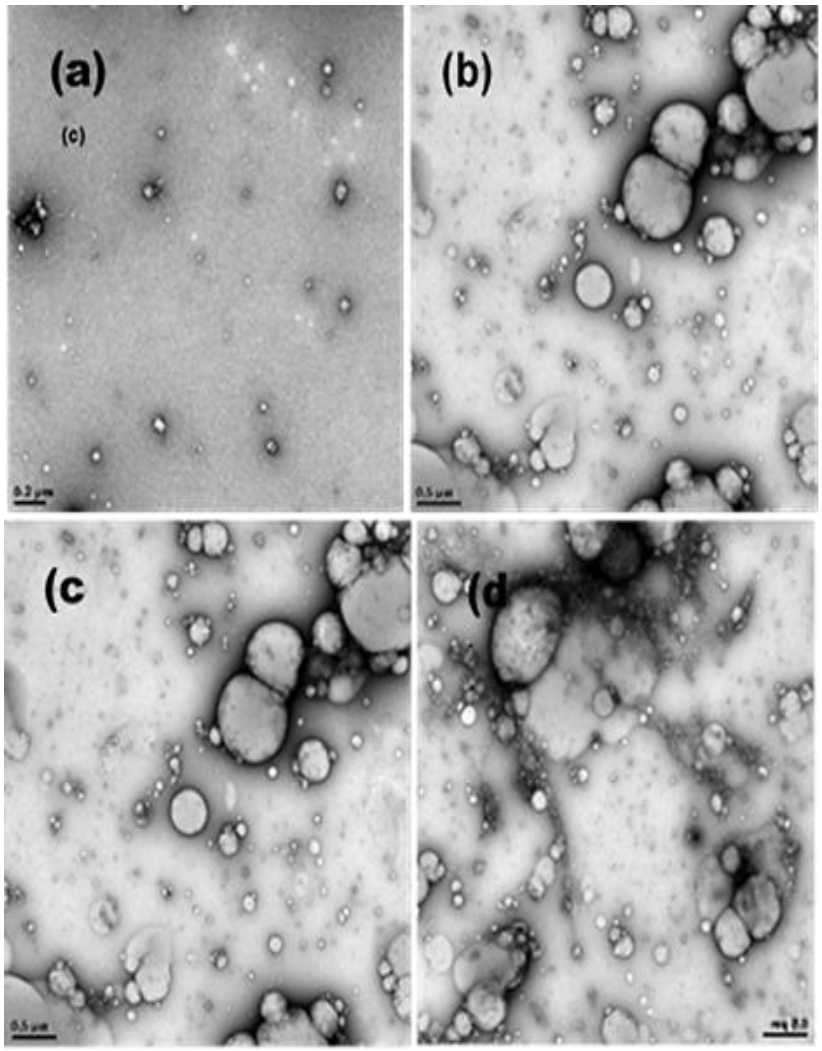

Figure 0.8: (a) Structural characteristics of ACM stabilised O/W-type nanoemulsions with emulsifier-ACM oil ratios of (a) 1:3.0 %, (b) 1:5.7 %, (c) 1:8.0%,and (d) 1:9.2 %.

The Cryo-TEM micrographs of the ACM stabilised O/W-type nanoemulsion showed that ACM encapsulated the O/W-type nanoemulsion and formed a consistent aggregate structure (

Figure 0.8, Figure 0.9 and Figure 0.10). Cryo-TEM studies also revealed that cross-linkage structure of mucins in ACM stabilised O/W-type nanoemulsions did not occur across the matrix but occurred preferentially via a heterogeneous distribution discretely in the networks matrix (

Figure 0.8, Figure 0.9 and Figure 0.10). The ACM contains amphiphilic filamentous threads that stabilises the network structure of stabilised emulsions. However, this stabilisation does not occur in every part of the matrix hence the stability is preferential as seen in Figure 5.8, 5.9 and 5.10. It is more pronounced with stabilised emulsions having EOR of 5:3, 5:4.6, 5:7.3, and 5:10 % as they

are more stable than emulsions containing 1 and 3 % ACM concentration. Hence, the structural stability of ACM stabilised O/W-type nanoemulsions was due to the presence of amphiphilic filamentous protein threads in ACM.

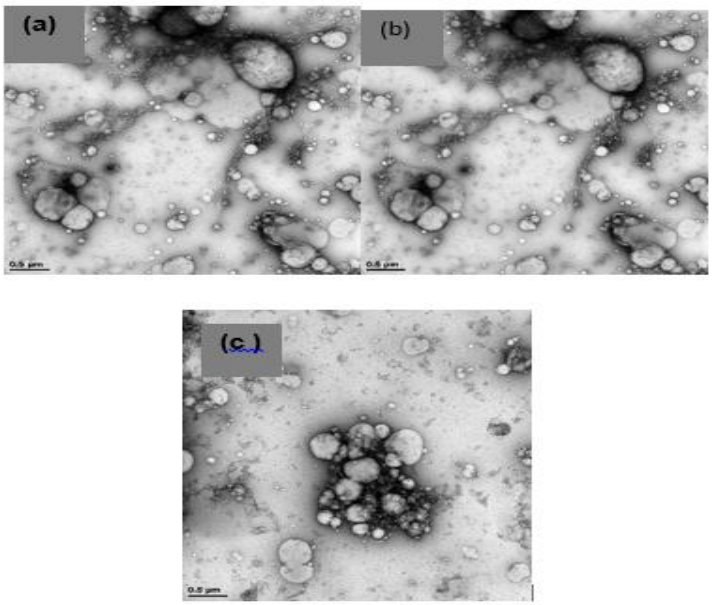

Figure 0.9: (a) Structural characteristics of ACM stabilised O/W-type nanoemulsions with emulsifier-ACM oil ratios of (a) 2.28:3 %, (b) 2.9:3.1 %, and (c) 3 3:6.2 %.

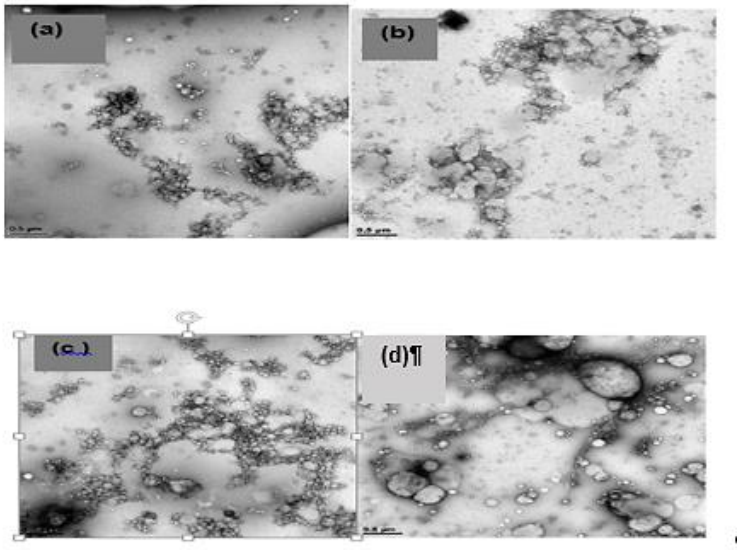

Figure 0.10: (a) Structural characteristics of ACM stabilised O/W-type nanoemulsions with emulsifier-ACM oil ratios of (a) 5:3 %, (b) 5:4.6 %, (c) 5:7.29 %, and (d) 5:10 %.

Authors have reported that cross-linkage structure of mucins in hagfish mucus did not occur across the matrix but occurred preferentially via a heterogeneous distribution discretely in the networks matrix (Fudge & Schorno, 2016). For instance, Fudge & Schorno (2016), investigated the predator defense functions of hagfish gland cells. The authors reported that hagfish gland thread cells contain fibers that were made-up of intracellular protein filaments. The authors proposed that the cross-linkage structure of mucins in hagfish mucus did not occur across the matrix but occurred preferentially via a heterogeneous distribution discretely in the networks matrix (Fudge & Schorno, 2016). The authors concluded that the filamentous threads of the mucins in hagfish mucus were the links that allowed cross-linkage to occur and result in the stable network structure of hagfish mucus (Fudge & .Schorno). Another study by on hagfish mucus gelation of soy milk gelation which resulted in creating flocculated fibrous emulsions revealed that the hagfish mucins influenced flocculation and enhanced cross-linking between hagfish slime and soya milk and resulted in a stable soy-slime emulsion. Based on literature claims, the stability of ACM stabilised O/W-type nanoemulsion is as a result of amphiphilic filamentous protein threads in ACM that enable a cross-linkage structure that does not occur across the matrix but occurs preferentially via a heterogeneous distribution discretely in the networks matrix as reported by (Fudge & Schorno, 2016).

The average particle size obtained using the TEM micrograph was consistent with that of the Zetasizer The particle size for ACM stabilised O/W-type nanoemulsion formulation is given as a function of $D_{(3,2)}$ in Table 5.5. It was observed that lower the oil concentration in the ACM stabilised O/W-type nanoemulsion the higher the stability as evidenced by lower $D_{(3,2)}$ (Table 5.5). Figure 5.9 shows the Cryo-TEM Images of O/W-type nanoemulsion stabilised with 2.28, 2.94, and 3.26 % concentration of ACM and oil concentration of 10, 3.14, and 6.15 % respectively. The Cryo-TEM micrographs of O/W-type nanoemulsion and the $D_{(3,2)}$ followed the same trend as that of ACM stabilised O/W-type nanoemulsion stabilised with 1 % ACM (Figure 5.2 and Table 5.1). The concentration of ACM influenced the stability of the stabilised O/W-type nanoemulsions despite the concentration of the oil in the ACM stabilised O/W-type nanoemulsion. The trend followed was the higher ACM concentrations (2.28 < 2.94 < 3.26 %), the higher the stability (lower $D_{(3,2)}$) of the ACM stabilised O/W-type nanoemulsion (Figure 0.2 and Table 0.1). Table 0.1 shows the of O/W-type nanoemulsion stabilised with ACM-emulsifier oil ratio of 5:3, 5:4.6, 5:7.3 and 5:10.0 % had a stability trend of (77.9 ± 0.1 %) followed by 4.6 % (75.8 ± 0.3 %), then 7.3 % (73.0 ± 0.5 % and 10.0 % (73.6 ± 0.1 %) respectively. The $D_{(3,2)}$ of O/W-type nanoemulsion stabilised with 1 % ACM concentration showed the same stability trend as that of ACM stabilised O/W-type nanoemulsion stabilised with 5 % ACM. The O/W-type nanoemulsion with oil concentration of 1

% had the stability trend of (63.36±0.2 %) followed by 5.73 nm (56.70±0.2 %), then 8.00 nm (46.85±0.2 %) and 9.64 nm (36.01±0.9 %) as seen in Table 5.1. Hence the $D_{(3,2)}$ influenced the stability of ACM stabilised O/W-type nanoemulsion and the trend was the higher the ACM concentration (ACM-EOR concentration) the higher the stability.

5.2.9 Functional group characteristics of ACM stabilised O/W-type nanoemulsion

The functional groups of the optimised selected ACM stabilised O/W-type nanoemulsion were confirmed through ATR-FTIR spectroscopy. The shifts in the wavelength peaks of ACM and ACM stabilised O/W-type nanoemulsion is compared in Table 0.100. There was a shift in the amide I of ACM 3301 cm^{-1} to 3344 cm^{-1} although comparable to the functional group of ACM it was modified which showed a kind of interaction (Table 0.100). This phenomenon was described by (Angulo & do Amaral Sobral, 2016), in the study of changes in the chemical composition of aloe vera and snail mucus composite scaffold using ATR-FTIR spectroscopy. The authors reported that when scaffolds of aloe vera and snail mucus was formulated shifts were observed which suggested an interaction in the spectra of the resulting compound. The interaction could be due to adhesions between the amino groups/protein micelles of ACM and oil globules of sunflower oil. Several authors have reported that amino groups/protein micelles interface with oil globules to form stable emulsions (Cagel et al., 2017; McClements et al., 2017; Reneeta et al., 2018; Liang et al., 2018; Bergenståhl & Spicer, 2019; Langevin, 2019). There was also a shift at the vibrational stretch of methyl groups from 2924 cm^{-1} in ACM to a peak of 2855 cm^{-1} in the ATR-FTIR spectra in ACM stabilised O/W-type nanoemulsion (Table 0.100). Furthermore, the glycoprotein methyl out of planar vibrations shifted from 2958 cm^{-1} to 2929 cm^{-1}, amide I at 1634 cm^{-1} shifted to 1645 cm^{-1}, C—O of carboxyl COO group accepting zero shifted from 1414 cm^{-1} to 1468 cm^{-1}, anti-symmetric C—O—C glycoside bond shifted from 1136 cm^{-1} to 1170 cm^{-1} (Table 0.10). Similar results were reported for wavelength peaks of ACM stabilised soya milk emulsions. The shift in the amide I of hydroxyl groups of hydrophilic amino acid groups of proteins from 3301 to 3344 cm^{-1} suggests that the proteins in the ACM are part of the stability mechanism of ACM stabilised O/W emulsion (Table 0.100). Authors have reported that amphiphilic proteins have been used to stabilise O/W emulsions (Burgos - Díaz et al., 2016; McClements et al., 2017; Maravić et al., 2019). Literature supports the claim that catfish mucus contains amphiphilic proteins or non-polar proteins which have been known to adsorb on nanoemulsion type interfaces (Hung et al., 2013; Shahkaramipour et al., 2017; Maravić et al., 2019). Hence it can be proposed that the non-polar proteins in ACM assist with stabilisng the O/W emulsions. This result that non-polar proteins in

ACM assist with stabilising the O/W emulsions.is consistent with reports by other authors Burgos - Díaz et al. (2016), McClements et al. (2017), and Maravić et al. (2019) .

Table 0.100: Comparison of wavenumbers of ACM and ACM stabilised O/W-type nanoemulsion

Wave number ACM (CM^{-1})	**Wave number O/W type nanoemulsion stabilised with ACM (CM^{-1})**	**Band assignments**	**References**
3301	3344	Possible broad peak stretching vibrations of hydroxyl groups of hydrophilic amino acids	(Angulo & do Amaral Sobral, 2016; Choo et al 2016)
2958	2929	Possible mucus/glycoprotein CH_2 out of plane vibration	(Angulo & do Amaral Sobral, 2016, Reneeta et al., 2018)
2924	2855	Possible CH_2 symmetric and out of plane vibration	(Angulo & do Amaral Sobral, 2016)
1634	1645	Possible Amide stretch, β-sheets absorption bands; Amide I	(Angulo & do Amaral Sobral, 2016; Pellegrini, et al., 2016)
1414	1468	Possible C-O of carbonyl COO group accepting zero or one H-bond	(Angulo & do Amaral Sobral, 2016, Fernando et al., 2017)
1136	1170	Anti-symmetric C-O-C glycoside bond; C-O strong bond stretch;	(Angulo & do Amaral Sobral, 2016, Tabrizi et al., 2016)

Chapter 6

FLOW AND VISCOELASTIC RHEOLOGICAL BEHAVIOR OF AFRICAN CATFISH MUCILAGE (ACM), ACM'S MOST STABLE EMULSION AND NANOEMULSIONS

6.1 Flow and viscoelastic rheological behaviour of ACM

This chapter provides results on the flow and visco-elastic rheological behavior of ACM, ACM stabilised soya milk emulsions and ACM stabilised O/W-type nanoemulsions. My original contribution to knowledge' is that this outcome could streamline the guidelines for process operations in the application of ACM for rheological quality and stability of ACMs' most stable emulsions and nanoemulsions. Also interpretations could result on guidelines dor the best fit models for ACM and ACMs' most stable emulsions and serve as a guidelines for the storage of the ACM and ACMs' most stable emulsions as it pertains to the linear viscosity range at low frequencies.

Oscillatory and rotational tests were performed to determine the flow and viscoelastic properties of ACM dispersion, soya milk, ACM stabilised O/W-type nanoemulsions, ACM stabilised soy milk emulsion, and African catfish mucus stabilised O/W-type nanoemulsion enriched with soya milk fiber respectively. Samples were equilibrated for 10 minutes before conducting the oscillatory tests (Adeyi et al.., 2014). Based on the results of two-way analysis of variance after Tukey's multiple comparisons test, the optimum African catfish mucilage (ACM) stabilised soy milk emulsion was chosen as emulsions having ACM-emulsifier soy milk ratio (ESMR) of 5:50 %. The methodology for achieving this research objective is described in section 3.3 of Chapter 3**.** The choice was based on recommendations of the highest stability (high BS % flux) and the level of significance (*p*-value < 0.05) of ACM stabilised soy milk emulsions. Based upon this choice, most stable emulsions with ACM-emulsifier soy milk ratio (ESMR) 5:50 % was selected. Also, the optimum ACM stabilised O/W-type nanoemulsion was chosen based on desirability functions to either maximise BS % flux (γ_1) and minimise Sauter mean diameter (γ_2) denoted as option A or maximise BS % flux (γ_1) and maximise Sauter mean diameter (γ_2) denoted as option B. Based on a D-optimal mixture design generated by the Design-Expert software (StatEase, Inc., Minneapolis, USA) and using mixture design surface methodology (RSM) two optimum concentrations were generated. The desirability functions led to ACM-emulsifier oil ratios (EORs) of 4.2:3 % for option A and 5:10 % for option B (**Error! Reference source not found.**, ection 5.2.7). The methodology for achieving this research objective is described in section 3.4 of

Chapter 3**.** However, the literature revealed that stabilised emulsions with higher oil concentration exhibited a higher degree of shear-thinning as the apparent shear viscosity decreased with increasing shear rate (Dokić et al., 2012; Xi et al., 2019). Hence, the emulsion with a higher oil ratio was chosen for the investigation to show the effect of ACM on flow and visco-elastic rheological behavior ACM stabilised O/W-type nanoemulsions. Therefore, this chapter details results and discussion on the experimental data obtained from performing the research objectives which involved investigating the effect flow and viscoelastic rheological behaviour of African catfish mucilage (ACM), and ACMs most stable emulsions and nanoemulsions. The methodology for achieving this research objective was described in section 3.5, Chapter 3**.**

6.2 Effect of African catfish mucilage on the viscosity of ACMs' most stable emulsions and nanoemulsions

Error! Reference source not found. shows the constituents in the ACM dispersion in MilliQ ater and ACMs' most stable emulsion and nanoemulsions used for the rheological characterisation in this work. Literature supports the claim that biopolymers improve the rheological roles of the continuous phase by reducing the interfacial tension between oil and water (Primozic et al., 2017; Junqueira et al., 2019). Hence, analysing changes in emulsion structure and rheology gives insights into the effects of biopolymers on stability (Primozic et al., 2017; Junqueira et al., 2019). Authors have reported that rotational steady-state operations reveal how the speed of mixing, pouring, and pumping operations influence emulsion quality (Junqueira et al., 2019). The effect on viscosity as the shear rate increases from 0.01 to 1000 s^{-1} for ACM (A), soya milk (B), ACM stabilised soya milk emulsion (C), ACM stabilised O/W-type nanoemulsion (D), and ACM stabilised O/W-type nanoemulsion enriched with soya milk Fiber (E), was performed using a controlled stress/strain rheometer (Physica MCR 502 rheometer, Anton Paar Com with parallel plate mode of 25 mm diameter stainless steel plates (PP25 S, Anton Paar, Austria) and a gap size of 0.5 mm. Samples were equilibrated for 10 minutes before conducting oscillatory tests as described by Adeyi et al. (2014)

Error! Reference source not found. shows the mean initial viscosity (MIV) of ACM (A), oy soya milk B), ACM stabilised soya milk emulsion(C), ACM stabilised O/W-type nanoemulsion (D), and ACM stabilised O/W-type nanoemulsion enriched with soya milk fiber (E), and at the lowest shear rate of 0.01 s^{-1}. In **Error! Reference source not found.** the results showed that the IV of ACM stabilised soy milk emulsions (2352.5 ± 1.3mPa.s) was higher than that of soy milk (661.3 ± 1.2 mPa-s). The data showed that ACM influenced the stability of the emulsion as it

affected the mean initial viscosity of the emulsion. This means that the viscosity i.e. the measure of soy milk's internal resistance to flow is less than that of ACM stabilised soy milk emulsions. The reason for this is that the ACM-emulsifier influences emulsion stability by forming films around the water drops in water/soy] milk interfaces. The films formed increases the stability of the emulsion by ensuring that the ACM adsorbs at smaller soy milk droplets interfaces. Hence the initial viscosity needed for flow to occur when shear stress is applied is higher than that for an emulsion with larger droplet size. Consequently, MIV of ACM stabilised soy milk emulsions were higher than that of soy milk. Hence the ACM stabilised soy milk emulsions were more stable than the soy milk because of higher MIV. Similarly, in **Error! Reference source not found.** the MIV of CM stabilised O/W-type nanoemulsion was lower

Table 0.1: Constituents in ACM dispersion in MilliQ water, soy milk, and ACMs' most stable emulsions.

		CONSTITUENTS			
TYPE	**SYMBOL**	**ACM (%)**	**Soy milk (%)**	**Oil (%)**	**Water (%)**
ACM dispersion in MIlliQ water	A	5	0	0	95
Soya milk	B		100		
ACM stabilised soy milk emulsion	C	5	50		45
ACM stabilised O/W-type nanoemulsion without fibre	D	5	0	10	85
ACM stabilised O/W-type nanoemulsion with fiber	E	5	50	10	35

[a] ACM African catfish mucilage

Table 0.2: Comparison of the Mean initial viscosity of ACM and its most stable nanoemulsions the lowest shear rate 0.01 s^{-1} [a]

TYPE	MEAN INITIAL VISCOSITY (mPa.s)
ACM	456.2 ± 1.2
Soy milk	661.3 ± 1.2
ACM stabilised soy milk emulsion	2352.5 ± 1.3
ACM stabilised O/W-type nanoemulsion without fibre	3476.1 ± 1.3
ACM stabilised O/W-type nanoemulsion with fibre	6468.0 ± 1.3

[a]ACM.African catfish mucilage

(3476.1 ± 1.3 mPa-s) than that of ACM stabilised O/W-type nanoemulsion enriched with soya milk fiber (6468.0 ± 1.3 mPa-s). The reason for this is that the ACM-emulsifier influences emulsion stability by forming films around the water globules in water/oil interfaces. The films formed increases the stability of the emulsion by ensuring that the ACM adsorbs at smaller oil droplets interfaces. This shows that the fibre enriched ACM stabilised O/W-type nanoemulsion was more stable than the ACM stabilised O/W-type nanoemulsion as a result of the higher MIV. Authors have reported that rotational steady-state operations reveal how the speed of mixing, pouring, and pumping operations influence emulsion stability and rheological properties (Liang et al., 2018; Junqueira et al., 2019). Authors have also reported that bioemulsifiers improve the stability and viscosity of the continuous phase by reducing the interfacial tension between oil and water give insights into the effects of biopolymers on stability (Primozic et al., 2017; Junqueira et al.2019). The result that the ACM influenced the viscosity of stabilised ACM stabilised soya milk emulsion(C), ACM stabilised O/W-type nanoemulsion (D), and ACM stabilised O/W-type nanoemulsion enriched with soya milk fiber (E) is consistent with reports by Primozic et al. (2017), Junqueira et al. (2019), and Maravić et al. (2019) that bioemulsifiers influence stability and rheological (viscosity) properties of emulsions.

6.3 Rheological behaviour of African catfish mucilage

The effect of viscosity as the shear rate increases from 0.01 to 1000 s^{-1} was investigated for African catfish mucilage (ACM) to study the effect of shear on ACM. As expected ACM showed a distinct shear-thinning behaviour (Figure 0.1). It was noted that the viscosity of the mucus decreased as the shear rate increased while the shear stress increased as the shear rate

increased. The result obtained that ACM had a shear-thinning behaviour and showed clear separations of

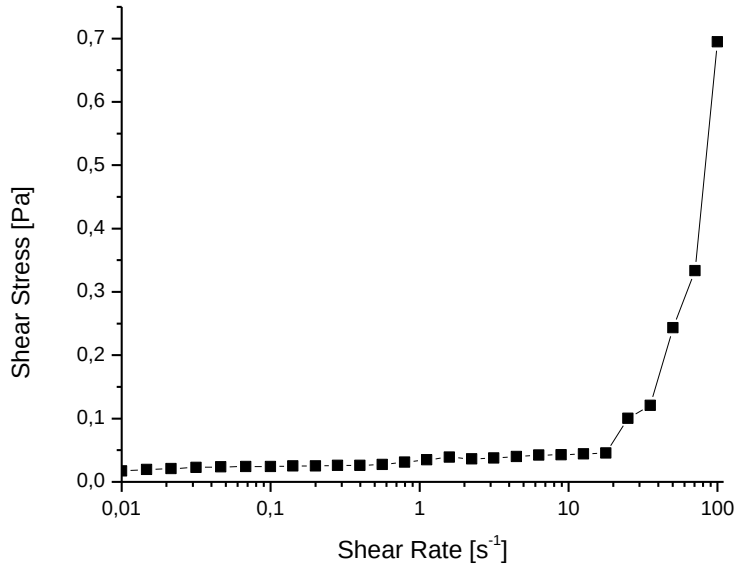

Figure 0.1: The effect of shear rate on the shear stress of African catfish mucilage

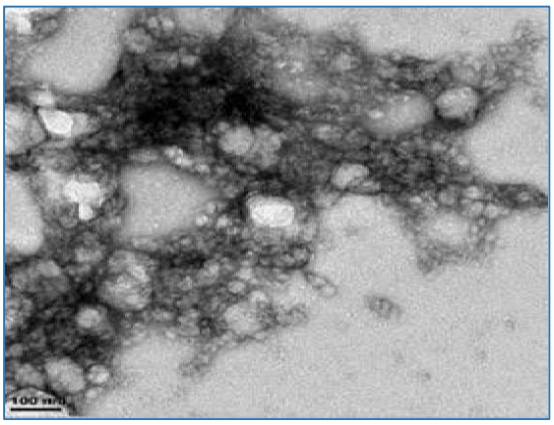

Figure 0.2: Cryo-TEM image of African catfish mucilage (ACM) with cross-linkages from filamentous protein threads that stabilise the network structure of ACM

dense gel and watery clusters is consistent with results reported by Böni et al. (2016b) for hagfish mucus. The authors investigated the effect of shear flow on the mucus properties of hagfish mucus at shear rates of 1, 10, and 100 s^{-1} and reported that hagfish mucus displayed a shear-thinning behaviour even when the shear rate was kept constant (Böni et al., 2016b). Figure 0.2

shows the TEM image of ACM with cross-linkages from filamentous protein threads that stabilise the network structure of ACM. The observed formation of a dense gel and watery clusters at different parts of the network matrix could be as a result of the ACM not forming a cross-linkage structure across the matrix but formed clear separations into a dense gel and watery clusters across the ACM matrix (Figure 0.2). This observation agrees with reports by Fudge & Schorno (2016) who proposed that the cross-linkage structure of mucins in hagfish mucus did not occur across the matrix but occurred preferentially via a heterogeneous distribution discretely in the networks matrix. The authors concluded that the filamentous threads of the mucins in hagfish mucus were the links that allowed cross-linkage to occur and result in the stable network structure of hagfish mucus (Fudge & Schorno, 2016). The authors further proposed that the filamentous protein threads of the mucins in hagfish mucins resulted in the inclusive viscoelasticity of the hagfish mucus by forming a viscoelastic network (Fudge & Schorno, 2016)). The phenomenon was ascribed to circling and entwining of the hagfish filaments or strands around the upper plate geometry of the rheometer which resulted in dissociation into a watery mass and a concentrated gel (Böni et al., 2016b; Böni et al., 2018). The authors further suggested that hagfish mucin was not stable under shear stress resulted in lower viscosity as it formed aggregates of dense gels and a watery portion (Böni et al., 2016b; Böni et al., 2018). The same phenomenon was observed when ACM was subjected to shear rates of 1, 10, and 100 s^{-1}. Hence, consistent with results obtained by authors such as Böni et al. (2016b) and Böni et al. (2018), it appears that ACM mucin is not stable to shear because of the clusters of dense gel and watery fraction formed after shear flow. Authors have described the phenomenon whereby shear stress results in cluster formation of mucins and a transition to dense gel solids is ascribed to interactions between inter-molecular hydrophobic protein fragments (Böni et al., 2016b; Esposito, Kirilov, & Roullin, 2018). Hence it is suggested that as a result of the large molecular weight and high amounts of protein in ACM mucin shear stress results in the ACM mucin cluster and enables interactions between inter-molecular hydrophobic protein fragments in agreement with Böni et al. (2016b) and Esposito et al. (2018).

6.4 Rheological behaviour of African catfish mucilage most stable emulsions

The effect on viscosity as the shear rate increases from 0.01 to 1000 s^{-1} for African catfish mucilage (ACM) stabilised O/W-type nanoemulsions, ACM stabilised O/W-type nanoemulsions enriched with soya milk fiber, soya milk fiber, and ACM stabilised soy milk fibre emulsion is shown in Figures 6.3 and 6.4 respectively. All ACMs' most stable emulsions and soya milk fibre (control) showed shear-thinning behaviour as it was observed that the viscosity of the mucus decreased

as the shear rate increased while the shear stress increased as the shear rate increased (Figures 6.3 and 6.4). The same shear-thinning behaviour observed with the viscosity of ACM was observed with the viscosities of ACM O/W-type nanoemulsions and ACM stabilised O/W-type nanoemulsion enriched with fibre. Similarly, the same shear-thinning behaviour was observed with the viscosity of soy milk the control and ACM stabilised soy milk emulsion (Figure 6.4). The mean initial viscosity (MIV) of ACM, soy milk (control), ACMs' most stable emulsions, and nanoemulsions are shown in Table 6.2. The MIV of soya milk (661.3 ± 1.2 mPa.s) was higher than that of ACM (456.2 ± 1.2 mPa.s) as seen in Table 6.2. Also, the MIV of ACM stabilised O/W-type nanoemulsions enriched with soya milk fiber (6468.0 ± 1.3 mPa.s) was higher than that of ACM stabilised O/W-type nanoemulsions (3476.1 ± 1.3 mPa.s) as seen in Table 6.2. However, the MIV of ACM stabilised O/W-type nanoemulsions enriched with soya milk fiber increased by a higher factor which suggested that a kind of synergy occurred between ACM and the soy milk fiber (Table 6.2). This viscosity increase has been explained by several authors who reported that amphiphilic proteins in bioemulsifiers such as mucins influence the rheological quality of O/W nanoemulsion interfaces (Primozic et al., 2017; Junqueira et al., 2019; Maravić et al., 2019). For instance a study by Böcker et al. (2016), who investigated the effect of fiber re-enforcement on hagfish mucus stabilised emulsions with the aid of biopolymers. The authors reported that hagfish slime in seawater loses its structural stability under shear as the shear rate increases from 0.01 to 100 s^{-1} (Böcker et al., 2016). The authors rectified this challenge with the aid of biopolymers such as chitosan, κ-Carrageenan, and starch and were able to obtain compounds with stable structures from the hagfish mucus and the biopolymers investigated (Böcker et al., 2016). The authors concluded that the re-enforced fiber compound formed had distinct cohesion and were stable to shear (Böcker et al., 2016). The stability in the re-enforced fiber compound might be due to the fact that as the shear rate increased it took a long time for the average cluster sizes to decrease hence leading to higher MIV. Authors have reported that shear-thinning is due to reduced average cluster sizes as the shear rate is being increased (Liu et al 2016). Also, shear-thinning could be due to deformation of emulsion droplet clusters under

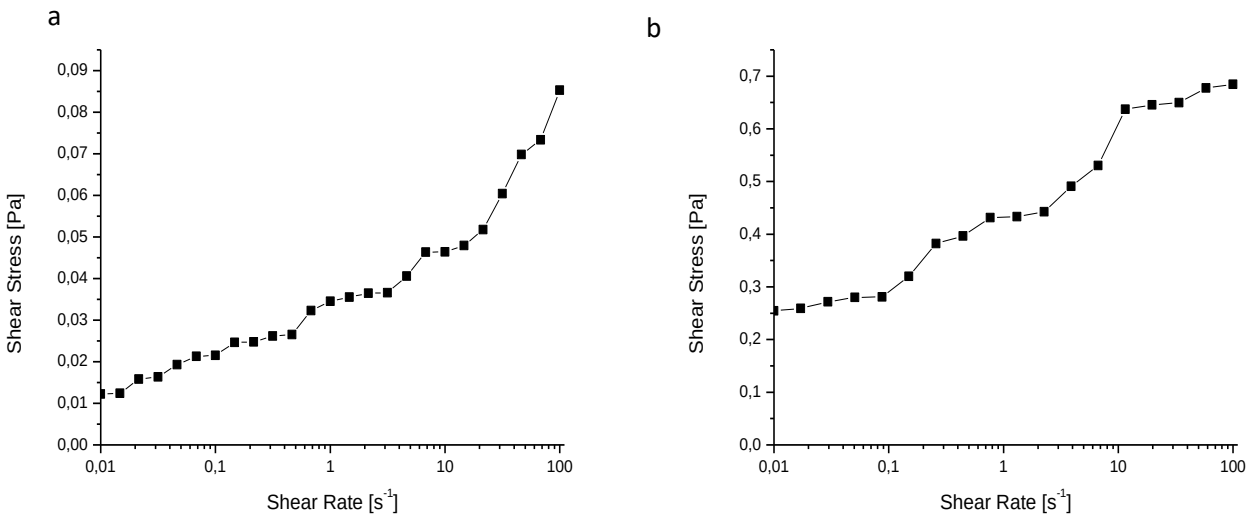

Figure 0.3: The effect of shear rate on the shear stress of (a) African catfish mucilage (ACM) stabilised O/W-type nanoemulsions, (b) ACM stabilised O/W-type nanoemulsions enriched with soya milk fiber

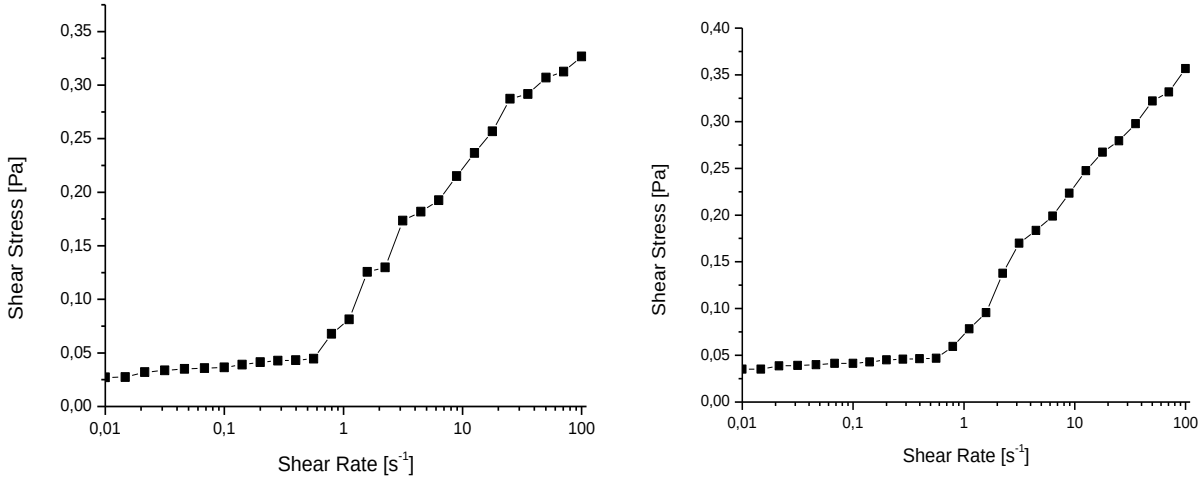

Figure 0.4: The effect of shear rate on the shear stress of (a) soya milk fiber, (b) ACM stabilised soy milk emulsion

shear stress (Liu et al 2016). Hence the higher structural stability in ACMs'most stable emulsion E in comparison with D might be due to delay in deformation of nanoemulsion droplet clusters under shear stress as a result of fibre re-enforcement. This is evidenced by the fact that the ACMs' most stable emulsion E (ACM stabilised O/W-type nanoemulsions enriched with soya milk fiber) had a higher MIV in comparison to D (ACM stabilised O/W-type nanoemulsions). The results obtained on ACM stabilised O/W-type nanoemulsions enriched with soya milk fiber show that synergy occurred between ACM and the soy milk fiber (Figure 0.3b and Table 0.2) and are consistent with results reported by Böcker et al. (2016) for the effect of fiber re-enforcement on hagfish mucus stabilised emulsions with the aid of biopolymers.

Figure 0.5 shows the Cryo-TEM images of ACM stabilised O/W-type nanoemulsion and ACM stabilised O/W-type nanoemulsion enriched with soy milk. It was observed that the network cross-linkage in Figure 0.5b was less deformed than that of Figure 0.5a which establishes that the structure of ACM stabilised O/W-type nanoemulsion enriched with soya milk could be more stable to shear. This was further established by the higher value of mean initial viscosity in ACM stabilised O/W-type nanoemulsion enriched with soya milk in comparison with ACM stabilised O/W-type nanoemulsion (Table 0.2). The Cryo-TEM images (Figure 0.5) and the mean initial viscosity values (Table 0.2) support the observation that there was a synergistic effect between ACM and soya milk fibe. This was the control soymilk fibre (B) which had an MIV of 661.3 ± 1.2 mPa.s and ACM (A) with 456.2 ± 1.2 mPa.s in comparison to 2352.5 ± 1.3 mPa.s (C), This can be explained by the fact that shear-thinning, could be due to the deformation of emulsion droplet clusters under shear stress (Liu et al 2016). Hence, the higher structural stability in ACMs' most stable emulsion E in comparison to D might be due to delay in deformation of nanoemulsion droplet clusters under shear stress as a result of fibre re-enforcement. Consequently, the ACM stabilised O/W- type nanoemulsions enriched with soya milk fiber had a higher MIV in comparison to ACM stabilised O/W-type nanoemulsions.

6.5 Flow behaviour of O/W emulsions as described by different models

Table 0.1 gives constituents in ACM dispersion in MilliQ water and ACMs' most stable emulsions while the flow curves of African catfish mucilage (ACM) dispersion in MilliQ water and its most stable emulsions are given in Figure 0.1, Figure 0.3, and

Figure 0.4. The flow curves of ACM) dispersion in MilliQ water (Figure 0.1) and ACMs' most stable emulsions (Figure 0.3, and

Figure 0.4) showed shear-thinning behaviour as it was observed that the viscosity of the mucus decreased as the shear rate increased while the shear stress increased as the shear rate increased. The mathematical expression of the time-independent behaviour used in this study for the Power Law, Herschel-Buckley, Casson, and Bingham models considered are given in Equations 6.1, Equation 6.2, 6.3 and Equation 6.4 respectively.

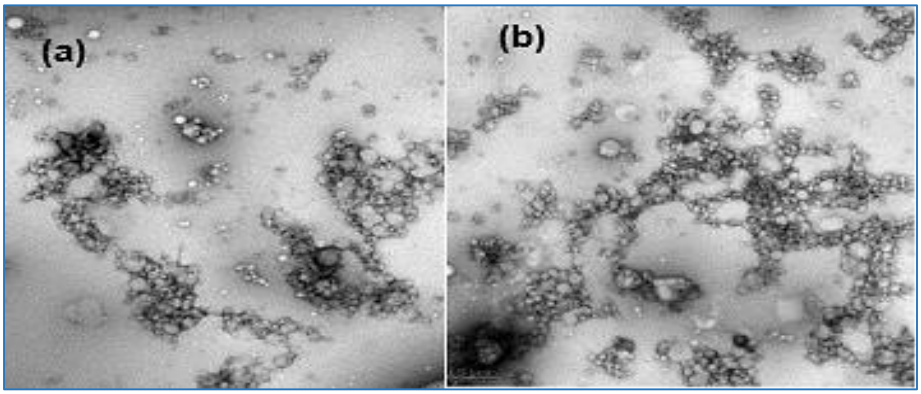

Figure 0.5: Cryo-TEM images of (a) ACM stabilised O/W-type nanoemulsion and (b) ACM stabilised O/W-type nanoemulsion enriched with soy milk fiber

6.6 Flow behaviour of O/W emulsions as described by different models

Table 0.1 gives constituents in ACM dispersion in MilliQ water and ACMs' most stable emulsions while the flow curves of African catfish mucilage (ACM) dispersion in MilliQ water and its most stable emulsions are given in Figure 0.1, Figure 0.3, and

Figure 0.4. The flow curves of ACM) dispersion in MilliQ water (Figure 0.1) and ACMs' most stable emulsions (Figure 0.3, and

Figure 0.4) showed shear-thinning behaviour as it was observed that the viscosity of the mucus decreased as the shear rate increased while the shear stress increased as the shear rate increased. The mathematical expression of the time-independent behaviour used in this study for the Power Law, Herschel-Buckley, Casson, and Bingham models considered are given in Equations 6.1, Equation 6.2, 6.3 and Equation 6.4 respectively.

The Power law model or the Ostwald de Waele law is expressed by Equation 6.1 and the Herschel–Buckley model which is used when yield stress is taken into consideration can be expressed by Equation 6.2 (Vadodaria et al., 2018; Kubo et al., 2019; Hentati et al., 2020).

$$\boldsymbol{\tau} = K\dot{Y}^{\eta} \qquad \textbf{Equation 6.1}$$

$$\boldsymbol{\tau} = \boldsymbol{\tau_0} + K\dot{Y}^{\eta} \qquad \textbf{Equation 6.2}$$

Where τ is the shear stress (Pa), $\boldsymbol{\tau_0}$ is the yield stress (Pa), $\dot{Y}$ is the shear rate (s^{-1}), K is consistency coefficient (Pa s^n), and η is flow behaviour index (where η = 1 represents Newtonian behaviour, η > 1 (shear-thickening) dilatant and η < 1 (Shear-thinning) pseudoplastic (Wang et al., 2016; Vadodaria et al., 2018; Kubo et al., 2019; Hentati et al., 2020). Other models like the Bingham and Casson, (Equations 6.3 and 6.4 respectively), have been used to characterise food-grade emulsions (Vadodaria et al., 2018; Kubo et al., 2019).

$$\boldsymbol{\tau} = \boldsymbol{\tau}^{B}_{0} + \eta^{B}\,\dot{Y} \qquad \textbf{Equation 6.3}$$

$$\boldsymbol{\tau}^{0.5} = \boldsymbol{\tau}(^{C}_{0})^{0.5} + (\eta^{C})^{0.5}\,\dot{Y}^{0.5} \qquad \textbf{Equation 6.4}$$

Where $\boldsymbol{\tau}$ is the shear stress, the $\boldsymbol{\tau}^{B}_{0}$ is the Bingham yield stress, the $\dot{Y}$ is the shear rate (s^1), η^{B} is the Bingham plastic viscosity (Pa.s), η^{C} is the Casson plastic viscosity (Pa.s), and $(\boldsymbol{\tau}^{C}_{0})^{0.5}$ is Casson yield stress, and $Y^{0.5}$ is the Casson shear rate (Vadodaria et al., 2018; Kubo et al., 2019).

The rheological models were used to fit the data using the Microsoft Excel Solver function. The model parameters of the Power Law, Herschel-Buckley, Bingham, and Casson models are described in **Error! Reference source not found.**, Table 0.4, Table 0.5, and Table 0.6 respectively. African catfish mucilage dispersion in MilliQ water (A), soy milk (B), ACM stabilised soya milk emulsion (C), ACM stabilised O/W-type nanoemulsion (D), and ACM stabilised O/W-type nanoemulsion enriched with soy milk fiber (E) experienced shear thinning (non-Newtonian behaviour) as η the flow behaviour index was less than 1.0 (**Error! Reference source not found.** nd Table 0.4). It was observed from **Error! Reference source not found.** and Table 0.4 that the flow behaviour index for ACM and studied emulsions were less than 1.0 hence ACM (A), soy milk (B), ACM stabilised soya milk emulsion (C), ACM stabilised O/W-type nanoemulsion (D), and ACM stabilised O/W-type nanoemulsion enriched with soy milk fiber (E) are non-Newtonian and displays shear-thinning and pseudoplastic. Authors have reported that the flow behaviour index measures the degree of pseudoplastic behaviour (Mandal & Bera, 2015; Paximada et al., 2016). Hence the results obtained on the flow behaviour index for ACM, soy milk, and ACMs' most stable emulsions that they are non-Newtonian as η the flow behaviour index was less than 1.0, are pseudoplastic in behaviour and displays shear thinning, are consistent with results reported by

Guo et al. (2017) and Quinzio et al. (2018). For instance, ACM (A) had η values of 0.5638 for Power-law and η value of 0.8488 for the Herschel–Buckley model (**Error! Reference source not ound.** and Table 0.4). The observations for the flow index behaviour of ACM (A) (**Error! Reference source not found.** and Table 0.4) agreed with the results observed for the effect of shear rate on the viscosity of ACM (Figure 0.1). This trend was observed for soy milk (B), ACM stabilised soya milk emulsion (C), ACM stabilised O/W-type nanoemulsion (D), and ACM stabilised O/W-type nanoemulsion enriched with soy milk fiber E based on η values for Power-law model and the Herschel–Buckley law model (**Error! Reference source not found.** and Table .4). For instance, ACM stabilised O/W-type nanoemulsion (D), had η values of 0.2080 for Power-law, and η value of 0.2475 for the Herschel–Buckley model (**Error! Reference source not found.** nd Table 0.4). The results obtained from the flow index behaviour of ACM stabilised O/W-type nanoemulsion (D) and ACM stabilised O/W-type nanoemulsion enriched with soy milk fibre (E) in **Error! Reference source not found.** and Table 0.4agree with the results observed for the effect f shear rate on the viscosity of ACM (Figure 0.3). A comparison of the η values obtained for Power-law and the Herschel–Buckley model for ACM and all emulsions showed that the Herschel–Buckley model had higher η values (**Error! Reference source not found.** and Table 0.4). For instance, the range of values was from 0.1270 to 0.5638 and 0.1669 to 0.8488 respectively for Power-law and the Herschel–Buckley model. ACM, soy milk (control), and ACMs' most stable emulsions all had yield stress (**Error! Reference source not found.** and Table 0.4). According to the Casson model, the yield stress for both ACM and ACM stabilised O/W-type nanoemulsion (D), was 0.0016 and 6.4668E-05 respectively (Table 0.5). For the Bingham model, the yield stress for both ACM and

Table 0.3: Model parameters for the Power Law fitting of ACM, soy milk, and ACMs' most stable emulsions at a constant shear rate of 100 s^{-1} for 10 minutes and varied from 100 to 1000 s^{-1} at 25°C [a].

TYPE	n	K (Pa.S^{-1})	R^2	adj R^2	SSE	RMSE
A	0.5638	0.0499	0.9961	0.9956	0.309	0.107
B	0.1270	0.2369	0.8041	0.7878	0.003	0.0011
C	0.2472	0.1273	0.9569	0.9533	0.0635	0.049
D	0.2080	0.0337	0.7278	0.7051	0.00023	0.000029
E	0.1682	0.3717	0.8720	0.8614	0.0389	0.0379

[a] A=African catfish mucilage ACM) dispersion in MillQ water, B=soy milk, C=ACM stabilised soya milk emulsion,

D=ACM type nanoemulsion, and E=ACM stabilised O/W-type nanoemulsion enriched with soy milk fiber.

Table 0.4: Model parameters for the Herschel–Buckley Law fitting of ACM, soy milk, and ACMs' most stable at a constant shear rate of 100 s^{-1} for 10 minutes and varied from 100 to 1000 s^{-1} at 25°C [a].

TYPE	n	K ($Pa.S^{-1}$)	τ_o	R^2	adj R^2	SSE	RMSE
A	0.8488	0.0131	0.0289	0.9989	0.9988	0.0289	0.0119
B	0.1669	0.1730	0.0601	0.7222	0.6983	0.0026	0.0098
C	0.2063	0.1356	0.0024	0.9579	0.9544	0.0076	0.0533
D	0.2475	0.0275	0.00524	0.7438	0.7224	0.0111	0.00269
E	0.4148	0.0906	0.3100	0.9764	0.9745	0.2651	0.0991

[a] A=African catfish mucilage ACM) dispersion in MillQ water, B=soy milk, C=ACM stabilised soya milk emulsion, D=ACM type nanoemulsion, and E=ACM stabilised O/W-type nanoemulsion enriched with soy milk fiber.

Table 0.5: Model parameters for the Casson Law fitting of ACM, soy milk, and ACMs' most stable emulsions at a constant shear rate of 100 s^{-1} for 10 minutes and varied from 100 to 1000 s^{-1} at 25°C. [a]

TYPE	n^C	$\tau(^c_0)^{0.5}$	R^2	adj R^2	SSE	RMSE
A	0.0016	0.0300	0.9878	0.9867	1.0757	0.1996
B	0.00092	0.03391	0.9503	0.9462	0.0206	0.0276
C	0.00138	0.00670	0.9618	0.9587	0.0285	0.0033
D	6.4668E-05	0.00047	0.9739	0.9718	0.0009	0.00059
E	0.0004	0.0728	0.9826	0.9811	0.2283	0.0911

[a] A=African catfish mucilage ACM) dispersion in MillQ water, B=soy milk, C=ACM stabilised soya milk emulsion, D=ACM type nanoemulsion, and E=ACM stabilised O/W-type nanoemulsion enriched with soy milk fiber.

Table 0.6: Model parameters for the Bingham Law fitting of ACM, soy milk, and ACMs' most stable emulsions at a constant shear rate of 100 s^{-1} for 10 minutes and varied from 100 to 1000 s^{-1} at 25°C [a]

TYPE	n^B	$\tau(^B)$	R^2	adj R^2	SSE	RMSE
A	0.005	0.01	0.9878	0.9867	0.0484	0.0042
B	0.003	0.2161	0.7041	0.6922	0.0603	0.0047
C	0.0051	0.0756	0.9561	0.9544	0.0132	0.0022
D	0.0007	0.0122	0.7266	0.7157	0.0038	0.0118
E	0.0058	0.1455	0.5127	0.4933	0.4983	0.1358

[a] A=African catfish mucilage ACM) dispersion in MillQ water, B=soy milk, C=ACM stabilised soya milk emulsion, D=ACM type nanoemulsion, and E=ACM stabilised O/W-type nanoemulsion enriched with soy milk fiber.

ACM stabilised O/W-type nanoemulsion (D), was 0.005 and 0.0007respectively (Table 0.6). The yield stress was also observed in the fitting of Herschel-Buckley law model, for instance, both ACM and ACM stabilised O/W-type nanoemulsion (D), had yield stress values of 0.02898 and 0.00524 respectively (Table 0.4). The literature suggests that the Herschel-Buckley model was developed to originally accommodate the poor result given by the Power-law model at an extremely low shear rate (Khalil & Mohamed Jan, 2012). Furthermore researchers have indicated that the Herschel-Buckley model could be used as a better fit for emulsions that have both Power law and Bingham law characteristics. (Adeyi et al., 2018). The literature has defined the apparent yield stress as the applied stress that must be exceeded to make an emulsion to flow and it is a significant factor in many industrial processes such as pumping, spreading, and coating (Paximada et al., 2016). A number of researchers have used flow models to quantify the yield stress of foods such as salad dressing as an indicator of quality because it describes the ability of the dressing to be retained on salad surfaces (Zhang & McClements, 2018; Gavahian et al., 2018. The quantified yield stress of ACM obtained in this study could relate to the ability/retention power of ACM to adhere to soy milk or O/W-type nanoemulsion surfaces. Hence quantified yield stress obtained could serve as guidelines for estimating the ability of African catfish mucilage as an alternative natural emulsifier feedstock in food, personal care, and pharmaceutical industry.

A comparison of the R^2 and adjusted R^2 values for ACM and ACMs' most stable emulsions showed that the R^2 and adjusted R^2 values were higher for Herschel-Buckley (HB) model than for the Power Law model. For instance, R^2 and adjusted R^2 values for ACM were 0.9989 and 0.9988,

and 0.9961 and 0.9956 for HB and Power-law model respectively (Table 0.3 and Table 0.4). A similar trend was observed for ACM stabilised soya milk emulsion (C), ACM stabilised O/W-type nanoemulsion (D), and ACM stabilised O/W-type nanoemulsion enriched with soy milk fiber E. However, the trend was reversed for soy milk as the R^2 and adjusted R^2 values (0.7222 and 0.6983 respectively) for HB model were lower than those of the Power-law (0.8041 and 0.7878 respectively) for the R^2 and adjusted R^2 values (Table 0.3 and Table 0.4. In the case of the Bingham model, the R^2 and adjusted R^2 values were the least for ACM (A), soy milk (B), and ACMs' most stable emulsions (C, D, and E). For instance the Power-law R^2 and adjusted R^2 values for ACM, soy milk, and ACMs' most stable emulsions were 0.9878 and 0.9867 (A), 0.7041 and 0.6922 (B), 0.9561 and 0.9544 (C), 0.7266 and 0.7157 (D), and 0.5127 and 0.4933 (E) respectively (Table 0.3) . The R^2 and adjusted R^2 values for the HB model were higher than those of the Power-law and Bingham-law models but were lower than those of the Casson model (Table 0.3, Table 0.4, and Table 0.5). The R^2 and adjusted R Power-law parameters for ACM, soy milk, and its most stable emulsions were 0.9961 and 0.9956 (A), 0.8041 and 0.7878 (B), 0.9569 and 0.9583 (C), 0.7278 and 0.7051 (D), and 0.8720 and 0.8614 (E) respectively. The R^2 and adjusted R^2 for Casson law parameters were the highest they were 0.9878 and 0.9867 (A), 0.9503 and 0.9462 (B), 0.9613 and 0.9587 (C), 0.9739 and 0.9718 (D), and 0.9826 and 0.9811 (E) respectively (Table 0.5). Hence from the R^2 and adjusted R^2 values, the HB and Casson laws better fitted the flow rheological data of ACM, soy milk (B) ACM stabilised soya milk emulsion (C), ACM stabilised O/W-type nanoemulsion (D), and ACM stabilised O/W-type nanoemulsion enriched with soy milk fiber (E). The R^2 and adjusted R^2 value of the HB model indicated it had a better fit than the Casson model for the ACM rheological data. However, R^2 and adjusted R^2 value of the Casson model indicated that it had a better fit than the HB model for the ACM stabilised soya milk emulsion (C), ACM stabilised O/W-type nanoemulsion (D), and ACM stabilised O/W-type nanoemulsion enriched with soy milk fiber (E). Authors have reported that the Bingham-model is not a good fit in predicting emulsion flow behaviour at a very low shear rate and is also not suitable at very high shear rates, except corrections are made for the Bingham viscosity and Bingham yield stress (Folayan et al., 2017; Pajouhandeh et al., 2017). However, the Casson rheological model accurately characterises emulsion flow behaviour at low and high shear rates because a correction factor of power 0.5 has been added to the Casson equation (Chivero et al., 2016; Glicerina et al., 2016; Folayan et al., 2017; Pajouhandeh et al., 2017). Equation 6.4 specifies that a condition (a correction factor of power 0.5) must be fulfilled to enhance the models' accuracy in predicting emulsion flow behaviour. This condition stipulates a correction factor for Casson viscosity and Casson yield stress to ensure that the Casson model better fits data

(Chivero et al., 2016; Glicerina et al., 2016; Folayan et al., 2017; Pajouhandeh et al., 2017). This is reflected in the results obtained in the R^2 and adjusted R^2 values for all studied emulsions (A, B, C, D, and E). Hence the results obtained in our study that the Casson model has a better fit for our data because it predicted the emulsion flow behaviour more accurately at a very low shear rate and very high shear is consistent with results obtained by Chivero et al. (2016), Glicerina et al (2016), Folayan et al. (2017), and Pajouhandeh et al. (2017).

A comparison of the SSE and RMSE values was conducted for all models to further evaluate the most suitable model. The results showed that the SSE and RMSE values for the Power and Bingham laws were higher for ACM and ACM stabilised soya milk emulsion (C), ACM stabilised O/W-type nanoemulsion (D), and ACM stabilised O/W-type nanoemulsion enhanced with soy milk fiber (E) in comparison to that of HB and Casson models. For instance, SSE and RMSE values for ACM were 0.02898 and 0.0119, and 0.0484 and 0.0423 for HB and Casson model respectively (Table 0.4, and Table 0.5). However the SSE and RMSE from Power and Bingham models were 0.3094 and 0.107, and 1.0757 and 0.1996 respectively (Table 0.3 and Table 0.6). Similar trends were observed for soy milk (B), ACM stabilised soya milk emulsion (C), ACM stabilised O/W-type nanoemulsion (D), and ACM stabilised O/W-type nanoemulsion enriched with soy milk fiber E. Authors have reported that the Power Law, Herschel-Buckley and Casson models can be used to describe the flow properties of O/W emulsions such as mayonnaise and salad dressing (Azari-Anpar et al 2017; Chetana et al 2019). Therefore, ACM, soy milk, and ACMs' most stable emulsions followed the same flow behaviour as other O/W emulsions such as mayonnaise and salad dressing. The Casson model was the best fit model that predicted the emulsion flow behaviour more accurately at a very low shear rate and very high shear. This is consistent with results obtained by Chivero et al. (2016), Glicerina et al (2016), Folayan et al. (2017), and Pajouhandeh et al. (2017).

6.7 Viscoelastic Properties

This segment seeks to discuss the viscoelastic properties of ACM, soya milk, ACM stabilised O/W-type nanoemulsion, ACM stabilised O/W-type nanoemulsion enriched with soya milk Fiber, and ACM stabilised soya milk emulsion at various strains, frequency, temperature and time.

6.7.1 Effect of strain on the viscoelastic properties of African catfish mucilage

The analysis was carried out to ascertain the point at which African catfish mucilage (ACM) remained stable as represented by the linear viscoelastic region (LVR), analyse ACMs' stability

and structure, and establish if there is a phase change i.e. at the cross-over point. Figure 0.6 shows the effect of strain on the viscoelastic properties of ACM at a fixed angular frequency of ω = 1 rad/s. The storage modulus of a food emulsion gives information about the structural stability of the emulsion {McClements, 2015; Lorenzo et al., 2018; Kubo et al., 2019). The storage modulus reflects the elastic behaviour of the emulsion and it signifies the energy stored in the emulsion before it loses its structural stability (Geremias-Andrade et al., 2016; Lorenzo et al., 2018; Kubo et al., 2019). On the other hand, loss modulus reflects the viscous behaviour of the emulsion and it signifies the energy dissipated by the emulsion when it loses its structural stability (Geremias-Andrade et al., 2016; Lorenzo et al., 2018; Kubo et al., 2019). Table 0.7 gives a comparison of mean initial storage (MIS) and miean initial loss modulus (MIL) of ACM, soy milk, and ACMs' most stable nanoemulsions as constituted in Table 0.1. The MIS and MIL modulus of ACM was 11.03 ± 0.1 and 1.39 ± 0.1 Pa respectively (Table 0.7). As the storage modulus of ACM was higher than the loss modulus it shows that ACM behaves more like a weak viscoelastic hydrogel. The linear viscoelastic region (LVR) shows the structural stability of ACM and the strains were G′ and G″ values that were relatively constant (Figure 0.6). Freeze-dried ACM in MilliQ water formed a viscoelastic web-like matrix with G′ and G″ values that were relatively constant at strains of up to 0.2 % (Figure 0.6 and Table 0.7) African catfish mucilage initially showed weak gel-like behaviour and its moduli in the linear viscosity range (LVR) was constant at low strains of up to 0.2 % and had cross-over points at about 10 % (Figure 0.6 and Table 0.7). Similar results were obtained by Radtke et al. (2018) for the viscoelastic properties G' and G' of the phlegm of convalescents with cystic fibrosis and the authors reported that the phlegm had fairly stable viscoelastic web-like matrix with G′ and G″ values that were almost constant at low concentrations (Radtke et al., 2018). Also, Chaudhary et al. (2018) investigated the storage and loss moduli properties of hagfish mucus as a function of the strain applied at a fixed angular frequency of ω = 1 rad/s. The authors reported that hagfish mucus had storage modulus values that were constant at a low strain range of up to 0.2 % (Chaudhary et al., 2018). The authors concluded that hagfish mucus behaved as a weak viscoelastic hydrogel

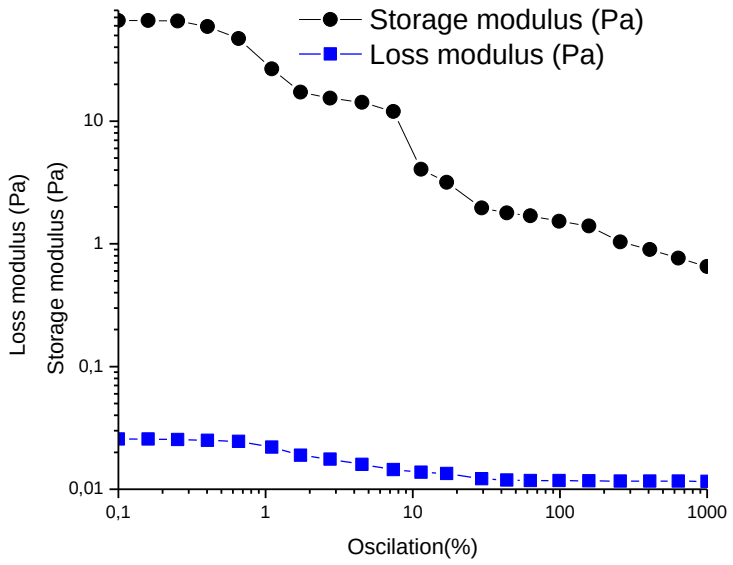

Figure 0.6: Effect of strain on viscoelastic properties of African catfish mucilage at a fixed angular frequency of 1 rad/s

Table 0.7: Comparison of mean initial storage and loss modulus of ACM and most stable nanoemulsions [a].

'MATERIAL AND EMULSION TYPE'	**STORAGE MODULUS (Pa)**	**LOSS MODULUS (Pa)**
ACM	11.0 ± 0.2	1.39 ± 0.1
ACM + O/W-type nanoemulsion without fibre	45.14 ± 0.3	6.57 ± 0.2
ACM + O/W-type nanoemulsion enriched with fiber	66.18 ± 0.3	8.37 ± 0.2

[a]ACM-African catfish mucilage

(Chaudhary et al., 2018). The result that ACM behaves as a weak viscoelastic hydrogel within a low LVR range is consistent with reports by. Böcker et al. (2016), Wu et al. (2017), and Chaudhary et al. (2018).

Figure 0.7 shows the ratio of the storage modulus to the loss modulus of ACM at an angular frequency of ω = 1 rad/s. The ACM was found to have a phase angle that was between 0 and 90° due to the vector contributions of the complex modulus and storage modulus (Figure 6.7). The ACM included elastic and viscous parts as no case was observed where either the storage (G') or loss (G'') modulus was zero (Figure 0.7). The complex modulus shows that ACM behaves as

a viscoelastic weak gel. The complex modulus is a direct measure of the rigidity of the gel's soft solid structure when exposed to stresses below the yield stress and it indicates the stability of the

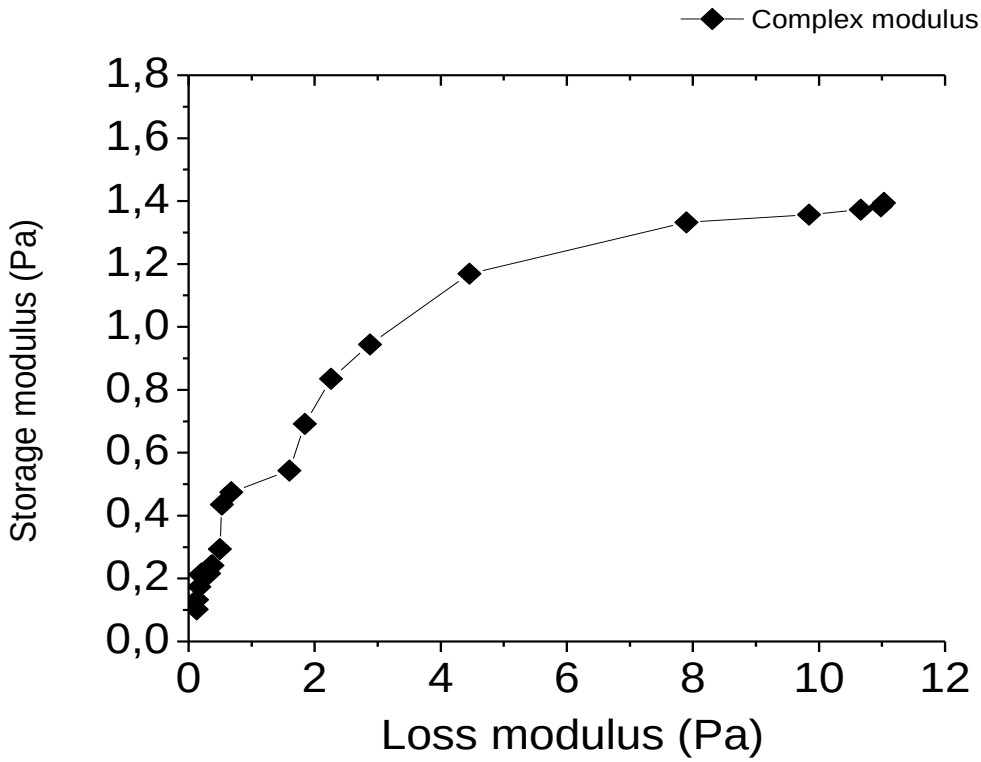

gel when exposed to shear stress (Geremias-Andrade et al., 2016; Lorenzo et al., 2018; Kubo et al., 2019). The result that ACM behaves like a weak viscoelastic hydrogel at low constant strains in the LVR, with a phase angle that is between 0 and 90° and a complex modulus that can stabilise an emulsion is in agreement with reports from Böcker et al. (2016), Geremias-Andrade et al. (2016), Lorenzo et al. (2018) and Kubo et al. (2019). Table 6.9 gives the mean initial values of tan δ for ACM and its most stable nanoemulsions. The mean initial value of tan δ for ACM was 0.1264 ± 0.01. The literature describes that a material with tan δ that is greater than one as one that exhibits more damping than a material with a tan δ than one (Anvari et al., 2016; Chi et al., 2019). Damping is higher in materials with a tan δ greater than one because the loss modulus of the material is greater than the storage modulus which means that the energy dissipating, viscous component of the complex modulus prevails and the material is less stable. Complex viscosity and damping factor are therefore vital in characterising the storage stability of dispersions (Anvari et al., 2016). For instance, Anvari et al. (2016) investigated the oscillatory rheological properties of anionic gum made from seeds of *Alyssum homolocarpum* at different concentrations of 0.5, 1, 2, 3, and 5 % w/v (Anvari et al., 2016).

Figure 0.7: Ratio of storage modulus to loss modulus of African catfish mucilage at an angular frequency 1 rad/s

Table 0.8: LVR and cross-over point of ACM and most stable nanoemulsions[a, b].

MATERIAL AND EMULSION TYPE	END-POINT OF LVR STRAIN (%)	CROSS OVER POINT OF LVR STRAIN (%)
A	0.2	10
D	0.4	30
E	0.6	50

[a]ACM-African catfish mucilage
[b]LVR-Linear viscosity region

Table 0.9: Tan δ of ACM and most stable nanoemulsions [a, b].

MATERIAL AND EMULSION TYPE	MEAN INITIAL TAN δ
A	0.1264 ± 0.01
D	0.1234 ± 0.01
E	0.1232 ± 0.01

[a]Indicated values are reported as means ± standard deviation (n = 3)
[b]ACM-African catfish mucilage

The authors also studied the effect of temperature increases from 5-50 ^{O}C on the viscoelastic properties of 1 % w/v aqueous anionic aqueous gum dispersions of *Alyssum homolocarpum* seeds (Anvari et al., 2016). The authors determined the limiting value of the linear viscosity region (LVR), critical strain and yield stress at 6.28 rad/s in the strain range of 0.01 to 100%, and the LVR storage and loss moduli, the limiting strain, complex modulus and damping factor (Anvari et al., 2016). The effect of frequency on the viscoelastic properties of the anionic gum was carried out at LVR strain of 0.1% and frequency ramps from 0.1 to 100 rad/s (Anvari et al., 2016). The authors reported that storage and loss moduli increased as the concentration of anionic gums increased in the aqueous dispersion which led to increased complex modulus i.e. rigidity and stability of the anionic gum dispersion. Also Increasing temperature led to decreases in storage and loss moduli values and showed that the microstructure of the anionic gum became less stable

as temperatures became higher (Anvari et al., 2016). The authors also reported that the values of the viscoelastic moduli for *A*. *homolocarpum* anionic seed gum compared favourably to values previously reported for food hydrocolloids such as *Lepidium perfoliatum* seed gum and gum tragacanth (Balaghi et al., 2011; Hesarinejad, Koocheki, & Razavi, 2014; Anvari et al., 2016) The authors concluded by reporting that large complex viscosity and low damping factor leads to greater structural stability for food colloids and emulsions (Anvari et al., 2016). It was observed that the mean initial tan δ of ACM was low (Table 6.9) this result coupled with the fact that ACM has a complex viscosity that could stabilise an emulsion shows that ACM dispersion in MilliQ water has a stable microstructure.

6.7.2 Effect of strain on the viscoelastic properties ACMs' most stable emulsions

The study was carried out to ascertain the point at which ACM stabilised O/W-type nanoemulsion and ACM stabilised O/W-type nanoemulsion enriched with soy milk fiber remained stable as represented by the linear viscoelastic region, analyse both nanoemulsions'' stability and structure, and establish if there is a phase change.

Figure 0.8 shows the effect of strain on viscoelastic properties of ACM stabilised O/W-type nanoemulsion and ACM stabilised O/W-type nanoemulsion enriched with soy milk fiber at a fixed angular frequency of ω = 1 rad/s. Table *0.7* compares the initial storage and loss modulus of ACM and the most stable nanoemulsions with constituents given in Table 0.1. The storage modulus of both nanoemulsions was higher than the loss modulus which shows that both emulsions behave more like viscoelastic nanoemulsions. The miean initial storage and mean initialloss modulus of ACM stabilised O/W-type nanoemulsion enriched with soy milk fiber (66.18 ± 0.3 and 8.37 ± 0.2 Pa) was higher than that of ACM stabilised O/W-type nanoemulsion (45.14 ± 0.13 and 6.57 ± 0.3 Pa) as shiwn in Table 0.8. The reason for the higher initial storage and loss modulus was due to the soy milk fiber which enhanced the stability properties of ACM on the microstructure of the nanoemulsion. The linear viscoelastic region (LVR) showed the stability of ACM (

Figure 0.8). The ACM stabilised O/W-type nanoemulsion formed a viscoelastic web-like matrix with G′ and G″ values that were relatively constant at strains of up to 0.4 % but there was crossover at about 30 % strain (

Figure 0.8a and Table 0.8). The result that ACM stabilised O/W-type nanoemulsion initially showed weak viscoelastic behaviour at strains of 0.4 %, a crossover point (30 %) and a complex modulus is consistent with reports on food hydrocolloids such as *Lepidium perfoliatum* seed gum

(Hesarinejad et al., 2014) and gum tragacanth (Balaghi et al., 2011), which are known to show weak viscoelastic behaviour at low strains, a cross over point abd a complex modulus Anvari et al. (2016).

The ACM stabilised O/W-type nanoemulsion enriched with soy milk fibre initially showed weak gel-like behaviour at strains of 0.6 % and a crossover point at 50% strain (

Figure 0.8b and Table 0.8). Also, ACM stabilised O/W-type nanoemulsion enriched with soya milk fiber had higher G' and G'' values in comparison to G' and G'' values of ACM stabilised O/W-type nanoemulsion. It has been established from the literature that fibres re-enforce the structural stability of emulsions as they work in synergy with ACM-bioemulsifiers by delaying deformation of oil droplet clusters in emulsions Sousa de et al. (2015), Fujisawa, Togawa, & Kuroda, (2017), Barkhordari, & Fathi, (2018), Ye et al, (2018), and Ruan et al. (2019). For instance, Ruan et al., (2019), investigated the effect of strain on the viscoelastic properties of high internal phase (HIP) O/W emulsions using corn peptide emulsifier re-inforced with citrus fibers (Ruan et al., 2019). The EORs for the HIP O/W emulsions were; 1.0: 75, 1.5: 75 and 2.0:75 % and the HIP O/W emulsions contained increasing citrus fibre concentrations of 0.5, 0.75 and 1.0 % (Ruan et al., 2019). Viscoelastic tests were performed on frequency sweep modes of 1 to 10 rad/s and amplitude sweeps of 0.1–1000 Pa was used to determine where the moduli in the LVR was constant (Ruan et al., 2019). The authors reported that, the G′ and G″ of HIP emulsions with citrus fibres was higher than the control that did not contain fibres (Ruan et al., 2019). The authors also reported that G' was always higher than G" and noted slight increases in G′ and G″ as the frequency increased from1 to 10 rad/s (Ruan et al., 2019). The authors indicated that slight increases in the value of G' as the concentration of the citrus fibre increased signified increased gel strength in the HIP emulsions with higher fibre concentration (Ruan et al., 2019).

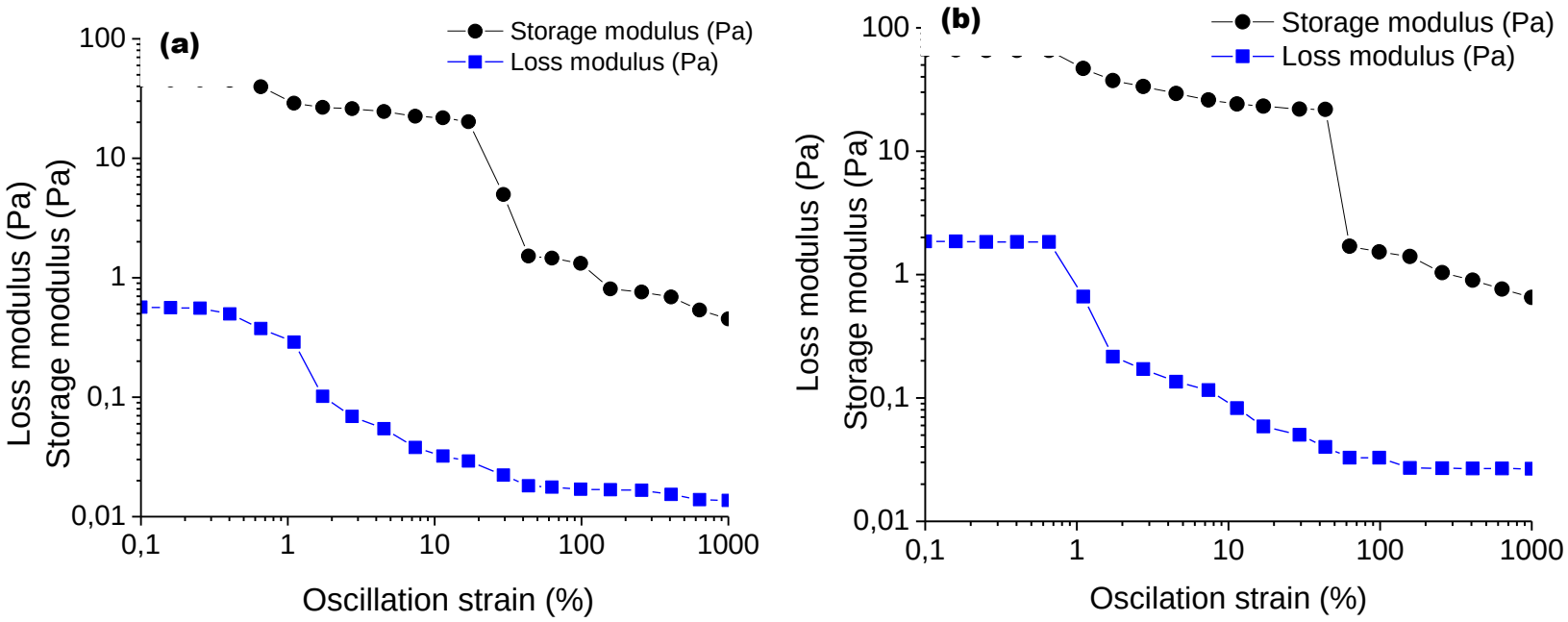

Figure 0.8: Viscoelastic properties (a) ACM stabilised O/W-type nanoemulsion (b) ACM stabilised O/W-type nanoemulsion enriched with soy milk fiber at a fixed angular frequency of 1 rad/s.

The authors concluded that the reason for the increase G' was due to the formation of a thicker interfacial layer which led to reinforced network structure of the corn peptide HIP emulsions that contained citrus fibres (Ruan et al., 2019). Therefore the higher storage modulus observed in the experimental data of ACM stabilised O/W-type nanoemulsion enriched with soy milk fibre in comparison to ACM stabilised O/W-type nanoemulsion was due to the synergy between the soy milk fibre and ACM which resulted in a thicker interfacial layer of the most stable nanoemulsion that contained soy milk fibre (Figure 0.9). The viscoelastic properties of ACM stabilised O/W-type nanoemulsion and ACM stabilised O/W-type nanoemulsion enriched with soy milk fibre showed that storage modulus had higher values than loss modulus over the LVR, signifying that both nanoemulsions had interconnected gel-like network structure with mainly elastic behaviour (Table 0.8). Zou et al (2018) studied the viscoelastic properties of Zein/tannic acid complex particles (ZTACPs) stabilised emulsion gels at a frequency range of 0.5-62.83 rad/s at 1 %. The authors reported that storage modulus had higher values than loss modulus over the fairly constant LVR and concluded that the ZTACP stabilised emulsion gels had interconnected gel-like network structure with mainly elastic behaviour (Zou et al., 2018). Similarly, Luo et al 2019) studied the viscoelastic properties of tea-seed O/W emulsions gels stabilised with citrus pectin concentrations of 1.5 4.5 % at a frequency of 0.62–62.8 rad/s at strains of 0.1%. The authors reported that storage modulus had higher values than loss modulus over the fairly constant LVR and concluded that the storage modulus value was always greater than that of the loss modulus within the LVR and both storage and loss moduli were dependent on low frequencies (Luo et al., 2019). Similarly, Primozic et al. (2017) investigated the viscoelastic properties of rapeseed O/W nanoemulsions that were stabilised with lentil protein isolate (LPI) of 1, 1.5, 2, 3 and 5% from 0.01 to 20 Hz, at a fixed angular frequency of 6.28 rad/s within the LVR. The authors established that all the nanoemulsions demonstrated viscoelastic behaviour with nanoemulsions stabilised with 3 and 5% LPI having higher viscoelasticity (Primozic et al. 2017). The authors also reported that the elastic part was dominant before the cross-over point (Primozic et al. (2017). The authors concluded that both storage and loss moduli were dependent on low frequencies (Primozic et al., 2017). Hence, the storage and loss moduli of both ACM stabilised nanoemulsions' and ACM stabilised O/W-type nanoemulsion enriched with soy milk fibre are dependent on low frequencies and both have interconnected stable gel-like network structure with mainly elastic behaviour. Figure 0.9 shows the ratio of the storage modulus to the loss modulus of ACM stabilised

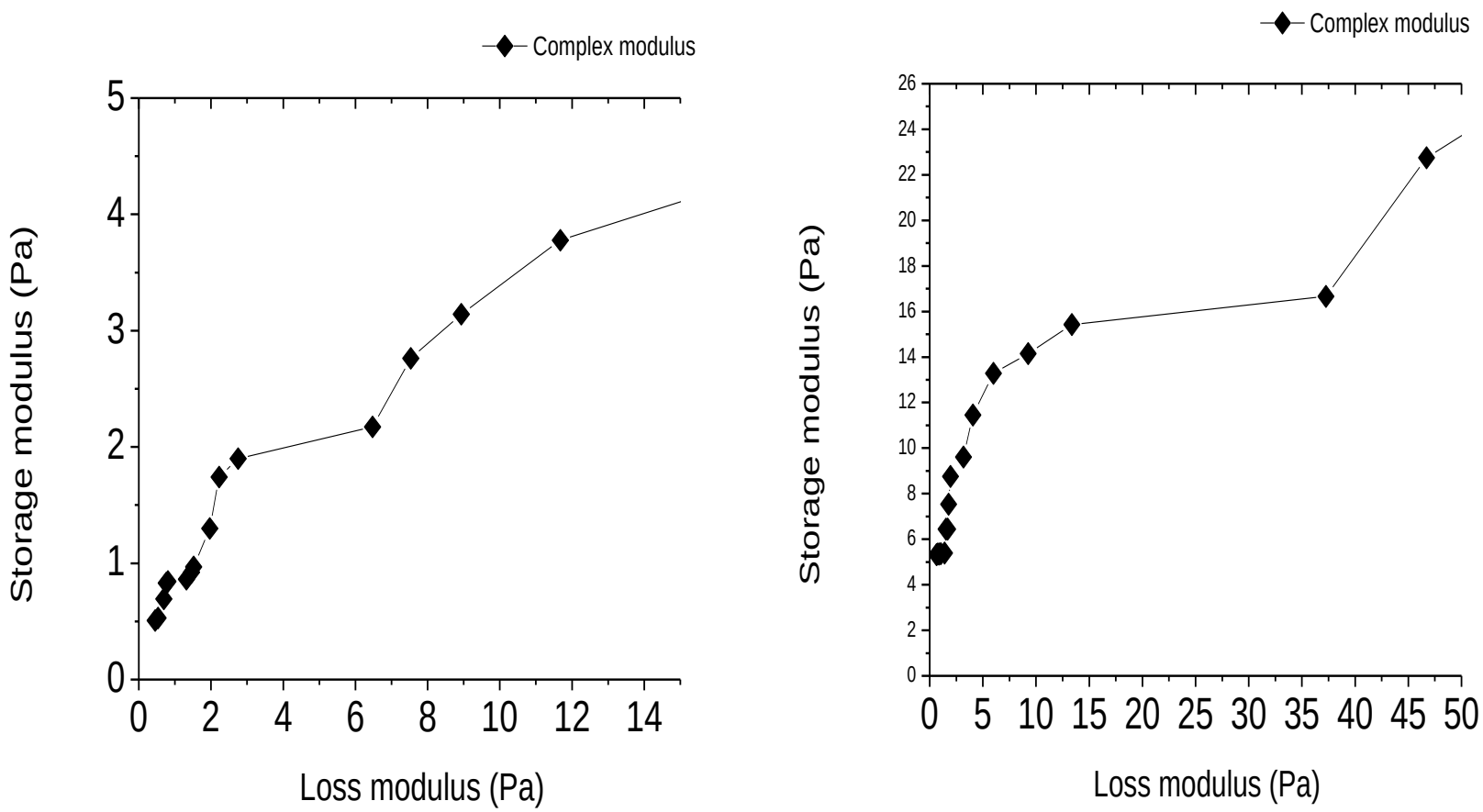

Figure 0.9: Ratio of loss modulus to storage modulus of African catfish mucilage (ACM) (a) (ACM stabilised O/W-type nanoemulsion and (b) ACM stabilised O/W-type nanoemulsion enriched with soy milk fibre at an angular frequency 1 rad/s

nanoemulsions' and ACM stabilised O/W-type nanoemulsion enriched with soy milk fibre at an angular frequency of ω = 1 rad/s. Both ACMs' most stable nanoemulsions were found to have a phase angle that was between 0 and 90° due to the vector contributions of the complex modulus and storage modulus (Figure 0.7). Both ACMs' most stable nanoemulsions included elastic and viscous parts as no case was observed were either the storage (G') or loss (G'') modulus was zero (Figure 0.7). The complex modulus shows that both ACMs' most stable nanoemulsions behave as a viscoelastic weak hydrogel. The complex modulus is a direct measure of the rigidity of the gel's soft solid structure when exposed to stresses below the yield stress and it indicates the stability of the gel when exposed to shear stress (Geremias-Andrade et al., 2016; Niu et al., 2016; Adeyi et al., 2018; Lorenzo et al., 2018; Kubo et al., 2019). It was observed that the complex modulus of ACM stabilised O/W-type nanoemulsion enriched with soy milk fibre was enhanced by the fibre in comparison to ACM stabilised O/W-type nanoemulsion (Figure 0.9). It was earlier established from the literature that fibres re-enforce the structural stability of emulsions as they work in synergy with ACM-bioemulsifiers by delaying deformation of oil droplet clusters in emulsions (Liu et al., 2016). Therefore the higher complex modulus in ACM stabilised O/W-type nanoemulsion enriched with soy milk fibre in comparison to ACM stabilised O/W-type nanoemulsion was due to the synergy between the soy milk fibre and ACM (Figure 0.9). The result that both stable nanoemulsions behave like a weak viscoelastic hydrogel at low strains, with a phase angle that is between 0 and 90° and a complex modulus is in agreement with reports from Geremias-Andrade et al. (2016), Liu et al. (2016), Wu et al. (2017), Lorenzo et al. (2018), and Kubo et al. (2019).

Table 0.9 gives the mean initial tan δ of ACM and ACMs' most stable nanoemulsions. The mean initial tan δ of ACM stabilised O/W-type nanoemulsion was 0.1234 ± 0.01 while that of the ACM stabilised O/W-type nanoemulsion enriched with soy milk fibre was 0.1232 ± 0.01. The literature describes that a material with tan δ = G'/G that is greater than one as one that exhibits more damping than a material with a tan δ than one (Anvari et al., 2016; Chi et al., 2019). Damping is higher in materials with a tan δ greater than one because the loss modulus of the material is greater than the storage modulus which means that the energy dissipating, viscous component of the complex modulus prevails and the material is less stable. Complex viscosity and damping factor are therefore vital in characterising the storage stability of dispersions (Anvari et al., 2016). For instance, Anvari et al. (2016) investigated the oscillatory rheological properties of anionic gum made from seeds of *Alyssum homolocarpum* at different concentrations (0.5, 1, 2, 3, and 5 % w/v) (Anvari et al., 2016). The authors also studied the effect of temperature increases from 5-50 ^{O}C

on the viscoelastic properties of 1 % w/v aqueous anionic aqueous gum dispersions of *Alyssum homolocarpum* seeds (Anvari et al., 2016). The authors determined the limiting value of the linear viscosity region (LVR), critical strain and yield stress at 6.28 rad/s in the strain range of 0.01 to 100%, and the LVR storage and loss moduli, the limiting strain, complex modulus and damping factor (Anvari et al., 2016). The effect of frequency on the viscoelastic properties of the anionic gum was carried out at LVR strain so 0.1% and frequency ramps from 0.1 to 100 rad/s (Anvari et al., 2016). The authors reported that storage and loss moduli increased as the concentration of anionic gums increased in the aqueous dispersion which led to increased complex modulus i.e. rigidity and stability of the anionic gum dispersion. Also Increasing temperature led to decreases in storage and loss moduli values and showed that the microstructure of the anionic gum became less stable as temperatures became higher (Anvari et al., 2016). The authors also reported that the values of the viscoelastic moduli for *A*. *homolocarpum* anionic seed gum compared favourably to values previously reported for food hydrocolloids such as *Lepidium perfoliatum* seed gum and gum tragacanth (Balaghi et al., 2011; Hesarinejad et al., 2014; Anvari et al., 2016) The authors concluded by reporting that large complex viscosity and low damping factor leads to greater structural stability food colloids and emulsions (Anvari et al., 2016). It was observed that the mean initial tan δ of the two ACMs' most stable nanoemulsions were low (Table 0.9) this result coupled with the fact that ACM has a complex viscosity that could stabilise an emulsion shows that ACM dispersion in MilliQ water could confer structural stability on its most stable nanoemulsions.

6.7.3 Effect of frequency on the viscoelastic of ACM

The analysis was carried out to ascertain the frequency at which ACM microstructure remained stable during long-term storage and establish the influence of slow and high movements on the viscoelastic characteristics of ACM. The effect of frequency was measured at a strain of 0.1% and frequency ramps from 0.06 to 100 rad/s. Figure 0.9 shows the effect of frequency on ACM over the frequency range 0.06 to 100 rad/s. An increase in frequency led to an increase in storage G') and loss (G'') modulus (Figure 0.9). It was also observed that no crossover points (G' = G") existed for ACM (Figure 6.9). A strain of 0.1 % was chosen to conduct the oscillatory frequency sweep test, as ACM was still at its LVR at this strain (Figure 0.9). The results showed that storage and loss moduli of both stabilised nanoemulsions increased as frequency increased (Figure 0.9). Felix et al. (2017) conducted frequency sweep tests for high-fatty acid O/W emulsions stabilised with crayfish protein concentrate (CPC) and xanthan gum at constant stress, within the LVR, from 0.06 to 100 rad/s with 40 mm serrate plates.

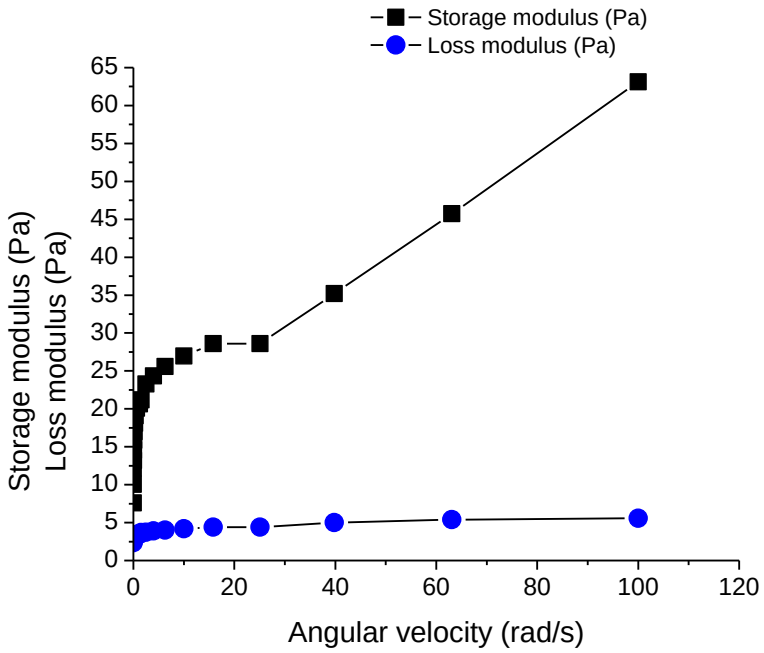

Figure 6.9: Effect of frequency on the moduli of African catfish mucilage

The authors reported that the G' and G'' of the CPC and xanthum gum stabilised high-fatty acid O/W emulsions increased as the frequency increased and the G' and G'' did not have cross over points (Felix et al., 2017). Hence the results obtained in this study that storage (G') and loss (G'') modulus increased and the G' and G'' did not have cross over points are consistent with results reported by Felix et al. (2017). Authors have established that the storage and loss moduli of both stabilised emulsions' are dependent on low frequencies and when the storage modulus is greater than the loss modulus the emulsion is more elastic (Felix et al., 2017; Primozic et al., 2017). Authors have reported that when storage modulus and the loss modulus increases without cross-over points there are no changes in phases hence the structural stability of the emulsion is maintained (Peng et al., 2018). Peng et al.(2018) investigated the effect of Milk fat globule membrane protein (MFGMP) on the viscoelastic properties of whipped cream at a range of 1 to 100 Hz at 0.5% strain and demonstrated that both the storage and loss modulus increased with increasing frequency. The authors reported that storage modulus had higher values than the loss modulus G″ values, which indicated that the whipped cream emulsion behaved as a stable weak gel (Peng et al., 2018). The result obtained showed that storage modulus was higher than loss modulus in ACM as frequency increased hence ACM behaves as a weak hyfrogel with a stable microstructure consistent with Felix et al. (2017), and Peng et al.(2018). Altso the observation of increases in both storage modulus and the loss modulus without cross-over points show that there

were no phases changes hence ACM had a stable microstructure as observed for othere food emulsions by Felix et al. (2017), and Peng et al.(2018).

6.7.4 Effect of frequency on the viscoelastic properties of ACMs' most stable emulsions

The effect of frequency on the viscoelastic properties of ACM stabilised O/W-type nanoemulsions and ACM stabilised O/W-type nanoemulsions enriched with soy milk fiber was carried out to ascertain the frequency at which the stabilised O/W-type nanoemulsion remained stable and to establish the influence of slow and high movements on its viscoelastic characteristics. A strain of 0.2 % was chosen from the amplitude test to perform the oscillatory frequency sweep test as all stabilised O/W-type nanoemulsion was still at their LVR at this strain. Figure 0.10 shows the effect of frequency increase from 0.06–100 rad/s on ACM stabilised O/W-type nanoemulsion and ACM stabilised O/W-type nanoemulsion enriched with soya milk fiber at 25°C. The results show that both ACM stabilised O/W-type nanoemulsions were influenced by low- frequency rates (Figure 0.10). It was also observed that G′ was greater than G″ values (Figure 0.10). Authors have reported that when the value of G′ is greater than that of G″ the material behaves like a weak gel (Peng et al., 2018; Irani et al., 2019). For instance, Peng et al (2018) conducted viscoelastic tests on whipped cream stabilised with different concentrations of milk fat globule membrane protein (MFGMP) The authors conducted frequency sweep analyses at 0.5% strain under the frequency range of 1.0–100 Hz at 25°C on whipped cream and revealed that all the whipped cream emulsions depended on low-frequency. The authors also reported that G′ was greater than G″ values and concluded that the whipped cream behaved as a weak gel (Peng et al., 2018). Furthermore, the authors stated that a pseudo-elastic gel network structure was formed by the adsorption of the MFGMP bioemulsifier on the oil/water interface of the stabilised whipped cream (Peng et al., 2018). Hence the application of MFGMP into whipped cream led to increases in G′ and G″ and resulted in a rugged structural protein network (Peng et al., 2018). It can be inferred that there was adsorption of ACM amphiphilic proteins at the oil/water interface of ACMs'most stable O/W-type nanoemulsions which resulted in the formation of a pseudo-elastic gel network structure hence, G′ was greater than G″ and increased with frequency (Figures 6.10).Therefore ACM acts as an emulsifier that influences viscoelasticl behaviour by ensuring that both ACM stabilised O/W-type nanoemulsions and ACM stabilised O/W-type nanoemulsions enriched

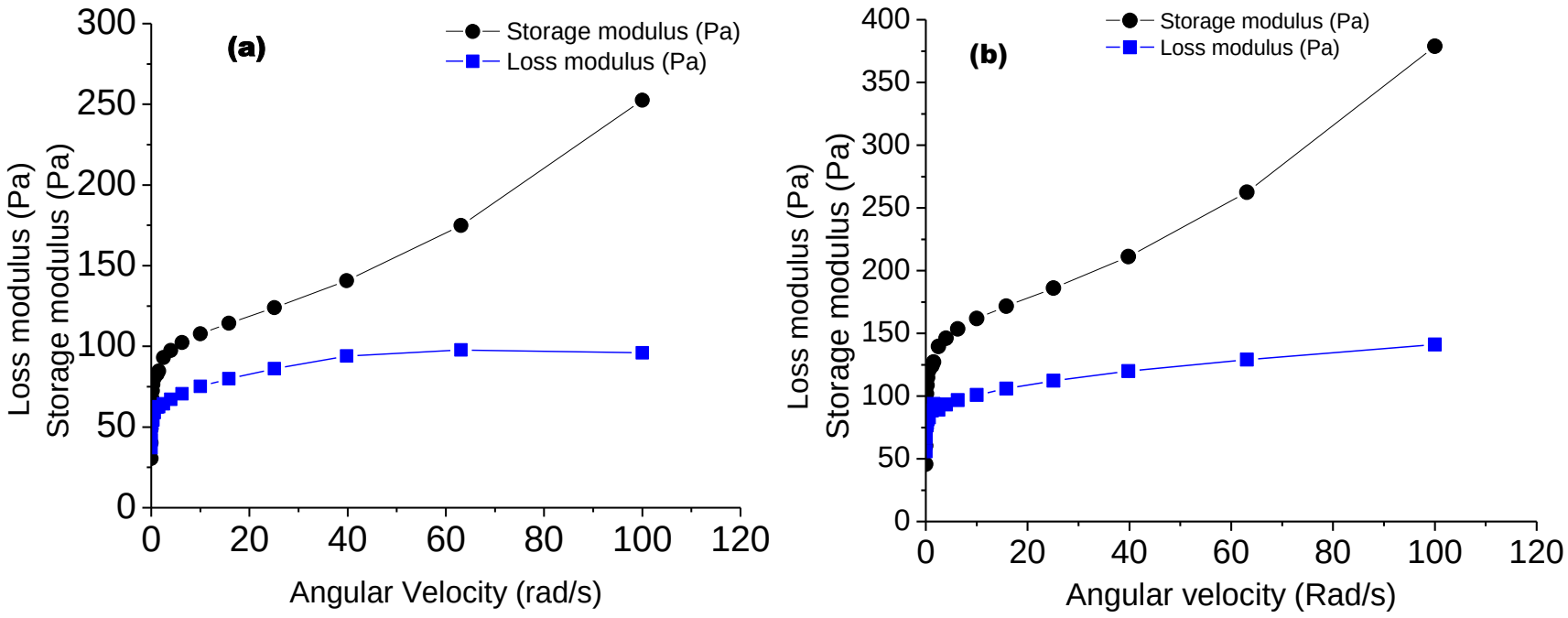

Figure 0.10: Effect of frequency on the moduli of (a) African catfish mucilage (ACM) stabilised O/W-type nanoemulsion and (b) ACM) stabilised O/W-type nanoemulsion enriched with soy milk fiber.

with soy milk fiber forms a strong cohesive network structure as a result of its amphiphilic proteins in African catfish mucilage. It was also observed that at low frequencies, the elastic portion dominated the curves as the G' was always higher than the G'' which shows that both ACM stabilised O/W-type nanoemulsions and ACM stabilised O/W-type nanoemulsions enriched with soy milk fiber were both stable (Figures 6.10). Also, the G' increased steeply initially at low-frequency for all ACM stabilised O/W-type nanoemulsions but at high frequencies, the increase became gradual (Figures 6.10). Although G'' increased as the frequency increased, the increase was not too high (Figures 6.10). The same trend was observed by Peng et al. (20118) on whipped cream stabilised with different concentrations of MFGMP. Hence the results obtained for the effect of frequency on the moduli of ACMs' most stable O/W-type nanoemulsions that both emulsions behaved as weak gel emulsions, had a stable rugged web-like matrix because storage modulus was always greater than loss modulus as the frequency increased in agreement with other authors Peng et al. (2018), and Irani et al. (2019).

Also, the G' value of ACM stabilised O/W-type nanoemulsions enriched with soy milk fiber was slightly higher than that of ACM stabilised O/W-type nanoemulsions (Figure 6.10). Table 6.7 gives the mean initial storage (MIS) modulus and mean initial loss (MIL) modulus of most stable nanoemulsions. The trend observed in Table 6.7 was that the MIS modulus for ACM stabilised O/W-type nanoemulsions enriched with soy milk fiber (66.18 ± 0.3) was higher than that of ACM stabilised O/W-type nanoemulsions (45.1 ± 0.3). Similarly, MIL modulus for ACM stabilised O/W-type nanoemulsions enriched with soy milk fiber (8.4 ± 0.2) was higher than that of ACM stabilised O/W-type nanoemulsions (6.6 ± 0.2).). It was earlier established from the literature that fibres re-enforce the structural stability of emulsions as they work in synergy with ACM-bioemulsifiers by delaying deformation of oil droplet clusters in emulsions (Böcker et al.; 2016; Lu et al., 2016). Therefore, the higher values of MIS and MIL modulus in stable emulsions with fibre could be attributed to the synergy between the emulsifier ACM and the soy milk fibre that delayed the deformation of oil droplet clusters in emulsions in ACMs' most stable emulsions

6.7.5 Effect of temperature on the viscoelastic properties

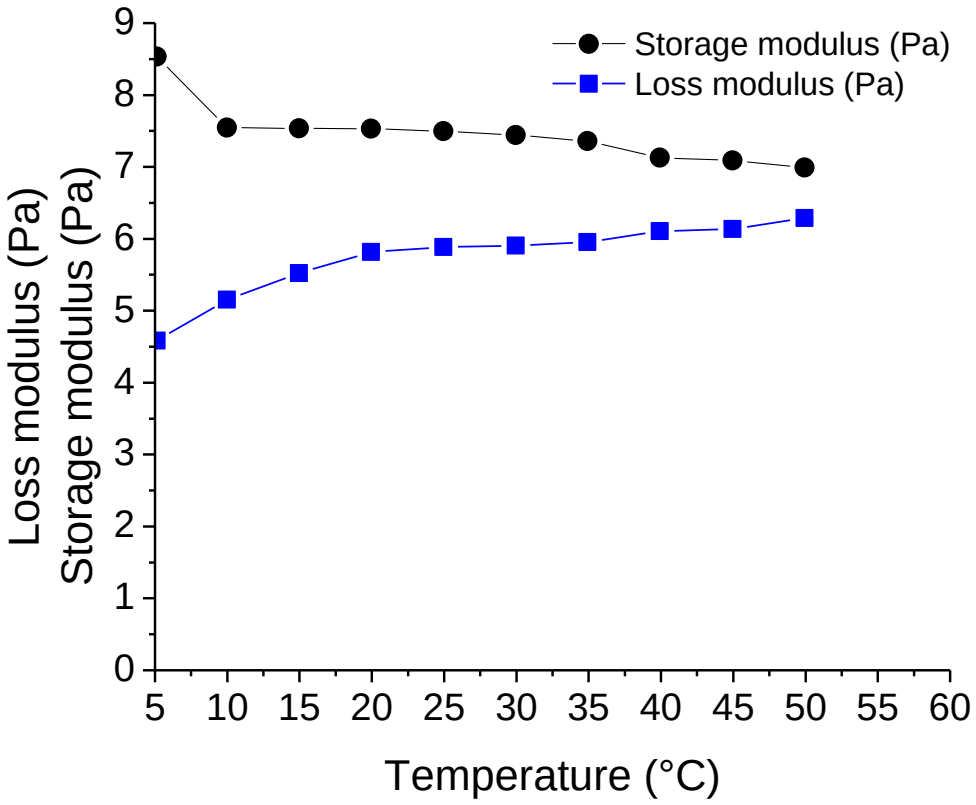

Figure 0.11 shows the effect of temperature on the viscoelastic properties of ACM. This analysis was conducted to observe the effect of storage temperature on ACM at refrigeration (5°C), room (25°C), and at higher temperatures of about 50°C. The measurements were carried out at a constant strain of 0.2 %, which was well within the linear viscoelastic region (LVR), while the frequency was fixed at 1 rad/s .The effect of temperature on the viscoelastic properties of ACM

showed that ACM moduli responded differently at different temperatures (

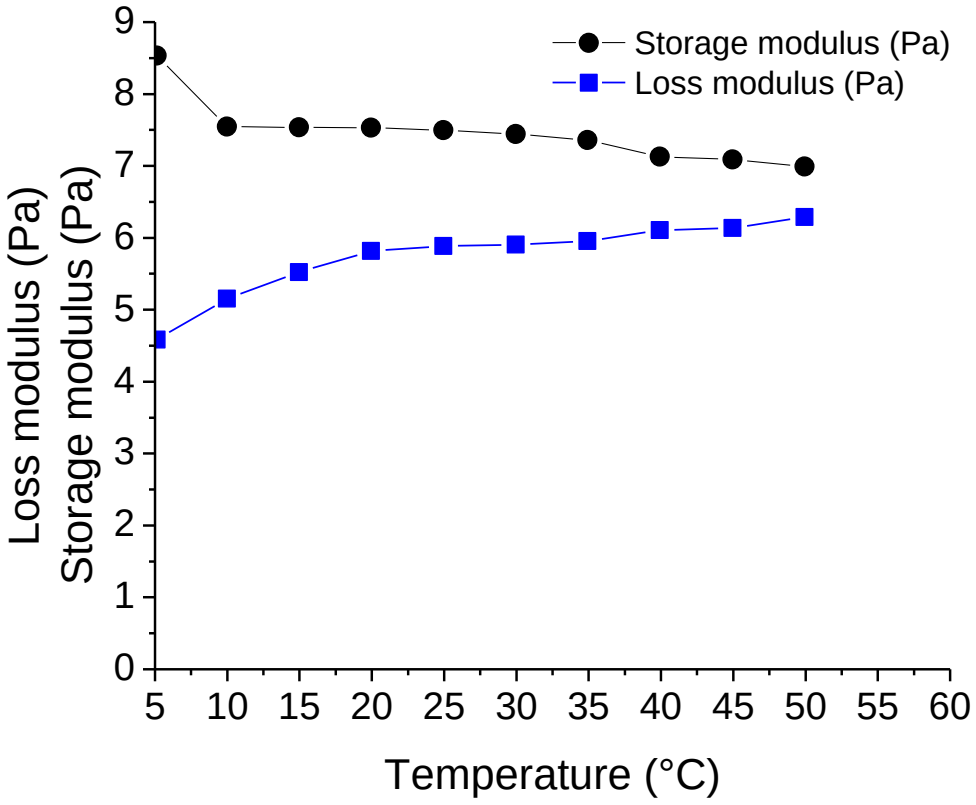

Figure 0.11). It was observed that there was no cross over points between the G' and G'' points of ACM which implied that there was no change in the phase for the ACM as the temperature was

increased (

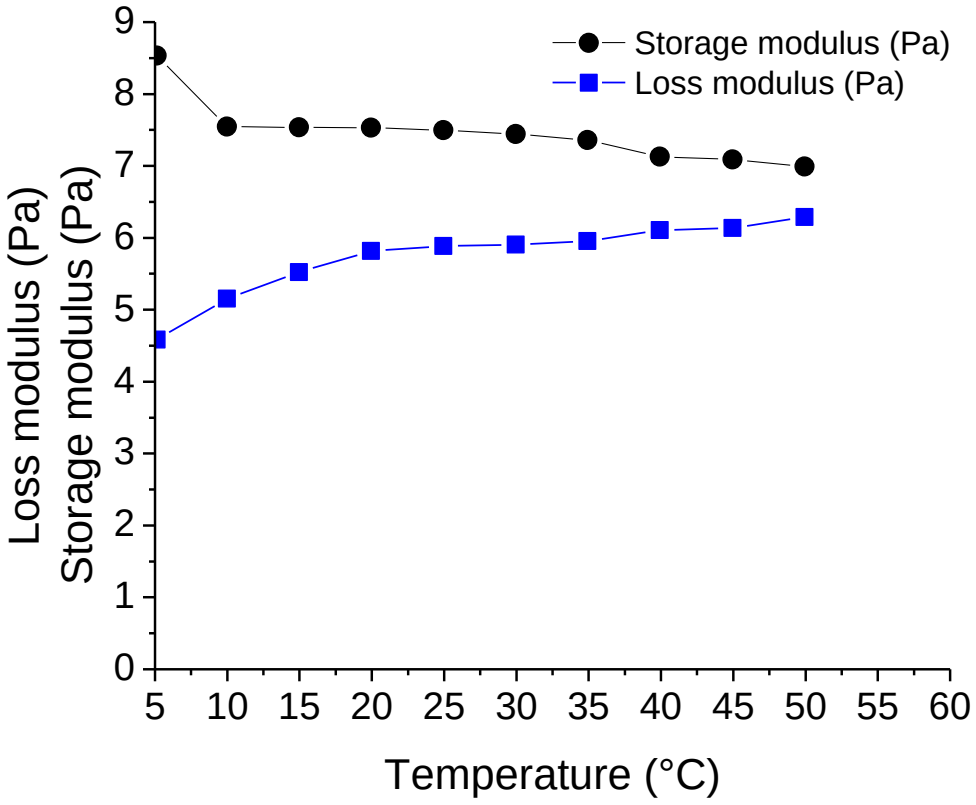
Storage modulus (Pa)
Loss modulus (Pa)
Loss modulus (Pa)
Storage modulus (Pa)
Temperature (°C)
0
1
2
3
4
5
6
7
8
9
5
10
15
20
25
30
35
40
45
50
55
60

Figure 0.11). Also, the G' of ACM was greater than G'' of ACM (

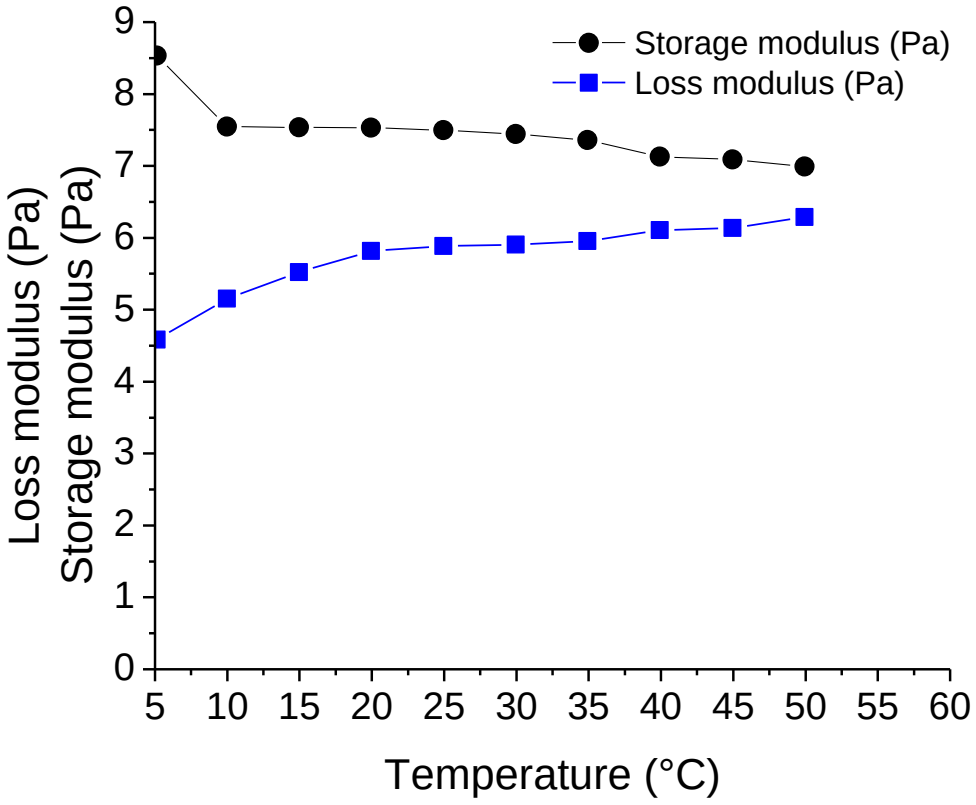

Figure 0.11). The effect of temperature on the moduli of ACM is shown in Table 0.10. At refrigeration temperature (5 °C), the storage modulus for ACM (8.5 ± 0.1 Pa) was higher than its loss modulus (1.9 ± 0.1 Pa) as seen in Table 0.10. At room temperature (25 °C), the storage modulus for ACM (7.5 ± 0.1 Pa) was higher than its loss modulus (2.5 ± 0.1 Pa) as seen in Table 0.10. The same trend of higher storage modulus (7.0 ± 0.1 Pa) in comparison with loss modulus (2.6 ± 0.1 Pa) was followed at increasedtemperatures of 50 °C. Also, the storage modulus of ACM slightly decreased as the temperature increased from 5 °C to 50 °C while the loss modulus slightly increased but the crossover point where storage modulus (G') values are equal to the loss

modulus (G") values were not observed (

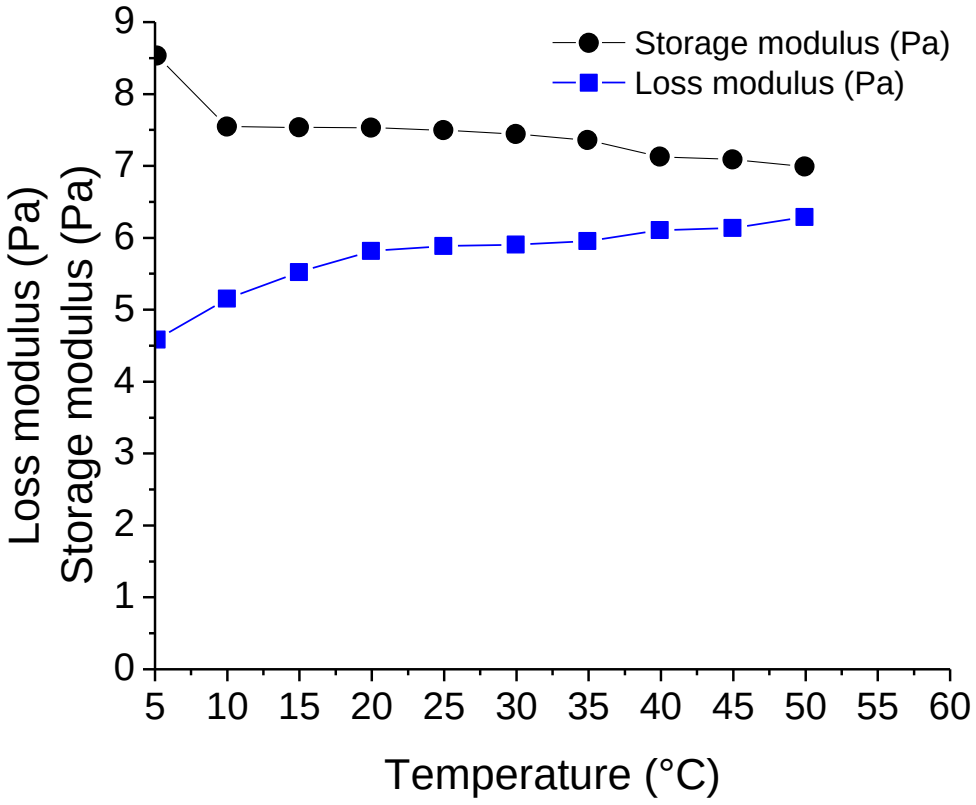

Figure 0.11). This implies that the ACM showed a slight weakening with an increase in temperature from 5 °C to 50 °C because there was no crossover point between G' and G", then.the ACM hydrogel did not transform but retained its soft weak gel phase. Also because the G' although higher than G" had small values then the ACM has a weak gel strength. This implies that the ACM showed a slight weakening in microstructure with an increase in temperature from 5 °C to 50 °C. However, because there was no crossover point between G' and G", then the ACM hydrogel did not transform but retained its soft weak gel phase. Also because the G' was higher than G" then the ACM has a weak gel strength. Hence the ACM stabilised O/W-type nanoemulsion had structural stability at refrigeration temperature Authors have reported that amphiphilic proteins can re-enforce the structural viscoelastic properties of gels (Geremias-Andrade et al., 2016; Lorenzo et al., 2018; Kubo et al., 2019). For instance, Geremias-Andrade et al. (2016) reviewed the rheological properties of emulsion stabilised with gels and concluded that the structural stability of emulsions is enhanced by interactions between the adsorbed milk proteins on the surface of the oil droplets and the protein gel network. Thus ACM is a weak

hydrogel that could impart structural stability properties on emulsions however, the structural stability of ACM is enhanced at refrigeration temperature. The reason for ACMs' stable microstructure is due to the presence of amphiphilic proteins in ACM which adsorb at the oil/water interface to reduce interfacial tension which leads to stable microstructure of the ACM at refrigeration temperatures. The effect of temperature on the stability of the ACM stabilised O/W-type nanoemulsion and ACM stabilised O/W-type nanoemulsion enriched with soy milk fiber is shown in Table 6.10. At refrigeration temperature (5 °C), the storage modulus for ACM (33.6 ± 0.1 Pa) was higher than its loss modulus (7.7 ± 0.1 Pa) as shown in Table 6.10.

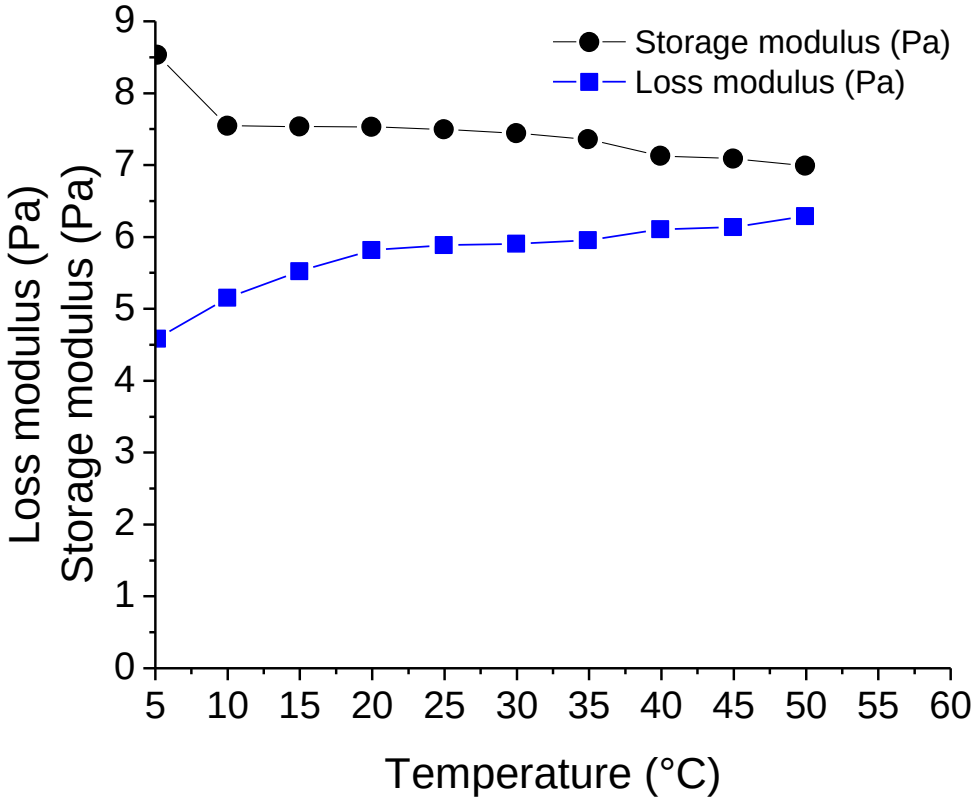

Figure 0.11: The effect of temperature on the viscoelastic properties of African catfish mucilage

At room temperature (25 °C), the storage modulus for ACM (28.6 ± 0.1 Pa) was higher than its loss modulus (9.9 ± 0.1 Pa) as shown in Table 6.9. The same trend of higher storage modulus (21.3 ± 0.1 Pa) in comparison with loss modulus (10.2 ± 0.1 Pa) was followed at higher temperatures of 50 °C. The storage modulus of ACMs' of most stable nanoemulsions slightly

decreased as the temperature increased from 5 °C to 50 °C while the loss modulus slightly increased and was almost constant but the crossover point where storage modulus (G') values are said to be equal to the loss modulus (G") values were not observed (Figure 6.12). This implies that although a slight weakening in structural stability could have occurred with increases in temperature from 5 °C to 50 °C but because there was no crossover point between G' and G", then the ACM stabilised O/W-type nanoemulsion did not change phases. Hence the ACM stabilised O/W-type nanoemulsion had structural stability at refrigeration temperature as observed with ACM.

Table 0.10: Temperature stability effect on the viscoelasticity of ACM and most stable nanoemulsions [a, b, c, d, e, and f]

	5°C		25°C		50°C	
TYPE	**G' (Pa)**	**G" (Pa)**	**G' (Pa)**	**G" (Pa)**	**G' (Pa)**	**G" (Pa)**
A	8.5 ± 0.1	1.9 ± 0.1	7.5 ± 0.1	2.5 ± 0.1	7.0 ± 0.1	2.6 ± 0.1
D	33.6 ± 0.1	7.7 ± 0.1	28.6 ± 0.1	9.9 ± 0.1	21.3 ± 0.1	10.2 ± 0.1
E	55.3 ± 0.1	11.7 ± 0.1	51.2 ± 0.1	15.9 ± 0.1	48.4 ± 0.1	17.9 ± 0.1

[a]A-African catfish mucilage (ACM);

[b]B-ACM stabilised Oil in Water-type nanoemulsion;

[c]C- ACM stabilised Oil in Water-type nanoemulsion enriched with soy milk fiber;

[d]G'-Storage modulus; [e]G"-Loss modulus

[f]4°C-refrigeration, 25°C-room and 50°C increased temperatures.

At refrigeration temperature (5 °C), the storage modulus for ACM stabilised O/W-type nanoemulsion enriched with soy milk fiber (55.3 ± 0.1 Pa) was higher than its loss modulus (11.7 ± 0.1 Pa) as seen in Table 0.10. Similarly, at room temperature (25 °C), the storage modulus for ACM (51.2 ± 0.1 Pa) was higher than its loss modulus (15.9 ± 0.1 Pa) as seen in Table 6.10. The same trend of higher storage modulus (48.4 ± 0.1 Pa) in comparison with loss modulus (17.9 ± 0.1 Pa) was followed at increased temperatures of 50 °C. The storage modulus of ACM stabilised O/W-type nanoemulsion enriched with soy milk fiber slightly decreased as the temperature increased from 5 °C to 50 °C while the loss modulus slightly increased but the crossover point where storage modulus (G') value was equal to the loss modulus (G") value was not observed (Figure 0.12). This implies that the ACM stabilised O/W-type nanoemulsion enriched with soy milk fiber showed a slight weakening with an increase in temperature from 5 °C to 50 °C because there was no crossover point between G' and G", then the ACM hydrogel did not change phases. Authors have reported that amphiphilic proteins can re-enforce the structural viscoelastic properties of emulsions (Geremias-Andrade et al., 2016; Lorenzo et al., 2018; Kubo et al., 2019). For instance, Geremias-Andrade et al. (2016) reviewed the rheological properties of emulsion stabilised with gels and concluded that the structural stability of emulsions is enhanced by interactions between the adsorbed milk proteins on the surface of the oil droplets and the protein gel network. Therefore, both ACM stabilised O/W-type nanoemulsion and ACM stabilised O/W-type nanoemulsion enriched with soy milk fiber are weak hydrogels that are stable at refrigeration temperatures. Furthermore, a comaparison of the effect of temperature on the moduli of ACM's most stable O/W-type nanoemulsion show that the fiber addition improved the structural stability properties of ACM stabilised O/W-type nanoemulsion enriched with soy milk fiber across all temperatures (5, 25 and 50 °C) as shown in Table 0.10.

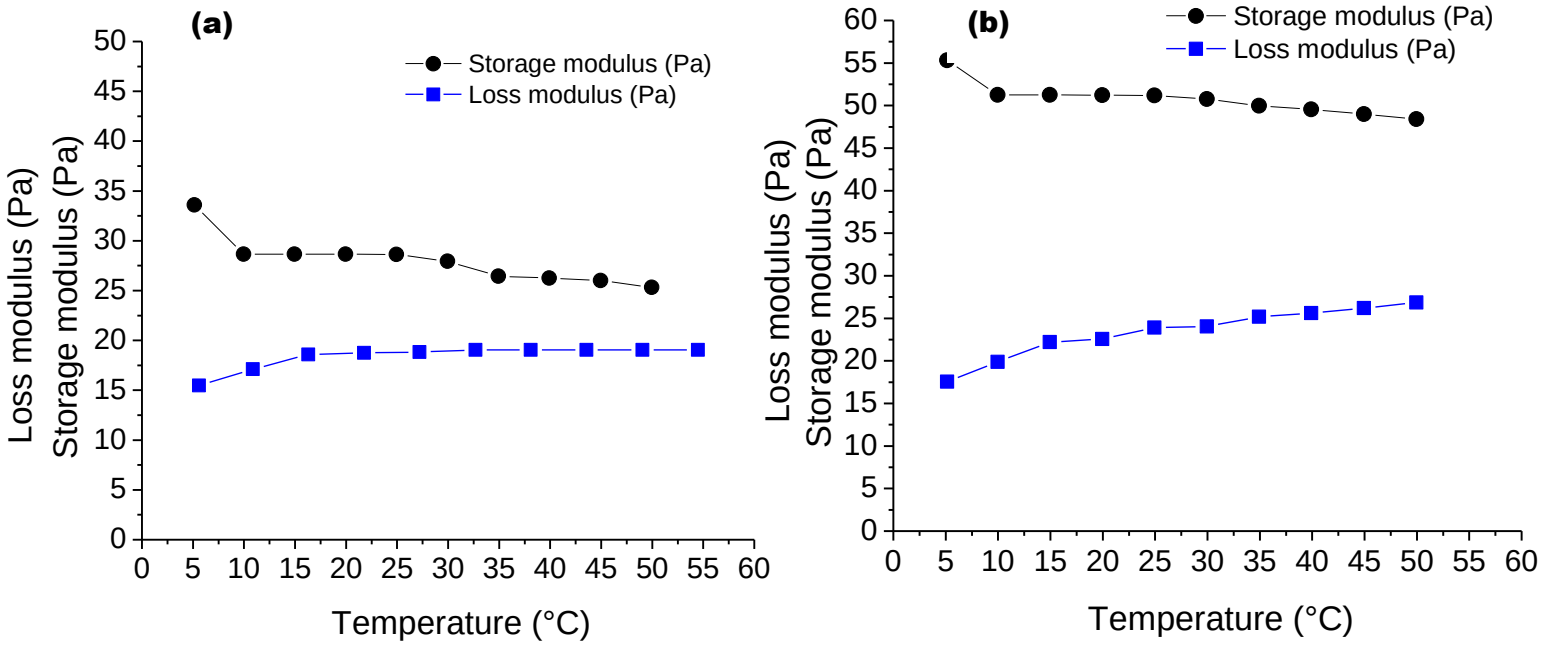

Figure 0.12: The effect of temperature on the viscoelastic properties of (a) African catfish mucilage (ACM) stabilised O/W-type nanoemulsions and (b) ACM stabilised O/W-type nanoemulsion enriched with soy milk fibre

Hence the addition of fiber could improve the structural stability of ACM stabilised O/W-type nanoemulsion enriched with soy milk fiber because ACM works in synergy with the soy milk fibre which is in agreement with reports by Sousa de et al. (2015), Ruan et al, (2019). Therefeore, refrigerating i.e keeping ACM, ACM stabilised O/W-type nanoemulsion and ACM stabilised O/W-type nanoemulsions enriched with soya milk fiber at temperatures of 5 °C results in enhancement of their structural stability. This study showed that storing ACM, ACM stabilised O/W-type nanoemulsion and ACM stabilised O/W-type nanoemulsions enriched with soya milk fiber at refrigeration temperatures of 5 °C sustains and improves its stability and rheological properties of ACM and its most stable nanoemulsions.. Sapei et al. (2017), carried out a kinetic study on the effect of temperature on the stability of o/w emulsion stabilised with different amounts of rice-husk silica and tween-20 (RHST). The authors reported that RHST stabilised O/W emulsions stored at 4-8 °C was two times more stable than RHST stabilised O/W emulsions stored at 28 °C (Sapei et al., 2017). The authors concluded that bioemulsifiers could be used to retard destabilisation rate constants of the O/W emulsions and improve stability and shelf life of O/W emulsions (Sapei et al., 2017). Consequently, the findings of Sapei et al. (2017) supports the inferences made from the data in this study on the temperature effects on the viscoelastic properties of ACM, ACM stabilised O/W-type nanoemulsion and ACM stabilised O/W-type nanoemulsions enriched with soya milk fiber. Therefore refrigerating i.e. keeping the ACM, ACM stabilised O/W-type nanoemulsion and ACM stabilised O/W-type nanoemulsions enriched with soya milk fiber at temperatures of 5°C sustains and improves its structural stability and viscoelastic properties ACM and ACMs' most stable O/W-type nanoemulsion.

6.7.6 Effect of time on the viscoelastic properties

Figure 0.13 and

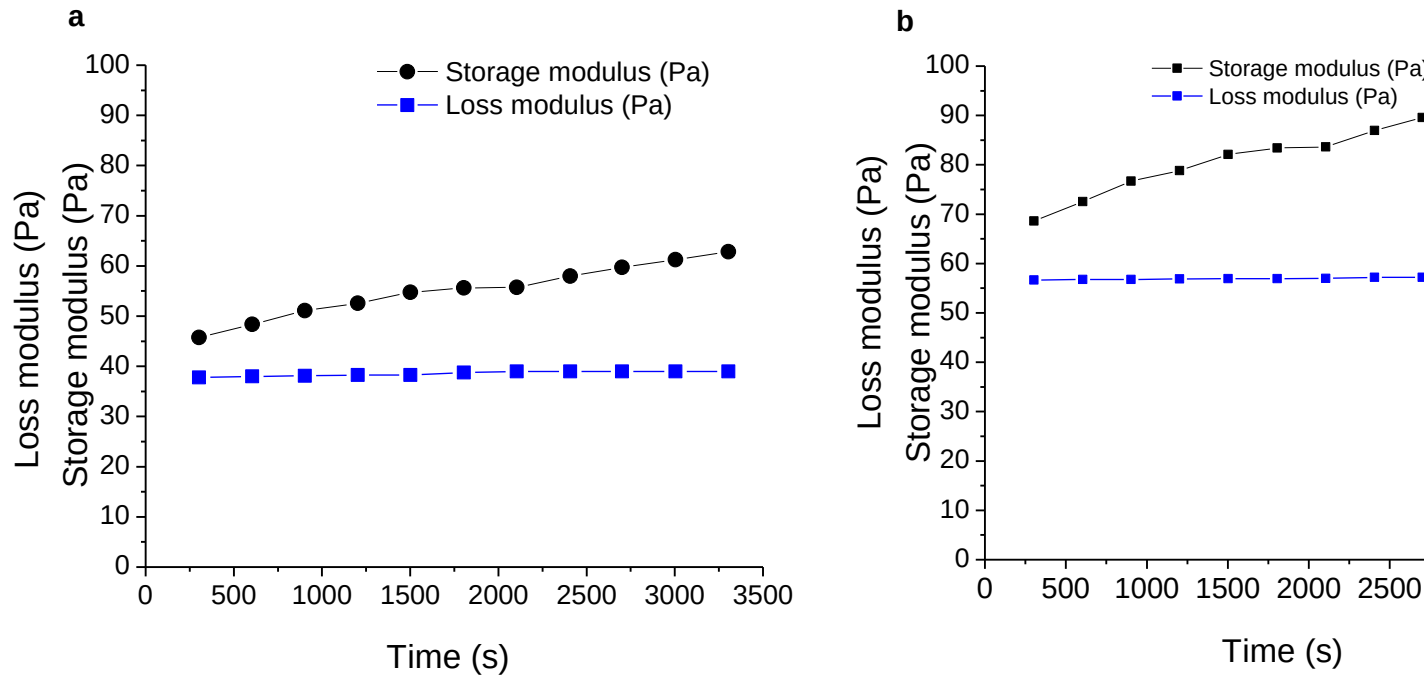

Figure 0.14 show the effect of time on the viscoelastic properties of ACM, ACM stabilised O/W-type nanoemulsion and ACM stabilised O/W-type nanoemulsions enriched with soya milk fiber. Changes that occurred in the viscoelastic properties of ACM and its most stable nanoemulsions was not significant as storage modulus increased gradually while loss modulus almost remained

constant (Figure 0.13 and

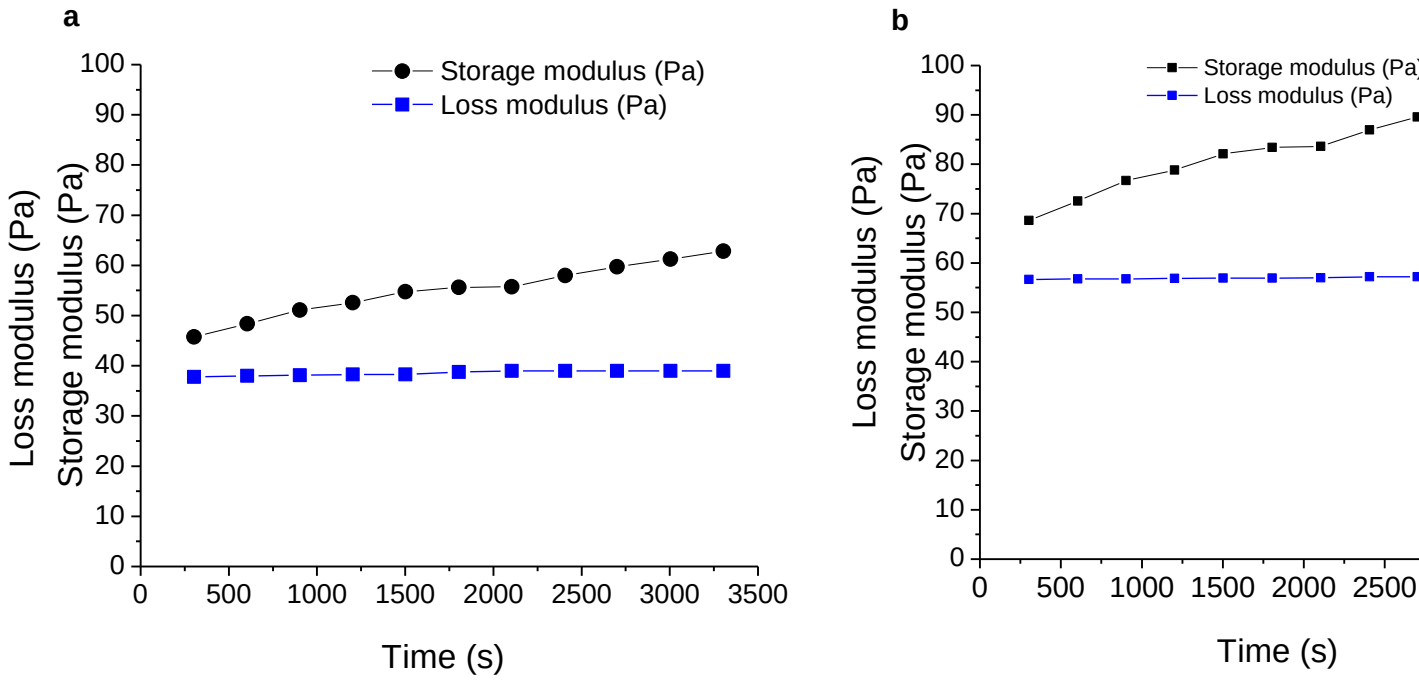

Figure 0.14). ACM and its most stable nanoemulsions emulsions were stable during the first hour as the storage modulus did not decline and the increase in loss modulus was gradual (Figure 0.13 and

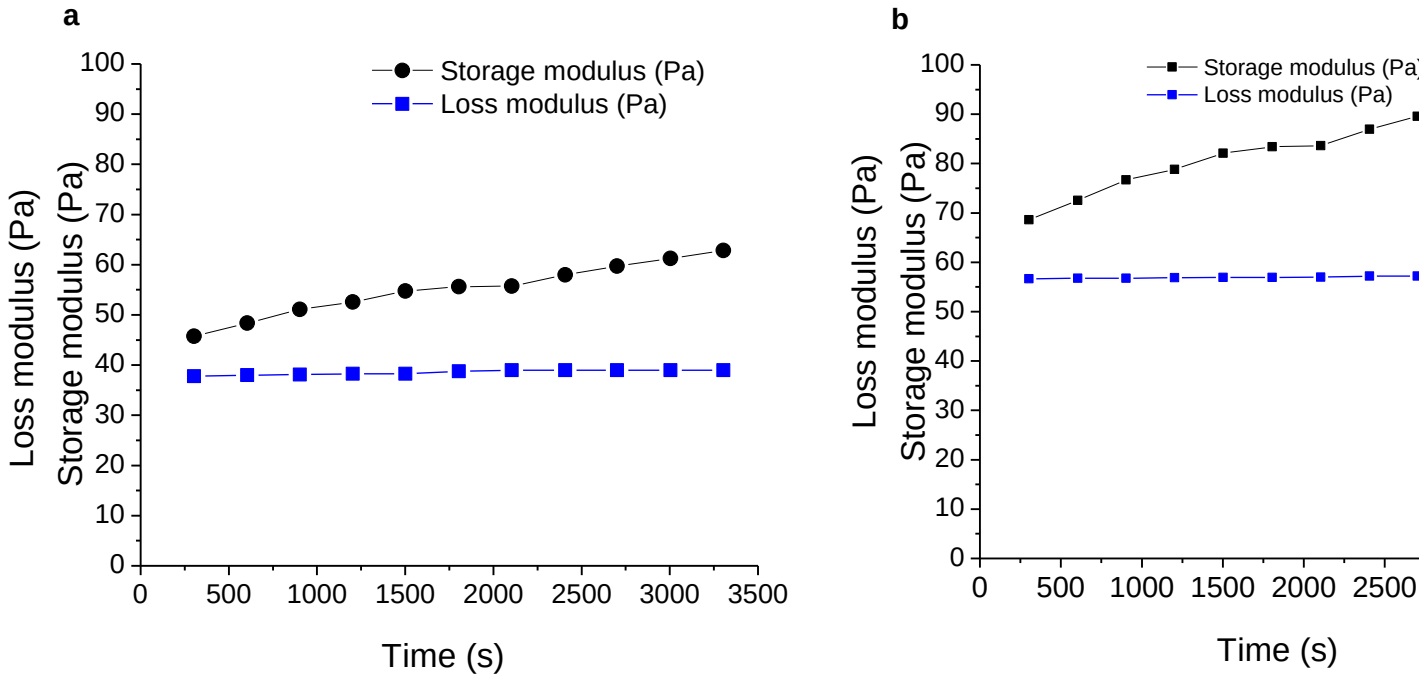

Figure 0.14). The structural stability of ACM and its most stable nanoemulsions was further confirmed because there was no phase change as there was no crossover point observed for storage and loss moduli (Figure 0.13 and

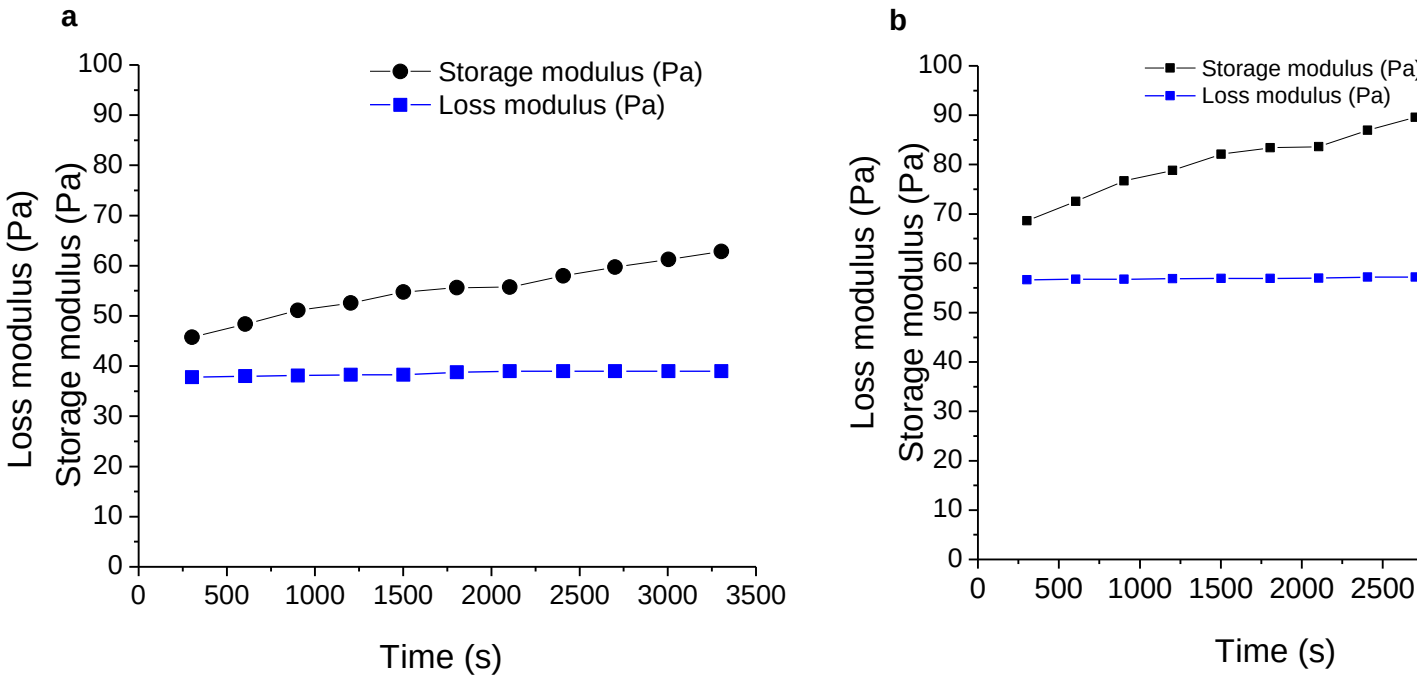

Figure 0.14).

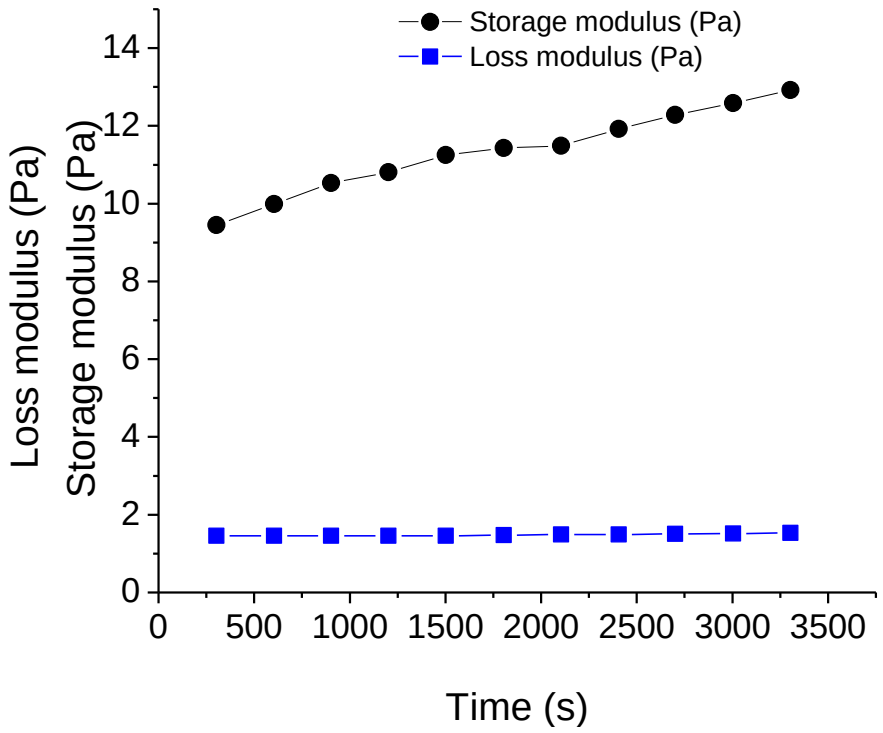

Figure 0.13: Effect of time on the moduli of (a) African catfish mucilage (ACM).

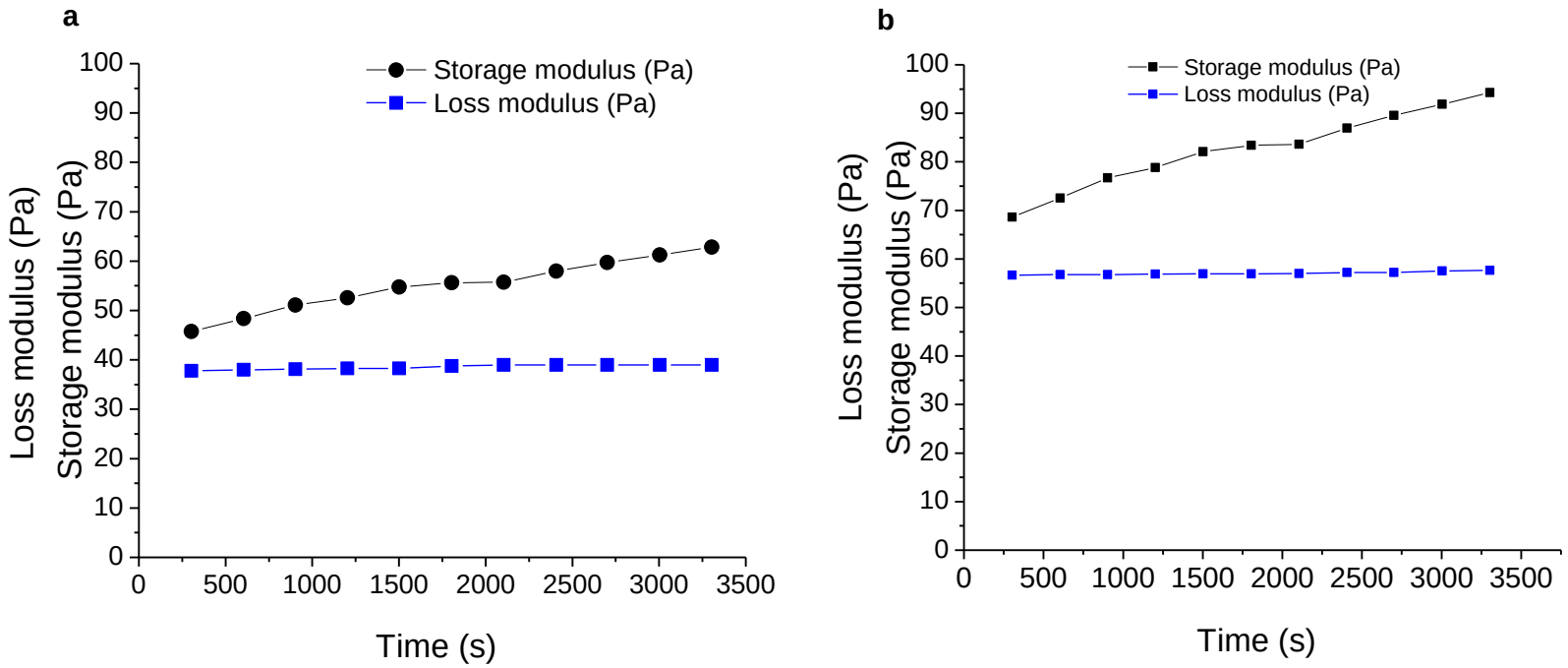

Figure 0.14: Effect of time on the moduli of African catfish mucilage (ACM) stabilised (a) O/W-type nanoemulsion and (b) O/W-type nanoemulsion enriched with soya milk fiber.

The effect of time on the viscoelastic properties of ACM and its most stable nanoemulsions showed that structural changes did not occur as storage modulus increased gradually while loss modus was constant hence, ACM and its most stable nanoemulsions remained stable (Figure 0.13 and

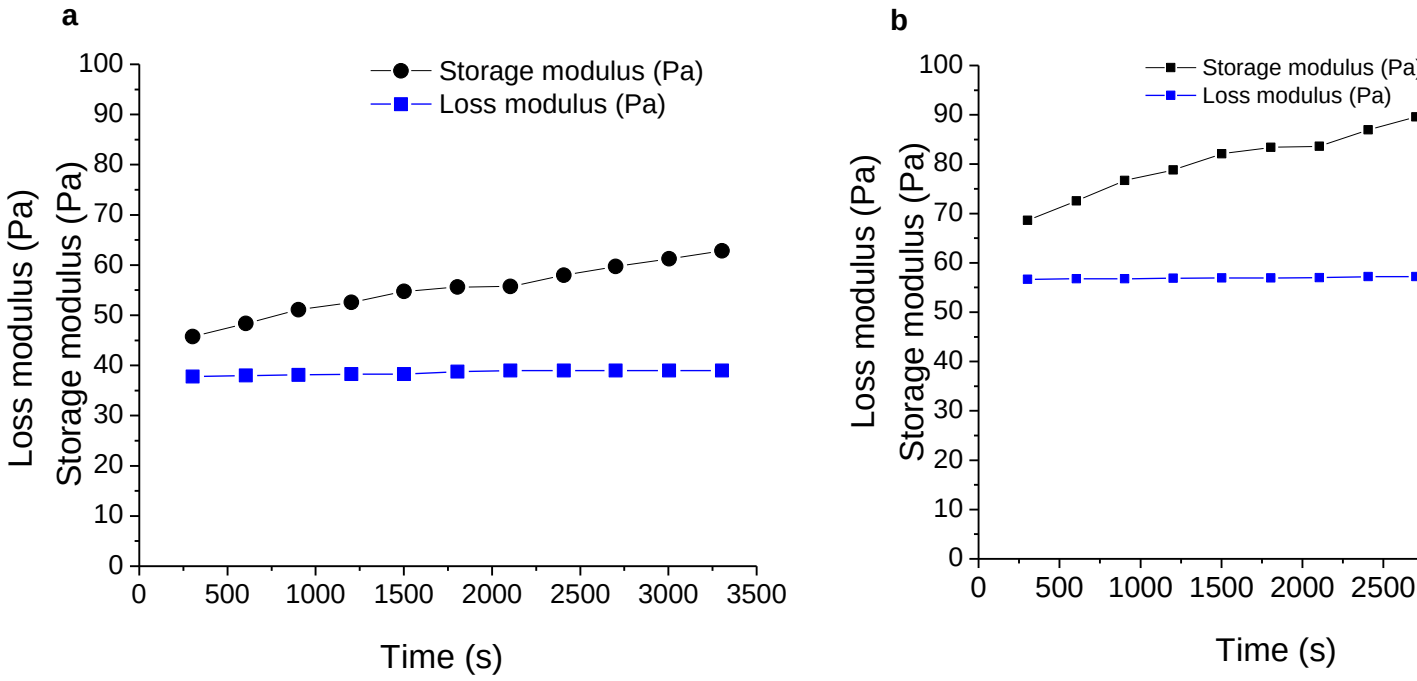

Figure 0.14). Earlier it was established that the stability of ACM and its stable nanoemulsions could be as a result of cross-linking due to filamentous protein threads in ACM which stabilised the network structure of ACM, ACM stabilised O/W-type nanoemulsion and ACM stabilised O/W-type

nanoemulsions enriched with soya milk fiber (Figure 0.13 and

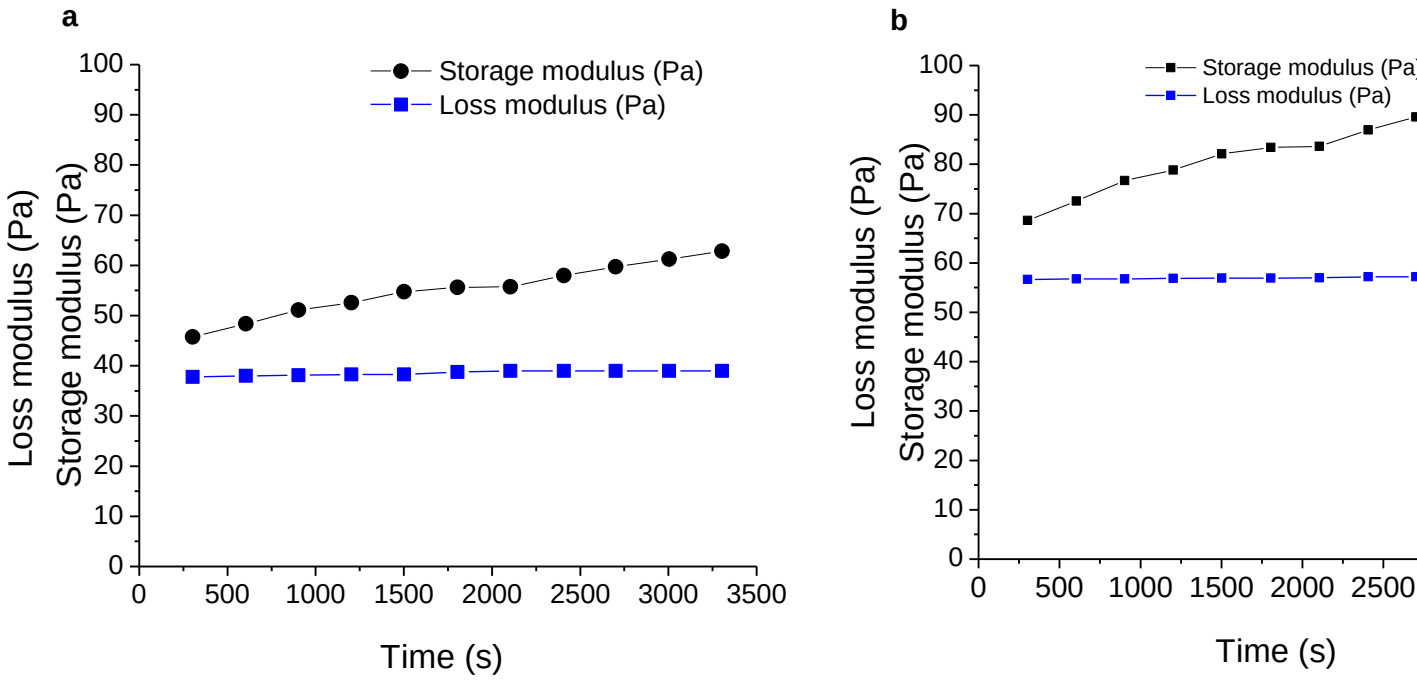

Figure 0.14).This observation is supported by the CryoTem images Figures 4.22 and 4.25 which showed that the network structure of ACM, ACM stabilised O/W-type nanoemulsion and ACM stabilised O/W-type nanoemulsions enriched with soya milk fiber was stabilised due to preferential heterogeneous distributions discretely within the network structure. This result that stability is achieved due to the cross-linking of filamentous protein threads that stabilise the network structure at discrete points consistent with results obtained by Böni et al. (2016b), Fudge & Schorno (2016), and Böni et al. (2018). Authors have reported that amphiphilic proteins in fish mucus influence the rheological properties of O/W-types nanoemulsion interfaces (Hung et al., 2013; Shahkaramipour et al., 2017; Maravić et al., 2019). Consequently, the findings that amphiphilic filamentous proteins are responsible for the cross-linkages in ACM and this sustains ACMs' structural stability and viscoelastic properties with time agrees with findings by Fudge & Schorno (2016), Böni et al. (2018), and Maravić et al. (2019) on the stability bioemulsifier stabilised emulsions. Also, ACM sustains the structural stability and viscoelastic properties of ACM stabilised O/W-type nanoemulsion with time. In the case of ACM stabilised O/W-type nanoemulsions enriched with soya milk the structural stability and viscoelasticity are due to the synergy between mucoadhesive ACM and soy milk fiber. It was earlier established from the literature that fibres re-enforce the structural stability of emulsions as they work in synergy with ACM-bioemulsifiers by delaying deformation of oil droplet clusters in emulsions Sousa de et al.

(2015), Fujisawa, Togawa, & Kuroda, (2017), Barkhordari, & Fathi, (2018), Ye et al, (2018), and Ruan et al., (2019). For instance, Ruan et al., (2019), investigated the effect of strain on the viscoelastic properties of high internal phase (HIP) O/W emulsions using corn peptide emulsifier re-inforced with citrus fibers (Ruan et al., 2019). The EORs for the HIP O/W emulsions were; 1.0: 75, 1.5: 75 and 2.0:75 % and the HIP O/W emulsions contained increasing citrus fibre concentrations of 0.5, 0.75 and 1.0 % (Ruan et al., 2019). Viscoelastic tests were performed on frequency sweep modes of 1 to 10 rad/s and amplitude sweeps of 0.1–1000 Pa was used to determine where the moduli in the LVR was constant (Ruan et al., 2019). The authors reported that, the G′ and G″ of HIP emulsions with citrus fibres was higher than the control that did not contain fibres (Ruan et al., 2019). The authors also reported that G' was always higher than G" and noted slight increases in G′ and G″ as the frequency increased from1 to 10 rad/s (Ruan et al., 2019). The authors reported that, the G′ and G″ of HIP emulsions with citrus fibres was higher than the control that did not contain fibres (Ruan et al., 2019). The authors indicated that slight increases in the value of G' as the concentration of the citrus fibre increased signified increased gel strength in the HIP emulsions with higher fibre concentration (Ruan et al., 2019). The authors concluded that the reason for the increase G' was due to the formation of a thicker interfacial layer which led to reinforced network structure of the corn peptide HIP emulsions that contained citrus fibres (Ruan et al., 2019). Therefore the higher storage modulus observed in the experimental data of ACM stabilised O/W-type nanoemulsion enriched with soy milk fibre in comparison to ACM stabilised O/W-type nanoemulsion was due to the synergy between the soy milk fibre and ACM which resulted in a thicker interfacial layer of the most stable nanoemulsion that contained soy milk fibre. Consequently, in the effect of time on the moduli of ACMs most stable nanoemulsions, the G' of ACM stabilised O/W-type nanoemulsion enriched with soya milk fiber was higher than that of ACM stabilised O/W-type nanoemulsion because of the synergy that existed between ACM< and soy milk fibre. This synergy resulted in reinforced network structure of ACM stabilised O/W-type nanoemulsion enriched with soya milk fiber. The reinforced network structure of ACM stabilised O/W-type nanoemulsion enriched with soya milk fiber was due to the formation of a thicker interfacial layer between its oi/water interfaces.

Chapter 7

CONCLUSION AND RECOMMENDATIONS

7.1 Introduction

The overall purpose of this research work and 'my original contribution to knowledge' is to assess the suitability of the African catfish mucilage (ACM) as a natural emulsifier that could be used as a feedstock in food-grade, personal care, and drug delivery emulsion systems. This work was conducted through the collection of the ACM from live African catfish (*Clarias gariepinus)* under anesthesia*.* The ACM was collected based on South African Bureau of Standards approved procedures, the Guidelines for Ethical conduct in the care and use of nonhuman animals in research and Ethical considerations for field research on fishes (SABS, 2008; Dunbar et al., 2012; Bennett et al., 2016). The properties investigated were characterising the ACM using physicochemical tests, quantifying the role of ACM as an emulsifier in stabilising soy milk and oil in water–type (O/W-type) nanoemulsions, and investigating the rheological properties of ACM, soy milk (control), ACM stabilised soy milk, and O/W–type nanoemulsions. Functional groups were determined through Attenuated Total Reflectance-Fourier Transform Infrared (ATR-FTIR) spectroscopy. Emulsion stability parameters were determined through morphology studies, particle size measurements, and by the backscattering (BS) flux %. The rheological measurements were carried out by determining the flow and viscoelastic properties of ACM, soy milk (control) ACM stabilised soy milk, ACM O/W–type nanoemulsions, and ACM O/W–type nanoemulsions enriched with soy milk fiber.

This dissertation was structured to achieve the following research objectives:

1. To collect and preserve African catfish mucilage (ACM) from the African catfish.
2. To characterise ACM by determining its physicochemical properties.
3. To investigate the effect of ACM on the stability of soya milk emulsions using Ultra-Turrax T-25 homogenizer.
4. To investigate the effect of ACM on the stability of oil in water-type (O/W-type) nanoemulsions prepared by ultrasonication using D-optimal mixture design.
5. To investigate the flow and viscoelastic rheological behaviour of ACM, ACM stabilised soya milk emulsions and ACM stabilised O/W-type nanoemulsions.

The next section presents findings of each of the set objectives.

7.2 Findings on research objectives

This section summaries the findings of the research based on the research objectives in the manner in which they are presented in the thesis. Section 4.2 presents findings on the first three research objectives one, two and three. Section 5.2 presents findings on research objective four while section 6.2 presents findings on fifth research objective.

7.3 African catfish mucilage extraction, characterisation, and role in stabilising soy milk

The research objective of collection, and preservation of African catfish mucilage (ACM) was achieved by following the South African Bureau of Standards approved procedures, the Guidelines for Ethical conduct in the care and use of nonhuman animals in research and Ethical considerations for field research on fishes (SABS, 2008; Dunbar et al., 2012; Bennett et al., 2016). African catfish mucilage (ACM) was extracted from live African catfish (Clarias gariepinus) by anesthetising the fish with 100 the fish with 100 mg per liter methanesulfonate. The ACM was collected from the African catfish under anesthesia with the aid of a fish stimulation gadget (HPG1, Velleman Instruments, (18 V, 80 Hz)). The fish stimulation gadget was used to enhance mucus discharge from mucus glands by placing the gadget on the ventral lateral section of the catfish to ensure that the ACM was not contaminated with blood, fish discharge and droplets. All the live African catfish were resuscitated after collecting the mucus by placing them in a recuperation bath. The live African catfish used for sampling was monitored for one week in other to ensure that they were stable and did not display any symptoms of stress. All live African catfish had fully recovered from stress conditions by day 2 and could be used to collect fresh ACM samples.

To achieve the second research objective, the morphology was determined with Transmission electron microscopy (TEM), while functional groups in ACM and ACM-stabilised soya milk emulsions were determined using ATR-FTIR spectroscopy. The objective of characterising African catfish mucilage (ACM) by determining its physicochemical properties was achieved as ACM was found to be a stable hydrogel with negatively charged (−36.2 mV) loosely bound electrons with polar and non-polar portions. Unmagnified freeze-dried African catfish mucilage (ACM) was found to be greyish-brown with a powdery appearance. Structural studies with the TEM revealed that the ACM dispersion in MilliQ water was spherical and formed aggregates with structural networking into gel fibers. Furthermore, ACM in MilliQ water was found to contain intermediate protein filaments and the mucins in ACM entrapped MilliQ water to form an elastic gel-like stable structure. The spectra of ACM revealed stretching vibrations of hydroxyl groups of

hydrophilic amino acid overtones, asymmetric stretch for biopolymers such as amphiphilic glycoprotein or mucus, amide I, II and III bands which affirmed protein secondary structure and stretching vibrations of protein-peptide bonds.

The third research objective which was to investigate the performanceof African catfish mucilage (ACM) on the stability of soya milk emulsions was carried out to test the ability of the African catfish mucilage as an emulsifier. A Turbiscan was used to measure stability, morphology was determined with TEM, while functional groups in ACM and ACM-stabilised soya milk emulsions were determined using ATR-FTIR spectroscopy. The objective of investigating the effect of African catfish mucilage (ACM) on the stability of soy milk emulsions was achieved as the variation in emulsion appearance over time, backscattering intensity and emulsion images were determined for soy milk concentrations of 10, 30, 50 and 75 % stabilised with 1, 3 and 5 % ACM for 180 mins of storage. The application of low concentration (1%, 3%, and 5%) ACM led to stabilised soy milk emulsions. Hence stability was achieved with ACM-emulsifier soy milk ratios (ESMRs) of 1:10, 1:30, 1:50 and 1:75 %, 3:10, 3:30, 3:50 and 3:75 % and 5:10, 5:30, 5:50 and 5:75 %. The stability of soy milk emulsions with ESMR of 1:75, 3:75 and 5;75 % was discontinued to showcase the effect of ACM in a soy milk emulsion that had MilliQ water concentrations of at least 45 %. The ESMR ratio of 5:10, 5:30, and 5:50 % had the highest stability i.e. highest back scattering (BS) % flux. The Turbiscan confirmed the role of ACM at low concentrations for the stability of soy milk emulsions. It also showed that the higher the concentration of ACM and the higher the ACM-ESMR the higher the stability of the emulsion i.e. the higher the BS % flux. The spectra of ACM stabilised soy milk emulsion revealed interactions between ACM and soya milk droplets. The zetasizer was used to determine the particle size and stability was expressed as a function of Sauter mean diameter ($D_{(3,2)}$) calculated from the particle size. The higher the concentration of ACM, the more stable the emulsion i.e. the lower the $D_{(3,2)}$ of stabilised emulsions. Also, the higher the ESMR the higher the stability i.e. the lower the $D_{(3,2)}$ of stabilised emulsions. The results from TEM, ATR-FTIR, $D_{(3,2)}$, and BS % flux analysis showed that the mucins in ACM formed strong cohesive connections with stabilised soy milk emulsions hence ACM exhibited adhesive properties. Consequently, ACM is a good natural emulsifier with mucoadhesive properties as it encapsulates soy milk to enhance stability. Two-way analysis of variance (ANOVA) with Tukey's multiple comparisons test was used to analyse the $D_{(3,2)}$ and BS % flux data. A significant difference ($\rho < 0.05$) was established on ACM stabilised soy milk emulsions with respect to BS % flux and $D_{(3,2)}$ for emulsions with ESMRs of 5:10, 5:30, and % 5:50 %. The ANOVA studies show that data obtained from BS % flux closely fit the regression

line by about 99.94% while the data for $D_{(3,2)}$ was 90% fit. Hence, both responses are good predictors of the stability of an emulsion.

7.4 African catfish mucilage role in stabilising oil in water-type nanoemulsions

The fourth research objective, which was to investigate the effect of ACM on the stability of oil in water-type (O/W-type) nanoemulsions prepared by ultrasonication using D-Optimal mixture technique was achieved. A Turbiscan were used to measure stability, a Zetasizer was used to measure the particle size, the morphology was determined with Cryo-Transmission electron microscopy (Cryo-TEM), and functional groups in ACM and ACM-stabilised soya milk emulsions were determined using ATR-FTIR spectroscopy. Turbiscan studies showed that when ACM concentration was highest regardless of oil concentration the initial average BS % flux of O/W-type nanoemulsions was high leading to higher stability. The results from the zetasizer showed that when ACM concentration was highest regardless of oil concentration, the Sauter mean diameter [D(3,2)] of emulsions was low leading to higher stability. Cryo-TEM studies revealed that cross-linkage structure of mucins in ACM stabilised O/W-type nanoemulsions did not occur across the matrix but occurred preferentially via a heterogeneous distribution discretely in the networks matrix. Hence, structural stability of ACM stabilised O/W-type nanoemulsions was due to the presence of amphiphilic filamentous protein threads in ACM. The spectra of ACM stabilised O/W-type nanoemulsion revealed interactions between ACM and oil droplets this was evidenced by shifts in the wavelength peaks of the key functional groups. The concentration of ACM to the oil ratio i.e. the emulsifier oil ratio (EOR) influenced the stability as a function of the BS % flux and the D(3,2). The trend was the higher the emulsifier-oil ratio (EOR) the higher the stability i.e. the higher the BS % flux and the lower the D (3,2), Consequently, the EOR influences the stability of O/W-type nanoemulsions.

Authors have reported the multi-faceted applications of O/W-type nanoemulsion in beverages, cosmetics, drug delivery, foods, nutraceuticals, and personal, and personal care products (Bai et al., 2017; Mikulcová et al., 2017; Azmi et al., 2019). Based on the multi-faceted applications of O/W-type nanoemulsions, the data on the effect of the independent variables (ACM, oil and MilliQ water) on the dependent variables Sauter mean diameter [$\mathbf{D_{(3,2)}}$] and backscattering (BS) % flux was modelled using mixture design surface methodology. In this study, mixture design surface methodology was combined with D-Optimal mixture method in order to investigate the effect of ACM in the stability of O/W-type nanoemulsions. The result indicated that the ability of RSM to select proper and precise formulations played a significant role in optimising the stability of ACM stabilised O/W-type nanoemulsion. Also, RSM was used to determine the

(main) linear, quadratic and synergy effects of main emulsion components on the BS % flux and $\mathbf{D_{(3,2)}}$ of ACM stabilised O/W-type nanoemulsion. Generally, D-Optimal mixture design was shown to be a useful experimental design that provided mixture design surface models that could explain the variation of two response variables as a function of three independent variables (ACM, oil and MilliQ water). The mixture design surface analysis provided a significant difference *p*-value of < 0.05 association with regression equations of high R^2 (0.9721 and 0.9992) and high adjusted R^2 (0.9567 and 0.9987) for the effect of the three independent variables on the dependent variables BS % flux and $\mathbf{D_{(3,2)}}$ responses. The quadratic mixture model for BS % flux obtained by analysng the experimental data was significant (F [557.86, 8.88] = 62.80; *p*-value < 0.0001) in describing the component effects (ACM, oil, and water) on BS % flux stability parameter. The quadratic mixture model for BS % flux was significant (F [557.86, 8.88] = 62.80; *p*-value < 0.0001). The model's lack of fit (F [19.98, *6.990E-003*] = *2858.24*; *p* < 0.0001) was also significant, however, the predicted R-squared value was 0.9123 and adequate precision was 20.186 indicating a model with adequate goodness-of-fit to the experimental data. Similarly, the quadratic mixture model for $\mathbf{D_{(3,2)}}$ was significant (F [235.71, 0.13] = 1805.99; *p*-value < 0.0001). The model lack of fit (F [0.17, 0.11] = 0.3104; *p* = 1.49) was not significant, and the predicted R-squared value was 0.9977 and adequate precision was 104.158 indicating a model with adequate goodness-of-fit. The results showed clearly that the African catfish mucilage content could be applied as a key independent variable in formulating stabilised O/W-type nanoemulsion based on BS % flux and $\mathbf{D_{(3,2)}}$ properties studied. Desirability functions were chosen to either maximise BS % flux (γ_1) and minimise Sauter mean diameter (γ_2) or maximise BS % flux (γ_1) and maximise Sauter mean diameter (γ_2). This desirability function was set to answer sub research objective questions on whether maximising BS % flux (γ_1) and minimising Sauter mean diameter (γ_2) or maximising BS % flux (γ_1) and maximising Sauter mean diameter (γ_2) would affect the desirability options. The overall desirability of the chosen formulation for option A (EOR 4.2:3) which involved maximising BS flux (γ_1) and minimising Sauter mean diameter (γ_2) was 100%. The overall desirability of the chosen formulation for option B EOR (5:10) which involved maximising BS flux (γ_1) and maximising Sauter mean diameter (γ_2) was 95%. Hence both desirability functions on the formulations substantially satisfied the targeted constraints. Based on the literature, the combination of independent variable constituents in option B (5 % ACM: 10 % oil: 85 % water) was selected for rheology tests because authors have reported that stabilised emulsions with higher oil concentration exhibited a higher degree of shear-thinning, viscosity, and viscoelastic rheological properties (Dokić et al., 2012; Xi et al., 2019). The predicted stability value for option B with EOR 5:10 % was BS % flux was 73.7 % while the $D_{(3,2)}$ value was 7.5 nm and the desirability was 95 %.

Results further showed that the protein functional groups in ACM and ACM concentrations critically influenced both BS % flux and $\mathbf{D_{(3,2)}}$ of ACM stabilised O/W-type nanoemulsions. It was observed that the higher the emulsifier oil ratio (EOR) the higher the stability i.e. the higher the BS % flux and the lower the $D_{(3,2)}$ (particle size). Hence, it was deduced that EOR influences the stability of O/W-type nanoemulsion. This was because the amphiphilic (hydrophilic and hydrophobic) proteins in ACM interfaced with oil and water simultaneously to ensure stability. Consequently, it was deduced that the emulsifier effect of ACM on ACM stabilised O/W emulsion could be explained by the micelle theory consistent with other authors. Hence African catfish mucilage highly influences the stability of O/W-type nanoemulsion and can be applied in cosmetics, food-grade, personal care, and drug delivery emulsions applications.

7.5 Flow and viscoelastic rheological behaviour of African catfish mucilage (ACM), ACM stabilised soy milk emulsion and ACM stabilised o/w-type nanoemulsions

The last research objective was to investigate the flow and viscoelastic rheological behaviour of African catfish mucilage (ACM), soy milk (control), ACM stabilised soy milk emulsion, ACM stabilised o/w-type nanoemulsions, and ACM stabilised o/w-type nanoemulsions enriched with soy milk fibre was achieved. The flow behavior tests were conducted by investigating the effect of viscosity as the shear rate increased from 0.01 to 1000 s 1. In summary, results showed that ACM, soy milk (control), ACM stabilised soy milk emulsion and ACM stabilised o/w-type nanoemulsion and ACM stabilised o/w-type nanoemulsion enriched with soy milk fibre were non-Newtonian and all showed a distinct shear thinning behaviour.. It was observed through Cryo-TEM studies that cross-linkage structure of mucins in African catfish mucilage did not occur across the matrix but occurred preferentially via a heterogeneous distribution discretely in the networks matrix. The stability of ACM, ACM stabilised O/W-type nanoemulsion and ACM stabilised O/W-type nanoemulsions enriched with soya milk fiber was established through visual observation, Cryo-TEM, and Turbiscan study. The stability results established correlated with the effects of strain, frequency, temperature, and time on viscoelastic properties as phase separation was not observed in ACM, ACM stabilised O/W-type nanoemulsion and ACM stabilised O/W-type nanoemulsions enriched with soya milk fiber. The results obtained through Cryo-TEM, and Turbiscan study on the stability of ACM, ACM stabilised O/W-type nanoemulsion and ACM stabilised O/W-type nanoemulsions enriched with soya milk fiber correlated with rheological properties as the viscoelastic properties were ascribed to the amphiphilic filamentous protein threads present in the ACM. The results confirmed that amphiphilic filamentous protein threads

in ACM influenced the rheological properties of O/W-type nanoemulsion interfaces by forming a stable network structure at different points within the matrix even though the system was watery.

The investigated African catfish mucilage (ACM), soy milk (control), ACM stabilised soy milk emulsion, ACM stabilised O/W-type nanoemulsions, and ACM stabilised O/W-type nanoemulsions enriched with soya milk fiber responded to low shear rates and had mean initial viscosity (MIV) values. The MIV value for ACM stabilised soy milk emulsion was higher than that of soy milk (control), they were 2352.5 ± 1.5 and 661.3 ± 2.2 mPa.s respectively. Hence ACM stabilised soy milk emulsion was more stable than soy milk (control) this was due to the influence of ACM-emulsifier on emulsion stability. ACM exhibited higher stability by forming films around the water drops in water/oil interfaces. The films formed increased the stability of the emulsion by increasing interfacial viscosity and decreasing interfacial tension. Hence the interfacial viscosity i.e. MIV of ACM stabilised soy milk emulsions is higher than that of soy milk. The MIV value of ACM stabilised O/W-type nanoemulsions enriched with soya milk fiber was higher than that of ACM stabilised O/W-type nanoemulsions they were 6468.0 ± 1.3 and 3476.1 ± 2.5 mPas respectively. This shows that the soy milk fiber worked in synergy with ACM and enhanced the stability of ACM stabilised O/W-type nanoemulsions enriched with soya milk fiber. The moduli in the linear viscoelastic region (LVR) of ACM was constant at low strains of 0.2 % and cross-over points of about 10 %. The moduli in the LVR of ACM stabilised O/W-type nanoemulsions, and ACM stabilised O/W-type nanoemulsions enriched with soya milk fiber was constant at low strains of 0.4 aand 0.6 % and cross-over points of about 30 and 50 % respectively. The moduli in the LVR of ACM was low and this is consistent with the results that microstructural stability and viscoelastic properties were conferred through the amphiphilic filamentous protein threads in ACM. Also the presence of soy milk fiber enriched the efficacy of ACM as it worked in synergy with ACM to improve the microstructural stability and viscoelastic properties of ACM stabilised O/W-type nanoemulsions enriched with soya milk fiber as evidenced by higher constany strains in the LVR. This is consistent with the mucoadhesive property of ACM, the ability of ACM to work in synergy with soy milk, the mucoadhesive theory proposed for ACM stabilised soy milk emulsions, and the micelle theory proposed for the stability of the ACM stabilised O/W-type nanoemulsions. The effect of temperature increase from 5 to 50°C showed a slight weakening of the microstructure of ACM and ACMs' most stable emulsions. Structural changes as a result of the effect of temperature was not significant as there was no phase changes observed in the microstructure of ACM and ACMs' most stable emulsions. However, refrigerating i.e. keeping the ACM, ACM stabilised O/W-type nanoemulsion and ACM stabilised O/W-type nanoemulsions

enriched with soya milk fiber at temperatures of 5°C sustained and improved its structural stability and viscoelastic properties. The presence of soya milk fiber influenced the ability of ACM as it worked in synergy with ACM to improve the rheological properties of ACM as evidenced by higher viscosity, storage, and loss moduli and resulted in improved stability and rheological properties. Time duration did not seem to have negative effects on the network structure of ACM, and ACMs' most stable O/W-type nanoemulsion as no pase changes occured within the time duration studied. Stability was due to cross-linking of filamentous protein threads that stabilised the network structure via a discrete heterogeneous preferential grouping in the structural network matrix.

Findings from rheological stability investigation indicates that the emulsion was stable despite the watery nature of ACM, ACM stabilised soy milk emulsions and ACM stabilised O/W-type nanoemulsions. The reason for the stability can be attributed to the amphiphilic filamentous protein threads present in the African catfish mucilage which occurred preferentially via a heterogeneous distribution discretely in the networks matrix and resulted in structural stability. This phenomenon was established by results obtained from morphology test I.e. structural stability, BS % flux and D(3,2) properties, and wavelength peak shifts in ACM stabilised soy milk emulsions, ACM stabilised O/W-type nanoemulsion and ACM stabilised O/W-type nanoemulsion enriched with soy milk fiber. The non-Newtonian flow of ACM, soy milk (control), ACM stabilised soya milk emulsion, ACM stabilised O/W-type nanoemulsion, and ACM stabilised O/W-type nanoemulsion enriched with soy milk fiber, could be modeled with either Power, Herschel-Buckley, Casson, or Bingham equations. The Casson model was the best fit for African catfish mucilage, soy milk (control), ACM stabilised soya milk emulsion, ACM stabilised O/W-type nanoemulsion, and ACM stabilised O/W-type nanoemulsion enriched with soy milk fiber.

7.6 Research contributions

The contributions of the study are discussed as follows:

1. The findings obtained from the first research objective of collecting and preserving African catfish mucilage from the live African catfish could give guidelines to enable the fish industry to collect and preserve ACM that could be used as an emulsifier in food-grade emulsions, cosmetic, and drug release products. Hence, 'my original contribution to knowledge' is that this outcome could give the guidelines to enable the fish industry to collect and preserve ACM that could be used as an emulsifier in food-grade emulsions, cosmetic, and drug release products.

2. After the collection of ACM, the live African catfish (under anesthesia) used in collecting the ACM were resuscitated and none of the live fish died. The resuscitation and full recuperation of live fish allowed the same fish samples to be reused to collect fresh samples of ACM. Also, because the resuscitated and fully recuperated catfish samples did not contain methanesulfonate, they could be harvested and sold for consumption after two weeks. The method used could be used as a guideline for the re-use of live African catfish for collection of ACM. Hence, 'my original contribution to knowledge' is that this outcome could give the guideline for the re-use of live African catfish for collection of ACM.
3. The research objective of investigating the effect of African catfish mucilage (ACM) on the stability of soya milk emulsions was used to establish the performance of ACM as a suitable emulsifier in food–grade emulsions. Hence, 'my original contribution to knowledge' is that this outcome could result in the application of African catfish mucilageas an emulsifier in food-grade emulsions.
4. Findings clearly showed that ACM is a tremendous natural emulsifier as the amphiphilic proteins in ACM entraps the O/W–type nanoemulsions to ensure stability through mucoadhesion by the micelle theory. Also, African catfish mucilage content could be applied as a key independent variable in formulating stabilised O/W-type nanoemulsion based on BS % flux and $\mathbf{D_{(3,2)}}$ properties studied because of its emulsifying properties. In general, the O/W-type nanoemulsions that contained a concentration of ACM (5 % w/w) and EOR 5:10 % was recommended to provide all separate and comprehensive desirable goals for cosmetic, food-grade, cosmetic, personal care, and drug delivery products. This outcome could result in the application of ACM in food-grade emulsions, cosmetic, personal care, and drug delivery products. Hence, 'my original contribution to knowledge' is that this outcome could streamline the conditions needed to determine the effect of process variables (ACM, oil and water) in the stability of O/W–type nanoemulsions in food-grade emulsions, personal care, and drug delivery emulsion systems.
5. The validation of predicted stability for food-grade, cosmetic, personal care, and drug delivery products showed that, the observed stability confirmed the suitability of the quadratic model. The outcome could be used as guidelines in predicting the stability of ACMs' most stable nanoemulsions. Hence, 'my original contribution to knowledge' is that this outcome could streamline the conditions needed to determine the most suitable models for stabilising food-grade emulsions, personal care, and drug delivery emulsion systems.

6. The results achieved from investigating the flow and rheological behavior of African catfish mucilage (ACM), ACM stabilised soy milk emulsion and ACM stabilised o/w-type nanoemulsions gave information on the process operations of the emulsifier ACM and how its effect on stabilised soy milk and O/W-type nanoemulsions. The outcome could be used as guidelines for process operations in the application of ACM for rheological quality and stability of ACMs' most stable emulsions and nanoemulsions. Hence, 'my original contribution to knowledge' is that this outcome could streamline the guidelines for process operations in the application of ACM for rheological quality and stability of ACMs' most stable emulsions and nanoemulsions.
7. The flow data achieved was described using rheological models. The results also showed that the non-Newtonian flow could be modeled with either Power, Herschel-Buckley, Casson, or Bingham equations. The Herschel-Buckley model was found to be the best fit model for African catfish mucilage while Casson model was the best fit model for soy milk (B), ACM stabilised soya milk emulsion (C), ACM stabilised O/W-type nanoemulsion (D), and ACM stabilised O/W-type nanoemulsion enriched with soy milk fiber (E). The flow data achieved could provide the guidelines to describe the best fit models for ACM and ACMs' most stable emulsions. Hence, 'my original contribution to knowledge' is that this outcome could streamline the guidelines to describe the best fit models for ACM and ACMs' most stable emulsions.
8. The rheological stability at refrigeration temperatures was prescribed by presenting the viscoelastic parameters that described the structural network of ACM dispersed in MilliQ water (A), ACM stabilised O/W-type nanoemulsion (D), and ACM stabilised O/W-type nanoemulsion enriched with soy milk fiber (E). This knowledge could serve as guidelines for estimating the rheological quality of African catfish mucilage as an emulsifier. The viscoelastic rheological behavior of African catfish mucilage (ACM), ACM stabilised soy milk emulsion and ACM stabilised o/w-type nanoemulsions could be used as a guideline for the storage of the ACM and ACMs' most stable emulsions as it pertains to the linear viscosity range at low frequencies. Hence, 'my original contribution to knowledge' is that this outcome could serve as a guideline for the storage of the ACM and ACMs' most stable emulsions as it pertains to the linear viscosity range at low frequencies.

The implications of the emulsifying qualities of the ACM which was established through physicochemical and time-independent rheological tests in this study are described in this section:

a) The result on soymilk emulsions implies that ACM can be applied as a feedstock in nutraceuticals that have nutritious benefits obtained from the identified proteins.
b) Oil in water (O/W) nanoemulsions stabilised with ACM can be feedstocks for nutrient packed nutraceutical products that contain proteins.
c) Rheological stability achieved in soymilk emulsions and O/W nanoemulsions can be employed in personal care products such as creams and ointment as shear-thinning is delayed until the applied force exceed the initial viscosity which could happen when it is applied on the skin. For instance, retaining the structural stability (consistency) of the cream or ointment is vital in anti-inflammatory drugs and formulations as it increases the residence time of drugs on the skin
d) Physicochemical and rheological stability achieved in O/W nanoemulsions can be employed in the biomedical industry as the mucoadhesive nature of ACM comes into play. This is due to the fact that regulated applied force/shear delays the release of drugs in a stabilised nanoemulsion implanted into the body. This can be used for the formulation of controlled release drugs which are used to reduce the speed of drug absorption by the body.

The overall contribution of this research work and 'its original contribution to knowledge' is to provide new scientific information to reveal how a suitable, eco-friendly alternative emulsifier such as African catfish mucilage (ACM) could be used in stabilising soy milk and O/W-type nanoemulsions, thereby contributing towards adding economic value to the African catfish mucilage. Hence, this research provides an original contribution to the knowledge of how African catfish mucilage could be used as an emulsifier in food-grade emulsions, cosmetic, and drug release products. Hence the application of this knowledge-base could lead to the creation of novel encapsulated ACM products with potential applications in food-grade, personal care, and pharmaceutical industry. Also, its application as an emulsifier could reduce the challenges of disposing ACM. The use of the ACM, a waste product as an emulsifier in feed-stocks for food-grade, personal care, and pharmaceutical industries would lead to economic growth through creating employment opportunities, improving food security, increasing income, and could increase the Gross Domestic Product (GDP). Also, the use of ACM as an emulsifier would lead to the development of a knowledge base that could enhance global competitiveness for the catfish industry in South Africa and overall contribute towards the South African National Development Plan vision for 2030.

7.7 Recommendations

This section provides recommendations based on results obtained from the data analysed. Although there is considerable information in the literature on the application of bioemulsifiers in stabilising emulsions, limited information is available on the physicochemical characteristics of African catfish mucilage (ACM) and the effects of ACM on emulsions. This is surprising, given the market and scientific bioresource potentials of African catfish mucilage in the South African fishing industry. Overall, the data obtained from research objectives one, two, three, four and five have shown that the use of ACM as a bioemulsifier could set the guidelines for the use of African catfish mucilage as a low cost, eco-friendly alternative emulsifier feedstock in the food-grade, cosmetics, and personal care industry and add value to African catfish (*Clarias gariepinus)* in South Africa and the African continent. Therefore, the following recommendations were prescribed for further study.

1. It is recommended that the knowledge obtained in this studies be implemented by South African fishing Industry to improve profitability, employment, boost the GDP, develop a knowledge base that could enhance global competitiveness for the catfish industry, and contribute towards the South African National Development Plan vision for 2030.
2. Investigate microbial counts of the African catfish mucilage (ACM) to clarify issues of food safety.
3. Investigate the sensory profile of ACM to enable skin clinical trials to determine pharmacological properties or benefits of ACM.
4. Investigate methods that accurately quantify the metabolic profile of ACM and its stabilised emulsions using internal standards. This would ensure that the active amphiphilic proteins are identified.
5. Investigate the flow-time-dependent models of ACM and ACM most stable emulsions for process design and control, sensory behavior and shelf life studies.
6. Investigate the effect of ACM protein isolates and hydrolysates with modified starches and surfactants.
7. Investigate the release kinetic properties of ACM peptide-based hydrogels for applications in food-grade products.

7.8 Limitations

Laboratory studies were conducted to determine, assess and predict the influence of various physicochemical factors on African catfish mucilage (ACM) and ACM stabilised emulsions (soy

milk and oil-in-water-type nanoemulsions. One of the limitations to this study is the resources, and equipment available within the scope of the research. This necessitated that the project was limited to establishing the role of ACM as an emulsifier. Hence, microbial and sensory studies were not conducted on the ACM, ACM stabilised soya milk emulsions and O/W-type nanoemulsions systems.

Also, the metabolic profiling of ACM was not carried out in this study because resources limited the purchase of internal standards for Liquid chromatography-mass spectrometry. This work did not focus on testing the freeze-dried ACM or its emulsion systems for its pharmacological properties or benefits. In addition, the work did not focus on skin trials for personal care or trials for drug delivery because of the scope of the work was limited to establishing the emulsifier role of ACM.

7.9 Conclusion

This thesis embodies the findings of pilot research aimed at evaluating how the physicochemical properties of African catfish mucilage (ACM) affect its efficacy as a potential emulsifier in soy milk and sunflower O/W emulsion and to optimise the emulsion formation to provide the food-grade, cosmetics and personal care industry with a low cost, eco-friendly alternative emulsifier. The use of live African catfish in the collection and preservation of African catfish mucilage could establish the necessary protocols for collecting and preserving ACM from fish farms. In our trials, physicochemical tests were conducted on stability and the rheological properties of ACM and ACM stabilised soy milk and O/W-type nanoemulsions were investigated based on resources available. The findings obtained from this work could enable the fish industry to understand how to collect and preserve ACM that could be used as bioemulsifier feedstock in food-grade emulsions, cosmetic, and drug release products. The outcome could be used as guidelines in predicting stability of ACMs' most stable emulsions and nanoemulsions, describe its best fit models and set the storage parameters of ACMs' most stable emulsions and nanoemulsions. The outcome could be used as guidelines for process operations in the application of ACM for rheological quality and stability of ACMs' most stable emulsions and nanoemulsions. The outcomes of the research findings would contribute to knowledge-based competitiveness for the South African fish industry, increase the economic value of African catfish and contribute to the economy by providing employment opportunities. Also, the use of the ACM collected would ensure that disposal costs on the farm are reduced. In general, the use of the results from each research finding would lead to more publications in peer-reviewed research journals. The implementation of the findings in this research would Improve profitability, employment, boost the

GDP, develop a knowledge base that could enhance global competitiveness for the catfish industry, and contribute towards the South African National Development Plan vision for 2030.

The overall contribution of the study is to provide new scientific information to reveal how a low cost, eco-friendly alternative emulsifier such as African catfish mucilage (ACM) could be used in stabilising soy milk and O/W-type nanoemulsions, thereby contributing towards adding economic value to the African catfish mucilage. This could lead to the creation of novel encapsulated ACM products with potential applications food, personal care, and pharmaceutical industry. Also, its application as an emulsifier could reduce the challenges of disposing ACM. The use of the ACM, a waste product as an emulsifier in feed-stocks for food, personal care, and pharmaceutical industries would lead to economic growth through creating employment opportunities, improve food security, increased income, and could increase the Gross Domestic Product (GDP). Also, the use of African catfish mucilage as an emulsifier would lead to the development of a knowledge base that could enhance global competitiveness for the catfish industry in South Africa and overall contribute towards the South African National Development Plan vision for 2030.

REFERENCES

Acevedo-Estupiñan, M. V., Gutierrez-Lopez, G. F., Cano-Sarmiento, C., Parra-Escudero, C. O., Rodriguez-Estrada, M. T., Garcia-Varela, R. & García, H. S. 2019. Stability and characterisation of o/w free phytosterols nanoemulsions formulated with an enzymatically modified emulsifier. *LWT*, 107, 151-157.

Adeyi, O., Ikhu-Omoregbe, D. & Jideani, V. 2014. Emulsion stability and steady shear characteristics of concentrated oil-in-water emulsion stabilised by gelatinized bambara groundnut flour. *Asian Journal of Chemistry*, 26, 4995-5002.

Adeyi, O., Ikhu-Omoregbe, D. I. O. & Jideani, V. A. 2018. Rheological properties of sunflower oil-in-water emulsion containing vinegar, stabilised with gelatinized bambara groundnut flour. *International Journal of Engineering Research in Africa,* Trans Tech Publ, 85-97.

Aditya, N., Espinosa, Y. G. & Norton, I. T. 2017. Encapsulation systems for the delivery of hydrophilic nutraceuticals: Food application. *Biotechnology Advances*, 35, 450-457.

Akunne, T., Okafor, S., Okechukwu, D.C., Nwankwor, S.S., Emene, J.O. and Okoro, B.N., 2016. Catfish (Clarias gariepinus) slime coat possesses antimicrobial and wound healing activities. *UK J. Pharmacol. Biosci*, *4*.

Agbekpornu, H., Yeboah, D., Pappoe, A., Ennin, J.E. & Oyih, M. 2017. The State of Farm Raised Catfish Consumption in Ghana: A Case of the Ashanti Region. *Current Journal of Applied Science and Technology*, 1-14.

Aguilera, J.M. 2018. Relating food engineering to cooking and gastronomy. *Comprehensive Reviews in Food Science and Food Safety*, *17*(4); 1021-1039.

Albaldawi, M. 2015. Chemical and physical strategies promoting nanoparticle permeation through intestinal mucus barrier. PhD Doctoral dissertation, Cardiff University.

Alghooneh, A., Razavi, S.M.A. & Behrouzian, F. 2017. Rheological characterization of hydrocolloids interaction: A case study on sage seed gum-xanthan blends. *Food Hydrocolloids*, *66*, 206-215.

Alkhatib, E. A., Grunzke, D. & Chabot, T. 2016 Multi-Regression Prediction of Metal Partition Coefficients under Various Physical/Chemical Conditions: Design of Experiments As, Cr, Cu, Ni and Zn. *Hydrology Current Research* 7:241.

Allam, B. & Espinosa, E.P. 2015. *Mucosal immunity in mollusks. In Mucosal Health in Aquaculture*. Academic Press. 325-370.

Amirdivani, S. & Baba, A. 2013. Rheological properties and sensory characteristics of green tea yogurt during storage. *Life Science Journal*, 378-390.

Angulo, D. E. L. & do Amaral Sobral, P. J. 2016. Characterisation of gelatin/chitosan scaffold blended with aloe vera and snail mucus for biomedical purpose. *International Journal of Biologica*l *Macromolecules*, 92, 645-653.

Anju, A., Jeswin, J., Thomas, P.C. & Vijayan, K.K. 2013. Molecular cloning, characterisation and expression analysis of F-type lectin from pearl oyster Pinctada fucata. *Fish & Shellfish Immunology,* 35(1): 170-174.

Anupam, K., Swaroop, V. & Lal, P. S. 2018. Antagonistic, synergistic and interaction effects of process parameters during oxygen delignification of melia dubia kraft pulp. *Journal of Cleaner Production,* 199, 420-430.

Anvari, M. & Joyner, H.S. 2017. Effect of formulation on structure-function relationships of concentrated emulsions: Rheological, tribological, and microstructural characterization. *Food Hydrocolloids*, *72*, 11-26.

Anvari, M., Tabarsa, M., Cao, R., You, S., Joyner, H. S., Behnam, S. & Rezaei, M. 2016. Compositional characterisation and rheological properties of an anionic gum from alyssum homolocarpum seeds. *Food Hydrocolloids*, 52, 766-773.

Arif, M., Chia, L.S. & Pauls, K.P. 2018. Protein-based bioproducts. In *Plant Bioproducts* (143-175). Springer, New York, NY.

Augusto, P. E. D., Falguera, V., Cristianini, M. & Ibarz, A. 2012. Rheological behavior of tomato juice: Steady-state shear and time-dependent modeling. *Food and Bioprocess Technology,* 5, 1715-1723.

Azari-Anpar, M., Khomeiri, M., Ghafouri-Oskuei, H. & Aghajani, N. 2017. Response surface optimization of low-fat ice cream production by using resistant starch and maltodextrin as a fat replacing agent. *Journal of Food Science and Technology*, 54(5): 1175-1183.

Azmi, N. A. N., Elgharbawy, A. A., Motlagh, S. R., Samsudin, N. & Salleh, H. M. 2019. Nanoemulsions: Factory for food, pharmaceutical and cosmetics. *Processes*, 7, 617.

Bahadir, T. C. H. S. I. & Tulun, S. 2019. Antibiotic applications in fish farms and environmental problems.*Turkish Journal of Engineering*., 3, 60-60.

Bai, L., Huan, S., Li, Z. & McClements, D. J. 2017. Comparison of emulsifying properties of food-grade polysaccharides in oil-in-water emulsions: Gum arabic, beet pectin, and corn fiber gum. *Food Hydrocolloids*, 66, 144-153.

Bai, L., Lv, S., Xiang, W., Huan, S., McClements, D. J. & Rojas, O. J. 2019. Oil-in-water pickering emulsions via microfluidization with cellulose nanocrystals: 1. Formation and stability. *Food Hydrocolloids*, 96, 699-708.

Balaghi, S., Mohammadifar, M.A., Zargaraan, A., Gavlighi, H.A. & Mohammadi, M. 2011. Compositional analysis and rheological characterisation of gum tragacanth exudates from six species of Iranian Astragalus. *Food Hydrocolloids*, *25*(7): 1775-1784.

Balasubramanian, S., Prakash, M., Senthilraja, P. & Gunasekaran, G. 2012. Antimicrobial properties of skin mucus from four freshwater cultivable fishes (Catla catla, Hypophthalmichthys molitrix, Labeo rohita and Ctenopharyngodon idella). *African Journal of Microbiology Research*, 6(24): 5110-5120.

Balasubramanian, S., Revathi, A. & Gunasekaran, G. 2016. Studies on anticancer, haemolytic activity and chemical composition of crude epidermal mucus of fish mugil cephalus. *International Journal of Fish and Aquatic Studies*. 4, 438-443.

Ballarin, L., Cammarata, M., Franchi, N. & Parrinello, N. 2013. *Routes in innate immunity evolution: galectins and rhamnose-binding lectins in ascidians. Marine protein and peptides*. *biological activities and applications*. Chichester: Wiley-Blackwell, 185-205.

Bansil, R. & Turner, B.S. 2018. The biology of mucus: Composition, synthesis and organization. *Advanced Drug Delivery Reviews*, *124*, .3-15

Barkhordari, M.R. & Fathi, M. 2018. Production and characterization of chitin nanocrystals from prawn shell and their application for stabilization of Pickering emulsions. *Food Hydrocolloids*, *82*, 338-345.

Barzic, A. I. & Ioan, S. 2016. *Multiphase polymer systems: Micro-to nanostructural evolution in advanced technologies*, CRC press, Boca Raton, Fl.

Basu, S. & Shivhare, U. 2013. Rheological, textural, microstructural, and sensory properties of sorbitol-substituted mango jam. *Food and Bioprocess Technology*, 6, 1401-1413.

Baugreet, S., Kerry, J. P., Allen, P. & Hamill, R. M. 2017. Optimisation of protein-fortified beef patties targeted to the needs of older adults: A mixture design approach. *Meat Science,* 134, 111-118.

Béné, C., Arthur, R., Norbury, H., Allison, E. H., Beveridge, M., Bush, S., Campling, L., Leschen, W., Little, D., Squires, D., Thilsted, S. H., Troell, M. & Williams, M. 2016. Contribution of fisheries and aquaculture to food security and poverty reduction: Assessing the current evidence. *World Development*, 79, 177-196.

Béné, C., Barange, M., Subasinghe, R., Pinstrup-Andersen, P., Merino, G., Hemre, G.I. & Williams, M. 2015. Feeding 9 billion by 2050–Putting fish back on the menu. *Food Security*, *7*(2); 261-274.

Bennett, R.H., Ellender, B.R., Mäkinen, T., Miya, T., Pattrick, P., Wasserman, R.J., Woodford, D.J. & Weyl, O.L. 2016. Ethical considerations for field research on fishes. *Koedoe*, *58*(1): 1-15.

Bergenståhl, B. & Spicer, P. T. 2019. *Physicochemical aspects of an emulsifier function. Food emulsifiers and their applications*. Springer Switzerland AG.

Bernards, M.A., Oke, I., Heyland, A. & Fudge, D.S. 2014. Spontaneous unraveling of hagfish slime thread skeins is mediated by a seawater-soluble protein adhesive. *Journal of Experimental Biology*, *217*(8):1263-1268.

Berton-Carabin, C.C., Sagis, L. & Schroën, K. 2018. Formation, structure, and functionality of interfacial layers in food emulsions. *Annual Teview of Food Science and Technology*, *9*, 551-587.

Bhardwaj, M., Singh, R. & Saxena, D. 2019. *Rheology: A tool to predict quality of foods. Technologies for value addition in food products and processes*. Apple Academic Press,. Palm Bay, Fl.

Bhattacharjee, S. 2016. Dls & zeta potential–what they are and what they are not? *Journal of Controlled Release*, 235, 337-351.

Bieczynski, F., Torres, W.D., Painefilu, J.C., Castro, J.M., Bianchi, V.A., Frontera, J.L., Paz, D.A., González, C., Martín, A., Villanueva, S.S. and Luquet, C.M., 2016. Alterations in the intestine of Patagonian silverside (Odontesthes hatcheri) exposed to microcystin-LR: Changes in the glycosylation pattern of the intestinal wall and inhibition of multidrug resistance proteins efflux activity. *Aquatic Toxicology*, *178*, pp.106-117.

Bishnoi, R., Khatri, I., Subramanian, S. & Ramya, T.N.C. 2015. Prevalence of the F-type lectin domain. *Glycobiology*, 25(8): 888-901.

Blau, P. J. 2015. How common is the steady-state? The implications of wear transitions for materials selection and design. *Wear*, 332, 1120-1128.

Böcker, L., Rühs, P.A., Böni, L., Fischer, P. & Kuster, S. 2016. Fiber-enforced hydrogels: Hagfish slime stabilized with biopolymers including κ-carrageenan. *ACS Biomaterials Science & Engineering*,*2*(1); 90-95.

Böni, L., Fischer, P., Böcker, L., Kuster, S. & Rühs, P. A. 2016a. Hagfish slime and mucin flow properties and their implications for defense. *Scientific Reports*, 6, 30371.

Böni, L., Rühs, P. A., Windhab, E. J., Fischer, P. & Kuster, S. 2016b. Gelation of soy milk with hagfish exudate creates a flocculated and fibrous emulsion-and particle gel. *Plos One*, 11, e0147022.

Böni, L. J., Zurflüh, R., Baumgartner, M. E., Windhab, E. J., Fischer, P., Kuster, S. & Rühs, P. A. 2018. Effect of ionic strength and seawater cations on hagfish slime formation. *Scientific Reports*, 8, 1-12..

Böni, L. J., Zurflüh, R., Widmer, M., Fischer, P., Windhab, E. J., Rühs, P. A. & Kuster, S. 2017. Hagfish slime exudate stabilization and its effect on slime formation and functionality. *Biology Open*, 6, 1115-1122.

Bonn, D., Denn, M. M., Berthier, L., Divoux, T. & Manneville, S. 2017. Yield stress materials in soft condensed matter. *Reviews of Modern Physics*, 89, 035005.

Borges, M.H., Andrich, F., Lemos, P.H., Soares, T.G., Menezes, T.N., Campos, F.V., Neves, L.X., Castro-Borges, W. & Figueiredo, S.G. 2018. Combined proteomic and functional analysis reveals rich sources of protein diversity in skin mucus and venom from the Scorpaena plumieri fish. *Journal of proteomics*, *187*, 200-211.

Brinchmann, M.F., Patel, D.M., Pinto, N. & Iversen, M.H. 2018. Functional aspects of fish mucosal lectins—Interaction with non-self. *Molecules, 23*(5): 1119.

Browne, M.J., Feng, C.Y., Booth, V. & Rise, M.L. 2011. Characterisation and expression studies of Gaduscidin-1 and Gaduscidin-2; paralogous antimicrobial peptide-like transcripts from Atlantic cod (Gadus morhua). *Developmental & Comparative Immunology*, 35(3): 399-408.

Burgos - Díaz, C., Rubilar, M., Morales, E., Medina, C., Acevedo, F., Marqués, A. M. & Shene, C. 2016. Naturally occurring protein–polysaccharide complexes from linseed (linum usitatissimum) as bioemulsifiers. *European Journal of Lipid Science and Technology*, 118, 165-174.

Bush, L., Stevenson, L. & Lane, K. E. 2019. The oxidative stability of omega-3 oil-in-water nanoemulsion systems suitable for functional food enrichment: A systematic review of the literature. *Critical Reviews in Food Science and Nutrition*, 59, 1154-1168.

Bustillo, M.E., Fischer, A.L., LaBouyer, M.A., Klaips, J.A., Webb, A.C. & Elmore, D.E. 2014. Modular analysis of hipposin, a histone-derived antimicrobial peptide consisting of membrane translocating and membrane permeabilizing fragments. *Biochimica et Biophysica Acta (BBA)-Biomembranes*, 1838(9):.2228-2233.

Cabillon, N. A. R. & Lazado, C. C. 2019. Mucosal barrier functions of fish under changing environmental conditions. *Fishes,* 4, 2.

Cagel, M., Tesan, F. C., Bernabeu, E., Salgueiro, M. J., Zubillaga, M. B., Moretton, M. A. & Chiappetta, D. A. 2017. Polymeric mixed micelles as nanomedicines: Achievements and perspectives. *European Journal of Pharmaceutics and Biopharmaceutics*, 113, 211-228.

Cammarata, M., Salerno, G., Parisi, M.G., Benenati, G., Vizzini, A., Vasta, G.R. & Parrinello, N. 2012. Primary structure and opsonic activity of an F-lectin from serum of the gilt head bream Sparus aurata (Pisces, Sparidae). *Italian Journal of Zoology,* 79(1): 34-43.Vasta

Capaldi, S., Faggion, B., Carrizo, M.E., Destefanis, L., Gonzalez, M.C., Perduca, M., Bovi, M., Galliano, M. & Monaco, H.L. 2015. Three-dimensional structure and ligand-binding site of

carp fishelectin (FEL). *Acta Crystallographica Section D: Biological Crystallography*, *71*(5); 1123-1135.

Capitani, M. I., Corzo-Rios, L., Chel-Guerrero, L., Betancur-Ancona, D., Nolasco, S. M. & Tomás, M. C. 2015. Rheological properties of aqueous dispersions of chia (salvia hispanica l.) mucilage*. Journal of Food Engineering*, 149, 70-77.

Cazón, P., Velazquez, G., Ramírez, J.A. & Vázquez, M. 2017. Polysaccharide-based films and coatings for food packaging: A review. *Food Hydrocolloids*, *68*, 136-148.

Chan, C.Y., Tran, N., Pethiyagoda, S., Crissman, C.C., Sulser, T.B. & Phillips, M.J. 2019. Prospects and challenges of fish for food security in Africa.*Global Food Scurity*, *20*, 17-25.

Chaudhary, G., Fudge, D.S., Macias-Rodriguez, B. and Ewoldt, R.H. 2018. Concentration-independent mechanics and structure of hagfish slime. *Acta biomaterialia*, *79*, 123-134.

Chen, H., Mao, L., Hou, Z., Yuan, F. & Gao, Y. 2020. Roles of additional emulsifiers in the structures of emulsion gels and stability of vitamin e. *Food Hydrocolloids*, 99, 105372.

Chen, T., Sun, A., Chu, C., Wu, H., Wang, J., Wang, J., Li, Z., Guo, J. & Xu, G. 2019. Rheological behavior of titania ink and mechanical properties of titania ceramic structures by 3d direct ink writing using high solid loading titania ceramic ink. *Journal of Alloys and Compounds*, 783, 321-328.

Cheong, A. M., Tan, K. W., Tan, C. P. & Nyam, K. L. 2016. Kenaf (hibiscus cannabinus l.) seed oil-in-water pickering nanoemulsions stabilised by mixture of sodium caseinate, tween 20 and β-cyclodextrin. *Food Hydrocolloids*, 52, 934-941.

Chetana, R., Bhavana, K.P., Babylatha, R., Geetha, V. & Kumar, G.S. 2019. Studies on eggless mayonnaise from rice bran and sesame oils. *Journal of Food Science and Technology,* 56(6): 3117-3125.

Chi, L., Lu, S. & Yao, Y. 2019. Damping additives used in cement-matrix composites: A review. *Composites Part B: Engineering*, *164*, 26-36.

Chivero, P., Gohtani, S., Yoshii, H. & Nakamura, A. 2016. Assessment of soy soluble polysaccharide, gum arabic and OSA-Starch as emulsifiers for mayonnaise-like emulsions. *LWT-Food Science and Technology*, *69*, 59-66.

Choi, S. J. & McClements, D. J. 2020. Nanoemulsions as delivery systems for lipophilic nutraceuticals: Strategies for improving their formulation, stability, functionality and bioavailability. *Food Science and Biotechnology*, 29, 149-168.

Choo, K., Ching, Y.C., Chuah, C.H., Julai, S. & Liou, N.S. 2016. Preparation and characterisation of polyvinyl alcohol-chitosan composite films reinforced with cellulose nanofiber. *Materials*, *9*(8): 644.

Chrom, C.L., Renn, L.M. & Caputo, G.A. 2019. Characterisation and antimicrobial activity of amphiphilic peptide ap3 and derivative sequences. Antibiotics, 8(1): 20.

Chung, C. & McClements, D. J. 2014. Structure–function relationships in food emulsions: Improving food quality and sensory perception. *Food Structure*, 1, 106-126.

Chung, C., Sher, A., Rousset, P., Decker, E.A. & McClements, D.J. 2017. Formulation of food emulsions using natural emulsifiers: Utilization of quillaja saponin and soy lecithin to fabricate liquid coffee whiteners. *Journal of Food Engineering*, *209*, 1-11.

Chylińska, M., Szymańska-Chargot, M. & Zdunek, A. 2016. FT-IR and FT-Raman characterization of non-cellulosic polysaccharides fractions isolated from plant cell wall. *Carbohydrate polymers*, *154*, 48-54.

Cipolari, O.C., de Oliveira Neto, X.A. & Conceição, K. 2020. Fish bioactive peptides: A systematic review focused on sting and skin. *Aquaculture*, 515, 734598.

Coelho, L.C.B.B., Silva, P.M.D.S., Lima, V.L.D.M., Pontual, E.V., Paiva, P.M.G., Napoleao, T.H. & Correia, M.T.D.S. 2017. Lectins, interconnecting proteins with biotechnological/pharmacological and therapeutic applications. *Evidence-Based Complementary and Alternative Medicine.*

Comtet, J., Chatté, G., Niguès, A., Bocquet, L., Siria, A. & Colin, A. 2017. Pairwise frictional profile between particles determines discontinuous shear thickening transition in non-colloidal suspensions. *Nature Communications*, 8, 1-7.

Conceição, P., Levine, S., Lipton, M. & Warren-Rodríguez, A. 2016. Toward a food secure future: Ensuring food security for sustainable human development in sub-saharan Africa. *Food Policy,* 60, 1-9.

Cordero, H., Cuesta, A., Meseguer, J. & Esteban, M.Á. 2016. Changes in the levels of humoral immune activities after storage of gilthead seabream (Sparus aurata) skin mucus. *Fish & Shellfish Immunology*, 58, 500-507.

Corfield, A.P. 2018. The interaction of the gut microbiota with the mucus barrier in health and disease in human. *Microorganisms*, 6(3): 78.

Costa, A. L. R., Gomes, A., De Andrade, C. C. P. & Cunha, R. L. 2017. Emulsifier functionality and process engineering: Progress and challenges. *Food Hydrocolloids*, 68, 69-80.

Costa, F.L., Lima, M.E.D., Pimenta, A.C., Figueiredo, S.G., Kalapothakis, E. & Salas, C.E. 2014. Expressed sequence tags in venomous tissue of Scorpaena plumieri (Scorpaeniformes: Scorpaenidae). *Neotropical Ichthyology*, 12(4): 871-878.

Dapčević Hadnađev, T., Dokić, P., Krstonošić, V. & Hadnađev, M. 2013. Influence of oil phase concentration on droplet size distribution and stability of oil-in-water emulsions. European *Journal of Lipid Science and Technology*, 115, 313-321.

Dash, S., Das, S.K., Samal, J. & Thatoi, H.N. 2018. Epidermal mucus, a major determinant in fish health: a review. *Iranian Journal of Veterinary Research*, 19(2): 72.

Delgado, M. A., Secouard, S., Valencia, C. & Franco, J. M. 2019. On the steady-state flow and yielding behaviour of lubricating greases. *Fluids*, 4, 6.

Derrien, M., Badr, A., Gosselin, A., Desjardins, Y. & Angers, P. 2017. Optimization of a green process for the extraction of lutein and chlorophyll from spinach by-products using response surface methodology (rsm). *LWT-Food Science and Technology*, 79, 170-177.

Dertli, E., Toker, O. S., Durak, M. Z., Yilmaz, M. T., Tatlısu, N. B., Sagdic, O. & Cankurt, H. 2016. Development of a fermented ice-cream as influenced by in situ exopolysaccharide production: Rheological, molecular, microstructural and sensory characterisation. *Carbohydrate Polymers*, 136, 427-440.

Dickinson, E. 2012. Emulsion gels: The structuring of soft solids with protein-stabilised oil droplets. *Food Hydrocolloids*, 28, 224-241.

Dickinson, E. 2017. Biopolymer-based particles as stabilising agents for emulsions and foams. *Food Hydrocolloids*, 68, 219-231.

Dickinson, E. 2018. On the road to understanding and control of creaminess perception in food colloids. *Food Hydrocolloids*, 77, 372-385.

Diedericks, C.F. & Jideani, V.A. 2015. Physicochemical and functional properties of insoluble dietary fiber isolated from bambara groundnut (Vigna subterranea [L.] Verdc.). *Journal of Food Science,* 80(9): C1933-C1944.

Djuris, J., Vasiljevic, D., Jokic, S. & Ibric, S. 2014. Application of D-optimal experimental design method to optimize the formulation of O/W cosmetic emulsions. *International Journal of Cosmetic Science*, 36(1): 79-87.

Dokić, L., Krstonošić, V. & Nikolić, I. 2012. Physicochemical characteristics and stability of oil-in-water emulsions stabilised by OSA starch. *Food Hydrocolloids*, 29, 185-192.

Douglas, J.F. 2018. Weak and strong gels and the emergence of the amorphous solid state. *Gels*, *4*(1); 19.

Drapala, K. P., Mulvihill, D. M. & O'mahony, J. A. 2018. A review of the analytical approaches used for studying the structure, interactions and stability of emulsions in nutritional beverage systems. *Food Structure*, 16, 27-42.

Ducloué, L., Pitois, O., Tocquer, L., Goyon, J. & Ovarlez, G. 2017. Yielding and flow of foamed metakaolin pastes a physicochemical and engineering aspects. *Colloids and Surfaces*. 513, 87-94

Dunbar, G., Higa, J., Jones, T., Kaminski, B. & Panicker, S. 2012. Guidelines for ethical conduct in the care and use of nonhuman animals in research. *American Psychological Association Committee on Animal Rights Research and Ethics 2010-2011*, 1-9.

Edwards, S.E., Flynn, S., Hobson, J.J., Chambon, P., Cauldbeck, H. and Rannard, S.P., 2020. Mucus-responsive functionalized emulsions: design, synthesis and study of novel branched polymers as functional emulsifiers. *RSC Advances*, *10*(51), pp.30463-30475.

Ekman, D.R., Skelton, D.M., Davis, J.M., Villeneuve, D.L., Cavallin, J.E., Schroeder, A., Jensen, K.M., Ankley, G.T. & Collette, T.W. 2015. Metabolite profiling of fish skin mucus: a novel approach for minimally-invasive environmental exposure monitoring and surveillance. *Environmental Science & Technology*, 49(5): 3091-3100.

Elavarasi, K., Ranjini, S., Rajagopal, T., Rameshkumar, G. & Ponmanickam, P. 2013. Bactericidal proteins of skin mucus and skin extracts from fresh water fishes, Clarias batrachus and Tilapia mossambicus. *Thai Journal of Pharmaceutical*. *Science,* 37, 194-200.

Ellis, J.E., Rowe, S. & Lotze, H.K. 2015. Expansion of hagfish fisheries in Atlantic Canada and worldwide. *Fisheries Research*, *161*, 24-33.

Esposito, C.L., Kirilov, P. & Roullin, V.G. 2018. Organogels, promising drug delivery systems: an update of state-of-the-art and recent applications. *Journal of Controlled Release*, 271, 1-20.

Esteban, M.Á. & Cerezuela, R. 2015. Fish mucosal immunity: skin. In *Mucosal health in aquaculture,* 67-92. Academic Press, Cambridge MA.

Ewoldt, R. H., Winegard, T. M. & Fudge, D. S. 2011. Non-linear viscoelasticity of hagfish slime. *International Journal of Non-Linear Mechanics*, 46, 627-636.

Faber, T., Van Breemen, L. & Mckinley, G. 2017. From firm to fluid–structure-texture relations of filled gels probed under large amplitude oscillatory shear. *Journal of Food Engineering*, 210, 1-18.

Falanga, A., Lombardi, L., Franci, G., Vitiello, M., Iovene, M.R., Morelli, G., Galdiero, M. & Galdiero, S. 2016. Marine antimicrobial peptides: nature provides templates for the design of novel compounds against pathogenic bacteria. International *Journal of Molecular Sciences*, 17(5): 785.

Falfushynska, H., Gnatyshyna, L., Yurchak, I., Sokolova, I. & Stoliar, O. 2015. The effects of zinc nanooxide on cellular stress responses of the freshwater mussels Unio tumidus are modulated by elevated temperature and organic pollutants. *Aquatic Toxicology*, *162*, 82-93.

Fasinu, E. G., Ikhu-Omoregbe, D. I. & Jideani, V. A. 2015. Influence of selected physicochemical factors on the stability of emulsions stabilised by bambara groundnut flour and starch. *Journa*l *of Food Science and Technology*, 52, 7048-7058.

Fecarotti, C., Celauro, C. Pirrotta, A. 2012. Linear Viscoelastic (LVE) behaviour of pure bitumen via fractional model. *Procedia-Social and Behavioral Sciences*, *53*, 450-461.

Felix, M., Romero, A. & Guerrero, A. 2017. Viscoelastic properties, microstructure and stability of high-oleic o/w emulsions stabilised by crayfish protein concentrate and xanthan gum*. Food Hydrocolloids*, 64, 9-17.

Felix, M., Romero, A., Sanchez, C. C. & Guerrero, A. 2019. Modelling the non-linear interfacial shear rheology behaviour of chickpea protein-adsorbed complex oil/water layers. *Applied* Surface *Science*, 469, 792-803.

Fernández-Alacid, L., Sanahuja, I., Ordóñez-Grande, B., Sánchez-Nuño, S., Herrera, M. & Ibarz, A. 2019. Skin mucus metabolites and cortisol in meagre fed acute stress-attenuating diets: correlations between plasma and mucus. *Aquaculture*, *499*, 185-194.

Fernando, I.P., Sanjeewa, K.K., Samarakoon, K.W., Lee, W.W., Kim, H.S., Kim, E.A., Gunasekara, U.K.D.S.S., Abeytunga, D.T.U., Nanayakkara, C., De Silva, E.D. & Lee, H.S. 2017. FTIR characterisation and antioxidant activity of water soluble crude polysaccharides of Sri Lankan marine algae. *Algae*, 32(1): 75-86.

Ferreira, C.D. and Nunes, I.L. 2019. Oil nanoencapsulation: development, application, & incorporation into the food market. *Nanoscale Research Letters*, 14(1): 9.

Firdaus-Nawi, M. & Zamri-Saad, M. 2016. Major Components of Fish Immunity: A Review. *Pertanika Journal of Tropical Agricultural Science*, 39(4).

Fischer, P. & Windhab, E. J. 2011. Rheology of food materials. *Current Opinion in Colloid & Interface Scienc*e, 16, 36-40.

Focsan, A. L., Polyakov, N. E. & Kispert, L. D. 2019. Supramolecular carotenoid complexes of enhanced solubility and stability—the way of bioavailability improvement. *Molecules*, 24, 3947.

Folayan, J. A., Anawe, P. a. L., Abioye, P. O. & Elehinafe, F. B. 2017. Selecting the most appropriate model for rheological characterisation of synthetic based drilling mud. *Internationa*l Journal *of Applied Engineering Research*, 12, 7614-7649.

Foudazi, R., Qavi, S., Masalova, I. & Malkin, A. Y. 2015. Physical chemistry of highly concentrated emulsions. *Advances in Colloid and* I*nterface Science*, 220, 78-91.

Fudge, D. S. & Schorno, S. 2016. The hagfish gland thread cell: A fiber-producing cell involved in predator defense. *Cells,* 5, 25.

Fujisawa, S., Togawa, E. & Kuroda, K. 2017. Nanocellulose-stabilized Pickering emulsions and their applications. *Science and Technology of advanced Materials*, *18*(1); 959-971.

Galloway, A.F., Knox, P. and Krause, K., 2020. Sticky mucilages and exudates of plants: putative microenvironmental design elements with biotechnological value. *New Phytologist*, *225*(4), pp.1461-1469.

Gavahian, M., Chen, Y.-M., Khaneghah, A. M., Barba, F. J. & Yang, B. B. 2018. In-pack sonication technique for edible emulsions: Understanding the impact of acacia gum and lecithin emulsifiers and ultrasound homogenisation on salad dressing emulsions stability. *Food Hydrocolloids*, 83, 79-87.

George, A., Shah, P.A. & Shrivastav, P.S. 2019. Natural biodegradable polymers based nano-formulations for drug delivery: A review. *International Journal of Pharmaceutics*, *561*, 244-264.

Geremias-Andrade, I. M., Souki, N. P., Moraes, I. C. & Pinho, S. C. 2016. Rheology of emulsion-filled gels applied to the development of food materials. *Gels*, 2, 22.

Gharehbeglou, P., Jafari, S. M., Hamishekar, H., Homayouni, A. & Mirzaei, H. 2019. Pectin-whey protein complexes vs. Small molecule surfactants for stabilization of double nano-emulsions as novel bioactive delivery systems. *Journal of Food Engineering*, 245, 139-148.

Gharibzahedi, S. M. T., Hernández-Ortega, C., Welti-Chanes, J., Putnik, P., Barba, F. J., Mallikarjunan, K., Escobedo-Avellaneda, Z. & Roohinejad, S. 2019. High pressure processing of food-grade emulsion systems: Antimicrobial activity, and effect on the physicochemical properties. *Food Hydrocolloids*, 87, 307-320.

Glassford, S. E., Byrne, B. & Kazarian, S. G. 2013. Recent applications of atr ftir spectroscopy and imaging to proteins. *Biochimica* et *Biophysica Act*a *(BBA*)-*Proteins and Proteomics*, 1834, 2849-2858.

Glicerina, V., Balestra, F., Dalla Rosa, M. & Romani, S. 2016. Microstructural and rheological characteristics of dark, milk and white chocolate: A comparative study. *Journal of Food Engineering*, *169*, 165-171.

Gobinath, R.A.C. & Ravichandran, S. 2011. Antimicrobial peptide from the epidermal mucus of some estuarine cat fishes. *World Applied Science Journal*, 12, 256-260.

Gonçalves, B., Pereira, C., Lago, A., Gonçalves, C., Giarola, T., Abreu, L. & Resende, J. 2017. Thermal conductivity as influenced by the temperature and apparent viscosity of dairy products. *Journal of Dairy Scienc*e, 100, 3513-3525.

Gonzalez Moreno, M., Lombardi, L. & Di Luca, M. 2017. Antimicrobial peptides for the control of biofilm formation. *Current Topics in Medicinal Chemistry*, 17(17): 1965-1986.

Gordiychuk, A., Svanera, M., Benini, S. & Poesio, P. 2016. Size distribution and Sauter mean diameter of micro bubbles for a Venturi type bubble generator. *Experimental Thermal and Fluid Science*, *70*, 51-60.

Guardiola, F.A., Cuartero, M., del Mar Collado-González, M., Baños, F.G.D., Cuesta, A., Moriñigo, M.Á. & Esteban, M.Á. 2017. Terminal carbohydrates abundance, immune related enzymes, bactericidal activity and physico-chemical parameters of the Senegalese sole (Solea senegalensis, Kaup) skin mucus. *Fi*sh *& Shellfish immunology*, 60, 483-491.

Guardiola, F.A., Cuesta, A. & Esteban, M.Á. 2016. Using skin mucus to evaluate stress in gilthead seabream (*Sparus aurata L*.). *Fish & shellfish immunology*, *59*, 323-330.

Guimarães, J. T., Balthazar, C. F., Scudino, H., Pimentel, T. C., Esmerino, E. A., Ashokkumar, M., Freitas, M. Q. & Cruz, A. G. 2019. High-intensity ultrasound: A novel technology for the development of probiotic and prebiotic dairy products. *Ultrasonics Sonochemistry*.

Guo, M. & Wang, G. 2016. Milk protein polymer and its application in environmentally safe adhesives. *Polymers*, *8*(9); 324.

Guo, X., Shang, X., Zhou, X., Zhao, B. & Zhang, J. 2017. Ultrasound-assisted extraction of polysaccharides from Rhododendron aganniphum: Antioxidant activity and rheological properties. *Ultrasonics Sonochemistry*, *38*, .246-255.

Gupta, A., Eral, H. B., Hatton, T. A. & Doyle, P. S. 2016. Nanoemulsions: Formation, properties and applications. *Soft Matter*, 12, 2826-2841.

Gürgen, S., Kuşhan, M. C. & Li, W. 2017. Shear thickening fluids in protective applications: A review. *Progress in Polymer Science,* 75, 48-72.

Gustafsson, H. & Holmberg, K. 2017. Emulsion-based synthesis of porous silica. *Advances in Colloid and Interface Science*, 247, 426-434.

Guzmán, R., Ancheyta, J., Trejo, F. & Rodríguez, S. 2017. Methods for determining asphaltene stability in crude oils. *Fuel,* 188, 530-543.

Habib, B.A. & AbouGhaly, M.H. 2016. Combined mixture-process variable approach: a suitable statistical tool for nanovesicular systems optimization. *Expert Opinion on Drug Delivery*, 13(6): 777-788.

Habib, B.A., Sayed, S. and Elsayed, G.M. 2018. Enhanced transdermal delivery of ondansetron using nanovesicular systems: Fabrication, characterisation, optimization and ex-vivo permeation study-Box-Cox transformation practical example. *European Journal of Pharmaceutical Sciences*, 115, 352-361

Hahn, C., Nöbel, S., Maisch, R., Rösingh, W., Weiss, J. & Hinrichs, J. 2015. Adjusting rheological properties of concentrated microgel suspensions by particle size distribution. Food *Hydrocolloids*, 49, 183-191.

Håkansson, A. 2019. Emulsion formation by homogenisation: Current understanding and future perspectives. *Annual Review of Food Science and Technology*, 10, 239-258.

Hamza, S. 2016. Modelling the effect of concentration on non-newtonian apparent viscosity of an aqueous polyacrylamide solution. *Global Journal of Physics*, 5.

Hentati, F., Pierre, G., Ursu, A.V., Vial, C., Delattre, C., Abdelkafi, S. & Michaud, P. 2020. Rheological investigations of water-soluble polysaccharides from the Tunisian brown seaweed Cystoseira compressa. *Food Hydrocolloids*, *103*, 105631.

Herr, J.E., Clifford, A.M., Goss, G.G. & Fudge, D.S. 2014. Defensive slime formation in Pacific hagfish requires Ca2+-and aquaporin-mediated swelling of released mucin vesicles. *Journal of Experimental Biology*, *217*(13): 2288-2296.

Herr, J.E., Winegard, T.M., O'Donnell, M.J., Yancey, P.H. & Fudge, D.S. 2010. Stabilization and swelling of hagfish slime mucin vesicles. *Journal of Experimental Biology*, 213(7): 1092-1099.

Hesarinejad, M. A., Koocheki, A. & Razavi, S. M. A. 2014. Dynamic rheological properties of lepidium perfoliatum seed gum: Effect of concentration, temperature and heating/cooling rate. *Food Hydrocolloids*, 35, 583-589.

Hess, M., Gratz, M., Remmer, H., Webers, S., Landers, J., Borin, D., Ludwig, F., Wende, H., Odenbach, S., Tschoepe, A., & Schmidt, A.M. 2020. Scale-dependent particle diffusivity and apparent viscosity in polymer solutions as probed by dynamic magnetic nanorheology.*Soft Matte*.

Hosono, M., Sugawara, S., Tatsuta, T., Hikita, T., Kominami, J., Nakamura-Tsuruta, S., Hirabayashi, J., Kawsar, S.M., Ozeki, Y., Hakomori, S.I. & Nitta, K. 2013. Domain composition of rhamnose-binding lectin from shishamo smelt eggs and its carbohydrate-binding profiles. *Fish Physiology and Biochemistry*, 39(6): 1619-1630.

Hu, Y.-T., Ting, Y., Hu, J.-Y. & Hsieh, S.-C. 2017. Techniques and methods to study functional characteristics of emulsion systems. *Journal of Food and Drug Analysi*s, 25, 16-26.

Hu, Z., Ballinger, S., Pelton, R. & Cranston, E. D. 2015. Surfactant-enhanced cellulose nanocrystal pickering emulsions. *Journal of Colloid and Interface Science*, 439, 139-148.

Hung, A., Mager, M., Hembury, M., Stellacci, F., Stevens, M. M. & Yarovsky, I. 2013. Amphiphilic amino acids: A key to adsorbing proteins to nanopatterned surfaces? *Chemical Scienc*e, 4, 928-937.

Hussein, Y. H. & Youssry, M. 2018. Polymeric micelles of biodegradable diblock copolymers: Enhanced encapsulation of hydrophobic drugs. *Material*s, 11, 688.

Hygreeva, D. & Pandey, M. 2016. Novel approaches in improving the quality and safety aspects of processed meat products through high pressure processing technology-a review. *Trends in Food Science & Technology*, 54, 175-185.

Ionescu, C.M., Birs, I.R., Copot, D., Muresan, C.I. & Caponetto, R. 2020. Mathematical modelling with experimental validation of viscoelastic properties in non-Newtonian fluids. *Philosophical Transactions of the Royal Society A*, *378*(2172); 20190284.

Irani, M., Razavi, S. M., Abdel-Aal, E.-S. M., Hucl, P. & Patterson, C. A. 2019. Viscoelastic and textural properties of canary seed starch gels in comparison with wheat starch gel. . *International Journal of Biological Macromolecules*, 124, 270-281.

Ivanova, R. & Kotsilkova, R. 2018. Rheological study of poly (lactic) acid nanocomposites with carbon nanotubes and graphene additives as a tool for materials characterisation for 3d printing application. *Applied* Rheology, 28.

Jamshidi, A., Hasan, M. R. M., Yao, H., You, Z. & Hamzah, M. O. 2015. Characterisation of the rate of change of rheological properties of nano-modified asphalt. Construction and Building Materials, 98, 437-446.

Javidi, F., Razavi, S. M. & Amini, A. M. 2019. Cornstarch nanocrystals as a potential fat replacer in reduced fat o/w emulsions: A rheological and physical study. *Food Hydrocolloid*s, 90, 172-181.

Jeewanthi, R.K.C. & Paik, H.D. 2018. Modifications of nutritional, structural, and sensory characteristics of non-dairy soy cheese analogs to improve their quality attributes. *Journal of food science and technology*, *55*(11); 4384-4394.

Jeirani, Z., Jan, B.M., Ali, B.S., Noor, I.M., Hwa, S.C. & Saphanuchart, W. 2012. The optimal mixture design of experiments: Alternative method in optimizing the aqueous phase composition of a microemulsion. *Chemometrics and Intelligent Laboratory Systems*, *112*, 1-7.

Jia, W., Ma, L., Le, Q., Zhi, C. & Liu, P. 2019. Deformation and fracture behaviors of AZ31B Mg alloy at elevated temperature under uniaxial compression. *Journal of Alloys and Compounds*,*783*, 863-876.

Jiang, Y.H., Mao, Y., Lv, Y.N., Tang, L.L., Zhou, Y., Zhong, H., Xiao, J. & Yan, J.P. 2018. Natural Resistance Associated Macrophage Protein Is Involved in Immune Response of Blunt Snout Bream, *Megalobrama amblycephala. Cells*, 7(4): p.27.

Jiao, D., Shi, C. & Yuan, Q. 2019. Time-dependent rheological behavior of cementitious paste under continuous shear mixing. *Construction and Building Materials*, 226, 591-600.

Jin, J., Ooi, C. H., Dao, D. V. & Nguyen, N.-T. 2017. Coalescence processes of droplets and liquid marbles. *Micromachines*, 8, 336.

Joshi, Y. M. & Petekidis, G. 2018. Yield stress fluids and ageing. *Rheologica Acta*, 57, 521-549.

Junqueira, L. A., Da Silva, V. M., Amaral, T. N., Prado, M. E. T. & De Resende, J. V. 2019. Effects of temperature and concentration on the rheological properties of mucilage extracted from pereskia aculeata miller. *Journal of Food Measurement and Characterisation*, 13, 2549-2562.

Kale, S. N. & Deore, S. L. 2017. Emulsion micro emulsion and nano emulsion: A review. *Systematic Reviews in Pharmacy*, 8, 39.

Karthik, P., Ezhilarasi, P. & Anandharamakrishnan, C. 2017. Challenges associated in stability of food grade nanoemulsions. *Critical Reviews in Foo*d *Science and Nutrition*, 57, 1435-1450.

Kasiri, N. & Fathi, M. 2018. Production of cellulose nanocrystals from pistachio shells and their application for stabilising pickering emulsions. *International Journal of Biological Macromolecules,* 106, 1023-1031.

Kazazi, H., Khodaiyan, F., Rezaei, K., Pishvaei, M., Mohammadifar, M. A. & Moieni, S. 2017. Rheology and microstructure of kefiran and whey protein mixed gels. *Journal of Food Science and Technology*, 54, 1168-1174.

Kelimu, A., Da Silva, D. F., Geng, X., Ipsen, R. & Hougaard, A. B. 2017. Effects of different dairy ingredients on the rheological behaviour and stability of hot cheese emulsions. *International Dairy Journal,* 71, 35-42.

Khalil, M. & Mohamed Jan, B. 2012. Herschel-bulkley rheological parameters of a novel environmentally friendly lightweight biopolymer drilling fluid from xanthan gum and starch. *Journal of Applied Polymer Science*, 124, 595-606.

Khayat, K.H., Meng, W., Vallurupalli, K. & Teng, L. 2019. Rheological properties of ultra-high-performance concrete—An overview. *Cement and Concrete Research*, *124*, 105828.

Kim, H., Beak, S.E. & Song, K.B. 2018. Development of a hagfish skin gelatin film containing cinnamon bark essential oil. *LWT*, *96*, 583-588.

Kim, H. S. & Mason, T. G. 2017. Advances and challenges in the rheology of concentrated emulsions and nanoemulsions. *Advances in Colloid and Interface Science*, 247, 397-412.

Kolawole, J.T., Combrinck, R. & Boshoff, W.P. 2020. Rheo-viscoelastic behaviour of fresh cement-based materials: Cement paste, mortar and concrete. *Construction and Building Materials*, *248*, 118667.

Koller, M. 2018. Biodegradable and biocompatible polyhydroxy-alkanoates (pha): Auspicious microbial macromolecules for pharmaceutical and therapeutic applications. *Molecules*, 23, 362.

Komaiko, J.S. & McClements, D.J. 2016. Formation of food-grade nanoemulsions using low-energy preparation methods: A review of available methods. *Comprehensive Reviews in Food Science and Food Safety*, *15*(2): 331-352.

Konar, N., Ozarda, O., Senocak, S., Unluturk, N. N. & Oba, S. 2019. Effects of process conditions on citrus beverage emulsions' creaming index: Rsm approach. International Journal of Food Engineering, 5.

Konkena, B. & Vasudevan, S. 2012. Understanding aqueous dispersibility of graphene oxide and reduced graphene oxide through p k a measurements. *The Journal of Physical Chemistry Letters*, 3, 867-872.

Konuskan, D. B., Arslan, M. & Oksuz, A. 2019. Physicochemical properties of cold pressed sunflower, peanut, rapeseed, mustard and olive oils grown in the eastern mediterranean region. *Saudi Journal of Biological Sciences*, 26, 340-344.

Kordon, A.O., Karsi, A. & Pinchuk, L. 2018. Innate immune responses in fish: antigen presenting cells and professional phagocytes. *Turkish Journal of Fisheries and Aquatic Sciences*, *18*(9); 1123-1139.

Kouhi, M., Prabhakaran, M.P. and Ramakrishna, S., 2020. Edible polymers: An insight into its application in food, biomedicine and cosmetics. *Trends in Food Science & Technology*.

Krasulya, O., Bogush, V., Trishina, V., Potoroko, I., Khmelev, S., Sivashanmugam, P. & Anandan, S. 2016. Impact of acoustic cavitation on food emulsions. *Ultrasonics Sonochemistry*, 30, 98-102.

Kubo, M.T., Rojas, M.L., Miano, A.C. and Augusto, P.E. 2019. Rheological Properties of Tomato Products, in *Tomato Chemistry, Industrial Processing and Product Development*, 2019, 1-25 Royal Society of Chemistry, Piccadilly, London.

Kumar, N. & Mandal, A. 2018. Surfactant stabilized oil-in-water nanoemulsion: stability, interfacial tension, and rheology study for enhanced oil recovery application. *Energy & Fuels*, *32*(6), 6452-6466.

Kuster, S., Böni, L.J., Fischer, P., Rühs, P.A. & Windhab, E.J. 2017, December. About hagfish, effective hydrogels and protein fiber enriched Tofu–an overview from our published work. In *General Information about Hagfish for Nestlé PTC Singen,* Germany.

Kwok, M.H., Sun, G. & Ngai, T. 2019. Microgel particles at interfaces: phenomena, principles, and opportunities in food sciences. *Langmuir*, *35*(12); 4205-4217.

Lamriben, L., Graham, J. B., Adams, B. M. & Hebert, D. N. 2016. N-glycan-based er molecular chaperone and protein quality control system: The calnexin binding cycle. *Traffic*, 17, 308-326.

Langevin, D. 2019. Coalescence in foams and emulsions: Similarities and differences. *Current Opinion in Colloid & Interface Science*.

Laredj-Bourezg, F., Bolzinger, M.-A., Pelletier, J. & Chevalier, Y. 2017. Pickering emulsions stabilised by biodegradable block copolymer micelles for controlled topical drug delivery. *International Journal* of *Pharmaceutics*, 531, 134-142.

Läuger, J. & Stettin, H. 2016. Effects of instrument and fluid inertia in oscillatory shear in rotational rheometers. *Journal of Rheology*, 60, 393-406.

Lee, M.K. & Nam, J. 2019. The determinants of live fish consumption frequency in South Korea. *Food Research International*, *120*, 382-388.

Legrand, T.P., Wynne, J.W., Weyrich, L.S. & Oxley, A.P. 2020. A microbial sea of possibilities: current knowledge and prospects for an improved understanding of the fish microbiome. *Reviews in Aquaculture*, 12(2):.1101-1134.

Leong, T. S., Martin, G. J. & Ashokkumar, M. 2017a. Ultrasonic encapsulation–a review. *Ultrasonics Sonochemistry*, 35, 605-614.

Leong, T. S. H., Zhou, M., Kukan, N., Ashokkumar, M. & Martin, G. J. O. 2017b. Preparation of water-in-oil-in-water emulsions by low frequency ultrasound using skim milk and sunflower oil. *Food Hydrocolloids*, 63, 685-695.

Lewis, A., Jones, K., Lewis, K., Jones, S. & Lewis, P. 2013. Detection of lewis antigen structural change by ftir spectroscopy. *Carbohydrate Polymers*, 92, 1294-1301.

Li, Z., Wu, H., Yang, M., Xu, D., Chen, J., Feng, H., Lu, Y., Zhang, L., Yu, Y. & Kang, W. 2018. Stability mechanism of o/w pickering emulsions stabilised with regenerated cellulose. *Carbohydrate Polymers*, 181, 224-233.

Liang, X., Wu, J., Yang, X., Tu, Z. & Wang, Y. 2018. Investigation of oil-in-water emulsion stability with relevant interfacial characteristics simulated by dissipative particle dynamics. *Colloids and Surfaces A*: *Physicochemical and Engineering Aspects*, 546, 107-114.

Lidon, P., Villa, L. & Manneville, S. 2017. Power-law creep and residual stresses in a carbopol gel. *Rheologica Acta*, 56, 307-323.

Liu, C., Ta, D., Fujita, F., Hachiken, T., Matsukawa, M., Mizuno, K. & Wang, W. 2014. The relationship between ultrasonic backscatter and trabecular anisotropic microstructure in cancellous bone. *Journal of Applied Physics*, 115, 064906.

Liu, J., Huang, X.-F., Lu, L.-J., Li, M.-X., Xu, J.-C. & Deng, H.-P. 2011. Turbiscan lab® expert analysis of the biological demulsification of a water-in-oil emulsion by two biodemulsifiers. *Journal of Hazardous Materials*, 190, 214-221.

Liu, L., Alva, G., Huang, X. & Fang, G. 2016. Preparation, heat transfer and flow properties of microencapsulated phase change materials for thermal energy storage. *Renewable and Sustainable Energy Reviews*, 66, 399-414.

Liu, Z., Bhandari, B., Prakash, S., Mantihal, S. & Zhang, M. 2019. Linking rheology and printability of a multicomponent gel system of carrageenan-xanthan-starch in extrusion based additive manufacturing. *Food hydrocolloids*, *87*, 413-424.

López-Martínez, A. & Rocha-Uribe, A. 2018. Antioxidant hydrophobicity and emulsifier type influences the partitioning of antioxidants in the interface improving oxidative stability in o/w emulsions rich in n-3 fatty acids. *European Journal of Lipid Science and Technology*, 120, 1700277.

Lorenzo, G., Zaritzky, N. & Califano, A. 2018. Food gel emulsions: Structural characteristics and viscoelastic behavior. *Polymers for Food Applications*. Springer.

Lourdes de Pérez-González, M.L., González-de la Rosa, C.H., Pérez-Hernández, G. & Beltrán, H.I. 2020. Nanostructured oleic acid/polysorbate 80 emulsions with diminished toxicity in NL-20 cell line: Insights of potential drug carriers. *Colloids and Surfaces B: Biointerfaces*, 187, 110758.

Lu, W., Kelly, A. L. & Miao, S. 2016. Emulsion-based encapsulation and delivery systems for polyphenols. *Trends in Food Science & Technology*, 47, 1-9.

Luo, S.Z., Hu, X.F., Jia, Y.J., Pan, L.H., Zheng, Z., Zhao, Y.Y., Mu, D.D., Zhong, X.Y. & Jiang, S.T. 2019. Camellia oil-based oleogels structuring with tea polyphenol-palmitate particles and citrus pectin by emulsion-templated method: Preparation, characterisation and potential application. *Food Hydrocolloids*, 95, 76-87.

Madhu, B., Srinivas, M. S., Srinivas, G. & Jain, S. 2019. Ultrasonic technology and its applications in quality control, processing and preservation of food: A review. *Current Journal of Applied Science and Technology*, 1-11.

Mahadevan, G., Mohan, K., Vinoth, J. & Ravi, V. 2019. Biotic potential of mucus extracts of giant mudskipper periophthalmodon schlosseri (pallas, 1770) from pichavaram, southeast coast of india. *The Journal of Basic and Applied Zoology*, 80, 13.

Mahajan, S., Khairnar, A., Bishnoi, R. & Ramya, T.N.C. 2017. Microbial F-type lectin domains with affinity for blood group antigens. *Biochemical and Biophysical Research Communications*, 491(3): 708-713.

Mahdizadeh Barzoki, Z., Emam-Djomeh, Z., Mortazavian, E., Akbar Moosavi-Movahedi, A. & Rafiee Tehrani, M. 2016. Formulation, in vitro evaluation & kinetic analysis of chitosan–gelatin bilayer muco-adhesive buccal patches of insulin nanoparticles. *Journal of Microencapsulation*, 33, 613-624.

Mahmood, K., Kamilah, H., Shang, P.L., Sulaiman, S. & Ariffin, F. 2017. A review: Interaction of starch/non-starch hydrocolloid blending and the recent food applications. *Food Bioscience*, *19*, 110-120.

Majumdar, S., Hazra, S., Choudhury, M.D., Sinha, S.D., Das, S., Middya, T.R., Tarafdar, S. & Dutta, T. 2017. A study of the rheological properties of visco-elastic materials using fractional calculus. *Colloids and Surfaces A: Physicochemical and Engineering Aspects*, *516*, 181-189.

Malkin, A., Kulichikhin, V. & Ilyin, S. 2017. A modern look on yield stress fluids. *Rheologica Acta*, 56, 177-188.

Malkin, A. Y. & Isayev, A. I. 2017. Rheology: Concepts, methods, and applications, Elsevier.

Mandal, A. & Bera, A. 2015. Modeling of flow of oil-in-water emulsions through porous media. *Petroleum Science*, 12, 273-281.

Maphosa, Y., Jideani, V. A. & Adeyi, O. 2017. Effect of soluble dietary fibres from bambara groundnut varieties on the stability of orange oil beverage emulsion. *African Journal of Science*, *Technology*, *Innovation and Development*, 9, 69-76.

Maravić, N., Šereš, Z., Nikolić, I., Dokić, P., Kertész, S. & Dokić, L. 2019. Emulsion stabilising capacity of sugar beet fibers compared to sugar beet pectin and octenyl succinate modified maltodextrin in the production of o/w emulsions: Individual and combined impact. *LWT*, 108, 392-399.

Marín, D., Alemán, A., Montero, P. & Gómez-Guillén, M. 2018. Encapsulation of food waste compounds in soy phosphatidylcholine liposomes: Effect of freeze-drying, storage stability and functional aptitude. *Journal of Food Engineering*, 223, 132-143.

Martinez, G.L., Poursadegh, F., Magnotti, G.M., Matusik, K.E., Duke, D.J., Knox, B.W., Kastengren, A.L., Powell, C.F. & Genzale, C.L. 2019. Measurement of Sauter mean diameter in diesel sprays using a scattering–absorption measurement ratio technique. *International Journal of Engine Research*, *20*(1); 6-17.

McClements, D. J. 2015. Food emulsions: Principles, practices, and techniques, CRC press, Boca Raton, Fl.

McClements, D. J., Bai, L. & Chung, C. 2017. Recent advances in the utilization of natural emulsifiers to form and stabilise emulsions. *Annual Review of Food Science and Technology*, 8, 205-236.

McClements, D. J. & Gumus, C. E. 2016. Natural emulsifiers—biosurfactants, phospholipids, biopolymers, and colloidal particles: Molecular and physicochemical basis of functional performance. *Advances in Colloid and Interface Science*, 234, 3-26.

McClements, D. J. & Jafari, S. M. 2018. Improving emulsion formation, stability and performance using mixed emulsifiers: A review. *Advances in Colloid and Interface Science*, 251, 55-79.

McGee, R., Dean, G.H., Mansfield, S.D. and Haughn, G.W., 2019. Assessing the utility of seed coat-specific promoters to engineer cell wall polysaccharide composition of mucilage. *Plant molecular biology*, *101*(4-5), pp.373-387.

Meerts, M., Cardinaels, R., Oosterlinck, F., Courtin, C. M. & Moldenaers, P. 2017. The interplay between the main flour constituents in the rheological behaviour of wheat flour dough. *Food and Bioprocess Technology*, 10, 249-265.

Melito, H., Daubert, C. & Foegeding, E. 2012. Validation of a large amplitude oscillatory shear protocol. *Journal of Food Engineering*, 113, 124-135.

Mendes, R., Vinay, G., Ovarlez, G. & Coussot, P. 2015. Modeling the rheological behavior of waxy crude oils as a function of flow and temperature history. *Journal of Rheology*, 59, 703-732.

Mendoza, L., Batchelor, W., Tabor, R.F. & Garnier, G. 2018. Gelation mechanism of cellulose nanofibre gels: A colloids and interfacial perspective. *Journal of Colloid and Interface Science*, *509*, 39-46.

Mikulcová, V., Kašpárková, V., Humpolíček, P. & Buňková, L. 2017. Formulation, characterisation and properties of hemp seed oil and its emulsions. *Molecules*, 22, 700.

Minami, S., Suzuki, D. & Urayama, K. 2019. Rheological aspects of colloidal gels in thermoresponsive microgel suspensions: Formation, structure, linear and nonlinear viscoelasticity. *Current Opinion in Colloid & Interface Science*.

Miyagawa, Y., Katsuki, K., Matsuno, R. & Adachi, S. 2015. Effect of oil droplet size on activation energy for coalescence of oil droplets in an o/w emulsion. *Bioscience*, *Biotechnology*, *and Biochemistry*, 79, 1695-1697.

Modarres-Gheisari, S. M. M., Gavagsaz-Ghoachani, R., Malaki, M., Safarpour, P. & Zandi, M. 2019. Ultrasonic nano-emulsification–a review. *Ultrasonics Sonochemistry*, 52, 88-105.

Moghaddam, L., Rencoret, J., Maliger, V. R., Rackemann, D. W., Harrison, M. D., GutiéRrez, A., Del RíO, J. C. & Doherty, W. O. 2017. Structural characteristics of bagasse furfural residue and its lignin component. An nmr, py-gc/ms, and ftir study. *ACS Sustainable Chemistry & Engineering*, 5, 4846-4855.

Mohammadi, M., Saffarian, M. & Mohammadi, M. 2015. Non-newtonian shear-thinning fluid passing through a duct with an obstacle, using a power law model. *Strojniš*ki vestnik-*Journal of Mechanical Engineering*, 61, 594-600.

Mohammadi, M., Taheri, B., Momenzadeh, N., Salarinia, R., Nabipour, I., Farshadzadeh, Z. & Bargahi, A. 2018. Identification and characterisation of novel antimicrobial peptide from hippocampus comes by In Silico and experimental studies. Marine Biotechnology, 20(6): 718-728.

Monaghan, M. G., Holeiter, M., Brauchle, E., Layland, S. L., Lu, Y., Deb, A., Pandit, A., Nsair, A. & Schenke-Layland, K. 2018. Exogenous mir-29b delivery through a hyaluronan-based injectable system yields functional maintenance of the infarcted myocardium. *Tissue Engineering Part A*, 24, 57-67.

Montgomery, D. C. 2017. Design and analysis of experiments, John wiley & sons, Hoboken, NJ.

Morales-Contreras, B. E., Rosas-Flores, W., Contreras-Esquivel, J. C., Wicker, L. & Morales-Castro, J. 2018. Pectin from husk tomato (physalis ixocarpa brot.): Rheological behavior at different extraction conditions. *Carbohydrate Polymers*, 179, 282-289.

Mortazavi-Manesh, S. & Shaw, J. M. 2014. Thixotropic rheological behavior of maya crude oil. *Energy & Fuels*, 28, 972-979.

Motohashi, S., Jimbo, M., Naito, T., Suzuki, T., Sakai, R. & Kamiya, H. 2017. Isolation, amino acid sequences, and plausible functions of the galacturonic acid-binding egg lectin of the sea hare aplysia kurodai. *Marine Drugs*, 15(6): 161.

Moussa, D. T., El-Naas, M. H., Nasser, M. & Al-Marri, M. J. 2017. A comprehensive review of electrocoagulation for water treatment: Potentials and challenges. *Journal of Environmental Management*, 186, 24-41.

Munesue, Y., Masui, T. & Fushima, T. 2015. The effects of reducing food losses and food waste on global food insecurity, natural resources, and greenhouse gas emissions. *Environmental Economics and Policy Studies*, 17, 43-77.

Muschiolik, G. & Dickinson, E. 2017. Double emulsions relevant to food systems: Preparation, stability, and applications. *Comprehensive Reviews in Food Science and Food Safety*, 16, 532-555.

Myers, R. H., Montgomery, D. C. & Anderson-Cook, C. M. 2016. Response surface methodology: Process and product optimization using designed experiments, John Wiley & Sons, Hoboken, NJ.

Nakamoto, M., Takeuchi, Y., Akita, K., Kumagai, R., Suzuki, J., Koyama, T., Noda, T., Yoshida, K., Ozaki, A., Araki, K. and Sakamoto, T. 2017. A novel C-type lectin gene is a strong candidate gene for Benedenia disease resistance in Japanese yellowtail, Seriola quinqueradiata. *Developmental & Comparative Immunology*, 76, 361-369.

Nasr, D. & Pakshir, A. H. 2019. Rheology and storage stability of modified binders with waste polymers composites. *Road Materials and Pavement Design*, 20, 773-792.

Nassar, A.I., Thom, N. & Parry, T. 2016. Optimizing the mix design of cold bitumen emulsion mixtures using response surface methodology. *Construction and Building Materials*, 104, 216-229.

Nejadmansouri, M., Hosseini, S. M. H., Niakosari, M., Yousefi, G. H. & Golmakani, M. T. 2016. Physicochemical properties and oxidative stability of fish oil nanoemulsions as affected by hydrophilic lipophilic balance, surfactant to oil ratio and storage temperature. *Colloids and Surfaces A*: *Physicochemical and Engineering Aspects*, 506, 821-832.

Nieto de Castro, C. A., Vieira, S. I., Lourenço, M. J. & Murshed, S. 2017. Understanding stability, measurements, and mechanisms of thermal conductivity of nanofluids. *Journal of Nanofluids*, 6, 804-811.

Nigam, A.K., Kumari, U., Mittal, S. & Mittal, A.K. 2012. Comparative analysis of innate immune parameters of the skin mucous secretions from certain freshwater teleosts, inhabiting different ecological niches. *Fish Physiology and Biochemistry*, 38(5): 1245-1256.

Niu, F., Niu, D., Zhang, H., Chang, C., Gu, L., Su, Y. & Yang, Y. 2016. Ovalbumin/gum arabic-stabilised emulsion: Rheology, emulsion characteristics, and raman spectroscopic study. *Food Hydrocolloids*, 52, 607-614.

Notani, M.A., Moghadas Nejad, F., Khodaii, A. & Hajikarimi, P. 2019. Evaluating fatigue resistance of toner-modified asphalt binders using the linear amplitude sweep test. *Road Materials and Pavement Design*,*20*(8); 1927-1940.

Obiero, K., Meulenbroek, P., Drexler, S., Dagne, A., Akoll, P., Odong, R., Kaunda-Arara, B. & Waidbacher, H. 2019. The contribution of fish to food and nutrition security in Eastern Africa: Emerging trends and future outlooks.*Sustainability*, *11*(6); 1636.

Ogawa, T., Watanabe, M., Naganuma, T. & Muramoto, K. 2011. Diversified carbohydrate-binding lectins from marine resources. *Journal of Amino Acids*, 2011.

Ogawa, Y., Motoba, T., Buchert, S.C., Häggström, I. & Nozawa, S. 2014. Upper atmosphere cooling over the past 33 years. *Geophysical Research Letters*, 41(15): 5629-5635.

Okuro, P. K., Gomes, A., Costa, A. L. R., Adame, M. A. & Cunha, R. L. 2019. Formation and stability of w/o-high internal phase emulsions (hipes) and derived o/w emulsions stabilised by pgpr and lecithin. *Food Research International*, 122, 252-262.

Ongey, E.L., Pflugmacher, S. & Neubauer, P. 2018. Bioinspired designs, molecular premise and tools for evaluating the ecological importance of antimicrobial peptides. *Pharmaceuticals*, 11(3): 68.

Ortiz-Viedma, J., Rodriguez, A., Vega, C., Osorio, F., Defillipi, B., Ferreira, R. & Saavedra, J. 2018. Textural, flow and viscoelastic properties of hass avocado (persea americana mill.) during ripening under refrigeration conditions. *Journal of Food Engineering*, 219, 62-70.

Ozturk, B. & McClements, D. J. 2016. Progress in natural emulsifiers for utilization in food emulsions. *Current Opinion in Food Science*, 7, 1-6.

Pajouhandeh, A., Kavousi, A., Schaffie, M. & Ranjbar, M. 2017. Experimental measurement and modeling of nanoparticle-stabilised emulsion rheological behavior. *Colloids and Surfaces A: Physicochemical and Engineering Aspects*, *520*, 597-611.

Palanisamy, R., Bhatt, P., Kumaresan, V., Pasupuleti, M. & Arockiaraj, J. 2018. Innate and adaptive immune molecules of striped murrel *Channa striatus*. *Reviews in Aquaculture*, 10(2): 296-319.

Paraskevopoulou, C., Perras, M., Diederichs, M., Amann, F., Löw, S., Lam, T. & Jensen, M. 2017. The three stages of stress relaxation-Observations for the time-dependent behaviour of brittle rocks based on laboratory testing. *Engineering Geology*, *216*, 56-75.

Parisi, M.G., Benenati, G. & Cammarata, M. 2015. Sea bass Dicentrarchus labrax (L.) bacterial infection and confinement stress acts on F-type lectin (Dl FBL) serum modulation. *Journal of Fish Diseases*, 38(11): 967-976.

Park, M. K., Jun, S., Kim, I., Jin, S. M., Kim, J. G., Shin, T. J. & Lee, E. 2015. Stepwise drug-release behavior of onion-like vesicles generated from emulsification-induced assembly of semicrystalline polymer amphiphiles. *Advanced Functional Materials*, 25, 4570-4579.

Patel, A.R., Dumlu, P., Vermeir, L., Lewille, B., Lesaffer, A. & Dewettinck, K. 2015. Rheological characterisation of gel-in-oil-in-gel type structured emulsions. *Food hydrocolloids*, *46,* 84-92.

Patil, L. & Gogate, P. R. 2018. Ultrasound assisted synthesis of stable oil in milk emulsion: Study of operating parameters and scale-up aspects. *Ultrasonics Sonochemistry*, 40, 135-146.

Paximada, P., Tsouko, E., Kopsahelis, N., Koutinas, A. A. & Mandala, I. 2016. Bacterial cellulose as stabiliser of o/w emulsions. *Food Hydrocolloids*, 53, 225-232.

Peatman, E., Lange, M., Zhao, H. & Beck, B. H. 2015. Physiology and immunology of mucosal barriers in catfish (ictalurus spp.). *Tissue Barriers*, 3, e1068907.

Pellegrini, D., Duce, C., Bonaduce, I., Biagi, S., Ghezzi, L., Colombini, M.P., Tinè, M.R. & Bramanti, E. 2016. Fourier transform infrared spectroscopic study of rabbit glue/inorganic pigments mixtures in fresh and aged reference paint reconstructions. *Microchemical Journal*, *124*, 31-35.

Peng, F., He, S., Yi, H., Li, Q., Xu, W., Wang, R. & Ma, Y. 2018. Physical, textural, and rheological properties of whipped cream affected by milk fat globule membrane protein. *Internationa*l *Journal of Food Properties*, 21, 1190-1202.

Perazzo, A., Preziosi, V. & Guido, S. 2015. Phase inversion emulsification: Current understanding and applications. *Advances in Colloid and Interface Science*, *222*, 581-599.

Pérez-Orozco, J.P., Sánchez-Herrera, L.M. & Ortiz-Basurto, R.I. 2019. Effect of concentration, temperature, pH, co-solutes on the rheological properties of Hyptis suaveolens L. mucilage dispersions. *Food Hydrocolloids*, *87*, 297-306.

Pérez-Sánchez, J., Terova, G., Simó-Mirabet, P., Rimoldi, S., Folkedal, O., Calduch-Giner, J. A., Olsen, R. E. & Sitjà-Bobadilla, A. 2017. Skin mucus of gilthead sea bream (sparus aurata l.). Protein mapping and regulation in chronically stressed fish. *Frontiers in Physiology*, 8, 34-34.

Peters, I.R., Majumdar, S. & Jaeger, H.M. 2016. Direct observation of dynamic shear jamming in dense suspensions. *Nature*, *532*(7598); 214-217.

Petrou, G. & Crouzier, T. 2018. Mucins as multifunctional building blocks of biomaterials. *Biomaterials science*, *6*(9); 2282-2297.

Piorkowski, D. T. & McClements, D. J. 2014. Beverage emulsions: Recent developments in formulation, production, and applications. *Food Hydrocolloids*, 42, 5-41.

Powell, K. C., Damitz, R. & Chauhan, A. 2017. Relating emulsion stability to interfacial properties for pharmaceutical emulsions stabilised by pluronic f68 surfactant. *International Journal of Pharmaceutics*, 521, 8-18.

Primozic, M., Duchek, A., Nickerson, M. & Ghosh, S. 2017. Effect of lentil proteins isolate concentration on the formation, stability and rheological behavior of oil-in-water nanoemulsions. *Food Chemistry*, 237, 65-74.

Qi, X., Wang, H., Wang, C. & Li, F. 2017. Application of Turbiscan in the homoaggregation and heteroaggregation of copper nanoparticles. *Colloids and Surfaces A: Physicochemical and Engineering Aspects*, *535*, 96-104.

Qian, Y. & Kawashima, S. 2018. Distinguishing dynamic and static yield stress of fresh cement mortars through thixotropy. *Cement and Concrete Composites*, *86*, 288-296.

Querol, N., Barreneche, C. & Cabeza, L. F. 2017. Storage stability of bimodal emulsions vs. Monomodal emulsions. *Applied Sciences*, 7, 1267.

Quinzio, C., Ayunta, C., de Mishima, B.L. & Iturriaga, L. 2018. Stability and rheology properties of oil-in-water emulsions prepared with mucilage extracted from Opuntia ficus-indica (L). Miller. *Food Hydrocolloids*, *84*, 154-165.

Radfar, R., Hosseini, H., Farhodi, M., Ghasemi, I., Średnicka-Tober, D., Shamloo, E. & Khaneghah, A.M. 2020. Optimization of antibacterial and mechanical properties of an active LDPE/starch/nanoclay nanocomposite film incorporated with date palm seed extract using D-optimal mixture design approach. *Internationa*l *Journal of Biological Macromolecules*.

Radtke, T., Böni, L., Bohnacker, P., Fischer, P., Benden, C. & Dressel, H. 2018. The many ways sputum flows–dealing with high within-subject variability in cystic fibrosis sputum rheology. *Respiratory Physiology & Neurobiology*, 254, 36-39.

Rafe, A. & Razavi, S. M. 2013. Dynamic viscoelastic study on the gelation of basil seed gum. *International Journal of Food Science & Technology*, 48, 556-563.

Rafe, A. & Razavi, S. M. 2017. Scaling law, fractal analysis and rheological characteristics of physical gels cross-linked with sodium trimetaphosphate. *Food Hydrocolloids*, 62, 58-65.

Rahman, M.A., Molla, M.H.R., Sarker, M.K., Chowdhury, S.H. & Shaikh, M.M. 2018. Snakehead fish (Channa striata) and its biochemical properties for therapeutics and health benefits. *SF J Biotechnol Biomed Eng*. 2018; 1 (1): 1005.

Rajak, V., Singh, I., Kumar, A. & Mandal, A. 2016. Optimization of separation of oil from oil-in-water emulsion by demulsification using different demulsifiers. *Petroleum Science and Technology*, 34, 1026-1032.

Rajanbabu, V. & Chen, J.Y. 2011. Applications of antimicrobial peptides from fish and perspectives for the future. *Peptides*, 32(2): 415-420.

Rao, M. A. 2014. Flow and functional models for rheological properties of fluid foods. Rheology of fluid, semisolid, and solid foods. Springer, New York, NY.

Rao, S.S. & Wong, H. 2018. The motion of long drops in rectangular microchannels at low capillary numbers. *Journal of Fluid Mechanics*, *852*, 60-104.

Rasouli-Pirouzian, H., Peighambardoust, S. H. & Azadmard-Damirchi, S. 2017. Rheological properties of sugar-free milk chocolate: *Comparative Study and Optimisation*.

Ren, Y., Zhao, H., Su, B., Peatman, E. & Li, C. 2015. Expression profiling analysis of immune-related genes in channel catfish (Ictalurus punctatus) skin mucus following Flavobacterium columnare challenge. *Fish &* Shellfish *Immunology*, 46(2): 537-542.

Reneeta, N. P., Thiyonila, B., Aathmanathan, V. S., Ramya, T., Chandrasekar, P., Subramanian, N., Prajapati, V. K. & Krishnan, M. 2018. Encapsulation and systemic delivery of 5-fluorouracil conjugated with silkworm pupa derived protein nanoparticles for experimental lymphoma cancer. *Bioconjugate Chemistry*, 29, 2994-3009.

Reverter, M., Tapissier-Bontemps, N., Lecchini, D., Banaigs, B. & Sasal, P. 2018. Biological and ecological roles of external fish mucus: a review. *Fishes*, 3(4): 41.

Ruan, Q., Yang, X., Zeng, L. & Qi, J. 2019. Physical and tribological properties of high internal phase emulsions based on citrus fibers and corn peptides. *Food Hydrocolloids*, *95*, 53-61.

Ruangsri, J., Salger, S.A., Caipang, C.M., Kiron, V. & Fernandes, J.M. 2012. Differential expression and biological activity of two piscidin paralogues and a novel splice variant in Atlantic cod (Gadus morhua L.). *Fish &* Shellfish *Immunology*, 32(3): 396-406.

Rubeena, A.S., Divya, M., Vaseeharan, B., Karthikeyan, S., Ringø, E. & Preetham, E. 2019. Antimicrobial and biochemical characterisation of a C-type lectin isolated from pearl spot (Etroplus suratensis). *Fish &* Shellfish *Immunology*, 87: 202-211.

Ruiz Ruiz, J. C., Ortiz Vazquez, E. D. L. L. & Segura Campos, M. R. 2017. Encapsulation of vegetable oils as source of omega-3 fatty acids for enriched functional foods. *Critical* Reviews *in Food Science and Nutrition*, 57, 1423-1434.

Saani, S. M., Abdolalizadeh, J. & Heris, S. Z. 2019. Ultrasonic/sonochemical synthesis and evaluation of nanostructured oil in water emulsions for topical delivery of protein drugs. *Ultrasonics Sonochemistry*, 55, 86-95.

SABS, 2008. South African National Standard: *The care and use of animals for scientific purposes* (SANS 10386:2008). Groenkloof, Pretoria: SABS Standards Division SABS-SANS 10388-

2008. In: SABS SOUTH AFRICAN BUREAU OF STANDARDS, S. D. (ed.) 1 ed. Groenkloof: Pretoria: SABS South African Bureau of Standards.

Safaei, F. & Castorena, C. 2017. Material nonlinearity in asphalt binder fatigue testing and analysis. *Materials & Design*, 133, 376-389.

Saini, C. S., Sharma, H. K. & Sharma, L. 2018. Thermal, structural and rheological characterisation of protein isolate from sesame meal. *Journal of Food Measurement and Characterisation*, 12, 426-432.

Salinas, I. 2015. The mucosal immune system of teleost fish. *Biology*, 4(3): 525-539.

Salinas, I. & Magadán, S. 2017. Omics in fish mucosal immunity. *Developmental & Comparative Immunology*, 75, 99-108.

Salles, M. S., D'abreu, L. F., Júnior, L. C. R., César, M. C., Guimarães, J. G., Segura, J. G., Rodrigues, C., Zanetti, M. A., Pfrimer, K. & Netto, A. S. 2019. Inclusion of sunflower oil in the bovine diet improves milk nutritional profile. *Nutrients*, 11, 481.

Salvia-Trujillo, L., Soliva-Fortuny, R., Rojas-Graü, M. A., McClements, D. J. & Martin-Belloso, O. 2017. Edible nanoemulsions as carriers of active ingredients: A review. *Annual Review of Food Science and Technology*, 8, 439-466.

Samson, S., Basri, M., Masoumi, H. R. F., Karjiban, R. A. & Malek, E. A. 2016. Design and development of a nanoemulsion system containing copper peptide by d-optimal mixture design and evaluation of its physicochemical properties. *RSC Advances*, 6, 17845-17856.

Sankhla, A., Sharma, R., Yadav, R. S., Kashyap, D., Kothari, S. & Kachhwaha, S. 2016. Biosynthesis and characterisation of cadmium sulfide nanoparticles–an emphasis of zeta potential behavior due to capping. *Materials Chemistry and Physics*, 170, 44-51.

Santos, J., Trujillo-Cayado, L., Calero, N., Alfaro, M. & Muñoz, J. 2016. Development of eco-friendly emulsions produced by microfluidization technique. *Journal of Industrial and Engineering Chemistry*, 36, 90-95.

Santos, P. H., Carignano, M. A. & Campanella, O. 2017. Effect of shear history on rheology of time-dependent colloidal silica gels. *Gels*, 3, 45.

Sapei, L., Sandy, I.G.Y.H., Suputra, I.M.K.D. & Ray, M. 2017, November. The effect of different concentrations of tween-20 combined with rice husk silica on the stability of o/w emulsion: A kinetic study. In *IOP Conference Series: Materials Science and Engineering* (Vol. 273). IOP Publishing, Bristol BS1 6HG.

Sarroukh, R., Goormaghtigh, E., Ruysschaert, J.-M. & Raussens, V. 2013. ATIR-FTIR: A "rejuvenated" tool to investigate amyloid proteins. *Biochimica et Biophysica Acta (BBA)-Biomembranes*, 1828, 2328-2338.

Sathyamoorthi, A., Kumaresan, V., Palanisamy, R., Pasupuleti, M., Arasu, M.V., Al-Dhabi, N.A., Marimuthu, K., Amin, S.N., Arshad, A., Yusoff, F.M. & Arockiaraj, J. 2019. Therapeutic cationic antimicrobial peptide (CAP) derived from fish aspartic proteinase Cathepsin D and its antimicrobial mechanism. *International Journal of Peptide Research and Therapeutics*, 25(1): 93-105.

Schmidt, U., Schütz, L. & Schuchmann, H. 2017. Interfacial and emulsifying properties of citrus pectin: Interaction of ph, ionic strength and degree of esterification. *Food Hydrocolloids*, 62, 288-298.

Scocchi, M., Furlan, M., Venier, P. & Pallavicini, A. 2016. Cathelicidins: an ancient family of fish antimicrobial peptides. In Lessons in Immunity (pp. 225-237). Academic Press, Cambridge, MA.

Selamat, S. N., Halmi, M. I. E. B., Abdullah, S. R. S., Idris, M., Hasan, H. A. & Anuar, N. 2018. Optimization of lead (pb) bioaccumulation in melastoma malabathricum l. By response surface methodology (rsm). *Rendiconti Lincei*. *Scienze Fisiche e Naturali*, 29, 43-51.

Seppola, M., Bakkemo, K.R., Mikkelsen, H., Myrnes, B., Helland, R., Irwin, D.M. and Nilsen, I.W. 2016. Multiple specialised goose-type lysozymes potentially compensate for an exceptional lack of chicken-type lysozymes in Atlantic cod. *Scientific Reports*, 6, 28318.

Shabir, U., Ali, S., Magray, A.R., Ganai, B.A., Firdous, P., Hassan, T. & Nazir, R. 2018. Fish antimicrobial peptides (AMP's) as essential and promising molecular therapeutic agents: a review. *Microbial Pathogenesis*, 114: 50-56.

Shahkaramipour, N., Tran, T. N., Ramanan, S. & Lin, H. 2017. Membranes with surface-enhanced antifouling properties for water purification. *Membranes*, 7, 13.

Shao, P., Ma, H., Zhu, J. & Qiu, Q. 2017. Impact of ionic strength on physicochemical stability of o/w emulsions stabilised by ulva fasciata polysaccharide. *Fish Hydrocollioids*, 69, 202-209.

Sharif, H. R., Williams, P. A., Sharif, M. K., Khan, M. A., Majeed, H., Safdar, W., Shamoon, M., Shoaib, M., Haider, J. & Zhong, F. 2017. Influence of osa-starch on the physico chemical characteristics of flax seed oil-eugenol nanoemulsions. *Food Hydrocolloids*, 66, 365-377.

Sharma, A. K., Tiwari, A. K. & Dixit, A. R. 2016. Rheological behaviour of nanofluids: A review. *Renewable and Sustainable Energy Reviews*, 53, 779-791.

Shavandi, A., Silva, T.H., Bekhit, A.A. & Bekhit, A.E.D.A. 2017. Keratin: dissolution, extraction and biomedical application. *Biomaterials science*, *5*(9); 1699-1735.

Sherahi, M. H., Shadaei, M., Ghobadi, E., Zhandari, F., Rastgou, Z. & Hashemi, S. M. B. 2018. Effect of temperature, ion type and ionic strength on dynamic viscoelastic, steady-state and dilute-solution properties of descurainia sophia seed gum. *Food Hydrocolloids*, 79, 81-89.

Shin, S.C., Ahn, I.H., Ahn, D.H., Lee, Y.M., Lee, J., Lee, J.H., Kim, H.W. & Park, H. 2017. Characterisation of two antimicrobial peptides from Antarctic fishes (Notothenia coriiceps and Parachaenichthys charcoti). *PloS one*, 12(1): e0170821.

Silva, C., Torres, M., Chenlo, F. & Moreira, R. 2017. Rheology of aqueous mixtures of tragacanth and guar gums: Effects of temperature and polymer ratio. *Food Hydrocolloids*, 69, 293-300.

Singla, N., Verma, P., Ghoshal, G. & Basu, S. 2013. Steady state and time dependent rheological behaviour of mayonnaise (egg and eggless). *International Food Research Journal*, 20, 2009.

Sohail, M., Sun, D.-W. & Zhu, Z. 2018. Recent developments in intelligent packaging for enhancing food quality and safety. *Critical Reviews in Food Science and Nutrition*, 58, 265

Sousa de, I. P., Steiner, C., Schmutzler, M., Wilcox, M. D., Veldhuis, G. J., Pearson, J. P., Huck, C. W., Salvenmoser, W. & Bernkop-Schnürch, A. 2015. Mucus permeating carriers:

Formulation and characterisation of highly densely charged nanoparticles. *European Journal of Pharmaceutics and Biopharmaceutics,* 97, 273-279.

Souza Mendes de, P.R. & Thompson, R.L. 2019. Time-dependent yield stress materials. *Current Opinion in Colloid & Interface Science*, *43*; 15-25.

Srivastava, A., Nigam, A.K., Mittal, S. & Mittal, A.K. 2018. Role of aloin in the modulation of certain immune parameters in skin mucus of an Indian major carp, Labeo rohita. *Fish &* Shellfish *Immunology*, 73: 252-261.

Staniszewska, E., Malek, K. & Baranska, M. 2014. Rapid approach to analyze biochemical variation in rat organs by atr ftir spectroscopy. Spectrochimica Acta Part A: Molecular and *Biomolecular Spectroscopy*, 118, 981-986.

Stettin, H. 2016. Resonances in oscillatory rheometry. *Applied Rheology*, 26, 8-19.

Stevens, J. R., Newton, R. W., Tlusty, M. & Little, D. C. 2018. The rise of aquaculture by-products: Increasing food production, value, and sustainability through strategic utilisation. *Marine Policy*, 90, 115-124.

Stounbjerg, L., Vestergaard, C., Andreasen, B. & Ipsen, R. 2018. Beverage clouding agents: Review of principles and current manufacturing. *Food Reviews International*, 34, 613-638.

Stowell, S.R., Ju, T. & Cummings, R.D. 2015. Protein glycosylation in cancer. *Annual Review of Pathology: Mechanisms of Disease*, 10: 473-510.

Su, Y. 2011. Isolation & identification of pelteobagrin, a novel antimicrobial peptide from the skin mucus of yellow catfish (Pelteobagrus fulvidraco). *Comparative Biochemistry and Physiology Part B: Biochemistry and Molecular Biology*, 158(2): 149-154.

Svensson, F., Lang, T., Johansson, M.E. & Hansson, G.C. 2018. The central exons of the human MUC2 and MUC6 mucins are highly repetitive and variable in sequence between individuals. *Scientific Reports*, 8(1): 1-10.

Tabrizi, L., Mcardle, P., Ektefan, M. & Chiniforoshan, H. 2016. Synthesis, crystal structure, spectroscopic and biological properties of mixed ligand complexes of cadmium (ii), cobalt (ii) and manganese (ii) valproate with 1, 10-phenanthroline and imidazole. *Inorganica Chimica Act*a, 439, 138-144.

Tadros, T. F. 2011. Rheology of dispersions: Principles and applications, John Wiley & Sons, Hoboken, New Jersey.

Tadros, T. F. 2013. Emulsion formation, stability, and rheology. Emulsion formation and stability, 1, 1-75. Weinheim, Germany: Wiley-VCH Verlag GmbH & Co. KGaA.

Tadros, T.F. 2015. *Interfacial Phenomena and Colloid Stability: Industrial Applications*. Walter de Gruyter GmbH & Co KG.

Tang, J., Sun, Y., Han, Z. and Shi, W., 2019. An illustration of optimal selected glycosidase for N-glycoproteins deglycosylation and crystallization. *International journal of biological macromolecules*, *122*, pp.265-271.

Tang, C.H. 2020. Globular proteins as soft particles for stabilising emulsions: Concepts and strategies. *Food Hydrocolloids*, *103*, 105664.

Tasumi, S., Yamaguchi, A., Matsunaga, R., Fukushi, K., Suzuki, Y., Nakamura, O., Kikuchi, K. & Tsutsui, S. 2016. Identification and characterisation of pufflectin from the grass pufferfish

Takifugu niphobles and comparison of its expression with that of Takifugu rubripes. *Developmental & Comparative Immunology*, 59: 48-56.

Tiong, T. J., Chu, J. K., Lim, L. Y., Tan, K. W., Yap, Y. H. & Asli, U. A. 2019. A computational and experimental study on acoustic pressure for ultrasonically formed oil-in-water emulsion. *Ultrasonics Sonochemistry*, 56, 46-54.

Torres, M. D., Chenlo, F. & Moreira, R. 2018. Rheological effect of gelatinisation using different temperature-time conditions on potato starch dispersions: Mechanical characterisation of the obtained gels. *Food and Bioprocess Technology*, 11, 132-140.

Townsend, J. M., Beck, E. C., Gehrke, S. H., Berkland, C. J. & Detamore, M. S. 2019. Flow behavior prior to crosslinking: The need for precursor rheology for placement of hydrogels in medical applications and for 3d bioprinting. *Progress in Polymer Science*, 91, 126-140.

Tran, T., Xi, X., Rades, T. & Müllertz, A. 2016. Formulation and characterisation of self-nanoemulsifying drug delivery systems containing monoacyl phosphatidylcholine. *International Journal of Pharmaceutics*, 502, 151-160.

Trapella, C., Rizzo, R., Gallo, S., Alogna, A., Bortolotti, D., Casciano, F., Zauli, G., Secchiero, P. & Voltan, R. 2018. Helixcomplex snail mucus exhibits pro-survival, proliferative and pro-migration effects on mammalian fibroblasts. *Scientific Reports*, 8, 17665.

Trujillo-Cayado, L. A., Santos, J., Calero, N., Alfaro, M. D. C. & Muñoz, J. 2019. Influence of the homogenisation pressure on the rheology of biopolymer-stabilised emulsions formulated with thyme oil. *Fluids*, 4, 29.

Tsang, Y., Choy, K., Wu, C., Ho, G., Lam, H. & Tang, V. 2018. An intelligent model for assuring food quality in managing a multi-temperature food distribution centre. *Food Control*, 90, 81-97.

Tsugawa, J.K., de Oliveira Romano, R.C., Pileggi, R.G. & Boscov, M.E.G. 2020. Rheology concepts applied to geotechnical engineering. *Applied Rheology*, *29*(1); .202-221.

Tsutsui, S., Komatsu, Y., Sugiura, T., Araki, K. & Nakamura, O. 2011. A unique epidermal mucus lectin identified from catfish (Silurus asotus): first evidence of intelectin in fish skin slime. *The Journal of Biochemistry*, 150(5): 501-514.

Tsutsui, S., Yamamura, N., Yoshida, T. & Nakamura, O. 2015. Fugu (Takifugu rubripes) serum GlcNAc-binding lectin is a kalliklectin but has different properties from those of a reported homologue. *The Journal of Biochemistry*, 158(3): 189-195.

Tsutsui, S., Yoshinaga, T., Komiya, K., Yamashita, H. & Nakamura, O. 2016. Differential expression of skin mucus C-type lectin in two freshwater eel species, Anguilla marmorata and Anguilla japonica. *Developmental & Comparative* Immunology, 61, 154-160.

Tsutsui, S., Yoshinaga, T., Watanabe, S., Tsukamoto, K. & Nakamura, O. 2019. Mucosal galectin genes in all freshwater eels of the genus Anguilla. *Journal of Fish Biology*, 94(4): 660-670.

Tyor, A. K. & Kumari, S. 2016. Biochemical characterisation and antibacterial properties of fish skin mucus of fresh water fish, hypophthalmichthys nobilis. *Int*. *J*. *Pharm*. *Pharmaceut*. *Sci*, 8, 132-6.

Vadodaria, S. S., Onyianta, A. J. & Sun, D. 2018. High-shear rate rheometry of micro-nanofibrillated cellulose (cmf/cnf) suspensions using rotational rheometer. *Cellulose*, 25, 5535-5552.

Valdenegro-Vega, V.A., Crosbie, P., Bridle, A., Leef, M., Wilson, R. & Nowak, B.F. 2014. Differentially expressed proteins in gill and skin mucus of Atlantic salmon (Salmo salar) affected by amoebic gill disease. *Fish & Shellfish Immunology*, 40(1): 69-77.

Valero, Y., Chaves-Pozo, E., Meseguer, J., Esteban, M.A. & Cuesta, A. 2013. Biological role of fish antimicrobial peptides. *Antimicrobial Peptides*, 2, 31-60.

Varki, A., Schnaar, R. L. & Schauer, R. 2017. Sialic acids and other nonulosonic acids. Essentials of glycobiology [internet]. 3rd edition. Cold Spring Harbor Laboratory Press, NY.

Vasta, G.R., Amzel, L.M., Bianchet, M.A., Cammarata, M., Feng, C. & Saito, K. 2017. F-type lectins: a highly diversified family of fucose-binding proteins with a unique sequence motif and structural fold, involved in self/non-self-recognition. *Frontiers in Immunology*, 8, 1648.

Velásquez-Cock, J., Serpa, A., Vélez, L., Gañán, P., Hoyos, C.G., Castro, C., Duizer, L., Goff, H.D. & Zuluaga, R. 2019. Influence of cellulose nanofibrils on the structural elements of ice cream. *Food Hydrocolloids*, *87*, 204-213.

Vignali, A., Iannace, S., Falcone, G., Utzeri, R., Stagnaro, P. & Bertini, F. 2019. Lightweight poly (ε-caprolactone) composites with surface modified hollow glass microspheres for use in rotational molding: Thermal, rheological and mechanical properties. *Polymers*, 11, 624.

Villalobos-Castillejos, F., Granillo-Guerrero, V. G., Leyva-Daniel, D. E., Alamilla-Beltrán, L., Gutiérrez-López, G. F., Monroy-Villagrana, A. & Jafari, S. M. 2018. Fabrication of nanoemulsions by microfluidization. Nanoemulsions. Elsevier.

Wang, F., Tang, J., Liu, H., Yu, G. & Zou, Y. 2019. Self-assembled polymeric micelles as amphiphilic particulate emulsifiers for controllable pickering emulsions. *Materials Chemistry Frontiers*, 3, 356-364.

Wang, H., Lin, M., Chen, D., Dong, Z., Yang, Z. & Zhang, J. 2018. Research on the rheological properties of cross-linked polymer microspheres with different microstructures.*Powder Technology*, *331*, 310-321.

Wang, T., Zhang, M., Fang, Z., Liu, Y. & Gao, Z. 2016. Rheological, textural and flavour properties of yellow mustard sauce as affected by modified starch, xanthan and guar gum. *Food and Bioprocess Technology*, 9(5): 849-858.

Watanabe, Y., Naganuma, T., Ogawa, T. & Muramoto, K. 2013. Lectins of marine origin and their clinical applications. In Antitumor Potential and other Emerging Medicinal Properties of Natural Compounds (pp. 33-54). Springer, Dordrecht, NE.

Weigel, F., Weiss, J., Decker, E.A. & McClements, D.J. 2018. Lutein-enriched emulsion-based delivery systems: Influence of emulsifiers and antioxidants on physical and chemical stability. *Food Chemistry*, *242*, 395-403.

Whaley, J. K., Templeton, C. & Anvari, M. 2019. Rheological testing for semisolid foods: Traditional rheometry. *Rheology of Semisolid Foods*. Springer, New York Ny.

Whitby, C. P., Anwar, H. K. & Hughes, J. 2016. Destabilising pickering emulsions by drop flocculation and adhesion. *Journal of Colloid and Interfac*e *Science*, 465, 158-164.

Whitby, C. P. & Wanless, E. J. 2016. Controlling pickering emulsion destabilisation: A route to fabricating new materials by phase inversion. *Materials*, 9, 626.

Wikström, F., Verghese, K., Auras, R., Olsson, A., Williams, H., Wever, R., Grönman, K., Kvalvåg Pettersen, M., Møller, H. & Soukka, R. 2019. Packaging strategies that save food: A research agenda for 2030. *Journal of Industrial Ecology*, 23, 532-540.

Wu, M., Shi, Z., Huang, H., Qu, J., Dai, X., Tian, X., Wei, W., Li, G. & Ma, T. 2017. Network structure and functional properties of transparent hydrogel sanxan produced by Sphingomonas sanxanigenens NX02. *Carbohydrate polymers*, *76*, .65-74.

Wu, X.M., Cao, L., Nie, P. & Chang, M.X. 2019. Histone H2A cooperates with RIP2 to induce the expression of antibacterial genes and MHC related genes. *Developmental & Comparative Immunology*, *101*, 103455.

Xi, Z., Liu, W., McClements, D. J. & Zou, L. 2019. Rheological, structural, and microstructural properties of ethanol induced cold-set whey protein emulsion gels: Effect of oil content. *Food Chemistry*, 291, 22-29.

Xie, J., Zhong, G., Cai, C., Chen, C. & Chen, X. 2017. Rapid and efficient separation of glycoprotein using ph double-responsive imprinted magnetic microsphere. *Talanta*, 169, 98-103.

Xu, X., Sun, Q. & McClements, D. J. 2019. Enhancing the formation and stability of emulsions using mixed natural emulsifiers: Hydrolyzed rice glutelin and quillaja saponin. *Food Hydrocolloids*, 89, 396-405.

Yadav, N.K., Nanda, S., Sharma, G. & Katare, O.P. 2017. Systematically optimized ketoprofen-loaded novel proniosomal formulation for periodontitis: in vitro characterisation and in vivo pharmacodynamic evaluation. *AAPS PharmSciTech*, 18(5): 1863-1880.

Yamashita, Y., Miyahara, R. & Sakamoto, K. 2017. Emulsion and emulsification technology. *Cosmetic Science and Technology*, 13.

Yang, Z.X. & Pan, K. 2017. Flow deformation and cyclic resistance of saturated loose sand considering initial static shear effect. *Soil Dynamics and Earthquake Engineering*, *92*,.68-78.

Ye, S., Yu, H.Y., Wang, D., Zhu, J. & Gu, J. 2018. Green acid-free one-step hydrothermal ammonium persulfate oxidation of viscose fiber wastes to obtain carboxylated spherical cellulose nanocrystals for oil/water Pickering emulsion. *Cellulose*, *25*(9); 5139-5155.

Yeom, D.W., Song, Y.S., Kim, S.R., Lee, S.G., Kang, M.H., Lee, S. & Choi, Y.W. 2015. Development and optimization of a self-microemulsifying drug delivery system for ator vastatin calcium by using D-optimal mixture design. *International Journal of nanomedicine*, *10*, 3865.

Yolmeh, M. & Jafari, S. M. 2017. Applications of response surface methodology in the food industry processes. *Food and Bioprocess Technology*, 10, 413-433.

Yuan, Q., Zhou, D., Khayat, K. H., Feys, D. & Shi, C. 2017. On the measurement of evolution of structural build-up of cement paste with time by static yield stress test vs. Small amplitude oscillatory shear test. *Cement and Concrete Research*, 99, 183-189.

Zhai, X., Lin, D., Liu, D. & Yang, X. 2018. Emulsions stabilised by nanofibers from bacterial cellulose: New potential food-grade pickering emulsions. *Food Research International*, 103, 12-20.

Zhang, C., Zhang, J., Liu, M. & Huang, M. 2018a. Molecular cloning, expression and antibacterial activity of goose-type lysozyme gene in Microptenus salmoides. *Fish &* Shellfish *Immunology*, 82, 9-16.

Zhang, H., Song, X., Wang, L., Kong, P., Yang, J., Liu, L., Qiu, L., Zhang, Y., Qiu, L. and Song, L. 2011. AiCTL-6, a novel C-type lectin from bay scallop Argopecten irradians with a long C-type lectin-like domain *Fish &* Shellfish *Immunology*, 30(1): 17-26.

Zhang, L., Ying, H., Yan, S., Zhan, N., Guo, Y. & Fang, W. 2018b. Hyperbranched poly (amido amine) as an effective demulsifier for oil-in-water emulsions of microdroplets. *Fuel*, 211, 197-205.

Zhang, X., Luo, X., Wang, Y., Li, Y., Li, B. & Liu, S. 2020. Concentrated O/W Pickering emulsions stabilised by soy protein/cellulose nanofibrils: Influence of pH on the emulsification performance. *Food Hydrocolloids* 106025.

Zhang, Z. & McClements, D. J. 2018. Overview of nanoemulsion properties: Stability, rheology, and appearance. Nanoemulsions. Elsevier.

Zheng, H. 2019. Introduction: Measuring rheological properties of foods. Rheology of semisolid foods. Springer.

Zhou, S., Zhao, H., Thongda, W., Zhang, D., Su, B., Yu, D., Peatman, E. & Li, C. 2016. Galectins in channel catfish, Ictalurus punctatus: characterisation and expression profiling in mucosal tissues. *Fish &* Shellfish *Immunology*, 49: 324-335.

Zhu, J., Lu, T., Yue, S., Shen, X., Gao, F., Busuttil, R.W., Kupiec-Weglinski, J.W., Xia, Q. & Zhai, Y. 2015. Rapamycin protection of livers from ischemia and reperfusion injury is dependent on both autophagy induction and mammalian target of rapamycin complex 2-Akt activation. *Transplantation*, 99(1): 48-55.

Zhu, Y., Gao, H., Liu, W., Zou, L. & McClements, D. J. 2019. A review of the rheological properties of dilute and concentrated food emulsions. *Journal of Texture Studies*.

Zide, D., Fatoki, O., Oputu, O., Opeolu, B., Nelana, S. & Olatunji, O. 2018. Zeolite 'adsorption'capacities in aqueous acidic media; The role of acid choice and quantification method on ciprofloxacin removal. Microporous *and Mesoporous Materials*, 255: 226-241.

Zielke, C., Stradner, A. & Nilsson, L. 2018. Characterisation of cereal β-glucan extracts: Conformation and structural aspects. *Food Hydrocolloids*, 79, 218-227.

Zou, Y., Yang, X. Scholten, E. 2018. Rheological behavior of emulsion gels stabilised by zein/tannic acid complex particles. *Food Hydrocolloids*, 77: 363-371.

Zhou, M.X., Classen, B., Agneessens, R., Godin, B. and Lutts, S., 2020. Salinity Improves Zinc Resistance in Kosteletzkya pentacarpos in Relation to a Modification in Mucilage and Polysaccharides Composition. *INTERNATIONAL JOURNAL OF ENVIRONMENTAL RESEARCH*, *14*(3), pp.323-333.

APPENDIX

Appendix A: Ethical certificate

Cape Peninsula
University of Technology

P.O. Box 1906, Bellville 7535 South Africa, Tel: +27 21 959 8669, Fax +27 21 595 6641, Symphony Road Bellville 7535

ENGINEERING FACULTY

On 22 January 2018, the Engineering Ethics Committee of the Cape Peninsula University of Technology granted ethics approval to **Adebanji Olasupo, 216278929** for research activities related to his **DEng: Chemical Engineering** studies at the Cape Peninsula University of Technology.

Title of thesis:	**Rheology and stability of oil in water emulsions stabilised with African catfish mucus.**

Comments:

Permission to collect Data attached.

Prof Tunde Ojumu	
Assistant Dean – Research and Innovation	22/01/2018